KIF18B, a nuclear kinesin, is involved in DNA damage response

Maryam Sakhteh

Genome Stability Laboratory,

Centre for Chromosome Biology,

Biochemistry, School of Natural Sciences,

National University of Ireland Galway

A thesis submitted to the National University of Ireland Galway for the degree of Doctor of Philosophy

Supervisor: Prof. Noel F. Lowndes

September 2020

Table of Contents

List of figures

List of Tables

Abbreviations

53BP1: p53 binding protein 1

aa: amino acids

Ahc1: ADA histone acetyltransferase

alt-EJ: alternative end-joining

APC/C: Anaphase promoting complex/Cyclosome

APR: Actin-binding protein

ANCHR: Abscission and NoCut checkpoint regulator

ATM: Ataxia Telangiectasia Mutated

ATR: Ataxia Telangiectasia and RAD3 related

ATRIP: ATR interacting protein

BER: Base excision repair

BIR: break-induced replication

BLM: Bloom syndrome protein

bp: Base pair

BRCA1: Breast Cancer associated gene 1

BRCA2: Breast Cancer associated gene 2

BRCT: BRCA1 carboxy-terminal

BrDU: Bromodeoxyuridine

BRE: Brain and Reproductive Organ-Expressed

BSA: Bovine Serum Albumin

CDC: cell division cycle

CDK: Cyclin dependent kinase

cDNA: complementary DNA

CHK1/2: Checkpoint Kinase 1/2

CHMP4B/C: Charged Multivesicular Protein 4 B/C

CIP1: Cyclin-dependent kinase inhibitor 1

C-NHEJ: classical NHEJ

CPC: Chromosome Passenger Complex

CSK: Cytoskeletal Buffer

CSR: class-switch recombination

CtIP: CtBP interacting protein

CTRL: control

DAPI: 4',6-diamidino-2-phenylindole

DDR: DNA damage response

dHJ: double Holiday junction

D-Loop: Displacement loop

DMEM: Dulbecco's Modified Eagle Medium

DMSO: Dimethyl sulfoxide

DNA: deoxyribonucleic acid

DNA2: DNA replication ATP-dependent helicase/nuclease DNA2

DNA-PKcs: DNA-dependent protein kinase catalytic subunit

Dox: DoxyCycline

DSB: DNA double-strand break

dsDNA: double-stranded DNA

DT-40: chicken lymphoma cell line

DTT: 1,4-Dithiothreitol

E2F: Transcription factor E2F

EB1: End Binding Protein 1

eIF4F: Eukaryotic initiation factor 4F

ESCRT: Endosomal Sorting Complex Required for Transport

FACS: Fluorescence-activated cell sorting

FAT: FRAP-ATM-TRRAP

FAT-C: FAT C-terminal domain

FISH: Fluorescence in Situ Hybridisation

FITC: Fluorescein isothiocyanate

FSC: Forward scatter

gH2AX: phosphorylated H2AX (ser139)

G1/2: Gap1/2 phase

GC: gene conversion

GFP: Green Fluorescent Protein

GST: Glutathione S-transferase

Gy: Gray

h: hour, hours

H2AX: variant histone H2AX

H3K9me3: tri-methylated lysine 9 on H3

H4K20me2: Histone H4 di-methylated on lysine 20

H2AK15ub: Histone H2A ubiquitinated on lysine 15

HCl: Hydrochloric acid

HDR: homology directed repair

HEK293: Human embryonic kidney cells

HeLa: Henrietta Lacks cell line

HR: homologous recombination

hTERT: human telomerase transcriptase

IF: Immunofluorescence

IP: Immunoprecipitation

IR: Ionizing Radiation

IRIF: ionizing radiation induced foci

J: Joules

kb: kilobases

kDa: kilo Dalton

KIF18B: Kinesin Family Member 18B

KIP1: Cyclin dependent kinase inhibitor p27

LAP2: Lamin Associated Protein 2

LINC: linker of nucleoskeleton and cytoskeleton

MAP: Microtubule Assembly Proteins

Mb: megabases

MCC: Mitotic Checkpoint Complex

MDC1: mediator of DNA damage checkpoint 1

MDM2: Mouse double minute 2 homolog

MEF: mouse embryonic fibroblast

MERIT40: Mediator of RAP80 Interactions and Targeting Subunit Of 40

MKLP1: Mitotic Kinesin-like Protein 1

mg: milligram

µg: microgram

ml: millilitre

mM: millimolar

MMR: mis-match repair

M-phase: Mitosis

MRN: MRE11-RAD50-NBS1 complex

mRNA: messenger RNA

MRE11: Meiotic Recomination11

N: Normality

NaCl: Sodium Chloride

NBA1: NAB1 and bud neck associated protein 1

NBS1: Nijmegen Breakage Syndrome 1

NCO: non-crossover

NEB: Nuclear Envelope Breakdown

NER: Nucleotide excision repair

NES: nuclear export signal

NHEJ: non-homologous end-joining

NLS: nuclear localisation signal

NPC: Nuclear Pore Complex

NUP153: Nucleoprotein 153

p53: tumour suppressor protein 53

PARP: Poly ADP ribose polymerase

PBS: Phosphate buffered Saline

PCR: Polymerase chain reaction

PFA: paraformaldehyde

PI: Propidium iodide

PI3K: phosphatidylinositole-3 kinase

PIKK: Phosphatidylinositol 3-kinase like kinase

PLK1/3: Polo-like kinase 1/3

PNK: Polynucleotide 5'-hydroxyl-kinase

PTIP: Pax transactivation domain interacting protein

PTM: post-translational modification

qPCR: quantitative PCR

RAP80: Receptor associated protein 80

RB: Retinoblastoma associated protein

RIF1: Rap1 interacting factor 1 homolog

RNA: ribonucleic acid

RNAse: Ribonuclease

RNF8: ring finger protein 8

RNF168: ring finger protein 168

ROS: reactive oxygen species

RPA: Replication protein A

RPE-1: retinal pigmented epithelial 1

RPMI: Roswell Park Memorial Institute media

RT: Room temperature

S-phase: DNA synthesis phase

SAC: Spindle assembly checkpoint

SD: standard deviation

SDS: Sodium dodecyl sulfate

SDSA: synthesis-dependent strand annealing

SEM: standard error of the mean

Ser: serine

shRNA: Short Hairpin RNA

SSA: Single-Strand Annealing

SSB: Single-Strand Break

SSC: side scatter

ssDNA: single-stranded DNA

SILAC: Stable isotope labelling with amino acids in cell culture

siRNA: small interfering RNA

SQ/TQ: Ser/Thr-Glu

TBS: Tris-buffered saline

TCE: total cell extract

TEMED: N, N, N', N'-tetramethyl ethylenediamine

TG: Tris-Glycine

TIP60: 60kDa Tat-interactive protein

TopBP1: Topoisomerase 2 binding protein 1

TRIP12: Thyroid Hormone Receptor Interactor 12

Tris: Tris(hydroxymethyl)aminomethane

TRITC: Tetramethylrhodamine Isothiocyanate

TRRAP: Transformation/Transcription domain associated protein

U2OS: U2 osteosarcoma cell line

UBR5: Ubiquitin Protein Ligase E3 Component N-Recognin

UDR: ubiquitination-dependent recruitment

UIM: ubiquitin interacting motif

USP28: Ubiquitin Specific Peptidase 28

UTR: untranslated region

UV: ultraviolet light

V: Volt

V(d)J recombination: Variable (Diversity) Joining recombination

VPS4: Vascular Protein Sorting 4

WB: Western Blot

WRN: Werner syndrome ATP dependent helicase

WT: wild type

XRCC3/4: X-Ray Repair Cross Complementing 3/4

Acknowledgements

Firstly, I would like to express my sincere gratitude to Noel for the continuous support of my Ph.D study, for his motivation, insightful comments and his guide, helping me with my research and writing of this thesis. I also appreciate the freedom he gave me to work in the lab as a scientist.

I would like to thank my best friend in the lab during my PhD, Janna, who helped me with ideas, troubleshooting and writing. Who kept me motivated when I was distressed. I also thank all former labmates; Louise, Nikolay, Marta and Stephen who I took advantage of their help and joyful research beside them. Muriel, I could not have produced such great microscopic images without your help and training. Shaylee and Sophie it was a short but sweet time to work with you two, wish you best of luck with the rest of your scientific life.

I'd also like to thank all of the past and present CCB members, who have helped me along the way.

Mahshid, Amin, Mona, Davoud, and all my Iranian friends in Galway and all over Ireland, thank you all to make this such a pleasant place for me to live so I never felt homesick.

To my parents, who I am so thankful to have. Thanks for all of their love and support and believing me. My love for them is beyond words. Thanks to my sister, Shaghayegh, who is always a good ear to hear all my complaints. I missed our load laughs together so much.

To Ryan, the apple of my eye, my love and motivation. Who carried out experiments with me in the lab for nine months. I also thank you and apologise to you for all the time missed to spend with you.

To Mohammadali, my soulmate. I could not have made it without the amount of love and support you gave me during these challenging years of my PhD. I won't forget those difficult days and nights you were minding Ryan and to let me work in lab. The power of our love makes everything possible. I am so lucky to have you in my life.

Thesis Declaration and Contributions

I declare that I have not obtained any previous qualification from NUI Galway or elsewhere based on any of the work contained in this thesis. I conducted all the experiments and wrote the thesis under supervision of Professor Noel Francis Lowndes. There is an exception which the experiment was performed by someone else but included in this thesis to complete the story. For clarity this is clearly indicated in the figure legend when appropriate and included below.

Chapter 3:

- The SILAC proteomic screen and initial confirmation of interaction in human cells were carried out by Dr. Silvia Maretto (Figure III.1.)

Abstract

DNA damage from both exogenous and endogenous sources occurs continuously in all cells. A multitude of DNA repair mechanisms have evolved to maintain genome stability. The 53BP1 tumour suppressor has been identified as a so-called mediator of the DNA double-strand break repair, promoting simple joining of breaks rather than a complex process of using an intact homologous strand as a template for repair. Additionally, 53BP1 is critical for class switch recombination in B-cells, a fusion of de-protected telomeres, and promotes the mobility of the broken ends of chromosomes. A previous proteomic screen for interacting partners of 53BP1 identified a kinesin, KIF18B, as a novel interactor. This interaction occurs via the Tudor domain of 53BP1 and a newly identified Tudor Interacting Motif (TIM) in KIF18B. KIF18B, is a kinesin-8 family member with a known role in maintaining the length of astral microtubules. Here we investigated the involvement of KIF18B in the DNA damage response and found it to be mainly nuclear in interphase and localised to DNA damage sites. We have also shown that 53BP1 focal recruitment to sites of DNA damage is KIF18B dependent. Furthermore, KIF18B is involved in the fusion of de-protected telomeres. Telomere fusion and 53BP1 recruitment to Telomere Dysfunction-Induced Foci, requires TIM, as well as the motor domain of KIF18B. Based on our observations, we propose a role for KIF18B in DNA damage response through mediating 53BP1 dependent DNA double-strand break mobility. Besides, we established that the KIF18B protein expression is cell cycle regulated, which increases as cells move from G1 to mitosis, and returns to low levels in late mitosis and early G1. Interestingly, we also showed a specific localisation of KIF18B to the midbody of cytokinetic cells, suggesting a role for KIF18B in abscission.

Chapter 1: General Introduction

1.1. The Cell Cycle

The duplication and segregation of all cellular components is termed the cell cycle and is conserved in all eukaryotes from yeasts to humans. The information required for growth and development is contained in nuclear DNA and packaged into chromosomes, collectively termed the genome. The genome is duplicated and segregated with high fidelity during each cell cycle. In general, the genome is duplicated during the S (synthesis) phase and segregated during M (mitosis) phase. Between S and M there are two 'gap' phases, termed the G1 and G2 phases (Barnum and O'Connell, 2014). The G1 and G2 phases are the intervals for cell growth and preparation for the subsequent S and M phases respectively (Bruce, 2008).

1.2. G1 and G1/S transition

The G1 phase is typically the longest and, with respect to cell growth and assessment of the environment for cells to proliferate, the most important phase of the cell cycle. The cell assesses the external environment (e.g., nutrient, growth factors), as well as cell size before making a decision to commit to another cell cycle. The decision point which cells irreversibly commit to proliferate rather than to exist the cell cycle is termed the 'Restriction point' in higher eukaryotes and the 'Start' in yeast (Bertoli et al., 2013). Cells exit the cell cycle at the Restriction point or Start if conditions are unfavourable and go into an un-dividing status termed G0 or quiescence (Martin and Stein, 1976).

Cyclins are the key regulators of cell cycle progression that activate Cyclin-dependent kinases or CDKs (Evans et al., 1983; Lees, 1995) (Figure1.1.). In higher eukaryotes, the major G1 Cyclins are the Cyclin Ds (Cyclin D1, D2 and D3, in human cells), with Cyclin E contributing to the G1/S transition, once the commitment to pass the restriction point has been made. Cyclin D partners with CDK4 or CDK6 and together these Cyclin D-CDK4/6 complexes phosphorylate the

retinoblastoma tumour suppressor, pRB (Morgan, 1997). Hypo-phosphorylated pRB associates with the E2F transcription factor and represses E2F-dependent transcription. Increasing phosphorylation of pRB, initially by Cyclin D-CDK4/6 and in late G1 by Cyclin E/CDK2, results in dissociation of the pRB transcription repressor from E2F. Therefore, the required proliferation genes for the progression of a cell through the remainder of the cell cycle will be transcribed. One of the genes upregulated by E2F is Cyclin E, which in a positive feedback process releases more E2F (Bartek and Lukas, 2001; Guan et al., 1994; Lukas et al., 1997). The waves of transcription following pRB phosphorylation have been studied in detail, as loss of appropriate control is associated with cancerous proliferation. Increasing levels of D-type Cyclins as cell size increases and in response to nutrient availability and growth factor stimulation are required for sufficient Cyclin D-CDK4/6 activity to trigger the restriction point. Cell cycle progression before the restriction point is entirely dependent upon Cyclin D levels, while after transit through the restriction point, expression of Cyclin E is also important (Honda et al., 2005). Interestingly, destruction of the inhibitor, $p27^{kip1}$, of Cyclin E-CDK complexes is regulated by its Cyclin D-dependent ubiquitination and degradation (Bartek and Lukas, 2001; Sheaff et al., 1997). Upon de-repression of pRB, increased expression of Cyclin E will also contributes to $p27^{kip1}$ degradation (Honda et al., 2005).

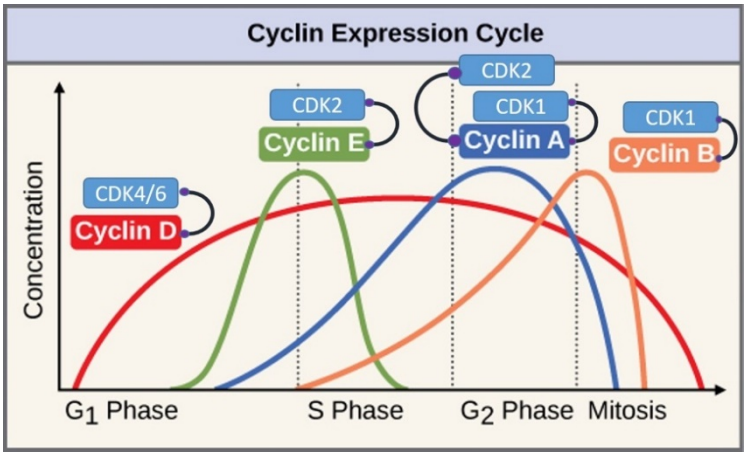

Figure 1.1. Cyclin activities during the cell cycle

The graph shows the cell cycle stages on the x axis and the relative concentration of the Cyclins during the time of cell cycle on the Y axis. The principle fluctuation of the Cyclins in partnership with the Cyclin-dependent kinases CDKs regulates the cell cycle progression through the four cell cycle stages. Once G1 is initiated, Cyclin D is synthesised and drives the G1/S transition. As the consequence of Cyclin D activation, the Cyclin E will be transcribed, expressed and associate with CDK2. The activation of Cyclin E-CDK2 will result in Cyclin A expression and allowing the cell to enter the S phase. Cyclin A promotes entering to the S phase while coupled with CDK2 and promotes entering M phase when binds to CDK1. The Cyclin A remained bound with CDK1 until the late G2, when it is replaced with Cyclin B. Cyclin A-CDK1, before getting ubiquitinated and degraded, activates and stabilises the Cyclin B-CDK1 complex. [Figure inspired by Bruce, 2008]

1.3. S phase progression

To efficiently drive cells through the G1/S transition, Cyclin E-dependent hyperphosphorylation of pRB is important for irreversible progress into the S phase (Satyanarayana and Kaldis, 2009). Subsequent synthesis of Cyclin A and the resulting Cyclin A-CDK2 complex is required to promote the initiation of DNA synthesis through phosphorylation of pre-replication complexes, already bound to origins of replication in early G1 (Coverley et al., 2002; Petersen, 1999). $P220^{NAPT}$ is another Cyclin E-CDK2 substrate accumulated in Cajal bodies in the nucleus. The Cyclin E-CDK2 phosphorylation of $p220^{NAPT}$ ensures that sufficient histones are expressed to package duplicated DNA (Ma, 2000). To ensure the stability of chromosome copy number and since the oncogenic activation of some proto-oncogenes and consequent tumour progression is associated with replication stress, DNA replication in the S phase must be precisely

controlled to prevent inappropriate replication of chromosomal DNA (Primo and Teixeira, 2020).

1.4. G2/M transition and mitosis

Cyclin-CDK complexes also regulate the G2/M transition (Figure 1.1.). Cyclin B-CDK1 is in charge of coordination of G2/M transition (Johnson and Kornbluth, 2012; Morgan, 1997; Nurse, 1990). The expression of Cyclin B starts in the mid S phase and peaks in G2. Cyclin B activity during the S phase is controlled by its cytoplasmic localisation, a consequence of Cyclin B having Nuclear Export Signal (NES). Once Cyclin B expression increases to a threshold level in G2, it will relocate to the nucleus and assure the progress to mitosis (Hagting et al., 1998; Moore, 2003). The CDK1 has to be phosphorylated at Thr 14 and Tyr 15, catalysed by WEE1 and MYT1 respectively right after partnered with Cyclin B to keep the Cyclin B-CDK1 complex in its inactive form (O'Farrell, 2001; Russell and Nurse, 1987) (Booher et al., 1997; Takizawa and Morgan, 2000). The dephosphorylation and subsequent activation of Cyclin B-CDK complex is coordinated by Cyclin A-CDK2 at late G2, which activates CDC25 through PLK1 dependent phosphorylation (Furuno et al., 1999). The Cyclin B-CDK1 complex is dephosphorylated at Thr14 and Tyr 15 by CDC25 (Gavet and Pines, 2010; Gheghiani et al., 2017; Izumi and Maller, 1993; Johnson and Kornbluth, 2012). Further WEE1 and MYT1 inactivation, including phosphorylation and dispatch for degradation, is promoted by active Cyclin B-CDK1 complex in a positive feedback loop (Lindqvist et al., 2007).

Active Cyclin B-CDK1 complex will phosphorylate the downstream targets for irreversible mitosis stages progression, including nuclear chromosome condensation, nuclear envelope breakdown (NEBD), chromosome segregation and eventually, the cytokinesis (Adhikari et al., 2012). The chromosome condensation required for the segregation of chromosomes is catalysed by condensin II which is

activated through CDK1 dependent phosphorylation (Abe et al., 2011; Kimura, 1998). At the same time, nuclear lamins are phosphorylated by Cyclin B-CDK1 complex, which promote their dissociation and NEBD (Peter et al., 1991). Through a negative feedback loop, the CDK1 kinase activity decreases to stimulate chromosome segregation in anaphase, while the anaphase promoting complex/cyclosome (APC/C) ubiquitinates Cyclin B and promotes its degradation (Murray, 2004). The degradation of Cyclin B results in the reduction of Cyclin B-CDK1 activity and therefore, allows the cell to progress through chromosome segregation in anaphase and cell separation in cytokinesis (Queralt and Uhlmann, 2008).

1.5. Cytokinesis and abscission

During telophase, the equally divided chromosomes start to de-condense, which is mediated by clearance of p97 dependent polyubiquitylated Aurora B. p97 is a hexameric ATPase implicated in membrane fusion and ubiquitin-dependent processes. However, the downstream targets of Aurora B kinase in chromosome de-condensation and other p97-dependent activities are poorly understood (Ramadan et al., 2007). Nuclear envelope reformation from the endoplasmic reticulum expansion around the segregated chromosomes is concurrent with chromosome de-condensation (Burke, 2001) (Prunuske and Ullman, 2006). The nuclear envelope is a bilayer membrane composed of an inner nuclear membrane (INM) and the outer nuclear membrane (ONM). The nuclear pore complexes (NPCs) form at the event of fusion of the INM and ONM. The NPCs police the trafficking of proteins between the cytoplasm and nucleus (Lu et al., 2011; Schooley et al., 2012a). At anaphase, the microtubules form a dense bundle at the centre of the mitotic spindle called the central spindle. The astral microtubules also contribute to define the position of the central spindle. Upon completion of chromosome segregation, ingression of the cytoplasm occurs upon formation of a contractile ring (CR), composed of actin and myosin II,

which pulls towards the central spindle (Fraschini, 2020). The final step of cytokinesis, known as abscission, requires Endosomal Sorting Complex Required for Transport (ESCRT) to progress (Christ et al., 2017). As cytokinesis advances, the CR contracts until a microtubule containing canal, about 1μm in diameter, forms between the two daughter with the antiparallel microtubules overlapping each other at the midbody (Henson et al., 2017). At this stage, actin and myosin have dissociated from the CR. The midbody within the intercellular canal provides a platform for recruitment of many proteins, including those required for abscission such as the ESCRTIII complex (Barr and Gruneberg, 2007; Pelham and Chang, 2002; Steigemann and Gerlich, 2009).

1.6. Checkpoints regulating the cell cycle

Cells are evolved to preserve the stability of genetic information in a very meticulous and organised way. A proper error-free cell proliferation is maintained by different checkpoints during the cell cycle. The checkpoints induce delays at key cell cycle transitions, such as G1/S and the G2/M, as well as ensuring error-free DNA replication in intra-S checkpoint (Figure1.2.). The two phosphotidylinositide 3-kinase like kinases (PIKKs); Ataxia telangiectasia mutated (ATM) and Ataxia telangiectasia and Rad3 related (ATR) are critical apical regulators of DNA damage checkpoints (Ciccia and Elledge, 2010). Checkpoints either delay cell cycle progression to facilitate DNA repair, or induce apoptosis to prevent lethal or carcinogenic DNA lesion transmission (Cimprich and Cortez, 2008; Flynn and Zou, 2011; Lowndes and Murguia, 2000).

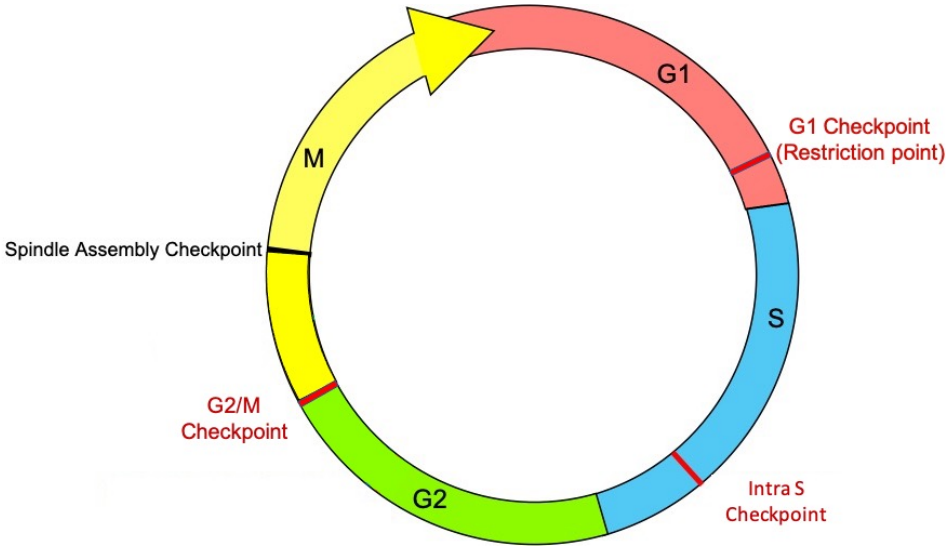

Figure 1.2. The cell cycle checkpoints

The cell cycle and checkpoints through four stages of the cell cycle including G1 (Gap1 phase), S (Synthesis phase), G2 (Gap2 phase) and M (mitosis or cell division). Genome integrity is guarded at major DNA damage dependent checkpoints. G1/S (Restriction point), Intra-S and G2/M, in addition to spindle assembly checkpoint, are ensuring the cell cycle progression. [The schematic inspired by Cheen Fei Chin and Foong May Yeong, 2010]

1.6.1. G1/S checkpoint

The Restriction point/Start in G1 is and environmental and DNA damage check point, preventing cells to progress through the cell cycle in unfavourable condition and propagate the damage in DNA in the S phase. The normal transition of G1/S is coordinated by Cyclin E when coupled with CDK2. CDK2 gets activated through the removal of inhibitory phosphorylation by CDC25A before partnering with Cyclin E (Satyanarayana and Kaldis, 2009). Upon DNA damage, the activation of ATR and ATM will result in CHK1 (Checkpoint kinase 1) and CHK2 (Checkpoint kinase 2) activation respectively, which will be followed by CDC25A phosphorylation (Canman, 1998). The phosphorylated CDC25A will be promoted to be degraded and in this way the G1/S transition will be halted until the DNA damage gets repaired (Figure1.2.) (Falck et al., 2001). Alternatively, ATR, ATM and

CHK2 will phosphorylate p53 on serine 20 and promote its dissociation from the E3 ubiquitin ligase, MDM2. Thereafter, the stabilised p53 can stimulate transcription of p21, a CDK2 inhibitor, halting the progression of the G1 to S phase to assure genome integrity (Bartek and Lukas, 2001; Li and Zou, 2005).

1.6.2. Intra S checkpoint

Although there is a DNA damage checkpoint in G1, there is no guarantee that fault-free DNA will enter the S phase as a template for DNA replication. Therefore, there is an intra-S phase checkpoint for policing genome integrity during synthesis as well (Figure1.2.). The intra-S checkpoint regulates origin firing, fork progression, and fork stability (Early et al., 2004; Iyer and Rhind, 2017; Santocanale and Diffley, 1998).

The intra-S checkpoint is activated by ATR and enforced by ATM if DSBs occur. ATR can respond to a variety of DNA lesions once they have been processed into single-stranded DNA (ssDNA), while ATM is specific to DSBs (Petermann et al., 2010; Shechter et al., 2004). Activation of the intra-S checkpoint will start with ATR and ATM-mediated CHK1 and CHK2 phosphorylation and results in stabilisation of the replication fork and inhibition of DNA replication initiation and DNA elongation (Lupardus, 2002; Tercero and Diffley, 2001; Tercero et al., 2003)

The CHK1 dependent regulatory complex inhibits DNA replication initiation through phosphorylation of the CDC7/DBF4. The kinase activity of CDC7 and its regulatory subunit, DBF4, is required for CDC45 loading on origins of replication and subsequent DNA polymerase α activity (Jiang, 1999; Petermann et al., 2010; Takisawa et al., 2000). Alternatively, CHK1 promotes Cdc25A phosphorylation and consequently degradation. This results in reduced Cyclin A/CDK2 and Cyclin E/Cdk2 activities which impedes the cell cycle progression

into the S phase (Busino et al., 2003; Falck et al., 2001; Zhang and Hunter, 2014; Zhao et al., 2002)

At the stalled fork, replication proteins are prevented from dissociating by the checkpoint (Cortez, 2015; Jossen and Bermejo, 2013). However, as a recent review on intra-S checkpoint (Iyer and Rhind, 2017) concludes, it remains controversial whether the dissociation of the replisome components is ATR dependent or depends on the whole checkpoint process involving other proteins (Cobb, 2005; Lucca et al., 2004; Trenz et al., 2006). Moreover, it is unclear whether the checkpoint regulates the physical association of the replisome components or just regulates their functionality (Cortez, 2015; Iyer and Rhind, 2017).

1.6.3. G2/M checkpoint

The Cyclin B/CDK2 complex regulates mitotic entry (FUNG and POON, 2005; Lindqvist et al., 2009; Lohka et al., 1988). Therefore, the G2/M DNA damage dependent checkpoint inhibits Cyclin B/CDK1 via ATR and ATM activation and subsequent CHK1 and CHK2 phosphorylation (Zhao et al., 2002). The activity of Cyclin B/CDK1 is regulated by the balance between WEE1 kinase (inhibitor) and CDC25 phosphatase (activator) activities (O'Farrell, 2001). The CHK1 and CHK2 phosphorylate CDC25 and promote its binding to 14-3-3 protein which blocks the CDC25 activity and stabilises phosphorylation of CDK1 at Thr14 and Tyr 15, leading to Cyclin B/CDK2 decreased activity (Chen et al., 2003; Schmidt et al., 2017; Watanabe et al., 2004). In addition, the G2/M checkpoint is modulated by p53 through upregulation of GADD45 and 14-3-3 transcription. Moreover, p53 promotes transcription of p21, an inhibitor of CDK2 (Taylor and Stark, 2001).

1.6.4. Spindle assembly checkpoint

Abscission is considered the final step of both cytokinesis and mitosis. To produce two normal and functional cells at the end of mitosis, the cytoplasmic canal between the daughter cells has to be severed (Mierzwa and Gerlich, 2014; Schroeder, 1972). Any chromatin bridges still present in the cytoplasmic canal should be cut if not resolved before abscission. The abscission checkpoint delays cytokinesis until such chromatin has been cleared from the canal (Hoffelder et al., 2004; Steigemann and Gerlich, 2009). A defective abscission checkpoint will result in aneuploidy, polyploidy or accumulation of DNA damage, all of which are hallmarks of cancer (Hanahan and Weinberg, 2011; Hoffelder et al., 2004).

The abscission delay in the presence of trapped chromatin in the cytoplasmic canal was first identified in budding yeast and known as “NoCut” (Norden et al., 2006), while in human cells it is called “Abscission checkpoint”(Steigemann and Gerlich, 2009). The chromatin bridge acts as the signal to trigger the NoCut checkpoint as long as the Ipl1/Aurora localises at the midbody and ADA histone acetyltransferase component (Ahc1) is not affected (Mendoza et al., 2009; Norden et al., 2006).

In human cells, Aurora B plays the pivotal role at the midbody in the abscission checkpoint (Steigemann et al., 2009). In addition to the presence of DNA bridges in the cytoplasmic canal, defects in nucleopore assembly can activate Aurora B dependent abscission checkpoint (Mackay et al., 2010). ANCHR protein (Abscission/NoCut checkpoint regulator) as an abscission regulator, together with the Chmp4c component of the ESCRT-III complex at the midbody and Vps4 (as an ATPase) form a trimeric complex that functions downstream of Aurora B to delay abscission until DNA bridges are completely resolved (Capalbo et al., 2016; Carlton et al., 2012; Thoresen et al., 2014).

1.7. DNA damage response

Each cell in our body repairs about 10^5 DNA lesions per day, caused by endogenous and exogenous damaging agents. Reactive oxygen species (ROS) produced during normal cellular metabolism or incorporation of mismatched nucleotides throughout DNA replication are examples of sources of endogenous DNA damage. Chemical agents such as those used for chemotherapy, ionizing radiation and ultra-violet radiation are examples of exogenous DNA damage (Cadet and Wagner, 2013).

Our cells have evolved to sense and repair a wide variety of different types of DNA damage using many different mechanisms, collectively called DNA damage response (DDR) (Giglia-Mari et al., 2011).

The types of DNA lesions vary, and as such cells repair them in a specific way. For example, base damage or incorrect base inclusion are repaired through base-excision repair (BER) and mismatch repair (MMR). Inclusion of bulky adducts are repaired by nucleotide excision repair (NER), while inter-strand crosslinks are repaired through inter-strand crosslink repair (ICLR) pathway. ICLR is mediated by the Fanconi anaemia (FA) proteins. The lesions most difficult to repair involve various nucleases, and multiple repair pathways. Single-strand breaks (SSBs) in DNA will use single-strand break repair pathway to be repaired. The most destructive type of damage, double-strand breaks (DSBs), are repaired by Non-homologues end joining (NHEJ) and Homologous recombination (HR) (Ciccia and Elledge, 2010; Fortini, 2003; Giglia-Mari et al., 2011; Kamileri et al., 2012; Li, 2008).

Unrepaired DNA damage results in cell death or imperfective genomic transfer through cell division (Cheung-Ong et al., 2013; Harper and Elledge, 2007; Norbury and Zhivotovsky, 2004).

1.7.1. Single-strand break

The base excision repair (BER) pathway involves an induction of single-strand break in DNA through recognition and excision of the damaged base (Kim and M. Wilson III, 2012; Lindahl, 1974). This excision will result in an AP site to be attacked by AP-endonuclease (APE1) and creates SSB (Jacobs and Schär, 2012; Li and Wilson, 2014). The abnormal deoxyribose phosphate is removed by BER and an insertion of the missing nucleotide is catalysed by DNA polymeraseβ (POLβ) (Matsumoto and Kim, 1995). A DNA ligase ensures the integrity of the repaired area by linking the nicks (Dianov and Lindahl, 1994).

Poly (ADP-ribose) synthetase, PARP1, known as a key component in SSB. PARP1 has a BRCT domain which mediates its interactions with the BER/SSBR proteins (Benjamin and Gill, 1980; Dantzer et al., 2000; Li and Wilson, 2014). PARP1 also has a well characterised interaction with XRCC1 through the BRCT domain which is important in the recruitment and coordination of repair factors to sites of DNA damage (Masson et al., 1998).

After recognition of DNA damage, PARP1 activation is the first event that occurs at DNA strand breaks (SSB and DSB). SSBs are rapidly repaired, but DSBs are more difficult to repair despite the PARylation at the breaks. Therefore, the DSBR takes over the repair process (Chen et al., 2020).

1.7.2. Detection of DSBs

Upon the occurrence of DSBs, DDR proteins are rapidly recruited to the damaged sites. ATM, as the primary DNA damage sensor, has a critical role in marking the sites of DSBs (Shiloh, 2003). The exact mechanism of ATM recruitment or sensing the damage by ATM remains unclear.

The ATM protein is predominantly nuclear and found as an active homodimer. DSBs result in autophosphorylation of ATM at Serine (S)1981 and its localisation to the damage sites (Bakkenist and Kastan, 2003). The autophosphorylation of ATM is also dependent upon the TIP60 (Tat interactive protein, 60 kDa) acetyl transferase, which promotes the monomerization and autophosphorylation of ATM (Sun et al., 2005). The Mre11-Rad50-Nbs1 (MRN) complex has also been implicated in the activation of ATM from inactive dimer to active monomer (Paull and Deshpande, 2014; Williams et al., 2007). The Nbs1 from the MRN complex interacts with ATM through a short interaction motif at its C-terminus, where it also interacts with ATR and DNA-PK (Kanu and Behrens, 2007; Zhu et al., 2001). Nbs1 as well as Mre11-Rad51 are required to promote the release of the inhibitory effect of homodimeric ATM and moreover, make the damaged DNA specifically accessible for ATM (Paull and Gellert, 1999; Uziel, 2003).

ATM, together with ATR and DNA-PK, are phosphatidylinositol (PI) 3-kinase-like kinases (PIKK) family members important for DDR signalling (Kim et al., 1999; Lovejoy and Cortez, 2009). Similar to ATM, ATR is also subjected to autophosphorylation that is regulated by its partner protein, (ATRIP), and RPA-bound single-stranded DNA (Liu et al., 2011). The association of DNA-PK with DSBs is also regulated by its autophosphorylation (DOUGLAS et al., 2002; Uematsu et al., 2007).

One of the key targets of PIKKs is the histone variant H2AX, which is phosphorylated by ATM on Serine (S)139 to form γH2AX (Burma et al., 2001; Rogakou et al., 1998). γH2AX is recognized by Mediator of DNA damage checkpoint 1 (MDC1) via its BRCA1 C-Terminus (BRCT) domain, resulting in the recruitment of more ATM and more H2AX phosphorylation to form a large domain of γH2AX spread over megabases of chromatin either side of the DSBs. (Stewart et al., 2003). Accumulation of γH2AX on the DSBs up to two megabases as the first step of DSBs repair, made the γH2AX an extensively used DSBs marker (Rogakou et al., 1998).

1.7.3. Sequential early events at the DSB

Once the chromatin flanking DSBs is marked by γH2AX, it acts as a platform for the recruitment of damage response proteins such as MDC1 and its downstream substrates (Paull et al., 2000; Rogakou et al., 1998). Upon ATM-dependent phosphorylation of MDC1, more ATM is recruited to the DSBs through a positive feedback loop (Lou et al., 2006). Moreover, the E3 ubiquitin ligase ring finger protein 8, (RNF8), together with a second E3 ubiquitin ligase, ring finger protein 168 (RNF168) are recruited to catalyse the ubiquitination of Histone H2A on Lysine 15 (H2AK15ub) (Goldberg et al., 2003; Mattiroli et al., 2012; Stewart et al., 2003).

RNF8, in partnership with the E2-conjugated enzyme UBC13, adds polyubiquitin chains to the linker histone H1, which in turn is recognised by RNF168 (Thorslund et al., 2015). RNF168 is regulated by further E3 ligases, TRIP12 and UBR5, to polyubiquitinate H2A on K15 (Gudjonsson et al., 2012). H2AK15ub is reported as a critical prerequisite for the recruitment of 53BP1 and BRCA1 to DSBs (Kolas et al., 2007; Wu et al., 2009).

MDC1, BRCA1, and 53BP1 are categorised in the group of large multidomain proteins called DDR mediators, which mainly recognise the phosphorylation events downstream of ATM via their C-terminal BRCT domains (Petrini, 2003; Williams et al., 2005). TopBP1 and Claspin are additional DDR mediators, which mainly mediate ATR/CHK1 signalling from single-stranded DNA (Kumagai et al., 2006; Liu et al., 2006).

BRCA1 (Breast cancer type 1 susceptibility protein), which is mutated in familial breast and ovarian cancer (King, 2003), is recruited to DSBs with its partner proteins, RAP80, Abraxas, Brcc36, BRE, NBA1, and MERIT40 to form complexes critical for mediating cell cycle checkpoints and DNA repair (Feng et al., 2009; Shao et al., 2009; Wang et al., 2009). The recruitment of BRCA1 is based on RNF8 and RNF168 mediated ubiquitination and recognised by RAP80 via its

ubiquitin interacting motif, UIM (Yan and Jetten, 2008). In partnership with CtIP, BRCA1 also plays an important role in DNA end resection, a critical early event in homologous recombination repair pathway (Huertas, 2010; Symington and Gautier, 2011).

Interestingly, loss of 53BP1 does not result in very significant defects in the repair of DSBs, created by ionizing radiation (Bouwman et al., 2010; Mirman and de Lange, 2020; Panier and Boulton, 2014). This suggests it is not a core component of NHEJ or HR. However, it plays a critical role in long range DSB repair required for class switch recombination (CSR) in B-cells and the fusion of de-protected telomeres in all cell types (Difilippantonio et al., 2008; Dimitrova et al., 2008; Mirman and de Lange, 2020).

Perhaps the most important role of 53BP1 in DSB repair is in the regulation of DSB repair pathway choice (Kakarougkas and Jeggo, 2014). Its initial recruitment to DSB prevents their resection and thus directs repair towards NHEJ and away from BRCA1-dependent resection (Lowndes, 2010; Shibata, 2017). Therefore, the equilibrium between the 53BP1 and BRCA1 is critical for repair pathway choice.

1.7.4. DSB Repair pathways

There are two main conserved pathways for the repair of the DSBs; homologous recombination (HR) and non-homologous end joining (NHEJ). HR is based on repairing the damage sites using a template, typically the sister chromatid, and therefore this pathway is typically error-free and confined to S and G2 phases of the cell cycle (Chapman et al., 2012a). However, HR can be subdivided into gene conversion (GC) and single-stranded annealing (SSA); of these, GC is template-driven and therefore error-free, while SSA is one of the most deleterious forms of repair. On the other hand, NHEJ is not based on homology, and essentially re-joins the DNA broken ends. It can therefore happen at any stage of the cell cycle but can be error-prone. NHEJ is divided into two sub-pathways: classical NHEJ (cNHEJ) and

alternative end joining (altEJ) (Ceccaldi et al., 2016). Despite being classified as error-prone, cNHEJ has high fidelity. Determining the repair pathway choice is heavily based on promoting or inhibiting DNA end resection.

1.7.4.1. Homologous recombination

HR is a process that enables the cell to use the intact sister chromatid as a template to repair the damaged DNA (Figure1.3.). Based on the cell cycle stage that the damage occurred and the mechanism of HR, it is divided into GC and SSA. The GC can progress through two sub-pathways: synthesis-dependent strand annealing (SDSA) and double-strand break repair (DSBR), forming double Holliday junction (DHJ) (Sung and Klein, 2006; Wright et al., 2018). Irrespective of the type of the HR pathway, the first few steps are common in all. DSBs undergo 5’ to 3’ resection, leaving 3’ overhangs. The resection is mediated by binding of the MRN complex to the broken ends, followed by CtIP recruitment and activation, which closely interacts with BRCA1 (Figure1.3.). The actual cutting of the DNA from 5’end is catalysed by Bloom helicase- Exonuclease1- DNA replication helicase/nuclease 2 (BLM-EXO1-DNA2) helicase activity which unwinds the DNA (Mimitou and Symington, 2009; Symington, 2014).

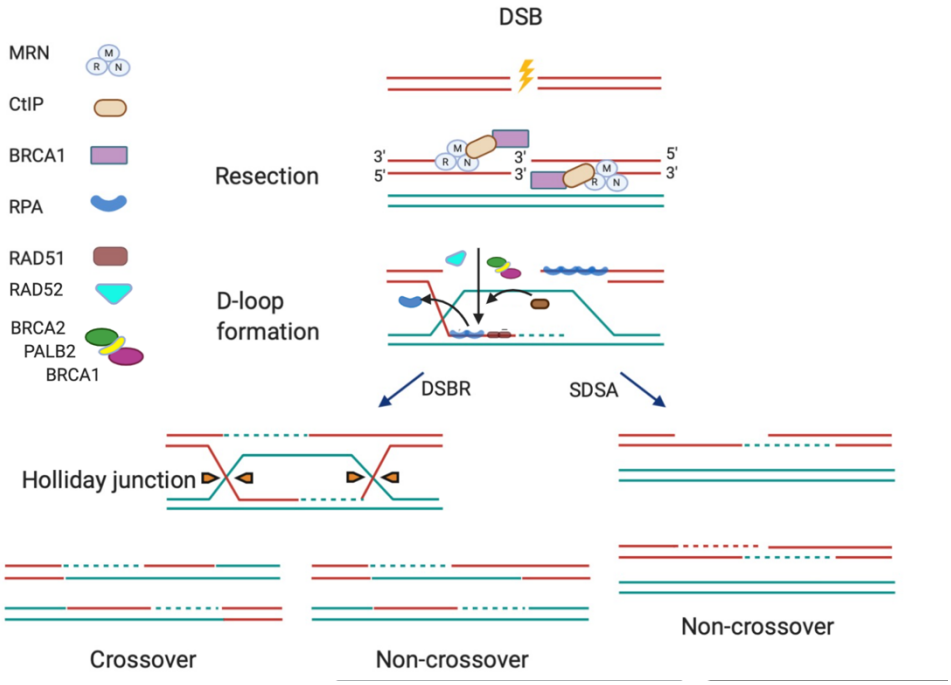

Figure 1.3. Homologous recombination

Homologous Recombination involves end resection of a DSB mediated by MRN complex and the speed of resection can be modulated by CtIP-BRCA1. The 3' overhangs will be covered by RPA, which in turn will be replaced by RAD51 to facilitate the invasion to find a homologous sequence and use it as a template to synthesise DNA. This replacement is mediated by BRCA1/BRCA2/PALB2 complex and RAD52/RAD51 paralogues. After homology search and invasion, the pathway can proceed with two main directions: DSBR and SDSA. The DSBR involved in DHJ formation and based on one cut or two cuts in HJ flanking sites the result would be repaired dsDNA with crossover or non-crossover respectively. In SDSA simply the new DNA strand will be synthetized based on the template and the result would be non-crossover repaired dsDNA. In one HR pathway, a Holliday junction is formed and resolved, which can result in a crossover or no-crossover product between the template and the invading sequence. However, during SDSA (synthesis dependent strand annealing) as the other pathway, the invading strand dissociates from the homologous template following synthesis and re-anneals with the other end of the break forming a non-crossover product.

The 3' overhangs are rapidly recognized as single-stranded DNA and coated by replication protein A (RPA) which prevents degradation or the formation of secondary structures (Wold, 1997). HR progression requires RPA to be replaced by RAD51, facilitated by a complex of proteins including BRCA1, BRCA2, PALB2, and BRG1 (Figure1.3.) (Hilario et al., 2009; Lee et al., 2018). Moreover, RAD52 and RAD51 paralogues are mediating the RPA replacement by RAD51 and work with the BRCA1/BRCA2/PALB2 complex epistatically in this regard (Qing et al., 2011). The nucleoprotein filament composed of RAD51-

bound 3'overhang will then start searching for the homologous sequence. Once the desired homology is found, it is invaded to form a displacement loop (D-loop) between the 3' overhang and the invaded duplex. After strand invasion, RAD54 mediates the RAD51 removal from the 3'overhangs (Ceballos and Heyer, 2011; Li et al., 2007; Onaka et al., 2016; San Filippo et al., 2008). The next step is the extension of the D-loop through DNA replication at the invading 3' strand by DNA polymerase. This extension will form a crossing DNA between the invading strand and complementary strand of the template, termed a Holliday-Junction (HJ) (San Filippo et al., 2008; Sung and Klein, 2006). The second invasion may happen to the extended D-loop and form a double Holliday-Junction (D-HJ). The described form of HR, called DSBR, can potentially result in chromosomal crossover when one of the D-HJs gets cut, or non-crossover as the consequence of cutting both D-HJs (Bzymek et al., 2010; Sarbajna and West, 2014; West et al., 2015).

Another type of HR, SDSA, occurs when the invading 3' extends but, instead of being cut at the HJ, the two strands slide over each other in a process called "branch migration". Finally, the newly synthetized DNA will anneal to the other overhang and result in a non-crossover chromosome (Allers and Lichten, 2001; Matos et al., 2011).

SSA, as the other type of HR, is intrinsically error-prone and occurs between repeating sequences (Morrical, 2015). Distinct from the GC pathways, in SSA there is no need to find a homologous sequence, as the break occurs between two repeated sequences. Therefore, it requires the post repeated sequences to anneal with the complementary single strands and cutting of non-hybridised ssDNA by exonucleases such as RAD1/10. Any mismatches can be repaired by mismatch repair (MMR) proteins (Li et al., 2013; Mehta and Haber, 2014; Morrical, 2015; Sugawara et al., 1997; W.-L. Toh et al., 2010). SSA is known to be dependent upon RAD52 replacement with the RPA coating the single-stranded DNA overhangs (Brouwer et al., 2017).

1.7.4.2. Non-homologous end joining

Non-homologous end joining is another type of DSB repair that happens when 53BP1 inhibits DNA resection at the broken ends toward its antagonism with BRCA1 (Figure1.4) (Callen et al., 2013; Chapman et al., 2012a, 2013; Zimmermann et al., 2013). Contrary to HR, NHEJ has not restricted to the cell cycle stages and its frequency is higher in G1 to compensate the absence of HR and is in competition with HR in S and G2 phases (Escribano-Díaz et al., 2013; Mao et al., 2008).

NHEJ is used for repairing the physiologically induced DSBs in lymphocytes for immunoglobulin class switch recombination and V(D)J recombination which are required for diversity in antibody production. (Li et al., 2011; Park et al., 2012). NHEJ is considered as an error-prone mechanism for DSB repair; re-joining the broken ends potentially can result in insertions or deletions in the DNA sequence (Ceccaldi et al., 2016). However, It has been shown recently that the precision of the repair and the frequency of error in repair mostly depends on the type of broken DNA ends, rather than the mechanism of NHEJ (Bétermier et al., 2014; Rodgers and McVey, 2016).

The DNA-dependent protein kinase (DNA-PK) is the initiator of the NHEJ pathway. DNA-PK has a regulatory subunit (Ku70/80) and a catalytic subunit (DNA-PKcs) (Mari et al., 2006; Uematsu et al., 2007). First, the heterodimer Ku70/80 binds to the DNA broken ends with a high sequence-independent affinity, then recruits and activates the catalytic subunit, DNA-PKcs (Figure1.4) (Downs and Jackson, 2004). DNA-PKcs becomes auto phosphorylated forming a ring shape complex with the Ku70/80 at DNA ends. DNA-PKcs holds the broken ends in close proximity to each other to facilitate ligation (Abraham, 2004; Bakkenist and Kastan, 2004; Uematsu et al., 2007).

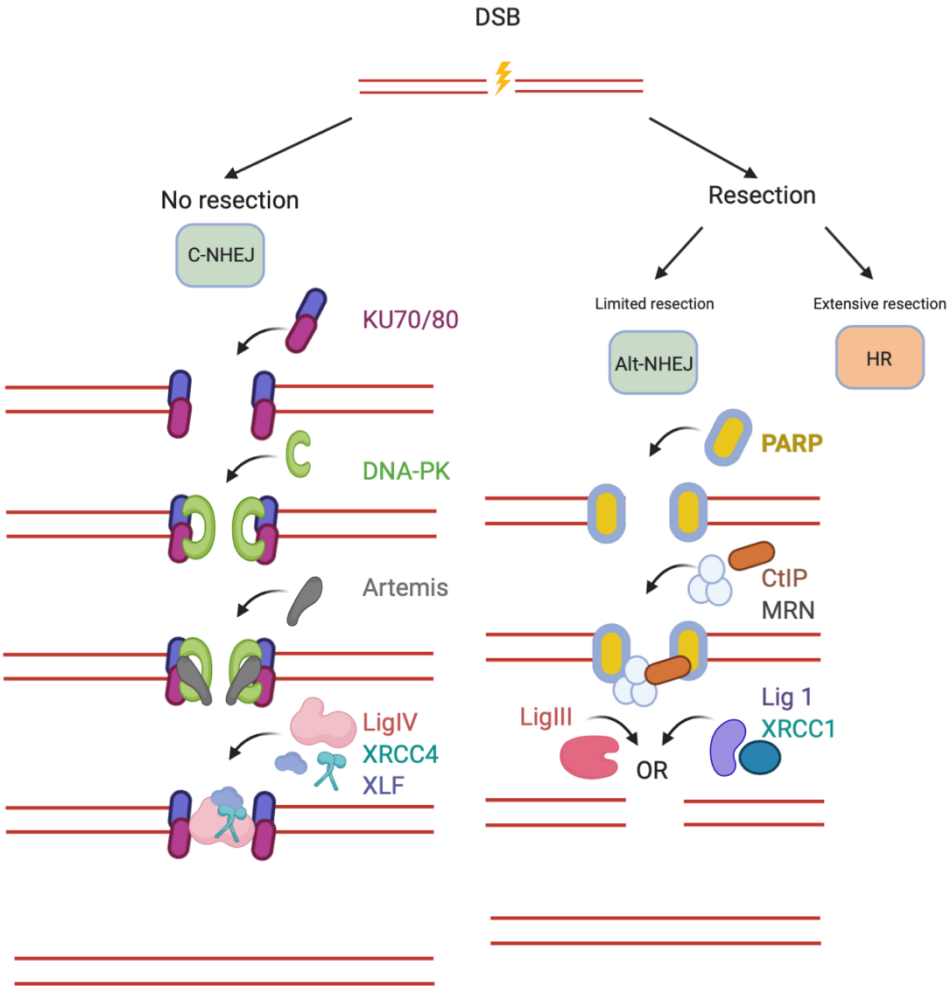

Figure 1.4. Non-homologous end joining

Upon the occurrence of DSB, C-NHEJ repair will happen when end resection is inhibited. There is another alternative DSB end joining pathway occurring after limited end resection in case of inaccessibility of C-NHEJ mediation factors, called microhomology or Alternative NHEJ. In C-NHEJ, the KU heterodimer binds to the DNA broken ends first and promotes the recruitment of DNA-PKcs. Subsequently, the DNA blunt ends will undergo end processing by factors including Artemis. Finally, XRCC4/XLF and LigIV complete the end joining process, ligating the broken ends. In Alt-NHEJ the KU heterodimer is replaced by PARP followed by MRN-CtIP recruitment and the ligation will be mediated by either LigI/XRCC1 or LigII.

In addition to the DNA-PKcs, there are several interventional proteins in NHEJ that directly or indirectly are recruited and activated by the Ku70/80 heterodimer, including: X-ray cross-complementing protein 4, XRCC4 (Costantini et al., 2007; Mari et al., 2006); Ligase IV (Nick McElhinny et al., 2000); XRCC4-like factor, XLF (Yano et al., 2008); and Aprataxin-and-PNK-like factor, APLF (Grundy et al., 2012).

XRCC4 and XLF form a complex and bind to either side of the break, tethering the DNA ends and facilitating ligation by the ligase IV (Andres et al., 2012; Malivert et al., 2010; Sibanda et al., 2001). Prior to the ligation, the DNA ends will undergo processing to remove any blocking end proteins, any minimal resection that might be required, and filling any gaps. PNKP, Aprataxin, APLF, Polymerases μ and λ, Werner (WRN) and Artemis, are end processing proteins which perform their role depending on the type and situation of the DSB, which are briefly described below.

PNKP, a 5'-kinase/3'-phosphatase, creates 5'-phosphate/3'-hydroxyl termini, as a necessary prerequisite for ligation (Bernstein et al., 2005). Aprataxin removes adenosine monophosphate when damaged DNA ligation by DNA Ligase IV is aborted and allows subsequent attempts at ligation (Ahel et al., 2006). APLF, Aprataxin, and PNK like factor, in coordination with PARP3, promotes the LIG4-XRCC4 complex retention at damaged sites to accelerate DNA ligation (Grundy et al., 2012). Polymerases μ and λ resyntheses damaged or missing nucleotides and also have BRCT domain facilitating their interaction with DDR proteins such as Ku and DNA ligase IV (Mahajan et al., 2002). Werner protein unwinds and separates double-stranded DNA via its helicase activity and removes the damaged nucleotides via its exonuclease activity (Oshima et al., 2002). Artemis is mostly important in V(D)J recombination; the loss of Artemis will result in severe combined immune deficiency (SCID) (Ma et al., 2002; Rooney et al., 2002).

Alternative NHEJ (alt-NHEJ) is another type of NHEJ which is normally inhibited by DNA-PK and XRCC4-LigIV (Figure1.4). Whenever C-NHEJ and HR fail to complete repair, alt-NHEJ is considered as an alternative DSB repair pathway (Dueva and Iliakis, 2013; Perrault et al., 2004). Alt-NHEJ is a high-risk strategy to repair DSB and is not favourable due to its low fidelity, frequently resulting in deletions, insertions, and translocations. (Ma et al., 2002; Pytel et al., 2007; Simsek and Jasin, 2010). Limited CtIP dependent resection is required

for initiation of the alt-NHEJ pathway (Bennardo et al., 2008; Wang and Xu, 2017). Once 5-25 nucleotides of homology have been revealed, the homologous sequences align, ssDNA is preserved and ends ligated; this frequently results in mutation through the loss of genetic information (Mladenov and Iliakis, 2011). In this pathway, Poly ADP-ribose polymerase 1 (PARP1) binds to the broken ends in competition with Ku70/80 (Mansour et al., 2010). Although the mechanism of alt-NHEJ is poorly understood, the MRN complex is involved, while Ligase I and III/XRCC1 are used rather than LIG4/XRCC4 in C-NHEJ (Boboila et al., 2012; Della-Maria et al., 2011).

1.8. 53BP1 and DNA damage response

53BP1 was first identified as a binding partner of the tumour suppressor protein p53 (Iwabuchi et al., 1994). Thereafter, 53BP1 has been mostly investigated as an important mediator and regulator of DSBs repair. 53BP1 is nuclear and a target of ATM (DiTullio et al., 2002). RAP1-interacting factor 1 (RIF1), is one of the main 53BP1 interacting partners within the chromatin to form the basis for other DSB signalling and repair proteins (Chapman et al., 2013; Silverman, 2004). Recent super resolution microscopy on 53BP1 localisation revealed that 53BP1 foci are composed of 4-7 smaller foci termed 53BP1 nanodomain (ND). Together these 53BP1 NDs form a single microdomain (MD), corresponding to a single 53BP1 IRIF from earlier work. Interestingly, Ochs et al. also established that RAP1-interacting factor 1 (RIF1), as one of the main 53BP1 interacting partners, is essential for stabilising the NDs within a MD. (Ochs et al., 2019). 53BP1-RIF1 in competition with the BRCA1-CtIP inhibits DNA end resection and NHEJ pathway promotion subsequently (Bouwman et al., 2010; Bunting et al., 2010; Chapman et al., 2012b; Escribano-Díaz et al., 2013). The prevention of the broken end resection requires the Shieldin complex recruitment by 53BP1-RIF1 (Gupta et al., 2018; Noordermeer et al., 2018).

1.8.1. 53BP1 protein structure

53BP1 localises to the chromatin surrounding DSBs. To be able to localise to the damaged sites requires methylation and ubiquitination events on histones. H2A ubiquitination on lysine 13 or 15 requires the γH2AX, MDC1, RNF8, and RNF168 pathway (Rogakou et al., 1998; Stewart et al., 2003). 53BP1 contains a ubiquitin dependent recruitment (UDR) domain that is specific for ubiquitinated lysine 13 and 15 of histones H2A and H2AX (Figure1.5) (Fradet-Turcotte et al., 2013). In addition, the Tudor domain of 53BP1 is a reader of H4 lysine 20 di-methylation (H4K20me2) (Figure1.7) (Botuyan et al., 2006). H4K20me2 is a widespread modification of chromatin, whilst H2A(X)K13/15ub is an induced modification upon DNA damage. A recent report has also implicated H4K16me1 in 53BP1 recruitment to chromatin flanking DSBs (Lu et al., 2019).

Furthermore, 53BP1 has an oligomerisation domain (OD), required for stable binding of 53BP1 sites of DNA damage (Lottersberger et al., 2013; Zgheib et al., 2009). The UDR motif, tandem Tudor domain, and OD domain, together with the glycine/arginine-rich (GAR) motif form the central focus forming region (FFR), which is the most investigated region of the 53BP1 protein (Figure1.5). 53BP1 also has an LC8 domain within the FFR, interacting with dynein light chain (DYNLL1) which participate in 53BP1 oligomerisation and recruitment at DSBs (Becker et al., 2018).

53BP1 has a BRCT domain at the C-terminal which is required to interact with p53 to target specific genes expression but does not have any direct effect on 53BP1 localisation at DSB or mediation of repair (Derbyshire, 2002). Moreover, it is reported that the BRCT domain interacts with H2AX, but not in line with the localisation at DSBs (Kleiner et al., 2015). The N-terminal of 53BP1 contains 28 SQ/TQ phosphorylation sites (Figure1.6). Having these phosphorylation sites enable 53BP1 to be phosphorylated by ATM and ATR, which

subsequently will result in the recruitment of the downstream effectors (Denchi and de Lange, 2007; Mirman and de Lange, 2020).

In G1 cells, there are some nuclear compartments which consist of unreplicated DNA due to replication stress and marked by 53BP1. They are called nuclear bodies and It is believed that they are a safekeeping core for the fragile DNAs (Lukas et al., 2011).

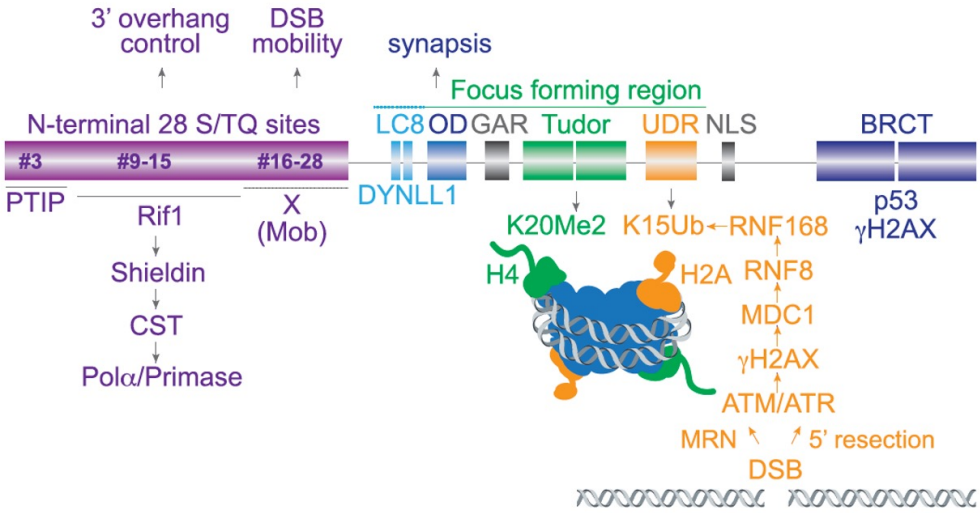

Figure 1.5. Schematic of structure and function of 53BP1

The central region is known as the focus forming region (FFR) is required for 53BP1 recruitment to the DSBs which includes dynein light chain binding domain (LC8), oligomerisation domain (OD), glycine–arginine-rich motif (GAR), a tandem Tudor domain and, ubiquitin-dependent recognition motif (UDR). 53BP1 reads the common histone modification, H4K20me2, via the Tudor domain. The UDR motif recognises the DSB induced histone modification, H2AK15ub. The orange demonstrated pathway indicates the phosphorylation events from DSB formation to H2AK15 ubiquitination. At N-terminal, there are 28 S/TQ phosphorylation sites critical in PTIP and RIF/Shieldin/CST interaction. Moreover, there is a currently unknown X motif at N-terminal proposed to be involved in DSB mobility promotion by 53BP1. The BRCT domain at the C-terminal mediates DNA damage unrelated to 53BP1 interaction with P53 and γH2AX. [Figure adapted from (Mirman and de Lange, 2020)].

1.8.2. 53BP1 functions

1.8.2.1. DNA repair pathway choice

Once DSBs have occurred, the choice of repair pathway will be directed by mutual antagonism between the two mediators, 53BP1 and BRCA1 (Chapman et al., 2012a). The two main pathways are HR and NHEJ, the first of which requires DNA end resection. Interestingly, in BRCA1 deficient cancers, the malignant cells become hypersensitive to PARP inhibitors, while the subsequent loss of 53BP1 rescues this PARPi sensitivity due to loss of Shieldin recruitment and resumption of DSB resection (Figure 1.6.) (Dev et al., 2018; Gupta et al., 2018; Wright et al., 2018).

The Shieldin complex, a 53BP1 downstream effector, consists of SHLD1, SHLD2, SHLD3, and Rev7, and localises to DSBs in a 53BP1-RIF1 dependent manner (Gupta et al., 2018; Mirman et al., 2018; Noordermeer et al., 2018). There are two models to describe how 53BP1 limits the resection at DSBs (Barazas et al., 2018; Dev et al., 2018; Findlay et al., 2018; Gao et al., 2018; Noordermeer et al., 2018). First, 53BP1 loads the Shieldin complex as an obstacle at ssDNA 5' end, preventing the nucleolytic attack. Second, the Shieldin inhibits EXO1 exonuclease activity by covering the ssDNA in the same way that RPA does (Nicolette et al., 2010; Soniat et al., 2019; Yang et al., 2012). Moreover, DNA2-WRN/BLM won't be activated upon substitution of Shieldin with RPA (Nimonkar et al., 2011; Sturzenegger et al., 2014).

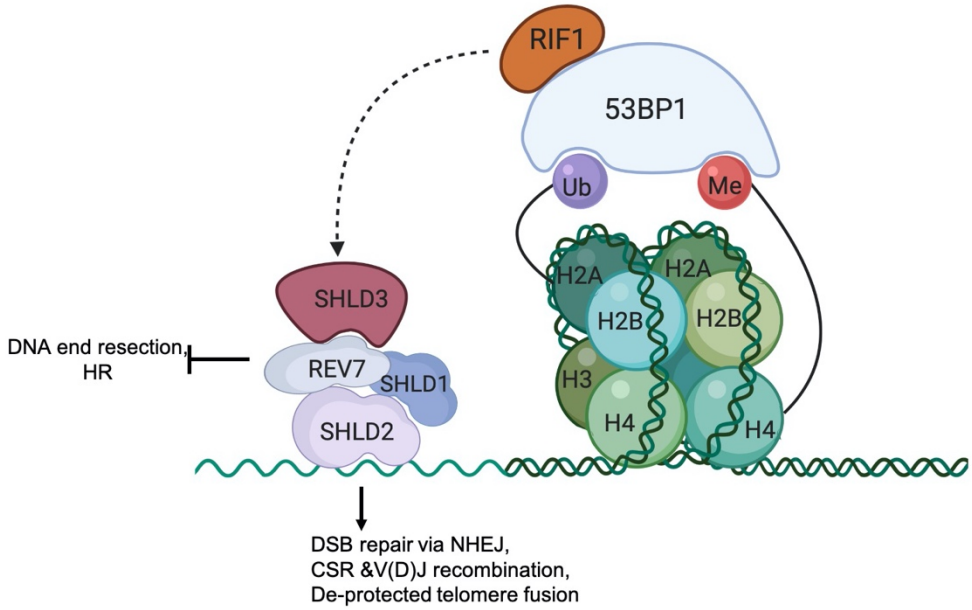

Figure 1.6. Damaged DNA end resection prevention by 53BP1 via Shieldin complex recruitment.

Downstream of 53BP1 activation via H4K20me2 and H2AK15/13ub, RIF1 is recruited to the DSB and activates SHLD3-Rev7 from the Shieldin complex. The Shieldin complex bind to the ssDNA to inhibit DNA end resection through its SHLD2-SHLD1 components.

1.8.2.2. V(D)J and class switch recombination

V(D)J recombination and antibody heavy chain class switch recombination (CSR) result from physiologically induced DSBs in lymphocytes that are essential for antibody diversity and an efficient immune system (Manis et al., 2004; Methot and Di Noia, 2017; Ward et al., 2004). These DSBs induction will occur at the immunoglobulin loci and are repaired by cNHEJ. 53BP1 is critical for CSR, a subset of V(D)J recombination resulting from long range DSBs. During V(D)J recombination, DSBs that are proximally located are not particularly 53BP1-dependent for their repair. (Callen et al., 2013; Difilippantonio et al., 2008; Mirman and de Lange, 2020).

Recombination-activating gene 1 and 2 (RAG1/2) proteins are responsible for DSB induction in V(D)J recombination; while

activation-induced cytidine deaminase (AID) activity is required for DSB formation during CSR (Chen, 2000; Jones and Gellert, 2004; Petersen et al., 2001). The repair pathway is classic NHEJ involving Ku70/80, DNA-PK, Artemis, XRCC4, and Lig4 as the classical members of the NHEJ (Costantini et al., 2007; Spagnolo et al., 2006; Yano et al., 2008)

While the presence of 53BP1 for most V(D)J recombination event is negligible, it has a critical role in CSR (Manis et al., 2004; Ward et al., 2004). There are two main characteristics of 53BP1 that make it critical for CSR. First, nucleic acid oligomerisation at the breaks to keep the broken ends at proximity as they are originally distantly located (Becker et al., 2018; Zimmermann et al., 2013). The second 53BP1 property is the recruitment of the RIF1/ Shieldin/ CST (Ctc1, Stn1, Ten1) complex at the breaks to prevent the end resection. The CSR products formed in absence of one or more of the RIF1/ Shieldin/ CST shows extensive resection (Barazas et al., 2018; Chapman et al., 2013; Gupta et al., 2018; Mirman and de Lange, 2020; Mirman et al., 2018)

1.8.2.3. Maintenance of de-protected telomeres

53BP1 as a major regulator of NHEJ is also shown to be required for the fusion of telomeres if they become de-protected (Dimitrova et al., 2008). Telomeres are protected by a complex called shelterin, analogous to Shieldin complex recruitment to DSBs. Shelterin is composed of six subunits: TRF1 (telomere repeat-binding factor 1), TRF2, POT1, RAP1, TIN2 (TRF1-interaction factor 2), and TPP1 (Figure1.7.) (de Lange, 2018; Lazzerini-Denchi and Sfeir, 2016). The main role of the shelterin complex is to ensure that chromosome ends are not recognized and processed as DSBs. TRF2 mediates the formation of a T-loop at the end of chromosomes reshaping the 3' overhang fold over the dsDNA and making it inaccessible to DDR signalling proteins, ATM/MRN, and telomerase (Figure1.7.)

(Dimitrova and de Lange, 2009; Doksani et al., 2013; Griffith et al., 1999). In the absence of TRF2, following ATM activation, the telomeres will join together through the classical NHEJ pathway involving Ku70/80- Lig4 (Celli et al., 2006; Denchi and de Lange, 2007; Smogorzewska et al., 2002). Depletion of 53BP1 in TRF2$^{-/-}$ cells considerably decreases the rate of telomere fusion (Dimitrova et al., 2008), presumably due to three independent 53BP1 mechanisms. First, 53BP1 is shown to be a stimulator of chromatin mobility, essential for dysfunctional telomeres to find each other within the nucleoplasm and to fuse together (Lottersberger et al., 2015). Second, its ability to oligomerise at DSBs, promoting telomere clustering. Finally, the recruitment of RIF1/ Shelterin/CST complex at the breaks minimises the telomeric overhang (Celli and de Lange, 2005; Deng et al., 2009; Lottersberger et al., 2013)

1.9. De-protected telomeres as a type of DSB

The word telomere is Greek originated “telos” (end) and “meros” (part). The telomeres are defined by an array of TTAGGG sequence repeats at the end of chromosomes and were identified for the first time in 1938 by Hermann J. Müller (Muller, 1938). In 1941 telomeres were further characterised by Barbara McClintock’s regarding its special role in chromosomal end protection from repair machinery (Chu and Autexier, 2016; McClintock, 1941).

Telomeres’ structure includes a G-rich ssDNA at the end of the chromosome which circles back on the preceding dsDNA, stabilised with the shelterin complex (Figure1.7.). Among the six shelterin components, TRF2 plays a key role in forming the T-loop through anchoring the telomeric ssDNA to the rearward dsDNA (Bilaud et al., 1997; Hartmann and Scherthan, 2005). The binding of the shelterin complex to the telomeres requires a minimal ssDNA overhang of a few hundred nucleotides. Therefore, telomeres with shorter ssDNA overhangs will not be able to recruit shelterin, and instead lead to the

aberrant recruitment of DDR proteins, (ATM/ATR/MRN) resulting in fusion, genomic instability, senescence or apoptosis (Greenberg et al., 1999; Perera et al., 2008).

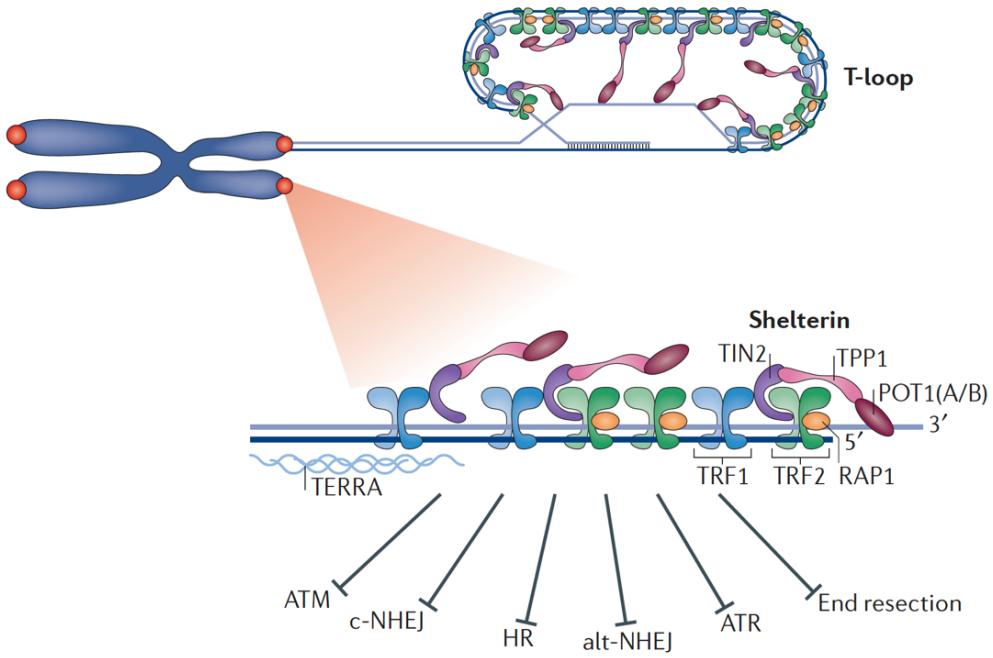

Figure 1.7. Composition of the shelterin complex at the telomere.

TRF1, TRF2, TIN2, RAP1, TPP1, and POT1 (protection of telomere 1; POT1A and POT1B in mice) are six-subunits of shelterin complex protecting chromosome ends from DNA damage signalling by ATM and ATR and subsequent DNA repair by c-NHEJ, alt-NHEJ, HR, and DNA end resection. [Figure adapted from (Lazzerini-Denchi and Sfeir, 2016)]

Inhibition or depletion of TRF2 will induce ATM activation, which in turn phosphorylates CHK2 and p53 (Denchi and de Lange, 2007; Karlseder et al., 2004). The sequential activation of the DDR signalling pathway will lead to form Telomere Dysfunction-Induced Foci (TIFs) sites for focal accumulation of 53BP1 and γH2AX at de-protected telomeres (Takai et al., 2003). There are two suggested mechanisms for the inhibition of ATM by TRF2. First, TRF2 dependent T-loop formation makes the telomeres inaccessible for binding by the MRN complex, an essential prerequisite for ATM activation (Amiard et al., 2007; Griffith et al., 1999). The other level of protection is thatTRF2

suppresses the activity of ATM and its downstream effectors' kinases activity (Karlseder et al., 2004). Recruitment of 53BP1, one of the main ATM effectors, will be prevented by TRF2 dependent RNF168 E3 ubiquitin ligase deactivation. This enzymatic inactivation is critical in telomeric protection in the S phase when DNA unwinds at the replication fork (Okamoto et al., 2013).

The de-protected telomeres mostly join through c-NHEJ in G1 before the replication, resulting in chromosome end fusion and dicentric or multicentric chromosomes, a detrimental type of fusion. Less frequent chromatid fusions are also observed, indicating the fusion occurred after replication (Maciejowski et al., 2015; Mirman and de Lange, 2020).

Although telomere fusion is mediated mainly by c-NHEJ, it is possible for the de-protected telomeres to join each other through HR. This might be less harmful but has the potential to change the length of telomeres. HR dependent telomere fusion takes place in three ways including telomere sister chromatid exchange (T-SCE) (Pierce, 2001), T-loop homologous recombination, in which the excision will occur within the telomere sequence (Wang et al., 2004), and those of recombination leading to alternative lengthening of telomeres (ALT) (Bryan et al., 1997).

Extensive investigation of the mechanisms by which telomeres are protected against telomeric uncapping and aberrant DNA repair provided a good model for dissecting the DDR signalling and DSB repair. Furthermore, understanding telomere structure and function has led to a better understanding of how telomere dysfunction and fusion can lead to cancer. (Lazzerini-Denchi and Sfeir, 2016).

1.10. Kinesin super family

Kinesin-1, an intracellular motor protein, was discovered as the first member of the kinesin superfamily 35 years ago through an investigation of the giant axon of squid (Brady et al., 1982; VALE et

al., 1985). Since then the number of identified kinesins has increased to more than 50 types (44 types occur in human), that have been subdivided into 14 families, forming the kinesin superfamily (Kim and Endow, 2000; Miki et al., 2005). Generally, kinesins consist of three main structural components: the motor domain, the coiled-coil (or stalk domain), and the tail. They all share the highly conserved motor domain containing binding sites for either ATP or microtubules that classifies them as kinesins (Endow et al., 2010; Miki et al., 2005). Based on the position of the motor domain at N-terminal, C-terminal, or middle of the protein, kinesins are categorised into three groups; N, C, and M, respectively (Lawrence et al., 2004).

The αhelical stalk domain is critical for dimerization of the protein and regulation of motor activity. The tail is where kinesins bind their cargos such as vesicles or mRNA-protein complex (Miki et al., 2005).

There are two other types of molecular motor proteins: dynein and myosin. Myosin uses actin filaments as the path for movement. Dynein moves along the same filaments as kinesin does (microtubules), typically in the opposite direction. Dynein moves toward the depolymerizing microtubule end, termed minus end, while most kinesins move in the plus end direction towards where microtubules are being polymerised (Hirokawa, 1998; Vale, 2003). Only kinesin-14 family members move toward the microtubule minus end (McDonald et al., 1990; Walker et al., 1990). The motor domain is the catalytic core of kinesins and hydrolyses the ATP to produce the force required for movement along microtubules. The direction preference of the motor domain is managed by the linking region between stalk and motor head, termed “neck”. Deletion of the sequence encoding neck in kinesins and dynein will result in losing directionality (Endow and Higuchi, 2000).

The most extensively studied kinesins are kinesin-1, kinesin-13 and kinesin-14. These three kinesins are structurally and functionally different so that the kinesin-1 is extremely processive and able to move

more than 800 nm in each motor and microtubule-binding event (Howard et al., 1989; Svoboda and Block, 1994). Contrarily, kinesin 14 is non-processive, so that in each ATP hydrolysis, the stalk only rotates toward the microtubules minus end (deCastro et al., 2000; Endow and Higuchi, 2000).

Kinesin 13 (MCAK, mitotic centromere associated kinesin; also known as KIF2C) differs from other kinesins as it lacks the stalk domain but surprisingly still exists as a dimer. Kinesin-13 does not move directionally and binds both microtubules plus and minus ends where it removes tubulin dimers and regulates microtubule dynamics (Hunter et al., 2003). Kinesin-8 family members are also plus end directed where they depolymerise microtubules in a length dependent manner (Gupta et al., 2006).

Kinesins are critical players in cell division, required for functional spindles, centrosome separation, and kinetochore fibre length maintenance in order to the bipolar separation of chromosomes (Endow et al., 2010). Some kinesins generate sliding force in the midzone of anaphase cells such as kinesin-5 (Eg5) and kinesin-6 (MKLP1) (Kapitein et al., 2005). The Budding yeast kinesin-8, Kip3, and human kinesin-8, KIF18A, are coordinated with MCAK, and participate in microtubules depolymerising at plus ends (Cottingham and Hoyt, 1997; Mayr et al., 2007).

1.10.1. Kinesin KIF18B

KIF18B, the focus of this study, belongs to the kinesin N-8 family (group 8 of the N-kinesins). As its name implies, the conserved motor domain is located at the N-terminal and has ATP binding pocket to produce the required force to walk along microtubules towards their plus end. The coiled-coil, stalk domain at the middle, helps KIF18B dimerization and facilitates the movement of this protein along the microtubules. At the C-terminal, it has multiple protein interacting

motifs including EB1, MCAK, and cargo binding domains (Locke et al., 2017; Varga et al., 2009)

Based on the most updated database in Ensembl 100 (2020 release) KIF18B has 150 orthologous which spans from Coelacanth fish, as the earliest species in its gene tree (Figure 1.8.).

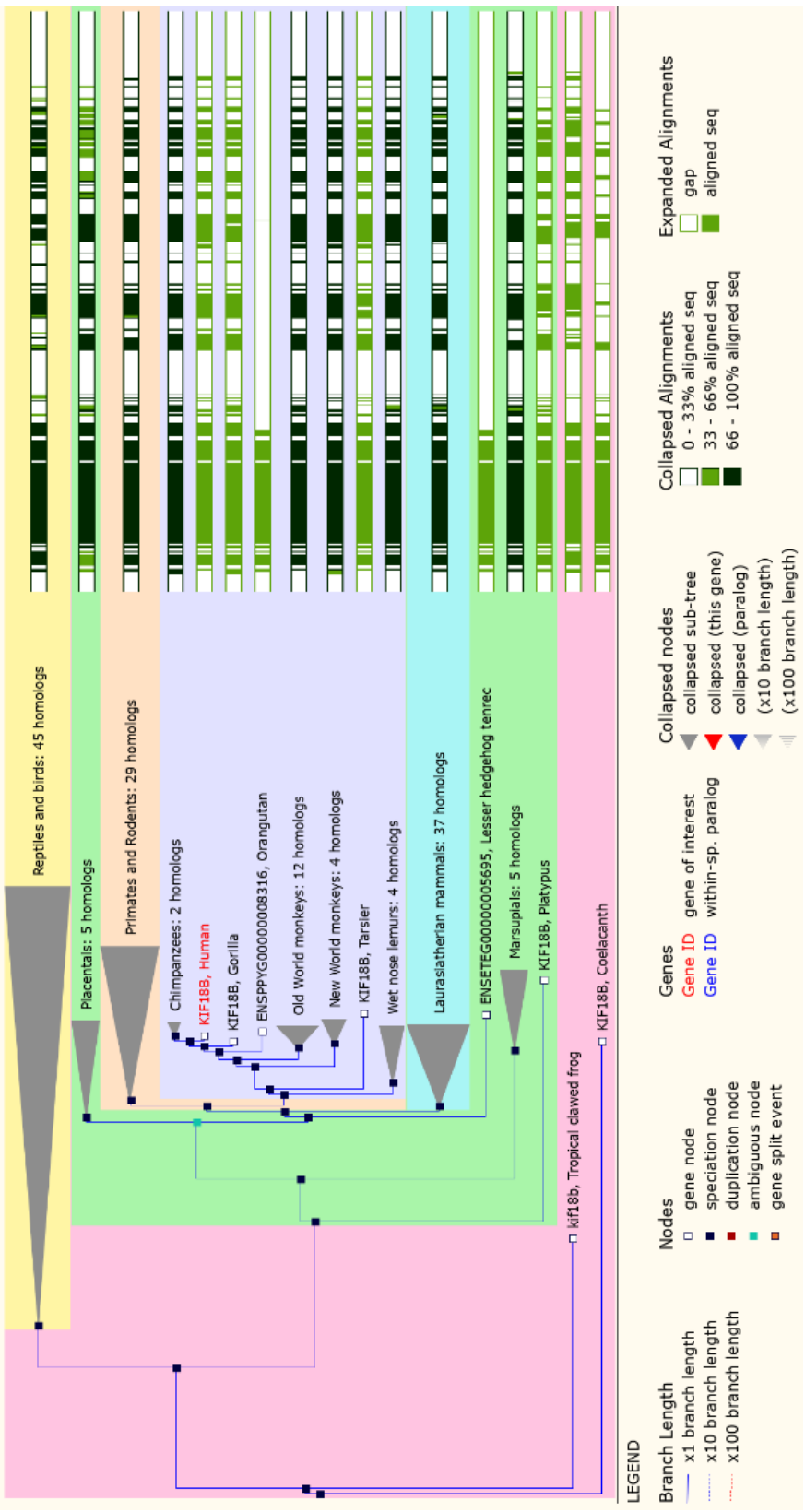

Figure 1.8. KIF18B gene tree

The gene tree is constructed in Ensemble version 100 released in 2020 based on the orthology/paralogy prediction method. The tree shows the KIF18B orthologues and their branching from a common ancestor. The conserved regions among the paralogues are also manifested in the alignment section on right.

KIF18B also has 41 paralogues as listed in Table1.1. which also highlighted in the phylogenetic tree generated through multiple alignments of the kinesin superfamily members using Clustal Omega online software (Figure 1.9.) KIF18B paralogues include most of the kinesin superfamily except the KIF16A and KIF20B. KIF18A, as the closest paralogues to KIF18B, branched from the same node. KIF19 and KIF22 stand at the next level of homology to KIF18B, respectively (Figure 1.9.).

The KIF2 family is also in close homology with KIF18B, which can be explained by the close cooperation of KIF2C (MCAK) and KIF18B in astral microtubule length maintenance (Tanenbaum et al., 2011).

KIF18B (*human*)	Target %ID	Query %ID	KIF18B (*human*)	Target %ID	Query %ID
KIF18A	32.85	34.62	KIF20A	15.96	16.67
KIF25	29.43	13.26	KIFC3	15.68	15.61
KIF3A	24.52	20.89	KIF23	15.21	17.14
KIF3B	23.56	20.66	KIF4A	15.02	21.71
KIF22	23.01	17.96	KIF4B	14.99	21.71
KIF3C	20.93	19.48	KIF16B	14.30	23.36
KIF12	20.66	12.44	KIF7	14.00	22.07
KIF19	19.94	23.36	KIF15	13.54	22.07
KIF2A	19.35	16.90	KIF27	13.20	21.71
KIF2B	19.17	15.14	KIF13A	12.02	25.47
KIF2C	19.17	16.31	KIF24	11.84	19.01
KIF9	17.85	16.55	KIF21B	11.79	22.65
KIF6	17.69	16.90	KIF1A	11.50	24.18
KIF5C	17.35	19.48	KIF1B	11.47	23.83
KIF5B	17.34	19.60	KIF21A	11.23	22.07
KIFC1	17.24	19.62	KIF13B	11.17	23.94
KIF17	16.42	19.84	KIF14	10.25	19.84
KIF11	16.38	20.31	KIF26A	8.40	18.54
KIF1C	16.23	21.01	KIF26B	7.35	18.19
KIF5A	16.18	19.60	KIF10(CENP	6.18	19.60
KIFC2	16.11	15.85			

Table 1.1. KIF18B paralogues

A total of 41 paralogues are identified for KIF18B (human) according to the most updated database on Ensembl version100. The target % ID column represents the amino acids identity percentage of the paralogue sequence matching KIF18B. The query % ID column represents the percentage of KIF18B amino acid sequence matching with the paralogue.

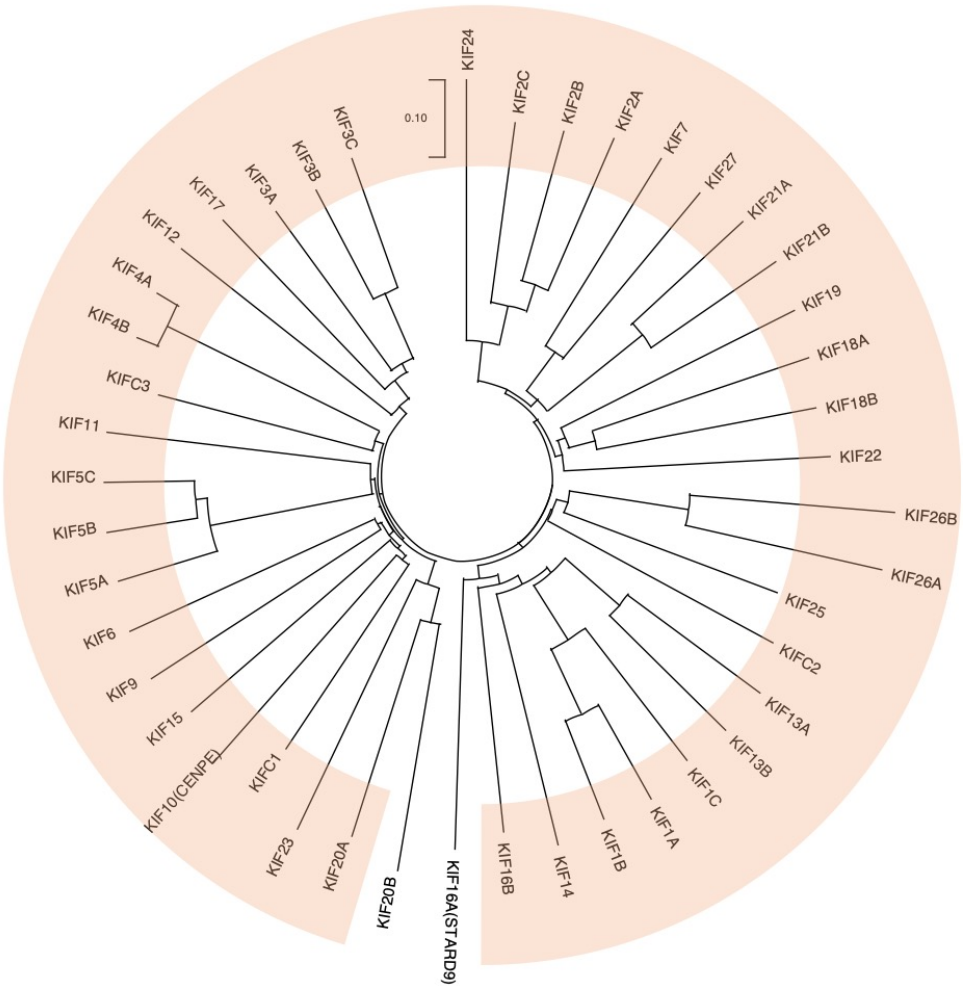

Figure 1.9. Kinesin super family phylogenetic tree in human

This tree is generated based on the multiple alignment of all 44 identified kinesin superfamily members. The KIF18B paralogues are highlighted and composed of 41 kinesin protein. The 0.1 scale bar indicates 10% genetic variation between the kinesin superfamily members.

KIF18B is predominantly nuclear in interphase thanks to an NLS sequence at the C-terminal. In total, three NLS sequences are found in the KIF18B coding gene. However, only one of the NLS sequences is shown to be responsible for sequestering KIF18B into the nucleus through the nucleopores (Lee et al., 2010), which is depicted in red in Figure 1.10.

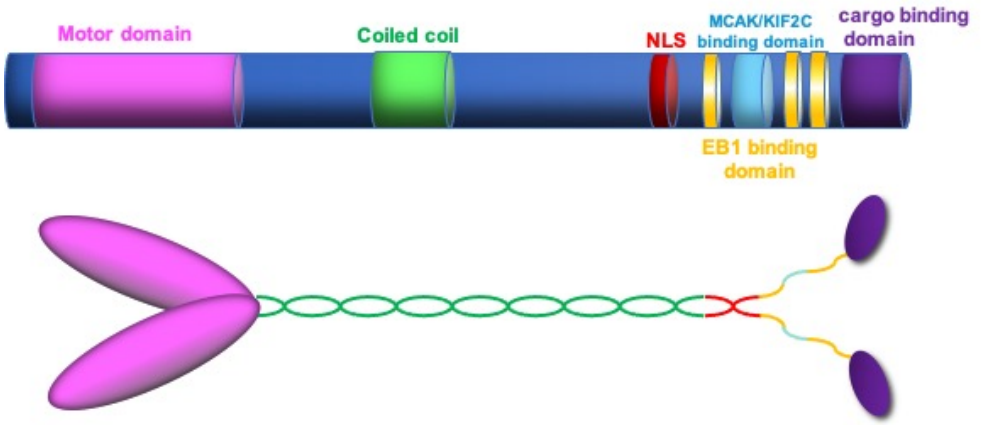

Figure 1.10. KIF18B protein structure schematic

The motor domain in KIF18B is located at the N-terminal, categorising this protein as an N-kinesin. The coiled-coil domain lets the protein dimerization. One NLS signal out of three is indicated in the schematic which is important in sequestering KIF18B to the nucleus in interphase. KIF18B has three EB1 and one MCAK binding domains at the C-terminal enabling this protein to localise at the microtubule plus ends and depolymerise them.

While KIF18B is mainly localised in the nucleus and to a lesser extent in the cytoplasm in interphase, it displayed concentration at the plus end of astral microtubules in mitosis (Tanenbaum et al., 2011; Walczak et al., 2016). Astral microtubules extending from centrosomes play an important role in spindle orientation and consequently chromosome segregation. Kinesin-8 family regulates microtubule dynamics by depolymerizing or capping the plus ends, a function performed in association with kinesin-13, MCAK (Manning et al., 2007; Varga et al., 2009). EB1, a well-characterized microtubule end-binding protein, is required for maintaining the microtubule plus ends. EB1 localises to the astral microtubule plus ends and interacts with KIF18B (Stout et al., 2011; Tirnauer and Bierer, 2000; Vitre et al., 2008). KIF18B localisation at the astral microtubule plus ends was shown to be EB1 dependent so that EB1 deletion, can result in misorientation of the mitotic spindle (McHugh et al., 2018; Shin et al., 2015; Stout et al., 2011). Accordingly, KIF18B uses its motor domain to walk along microtubules with a speed of 635 ± 163 nm/s and upon reaching the microtubule plus ends, where EB1 is localised, interacts with the EB1 via its c-terminal EB1-binding-domain to regulate astral microtubule length in assistance with microtubule depolymeriser, MCAK (Tanenbaum et al., 2011, 2014, Stout et al., 2011).

Regulation of MCAK-KIF18B microtubule destabilizing activity is regulated by Aurora A and B kinases dependent MCAK phosphorylation (Tanenbaum et al., 2011).

Bioinformatics studies have implicated KIF18B in carcinogenesis (Itzel et al., 2015; Jalali et al., 2015; Yang et al., 2020). The dynamics of microtubules is important to proper chromosome segregation and any malfunction in mitosis makes the cell prone to cancer. Therefore, the role of KIF18B in spindle orientation could be the underlying reason for KIF18B's association with breast, ovarian, kidney, liver, and lung cancers. Alternatively, KIF18B might have a role in cancer due to unknown roles in the nucleus during interphase. For instance, KIF4A is another nuclear kinesin, reported to be involved in DNA damage repair, interacting with BRCA2-RAD51 (Wu et al., 2008). KIF4A interacts with BRCA2 via its C-terminal tail and is impaired in HR repair pathway so that KIF4A deletion reduced RAD51 activation and increased cells IR sensitivity. Moreover, using laser micro-irradiation, immediate recruitment of KIF4A to DSBs was shown (Wu et al., 2008).

1.11. Movement of DSB

The nucleus can be considered as the information centre of the cell. It carries almost all the genome, except the mitochondria, and has a large, complex proteome. Chromatin maintenance in such a busy compact space requires mobility to allow all the genome metabolic processes, such as transcription, replication, segregation, and repair. DNA damage response also requires DSBs clustering, homology search, heterochromatin relocation and anchoring to subnuclear structures, and more highly dynamic processes (Marnef and Legube, 2017).

Recent studies on genome organization and transcription in interphase cells, which were performed in yeast, revealed a chaperon-dependent mobility induction of a gene promoter, based on the nuclear actin network. The promoter movement is mediated by Hsp90

dependent nucleation of myosin, and the interaction of myosin and nuclear actin network is mediated by ARP-containing chromatin remodelers (Soutoglou and Misteli, 2007; Wang et al., 2020).

Following DSB, H2AX is phosphorylated by ATM, triggering the DDR cascade. Considering the expansion of γH2AX flanking the DSB spreads about 1-2 Mb in mammals and 200-300 kb in yeast, yet phosphorylated ATM is localised to just 2-10 kb flanking the DSB, intra TAD (topologically associated domains, physically interacting regions of chromatin) chromatin movement likely explains the spread of H2AX phosphorylation (Aymard and Legube, 2016; Caron et al., 2015; Clouaire and Legube, 2019; Dekker and Mirny, 2016; Iacovoni et al., 2010; Lee et al., 2014; Lukas et al., 1997) In this model, intra-TAD movement around the ATM marked breaks facilitate all the H2AX phosphorylation within a TAD (Marnef and Legube, 2017; Savic et al., 2009).

Initial access of damaged DNA to DDR proteins involves the coordinated activity of PARP1, ATM, and γH2AX to relax chromatin structure and re-condensation (Downs et al., 2000; Strickfaden et al., 2016). This transition between condensation and de-condensation termed ‘chromatin breathing’ will result in DSBs movement (Rother et al., 2020). There are a couple of factors influencing the range of movement from no movement to limited or long-range movement. The damaging agent is one of the factors, as etoposide will induce more movement rather than gamma irradiation (Krawczyk et al., 2012). Also, a DSB within a telomeric area is more prone to movement in comparison to the central area within the chromosome (Cho et al., 2014). Furthermore, it has been shown that DSBs within active genes stimulate more movement versus DSBs in non-coding DNA (Gandhi et al., 2012; Soutoglou and Misteli, 2007). Finally, the scale of DSB movement depends on the chosen pathway for repair (Dion et al., 2012).

Another type of DSB movement is DSB clustering, evident by one RAD52 focus formation at two DSBs in yeast (Lisby et al., 2003). While

clustering would promote quicker recruitment of DDR proteins to DSB, it also leads the damaged foci to be isolated from the rest of chromatin (van Sluis and McStay, 2015; Tsouroula et al., 2016). The DSB clustering must be tightly controlled otherwise one possible detrimental outcome could be chromosome translocation (Roukos et al., 2013).

Heterochromatic DSBs are mostly repaired by HR. Persistent or unrepairable DSBs within the heterochromatin after irradiation moves toward the nuclear periphery, perhaps to be in a safe position and far from repetitive copies of breaks ends resulting in aberrant DNA repair (Chiolo et al., 2011). Another hypothesis explaining unrepairable DSBs movement is interaction with subnuclear compartments such as the LINC complex, which transmits the message from nucleus to cytoplasm to mediate apoptotic morphological changes (Starr and Fridolfsson, 2010). The LINC is a protein complex linking nucleoskeleton and cytoskeleton and is implicated in various cell activities by providing internal cell connectivity (Crisp et al., 2006).

Chromosome translocations and subsequently unusual chromosome rearrangement is a hallmark of cancer and in particular, leukemia. The movement of DSBs within the nucleus is described as the mechanism of chromosome translocation formation through spatial and dynamic investigations. Roukos Vasiliss and colleagues studied the spatiotemporal movement of fluorescently tagged chromosomes after induction of DSBs. They observed movement of distally located breaks as well as breaks in proximity and reported these movements as a salutatory movement which is statistically different from Brownian movement and needs a kind of force through fibres (Roukos et al., 2013).

Whether the movement of DSBs is through diffusion in the nucleus or directional is a source of conflict in the field. Chromatin changes at the breaks, leading to relaxation and roaming in higher volume in the nucleus supports the DSB diffusion hypothesis (Zhang and Heermann, 2014). The detachment of chromatin from anchoring components and

freedom in movement within the nucleus, as the consequence of break, is also consistent with the hypothesis of movement of DSB through diffusion (Strecker et al., 2016).

Regarding the directional movement of DSB, movement of sub telomeric DNA has been reported by Cho. N.W. and colleagues and suggested allowing long range RAD51 dependent directional movement of damaged telomeres in order to search for homology (Cho et al., 2014). Actin filament polymerization in the nucleus upon DNA damage is another provoking hint requiring more investigation on the possibility of the directed movement of DSB within the nucleus (Belin et al., 2015). Impairment of DNA repair after treatment with microtubule destabilising agents, plus involvement of few kinesins in DDR, are also some indications of microtubules involvement in DSB movement in the nucleus (Chung et al., 2015; Poruchynsky et al., 2015; Wu et al., 2008)

1.12. Aims and objectives

KIF18B was previously identified as a novel interacting partner for 53BP1 and the domains of each protein required for this interaction have been mapped. In this study, we aimed to further investigate KIF18B localisation and expression throughout the cell cycle.

We also aimed to explore the role of KIF18B in the DNA damage response in relation to 53BP1.

Furthermore, we carried out a structure-function investigation to elucidate the mechanism of KIF18B involvement in DDR if it shows any role.

Chapter 2: KIF18B subcellular localisation and expression during cell cycle

2.1. Summary

We show that KIF18B is mainly nuclear during interphase and appears as nuclear spots in immunofluorescent staining with regions of more intense staining that co-localise with regions of brighter DAPI staining suggestive of co-localisation with heterochromatin. Our data also support KIF18B localisation at astral microtubules, in accordance with previous studies. In addition, we report KIF18B localisation during cytokinesis to the midbody and primary abscission cut site. The presented data are suggesting that its localisation at the midbody is regulated by Aurora B, DNA-PK, and ATM kinase activity. Cytokinetic profiling upon KIF18B depletion suggests a probable role for KIF18B in the regulation of abscission timing, serving as a checkpoint regulator in cell cycle regulation. This novel role requires further investigation to elucidate its mechanism of action.

2.2. Introduction

Several cellular functions have been identified for kinesins. Vesicle and organelle transport are amongst their important roles. Neuronal vesicles containing neurotransmitters require to be delivered to the presynaptic region for efficient signal transmission. The vesicle transporter involved in this process is Kinesin-1 (Hurd and Saxton, 1996; Saxton et al., 1991). Kinesin-2 is required for flagella and cilia maintenance for precursor transportation for cilia assembly (Rosenbaum and Witman, 2002).

Kinesins are also involved in mitosis and meiosis. The kinesin-5 family member, Eg5 and kinesin-6, MKLP, are involved in cell division through generating sliding forces in the midzone of late anaphase and cytokinetic cells (Shimamoto et al., 2015; Zhu et al., 2005). CENPE is a kinesin-7 family member and together with kinesin4 is involved in chromosome and microtubule interaction during chromosome segregation (Mazumdar et al., 2004; She et al., 2020). Kinesins also play an essential role in microtubule dynamics. MCAK, a Kinesin-13, as well as KIF18A and KIF18B, are kinesin-8 family members which reported to be involved in microtubule dynamics through depolymerisation of microtubules (Goshima et al., 2005; Tanenbaum et al., 2011). The budding yeast kinesin-8, KIP3, is also a microtubule depolymerising kinesin (Gupta et al., 2006). On the other hand, Ncd, a kinesin-14, maintains microtubule length by stabilising them (Endow et al., 2010; Wordeman, 2010).

The distinct roles for the kinesins are related to their subcellular localisation and also their expression pattern, which can be either steady or cell-cycle regulated expression.

The cell-cycle regulated genes have a peak in expression in either G1/S or G2/M phase. While E2F/DP1 regulates G1/S transcription, FOXM1 is generally proposed as the main transcription factor for G2/M expressing genes (Grant et al., 2013; Liu et al., 2017).

We carried out a microscopic analysis of immunofluorescent stained cells to broaden our understanding of the KIF18B subcellular localisation in each cell cycle stage. KIF18B has a nuclear localisation in interphase and from prophase to anaphase localises to the plus end of astral microtubules, underlying its defined role in astral microtubule dynamics (Tanenbaum et al., 2011). However, the role if any, of nuclearly localised KIF18B during interphase is unknown. Interestingly, we noticed KIF18B localisation at the midbody in cytokinesis which could define a new role for KIF18B in cytokinesis.

Cell cycle analysis revealed a distinct pattern of regulation for KIF18B. Its expression steadily increases from low levels in early G1 to its highest level in late G2/early mitosis.

2.3. Materials and Methods

2.3.1. Cell Culture

Cells were cultured at 37°C in a humidified atmosphere of 5% CO_2. U2OS, HeLa, and HEK293T were cultured using DMEM supplemented with 10% FBS (Biosciences). hTERT immortalized RPE-1 cells were cultured in DMEM-F12 media supplemented with 10% FBS. All cell lines were cultured in 1% penicillin-streptomycin (Biosciences).

2.3.2. Drug treatments

For fixed cell immunofluorescence experiments, cells were treated with inhibitors (Table 2.3.) and harvested after 3 h except for the Aurora B and CHK1 inhibitor experiments where cells were treated for 45- 60 mins. They were all used at the 10 μM concentration.

2.3.3. Protein Extraction

Protein extracts were prepared by lysing cells in lysis buffer (50mM Tris-HCl, 0.5% NP40, 150mM NaCl, 10% glycerol, 1mM $MgCl_2$, protease and phosphatase inhibitors) and a 1:1000 dilution of Benzonase nuclease (Sigma Aldrich) for 45 min at 4°C. Samples were centrifuged for 20 min at 14,000 rpm at 4°C, the supernatant was used for downstream applications. The protein concentrations were measured using Bradford reagent.

2.3.4. Western Blotting

The concentration of proteins was adjusted to be the same and diluted with 4X sample buffer (2.0 ml 1M Tris-HCl pH 6.8, 0.8 g SDS, 4.0 ml 100% glycerol, 0.4 ml 14.7 M β-mercaptoethanol, 1.0 ml 0.5 M EDTA, 8 mg bromophenol Blue). The separation of proteins carried out on sodium dodecyl sulphate polyacrylamide gel electrophoresis (SDS-

PAGE). Proteins were transferred to a nitrocellulose membrane using 0.35 mA for 1h at 4°C. Membranes were blocked in 5% milk-TBST for 20 min at RT. The conditions for probing with the primary and secondary antibodies are mentioned in Table 2.1. Following overnight probing for the primary Ab, membranes were washed 3 times with TBST and incubated with the relevant secondary antibody for 60 min at RT.

Table 2.1. List of antibodies and conditions used for Western blotting

Antibody	**Dilution**	**Blocking**	**Species**	**Manufacturer**	**Catalogue Number**
Primary antibodies					
KIF18B	1:1000	5% milk	Rabbit	Sigma Aldrich	HPA024205
Actin	1:5000	5% milk	Rabbit	Sigma Aldrich	A2066
ATR	1:1000	5% milk	Goat	Santa Cruz	Sc1887
Nup15.3	1:1000	5% milk	Rabbit	Bethyl	A301-788A
H3S10p	1:1000	5% milk	Rabbit	Millipore	06-570
Cyclin B1	1:1000	5%milk	Rabbit	Cell Signalling	4138S
H3	1:80000	5%milk	Rabbit	Abcam	Ab1791
Secondary antibodies					
Goat Anti-Rabbit IgG	1:5000	5%milk	Goat	Thermoscientific	31460
Anti-mouse IgG	1:5000	5%milk	Rabbit	Thermoscientific	31450

2.3.5. Immunofluorescence staining

Coverslips sterilized under UV for 20 min before seeding cells. $2.5x10^5$ to $1.5x10^5$ (depending on the purpose of the experiment) cells were grown on a sterile coverslip. 24 to 48 h following the seeding, coverslips were briefly washed twice with PBS. Cells were fixed in 4% PFA for 10 min at RT, or in ice-cold methanol for 20 min at -20°C depending on the antibody staining required. Coverslips were then washed three times in PBS and permeabilised with 0.25% Triton X-100 for 5-10 min. The cells were again washed in PBS three times before blocking in 5 % BSA for 1h at RT or overnight in 4°C and followed by 1h at RT. The primary and secondary antibody staining conditions are mentioned in Table 2.2. Cells were stained 1h at 37°C in a humidified chamber with primary and secondary antibodies, with three PBS washes after each incubation. Slides were mounted using vectashield media with DAPI. Images were captured on a Deltavision integrated microscope system mounted on an IX71 Olympus microscope and using Softworx software. 0.2-0.5 µm Z-stacks were collected, deconvolved, projected, and merged. Microscopy analysis performed using ImageJ 1.52n software.

If cytoskeletal pre-extraction is needed, cells were treated with CSK buffer (100 mM NaCl, 300 mM sucrose, 3 mM MgCl2, 10 mM PIPES (pH 6.8), 0.2% Triton X-100) for 10 min at RT prior to PFA fixation.

Table 2.2. List of antibodies and conditions used for Immunofluorescence staining

Antibody	Dilution	Blocking	Species	Manufacturer	Catalogue Number
Primary antibodies					
53BP1	1:500	5% BSA	Mouse	Thanos	Non-commercial
KIF18B	1:200	5% BSA	Rabbit	Sigma Aldrich	HPA024205
αTubulin-B512	1:200	5% BSA	Mouse	Sigma Aldrich	T5168
Lap2β	1:200	5% BSA	Mouse	BD Biosciences	611000
Aurora B	1:200	5% BSA	Mouse	BD Biosciences	611082
EB1	1:200	5% BSA	Rabbit	Bethyl	A302-332A
ZFYVE19 (Anchr)	1:500	5% BSA	Rabbit	Bethyl	A301-808A
Secondary Antibodies					
FITC anti-mouse IgG	1:200	5% BSA	Goat	Jackson Immunoresearch	115-096-062
FITC anti-rabbit IgG	1:200	5% BSA	Goat	Jackson Immunoresearch	111-096-045
TRITC anti-mouse IgG	1:200	5% BSA	Donkey	Jackson Immunoresearch	711-025-152
TRITC anti-rabbit IgG	1:200	5% BSA	Donkey	Jackson Immunoresearch	711-025-151

2.3.6. siRNA Transfection

$1.5x10^5$ RPE1 cells were seeded in 35 mm dishes and transfected with 40 pmol of negative control siRNA (Dharmacon) or siRNA targeting Luciferase (Eurofins) as control, and targeting siRNA (Ambion, Dharmacon or Eurofins) using Oligofectamine (Invitrogen) according to manufacturer's instructions. Cells were harvested 48 h following the siRNA transfection. Biological triplicates were used for each siRNA treatment. siRNA sequences are listed in Table 2.3.

Table 2.3. RNAi targeting sequences, inhibitors, and drugs

Target gene	siRNA sequence	Manufacturer
KIF18B	GGUGUAUAAUGAACAGAUC	Eurofins
KIF18B	CGUACAACAACCCUCAAAUA	Eurofins (for rescue)
KIF18B	CGUACAACACCCUCAAAUA	Ambion
53BP1	(OnTargetplus SMARTpool of four)	Dharmacon
Nup13.5	CAAUUCGUCUCAAGCAUUA GAUAGGAGUGGGAUAGAUA CAAGAUAGCAAACUAGCAA GUUCCACGCUGGCCAGAAA	Dharmacon
ATR	CCU CCG UGA UGU UGC UUG A dtdt	Eurofins
ATM inhibitor	KU55933	Selleckchem
ATR inhibitor	S8050	Selleckchem
Aurora B inhibitor	SML0268	Sigma Aldrich
Chk1 inhibitor	559402	Sigma Aldrich
DNA-PK inhibitor	NU7026	Sigma Aldrich
Nocodazole	M1404	Sigma Aldrich
Thymidine	T1895	Sigma Aldrich
Deoxycytidine	D3897	Sigma Aldrich

2.3.7. cDNA transfection

HeLa cells were grown to 80-90% confluency and transfected with 1µg of DNA and 2µl of Lipofectamine2000 (Life Technologies) diluted in 500 µl Opti-MEM (Gibco) added into 2ml DMEM with 10% FBS per 35 mm dish. Cells were grown for 48 h prior to analysis by immunofluorescence and western blot.

2.3.8. Cell synchronization by Nocodazole

HeLa cells were seeded in 10cm dishes and cultured until 90% confluent. Cells were then grown in DMEM media containing 25 ng/ml of Nocodazole for 16-18 h. Nocodazole arrested cells were harvested by mitotic shake-off and washed 4 times with 50 ml 1x PBS (pre-warmed at 37°C). Cells were then released into fresh DMEM media and harvested in different time points for western blot and immunofluorescence (Jackman and O'Connor, 1998). The method was adjusted in our lab to achieve the most efficient synchronisation.

2.3.9. Double thymidine block

HeLa cells were seeded at $8x10^5$ cells/10 cm dish to have 50-60 % confluency at the time of the first block. 1mM Thymidine was added to the cells, followed by 22 h incubation. Cells were washed with PBS three times and 25 µM Deoxycytidine in addition to 25 µM Thymidine was added to the cells to release them for 6 h. Cells were then blocked again with 2.5 mM Thymidine for 16 h. Cells were then subjected to three washes with PBS and fresh media containing 25 µM Deoxycytidine. Cells were harvested for Immunofluorescent imaging, FACs analysis, and Western blotting every 2 h for the period of 24 h after the second release (Shelby et al., 1997).

2.3.10. FACs analysis

Cells were pelleted by centrifugation at 1200 rpm for 5 min at 4°C then washed in PBS and resuspended in 1ml cold PBS. The cell suspension was added to 3 ml 100% ice-cold Ethanol, while vortexing at low speed. Cells in 75% final concentration of ethanol were fixed and kept at least 24 hours before the staining for FACS analysis.

Cells were pelleted at 1200 rpm for 5 min after addition of 3 ml PBS, then washed in 1% BSA in PBS and resuspended in 50ul of 1% BSA-PBS- 0.5% Triton X-100 containing a 1:50 dilution of primary antibody and incubated for 2 h at RT. Cells were washed three times in 1% BSA-PBS and resuspended in 50ul of 1% BSA-PBS-0.5% Triton X-100 containing a 1:50 dilution of FITC-conjugated anti-rabbit secondary antibody (Jackson Immunoresearch 111-096-045). Samples were incubated for 1h at RT in the dark and were then washed three times in 1% BSA-PBS. After final pelleting, cells were resuspended in 300µl PBS containing 40ug/ml Propidium Iodide (Sigma Aldrich) and 250ug/ml RNAse A and incubated for 30 min at RT before being analysed using a FACS Canto II (BD Biosciences).

2.3.11. Statistical analysis

For quantified microscopy experiments three biological replicates were completed with a constant number of cells per condition per biological replicate which is indicated in each figure legend. Sample sizes were selected to be as large as biologically and technically feasible within our experimental conditions. The mean difference of each condition in Figures 2.13. and 2.14., individually compared to control via Student t-test. The variance was similar between the groups that are being compared. GraphPad Prism 8.2.1 software was used for all standard statistical analyses.

2.4. Results

2.4.1. KIF18B exponential subcellular localisation

To have an overview of KIF18B subcellular localisation, we stained exponentially growing (80% confluent) asynchronous HeLa, U2OS and hTERT-RPE1 cells for KIF18B. The antibody (Sigma Aldrich HPA024205) used for KIF18B staining, was first evaluated for its specificity to KIF18B, using genetically depleted cells for KIF18B (Figure 2.1.). Similar to the first study of KIF18B by Lee YM. et al, 2010, we observed a predominant but, not absolute nuclear localisation of KIF18B, while a small proportion of KIF18B is diffused over the cytoplasm with slightly more concentration at the proximity of the nucleus (Figure 2.2.).

We noted the diversity in KIF18B signal intensity throughout the cell population, which was consistent in the three cell lines examined (Figure 2.2.). The variation in KIF18B signal intensity in interphase cells is observable, which could be explained by the cell cycle-regulated expression of KIF18B in further investigation.

We also noticed KIF18B localisation to the midbody in cytokinetic cells as shown in (Figure 2.2.). This localisation of KIF18B is comparable to KIF4A which is also nuclear in interphase and localise at the midbody in cytokinesis.

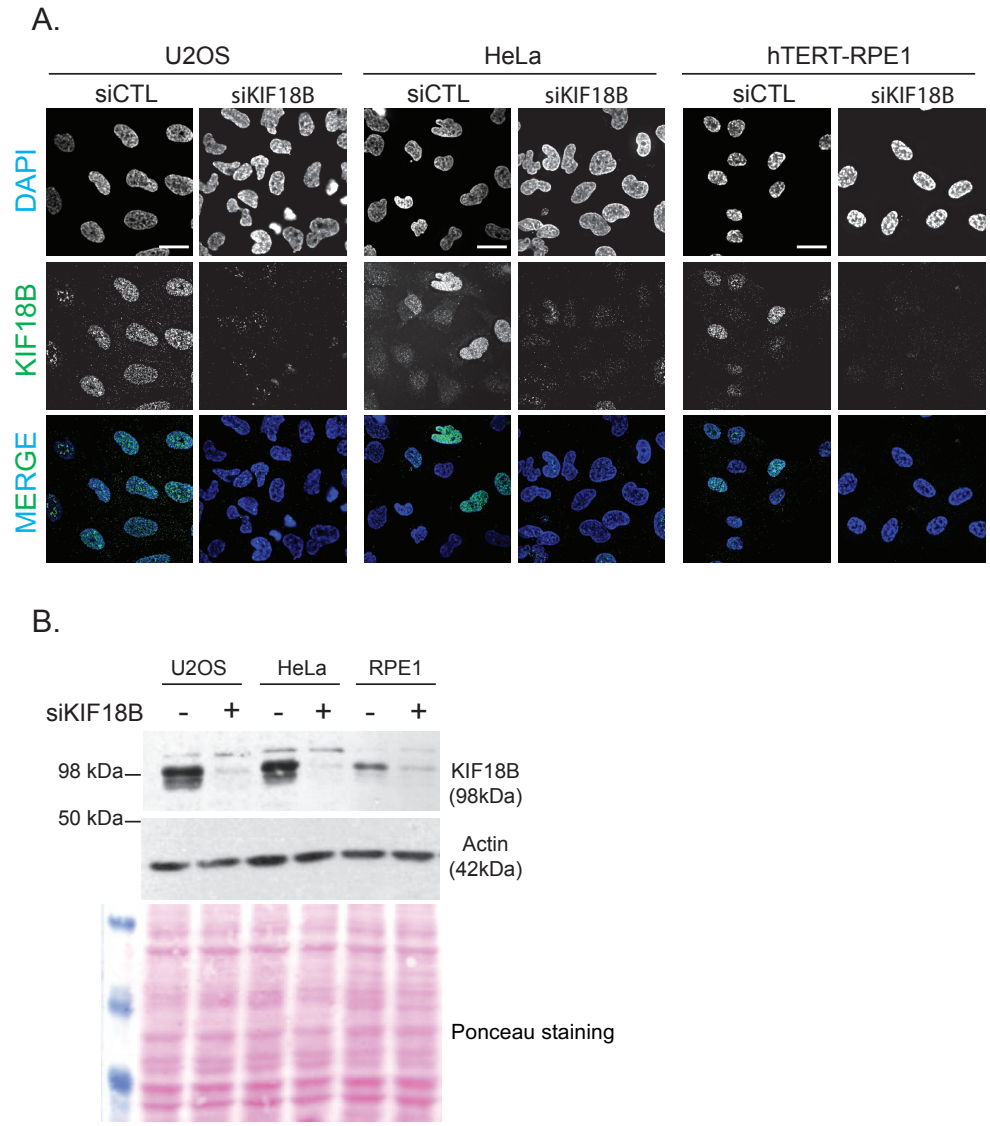

Figure 2.1. Evaluation of KIF18B antibody for its specificity

(A) Representative images from immunofluorescent staining of U2OS, HeLa, and hTERT-RPE1 cells for KIF18B in normal (transfected with siControl) and KIF18B depleted (transfected with siKIF18B) cells. DAPI staining is indicated as blue and KIF18B as green. The third row is showing the merged image from the two channels. The scale bar is equal to 25 µm. (B) The Western blot confirms the successful depletion of KIF18B in U2OS, HeLa, and hTERT-RPE1 cells. The Actin and ponceau staining are shown as a loading control and successful transfer of proteins to the membrane, respectively.

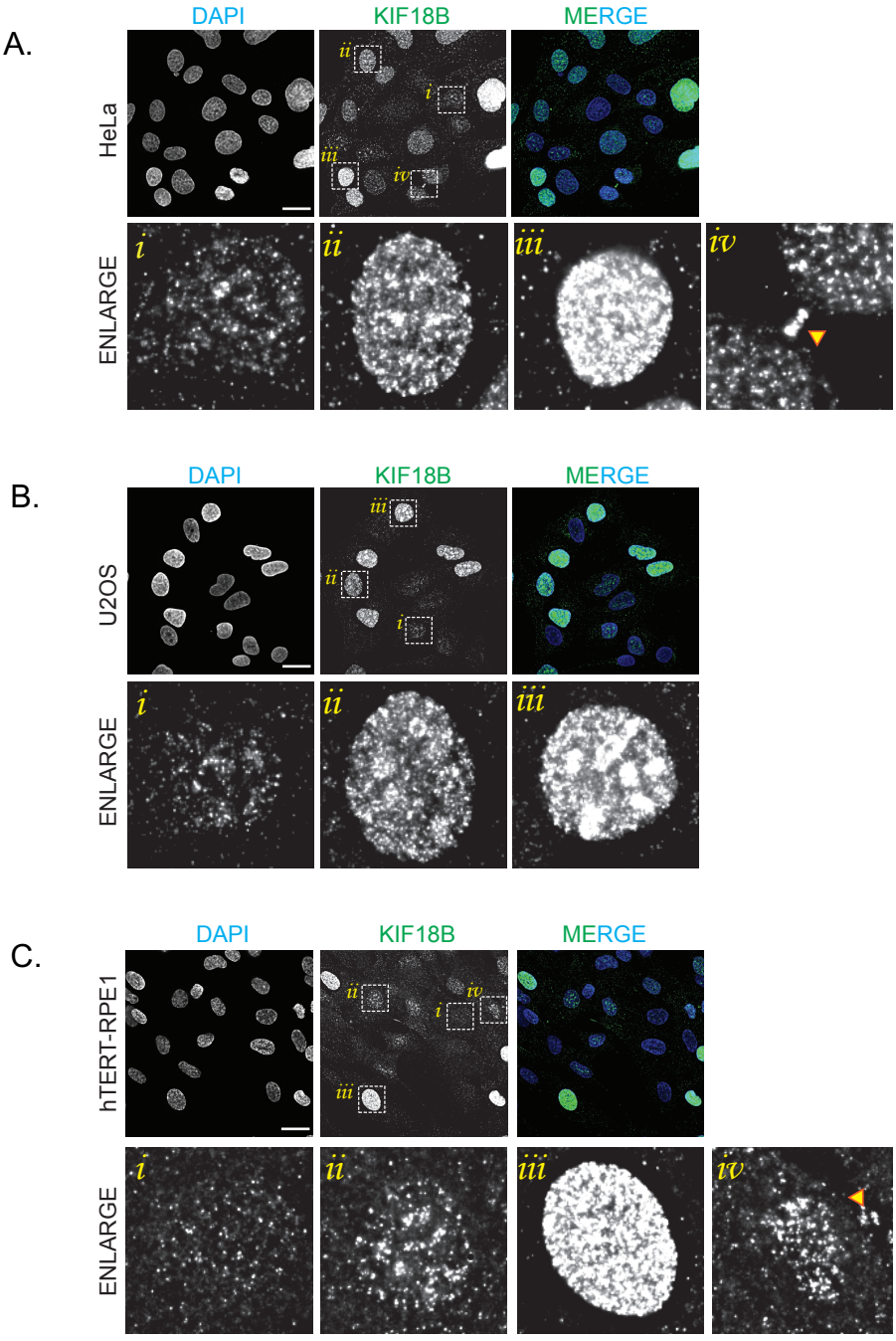

Figure 2.2. KIF18B immunostaining in HeLa, U2OS and hTERT-RPE1 cells

(A) HeLa cells are stained for KIF18B (SigmaAldrich HPA024205). Three distinctive KIF18B signal intensities, including low (i), medium (ii), and high (iii) are denoted and enlarged. KIF18B signal at the midbody of two cytokinetic cells (iv) is also shown. (B) KIF18B staining of U2OS cells and representative enlargement of three different signal intensities of KIF18B. (C) KIF18B staining of hTERT-RPE1 cells, which is showing the three different intensities, and KIF18B at the midbody of two cytokinetic cells (A). The scale bar represents 25μm.

2.4.2. KIF18B expression is cell cycle regulated

We studied the KIF18B expression level in different cell stages using synchronized HeLa cells. The cells were treated with the microtubule depolymerising agent, Nocodazole, to arrest them at late G2/prophase (Figure 2.3.). A western blot on harvested cells after Nocodazole release in five indicated time points was performed (figure 2.3.). Accordingly, KIF18B was expressed at very high levels in Nocodazole arrested cells, corresponding to an induced and extended arrest in late G2/M phase (0–60 min after release). Subsequently, KIF18B levels gradually decreased upon release up to 120 minutes after Nocodazole wash out, but still not returned to the level seen in asynchronously growing cells. The result of this experiment suggested that KIF18B is cell cycle-regulated with pronounced up-regulation during the G2/M phase. The levels of H3S10p were examined as control, as this phosphorylation event is specific to the M phase (Figure 2.3.). The gradual reduction in H3S10p levels upon Nocodazole release indicates a degree of release from the Nocodazole block. The pattern of KIF18B expression in this experiment is similar to H3S10p, although not identical.

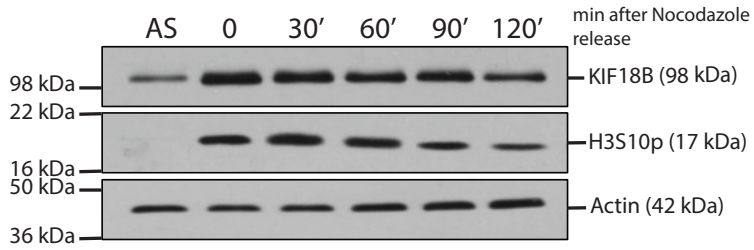

Figure 2.3. Analysing the KIF18B cell cycle regulated expression

HeLa cells were synchronised at G2/M by Nocodazole treatment. The synchronisation was carried out by Nocodazole arrest and mitotic shake off. At the indicated times after release, cells were harvested and subjected to western blot analysis and probed for KIF18B and phosphorylation of H3S10 (H3s10p) as a mitotic marker. Actin served as loading control.

The preliminary result from arresting cells at G2/M by Nocodazole showed KIF18B to be cell cycle-regulated. Therefore, we decided to confirm it by using the double thymidine block and release protocol.

The high concentration of thymidine, interrupts the deoxynucleotide metabolism pathway, thereby depriving cells of the deoxynucleotide required for DNA replication (Bjursell and Reichard, 1973). As treatment of exponentially growing cells with thymidine arrests all cells undergoing DNA synthesis shortly after the addition of thymidine, a double thymidine block procedure, which involves releasing cells from a first thymidine block before trapping them with a second thymidine block is generally used to result in a more uniform arrest of cells at the G1/S or early S phase boundary (BOSTOCK, 1971). We arrested HeLa cells at G1/S and early S by using double thymidine block and released the cells into the cell cycle with synchrony. After release, cells were harvested every 2 hours for 24 hours. Analysis of DNA content through PI staining and flow cytometry confirmed the cell's synchronisation (Figure 2.4.). Immunoblotting for H3S10p and Cyclin B also confirmed a reasonable level of synchrony (Figure 2.5. B).

Immunoblotting for KIF18B showed a steady increase in expression level as cells transited the S phase into G2 and M phases. Once cells exited M and entered into the subsequent G1 phase, the level of KIF18B decreased and remain low, which is consistent with the immunofluorescent staining for KIF18B (Figure 2.5.).

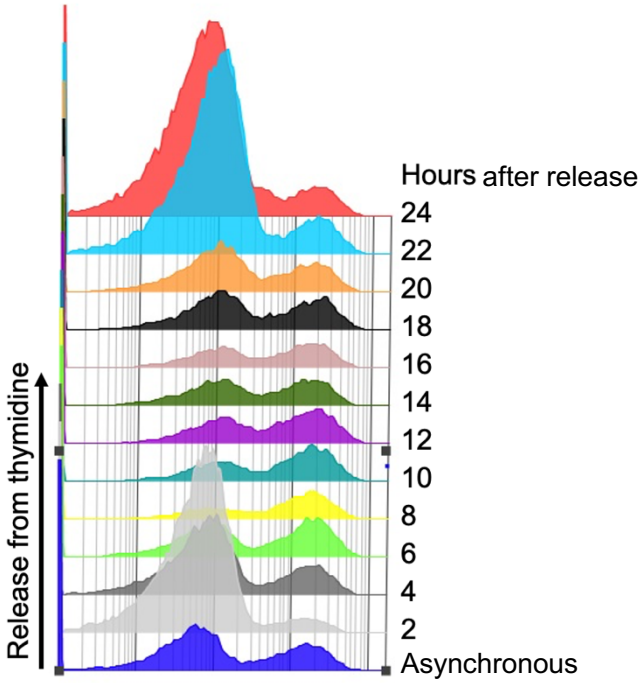

Figure 2.4. Staggered histogram of flow cytometric analysis of synchronised HeLa cells

HeLa cells were blocked twice with thymidine and released. The **c**ells were harvested at indicated time points after the last release**.** Ethanol fixed samples were analysed by Flowcytometry**.** Cell's DNA content is stained with Propidium Iodide, representing the number of alive cells proceeding through the cell cycle. The Y-axis of the histogram is indicating the number of cells and the X-axis is indicating the DNA content/Cell.

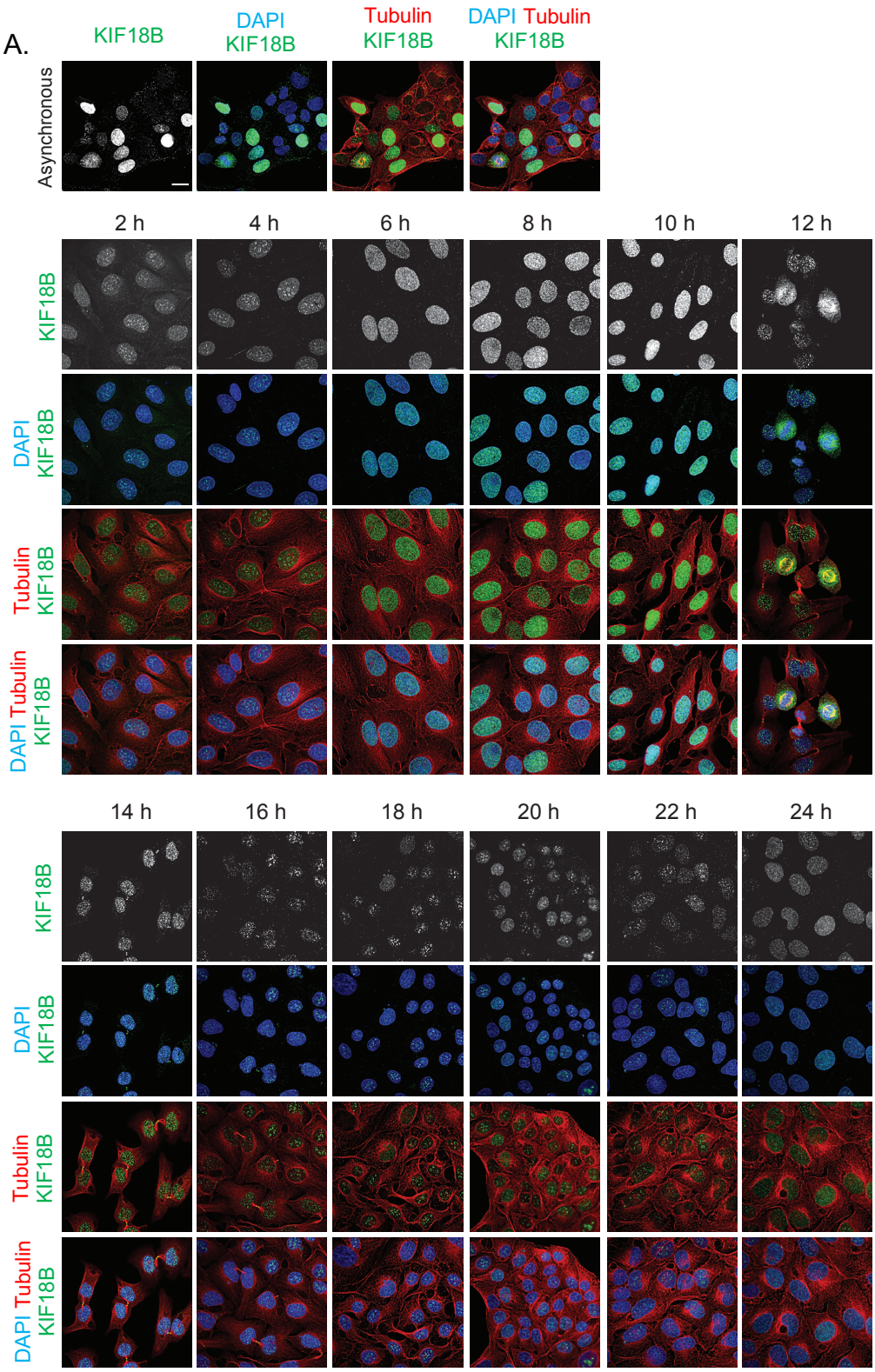
A.
KIF18B
DAPI KIF18B
Tubulin KIF18B
DAPI Tubulin KIF18B
Asynchronous
2 h
4 h
6 h
8 h
10 h
12 h
KIF18B
DAPI KIF18B
Tubulin KIF18B
DAPI Tubulin KIF18B
14 h
16 h
18 h
20 h
22 h
24 h
KIF18B
DAPI KIF18B
Tubulin KIF18B
DAPI Tubulin KIF18B

Figure 2.5.

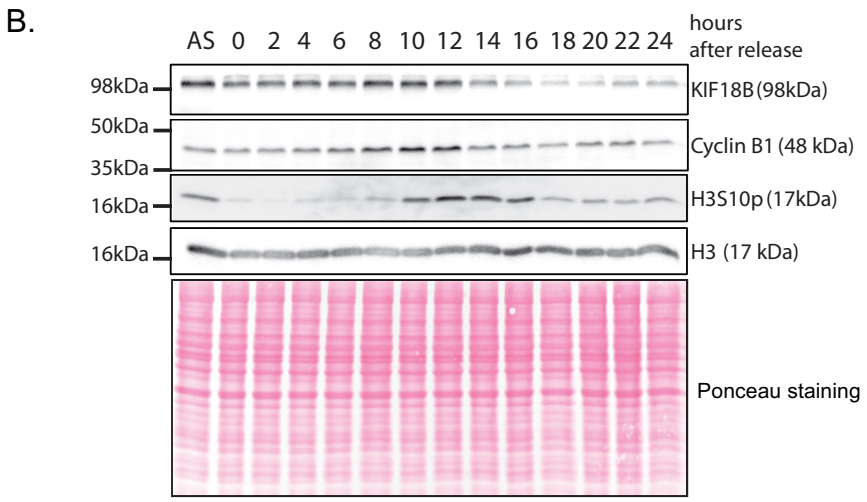

Figure 2.5. Cell cycle regulated expression of KIF18B

(A) HeLa cells were arrested at G1/S by double thymidine block and harvested at indicated time points. Cells were stained for KIF18B (green) and Tubulin (red) and imaged. KIF18B, Merge of DAPI- KIF18B, Merge of Tubulin- KIF18B, and Merge of DAPI-Tunulin-KIF18B are shown respectively in Asynchronous condition and all time points. The scale bar represents 25µm. (B) The western blot of the cells harvested at indicated time points after double thymidine block and release was probed for KIF18B, CyclinB1, H3S10p, and H3. Ponceau staining is used as loading and protein transfer control.

For further confirmation of the cell cycle regulation of KIF18B expression, we used the Fluorescent Ubiquitination-based Cell Cycle Indicator (FUCCI) system (Sakaue-Sawano et al., 2008). FUCCI is a set of two fluorescent fusion proteins: FUCCI-G1 Red and FUCCI-S/G2/M Green. FUCCI-G1 Red is a fusion protein of a fragment of human CDT1 with the red fluorescent protein, m-Cherry, which is expressed in the G1 phase. FUCCI-S/G2/M Green is a fusion protein of a fragment of human Geminin with the green fluorescent protein mAG1 (monomeric Azami-Green1), that is expressed in S, G2, and M phases. Cells expressing both Cdt1 and Geminin are in transition from G1 to S phase and exhibit a yellow colour. This technology utilises red and green florescent staining to analyse cells in a spatio-temporal manner. We used a far-red dye, Cy5, to stain KIF18B. (Figure 2.6. A, B, C).

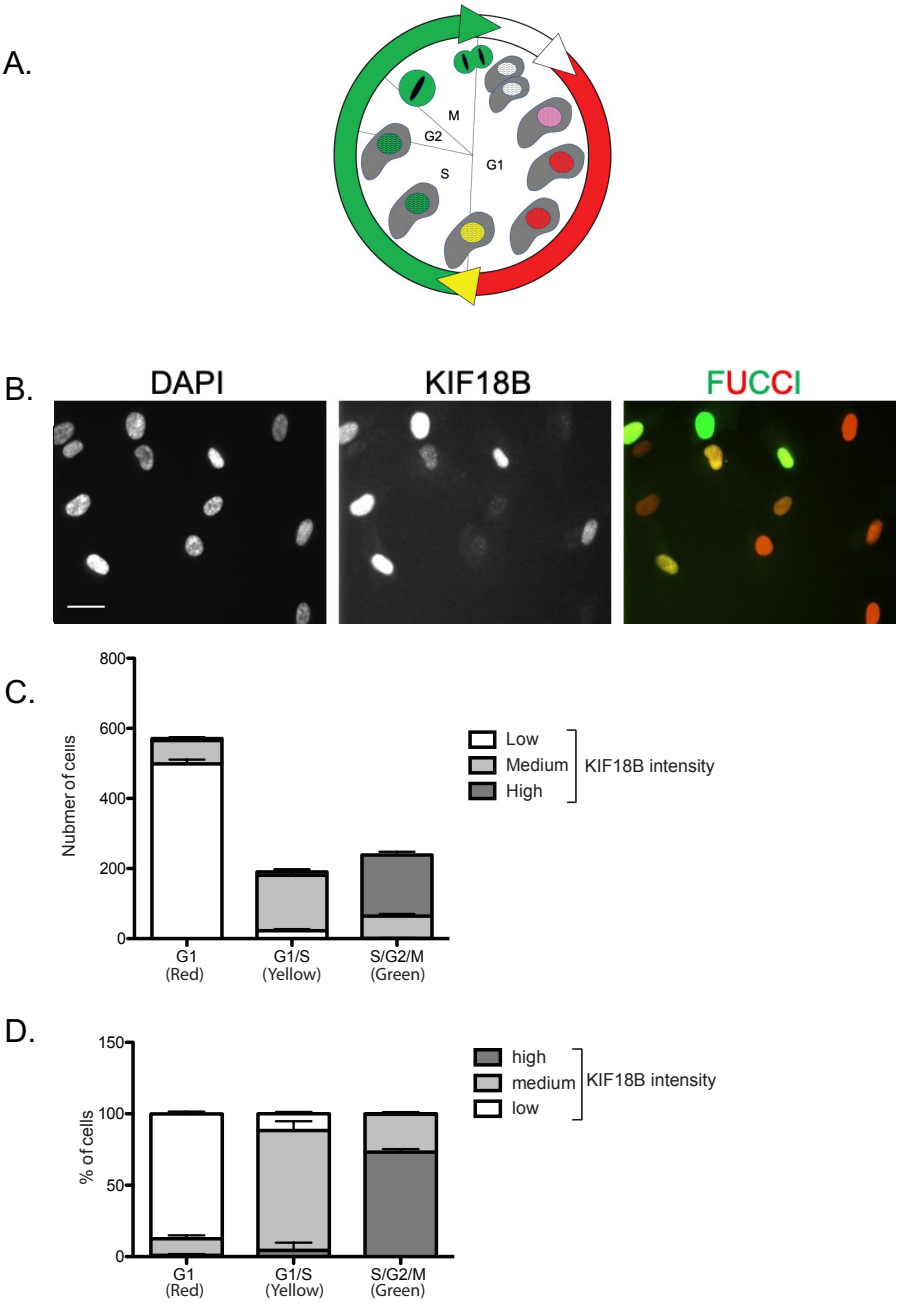

Figure 2.6. KIF18B cell cycle profiling by FUCCI system

(A) Schematic of the FUCCI system application for recognising the cells in different stages of the cell cycle. (B) A representative image of the hTERT-RPE1 cells, stably expressing CDT1-mcherry (red), in G1 phase and Geminin-mAG1 (green), in S/G2/M phases and presents the G1/S transition in yellow (on the far-right). The cells stained for KIF18B and categorised in three levels of KIF18B signal intensity (panel in the centre): low, medium, and high. DAPI staining is presented in the far-left panel. The scale bar represents 25µm. (C) Quantification of the absolute count of cells at different cell cycle stages based on their colour in low, medium, and high categories of KIF18B signal intensity. (D) Quantification of the percentage of cells with low, medium and high KIF18B signal intensity at different cell cycle stages. The quantification is performed by Fiji ImageJ version 1.52n software by defining a region of interest (ROI) around each cell's nucleus and measurement of the KIF18B signal intensity within the ROI. 1000 cells were counted in each experiment and categorised in three groups of low (<100), medium (100-150), and high (>150), based on KIF18B intensity (pixels in ROI). The Error bars represent the SEM across 3 independent repeats.

We divided the cells into three groups, low, medium, and high, based on the level of KIF18B intensity. The distribution of red, yellow, and green cells in three different cell cycle stages, G1, G1/early S, and late S/G2/M, based on the absolute count of cells, was typical for a proliferating population of cells. Most of the cells counted as red (60%), indicating G1 and a smaller population (20%) were detected in S/G2/M by green colour, followed by a smaller number of cells (10%) in G1/S transition staining as yellow (Figure 2.6. B). The percentage of the cells in each group of the high, medium, and low signal intensity for KIF18B indicates that KIF18B intensity correlates with the cell cycle progression. The majority of the cells in the S/G2/M phase showed high KIF18B intensity, indicating that KIF18B is cell cycle-regulated with a gradual increase from G1 to G1/S and reach the highest in S/G2/M phases (Figure 2.6. C). Although all methods of cell cycle analyse have limitations, this method confirms the result of our previous Nocodazole arrest and double thymidine block and release analysis, indicating that KIF18B expression is cell cycle-regulated with low levels in early and high levels in the late phases of the cell cycles.

2.4.3. KIF18B localisation throughout the cell cycle

To investigate KIF18B subcellular localisation in interphase and specific stages of mitosis, HeLa cells were stained for KIF18B and tubulin and captured at different cell cycle stages (Figure 2.8.).

Unlike the most kinesins, we found KIF18B predominantly, but not exclusively, localised in the nucleus during interphase. This observation is in accordance with a previous study reporting the nuclear localisation of KIF18B (Lee et al., 2010).

Furthermore, we noticed that KIF18B co-localises with the area of the nucleus, which shows the most intense DAPI staining, corresponding to heterochromatin particularly around the nucleoli, which recognised as a black cavity in the nucleus due to a lower concentration of DNA

(Pontvianne et al., 2016) (Figure 2.7.). There is also a small fraction of the KIF18B signal found within the cytoplasm.

KIF18B is released from the nucleus upon nuclear envelope breakdown in mitosis and localises to the plus end of the astral microtubule, where it is required, together with EB1 and MCAK, for astral microtubule dynamics in interaction with the proteins (Stout et al., 2011; Tanenbaum et al., 2011).

In our analysis of KIF18B cellular localisation by immunofluorescence staining, we found KIF18B at the appointed position to the astral microtubule plus ends, which is more visibly in prometaphase and metaphase (Figure 2.8.). Although KIF18B is detectable throughout the cytoplasm in mitotic cells, more abundant aligned with polar and kinetochore microtubules in the middle of the cell in anaphase (Figure 3.8.). Noticeably, it starts localising on or around the chromosomes from telophase, when the nuclear envelope re-forms and KIF18B would be able to move to the nucleus through NPCs.

Surprisingly, in cytokinesis, a proportion of KIF18B clearly localises to the midbody (Figure 2.8.). However, any role for KIF18B in cytokinesis is not yet been reported.

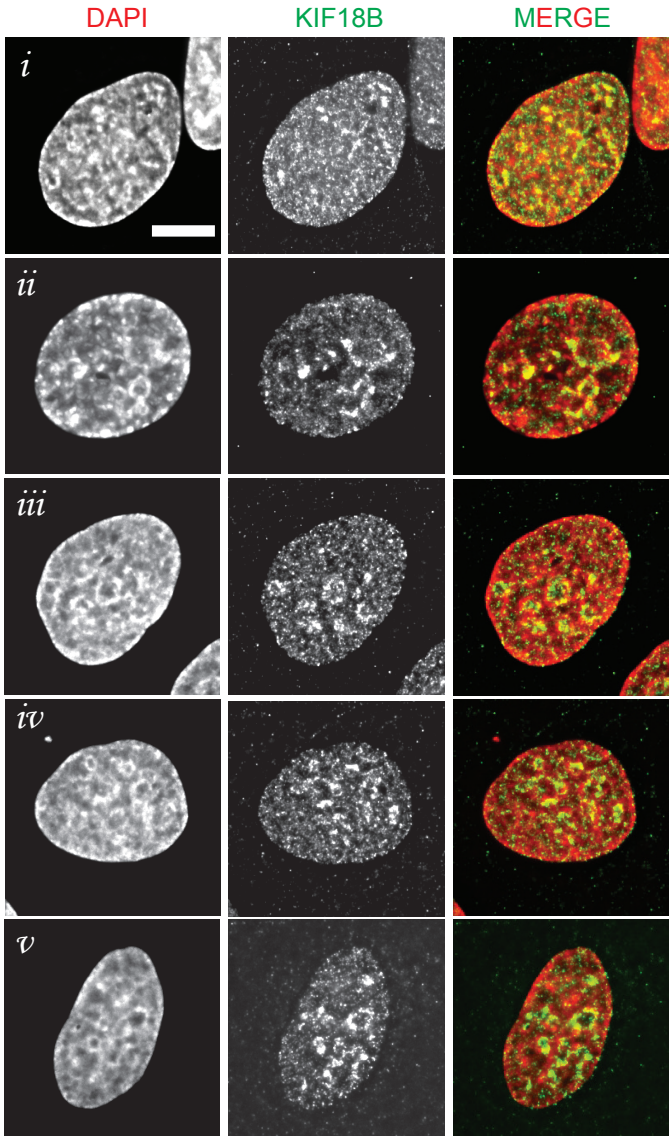

Figure 2.7. KIF18B co-localisation with intense DAPI stained areas in the nucleus in interphase human cells

Five representative images of HeLa cells in interphase (*i* to *v*), showing the distribution of KIF18B intensity in the nucleus. KIF18B staining is indicated in green and the DAPI staining is shown in red. The scale bar represents 25µm.

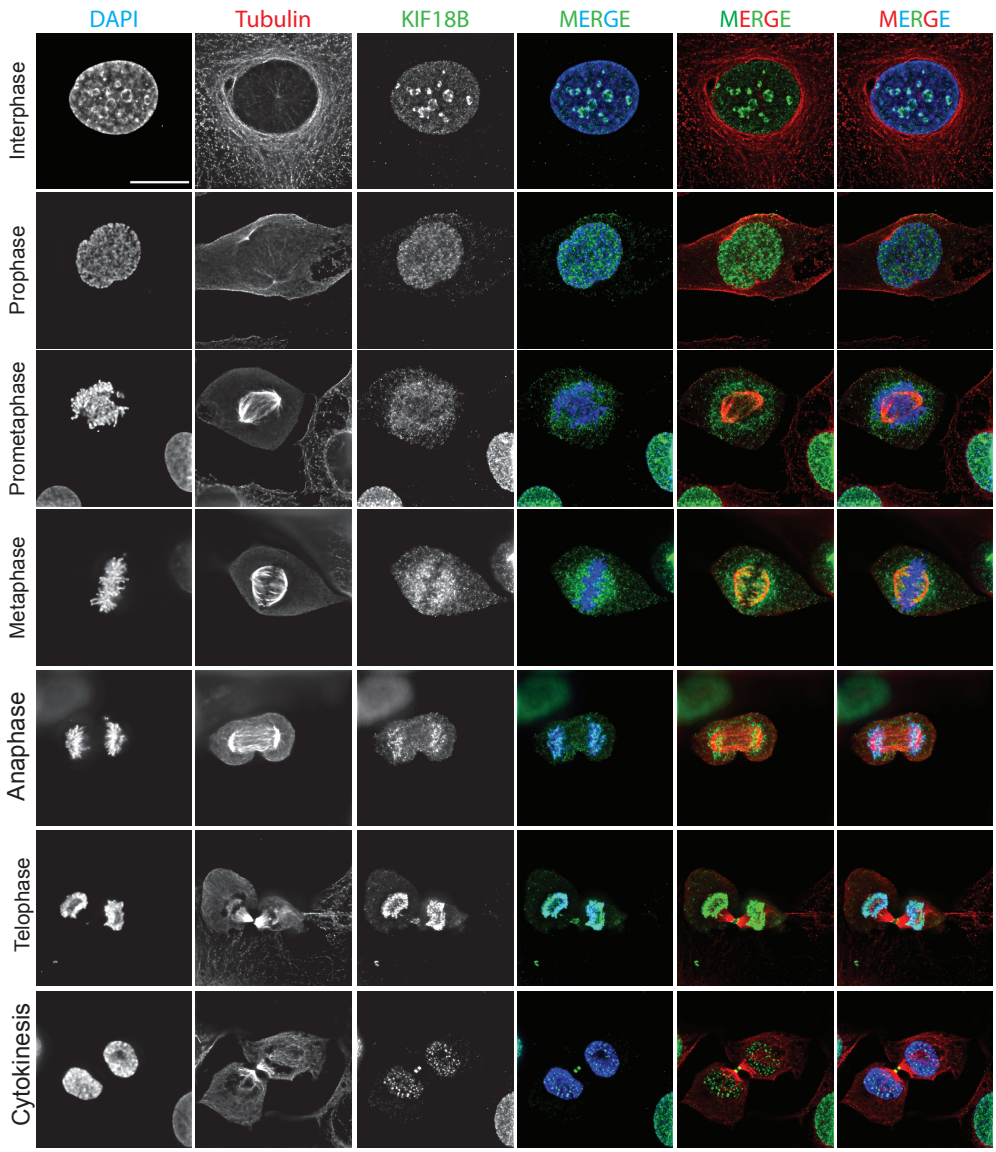

Figure 2.8. KIF18B staining at different cell cycle stages

Representative immunofluorescence staining of KIF18B and Tubulin in HeLa cells, at different cell cycle stages. DAPI staining is shown in blue, Tubulin in red and KIF18B in green as indicated. DAPI and KIF18B are merged in the fourth column, Tubulin and KIF18B are merged in the fifth column and in the last column, all channels are merged. The scale bar is 25μm. The cell cycle stages are shown on the left of each row.

2.4.4. KIF18B localises to the midbody and primary cut site

While studying KIF18B at different cell cycle stages on synchronised and asynchronised HeLa, as well as U2OS cells, we noticed the localisation of KIF18B to the midbody during cytokinesis (Figure 2.8.).

To further investigate KIF18B localisation to the midbody during cytokinesis, we utilised the hTERT-RPE1 cell line, which is karyotypically normal immortalised cell line and expected to exhibit more normal phenotypes. RPE1 cells stained for KIF18B and tubulin, the cleavage furrow ingression, and midbody stage cells were recognised by the appearance of a distinctive tubulin signal along the cytoplasmic canal. Imaging cytokinetic cells, KIF18B was consistently observed at the midbody from early to late cytokinesis (Figure 2.9.). We noticed that KIF18B localisation is dynamic during cytokinesis. It is accumulated at the midbody in early cytokinesis. In later stages of cytokinesis, a proportion of KIF18B moves toward either side of the midbody, also known as midbody arms (Figure 2.9.).

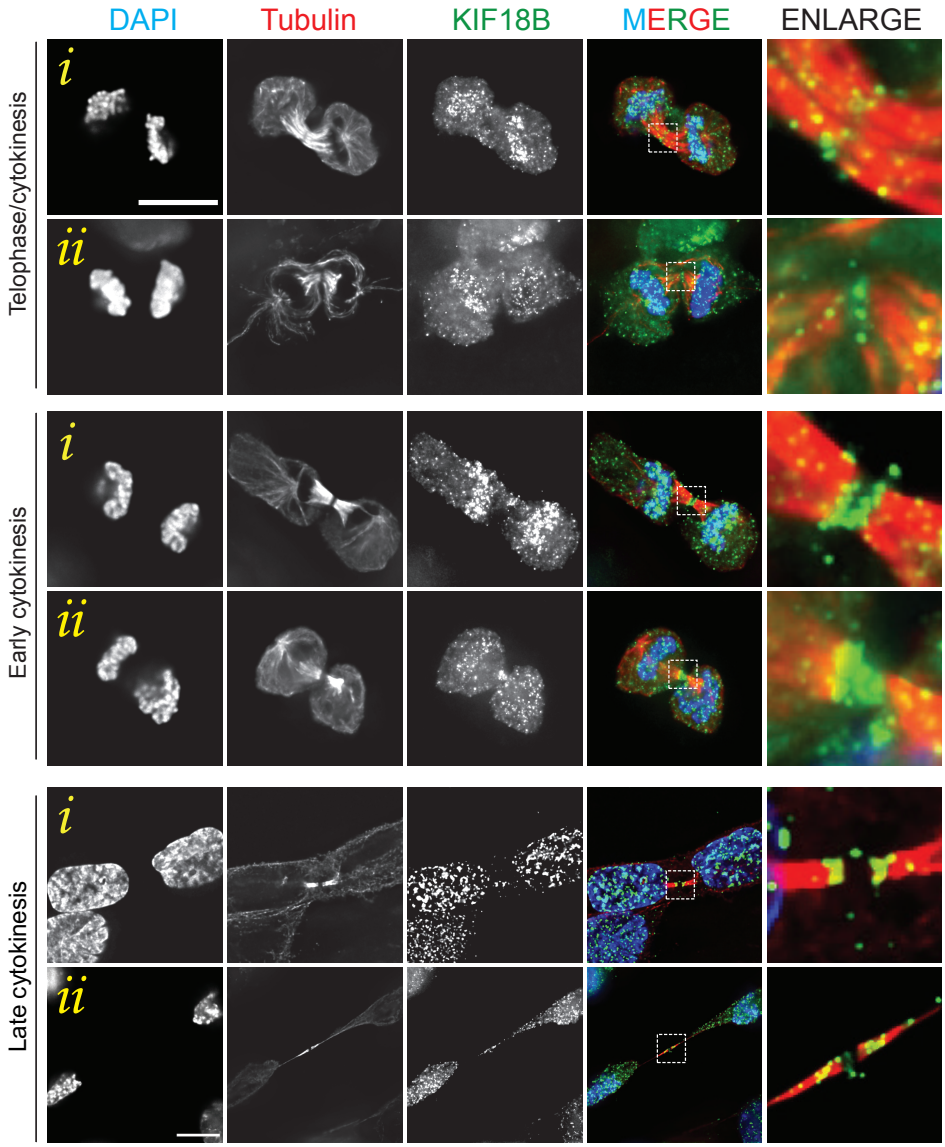

Figure 2.9. KIF18B localises at the midbody in cytokinesis

hTERT-RPE1 cells in different cytokinetic stages as indicated on the left were stained for KIF18B and Tubulin. DAPI staining is shown as blue (1st column), Tubulin is shown in red (2nd column), and KIF18B is presented in green (3rd column). They are all merged in the fourth column. The fifth column is the enlargement of the selection in the fourth column. Images from early to late cytokinesis showing the dynamic localisation of KIF18B to the midbody. " *i* " and " *ii* " represent two examples of each cytokinesis stage. The scale bar represents 25 µm.

To confirm the KIF18B localisation at the midbody, we co-stained RPE1 cells for KIF18B and Aurora B, as a protein with a distinctive localisation at the midbody (Figure 2.10.). Aurora B is a relatively well characterised mitotic kinase, which is localised at midbody arms throughout cytokinesis and activated from early mitosis and in

association with its partners in the chromosome passenger complex regulates the abscission timing (Carmena et al., 2012).

While Aurora B localises merely on the midbody arms during cytokinesis, we found that KIF18B localisation varies from early to late cytokinesis (Figure 2.10.). Comparing the localisation of KIF18B and Aurora B, they appear to have some overlap in early cytokinesis as KIF18B is mostly localised to the midzone, the midbody centre, and Aurora B mostly localises to the midbody arms. However, in late cytokinesis, they show the same localisation pattern and co-localise at the midbody arms, while a small proportion of KIF18B remained at the midzone.

As EB1 is essential for KIF18B targeting microtubules plus ends and regulating the dynamics of the microtubule, in mitosis (McHugh et al., 2018), we explored the localisation of EB1 at the midbody during cytokinesis to see if it does have any connection to KIF18B at the midbody as well as the microtubules plus ends (Figure 2.11.). We imaged RPE1 cells stained for EB1 and Tubulin from prometaphase to late cytokinesis. At prometaphase and anaphase, EB1 was mainly detectable at its known location at the plus ends of the astral microtubule (Figure 2.11.). In anaphase, we found EB1 with relatively intense localisation at the centre of the spindle, appointed to the kinetochore microtubules. Images of the cytokinetic progression showed EB1 localises to the midbody, which two examples are showed (Figure 2.11.). This result suggests the requirement of EB1 for KIF18B localisation at the midbody as well as astral microtubule plus ends.

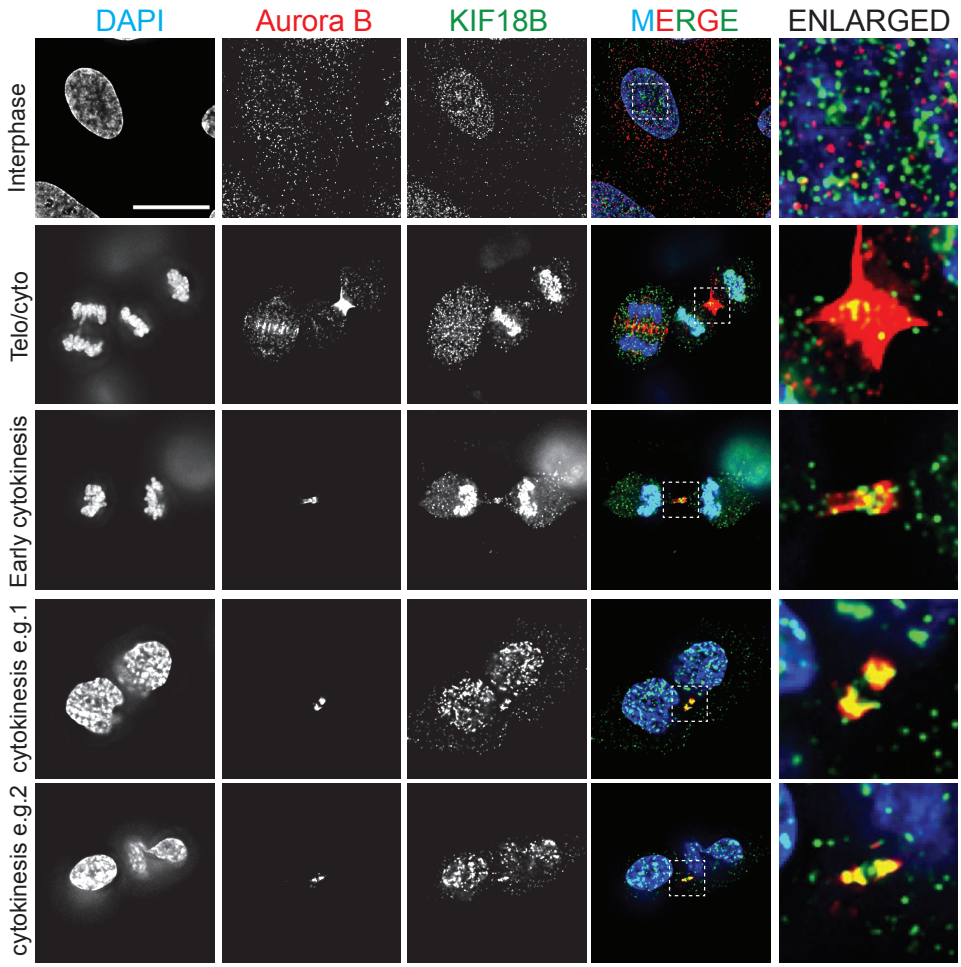

Figure 2.10. KIF18B and Aurora B localisation during cytokinesis

Immunofluorescence of KIF18B and Aurora B in hTERT-RPE1 cells. DAPI staining is shown in blue (1st column), Aurora B is presented in red and KIF18B in green (2nd and 3rd column, respectively). In the fourth column, they all merged. The fifth column is the enlargement of selection in the fourth column. At early cytokinesis the KIF18B and Aurora B are overlapping and in later cytokinetic stages (e.g., 1&2) they co-localised at midbody arms. The scale bar represents 25μm.

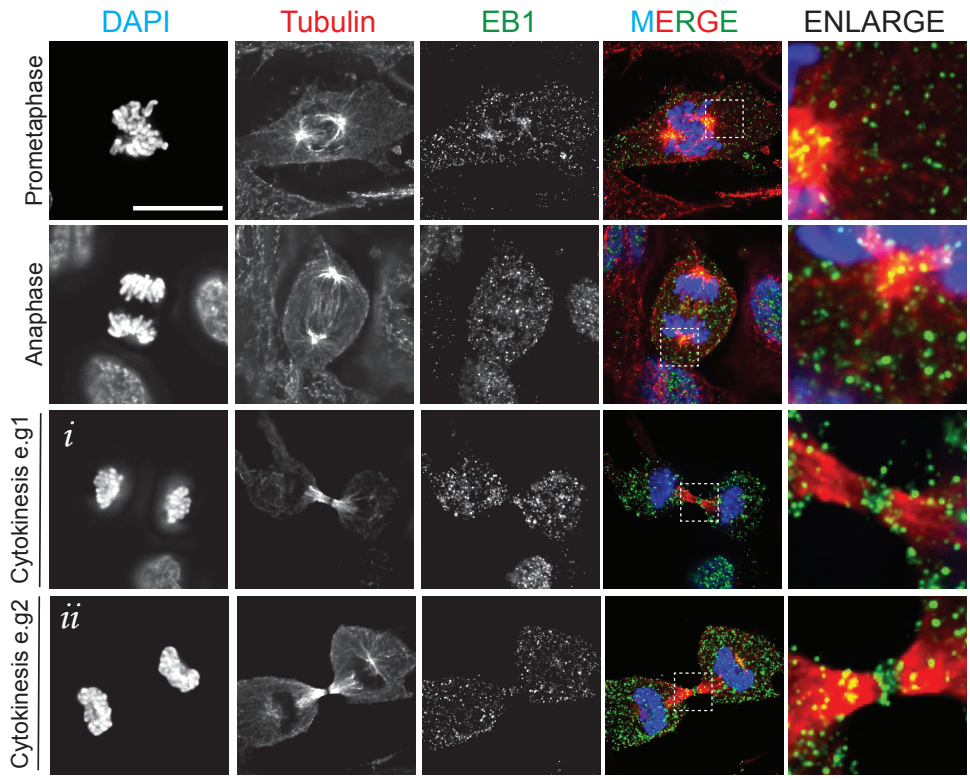

Figure 2.11. EB1 localisation in different cell cycle stages.

Immunofluorescence of EB1 and Tubulin in hTERT-RPE1 cells in mitosis and cytokinesis. DAPI staining is presented in blue (1st column), Tubulin is shown in red (2nd column), and EB1 in green (3rd column). In the fourth column, the three of them are merged. The fifth column is the enlargement of the selection in the fourth column. As shown in prometaphase and anaphase, EB1 localises at astral microtubule plus ends appointed position. Two examples of cytokinetic cells (*i* and *ii*, in the 3rd and 4th row) are showing EB1 localisation at the midbody. The scale bar represents 25μm.

Abscission is the final step of cytokinesis, characterised by the occurrence of a cut in flanking region of the midbody in one of the arms (Steigemann et al., 2009).The abscission results from the coordinated action of a set of proteins acting as a cascade leading to the constriction of the action-myosin cortex. The ESCRTIII complex is the key for successful cytoskeletal structure removal and the plasma membrane cleavage (Fededa and Gerlich, 2012). The antiparallel microtubule bundle, which is densely compacted in the cytoplasmic canal, must be cut by the microtubule severing protein, Spastin (D'Avino et al., 2015). We also observed KIF18B localises to the cut site at late cytokinesis (Figure 2.12.). As KIF18B is recognised as a destabiliser for microtubules that depolymerises them at their plus

ends, the presence of KIF18B at the primary cut site is an indicative of a potential role for KIF18B in abscission.

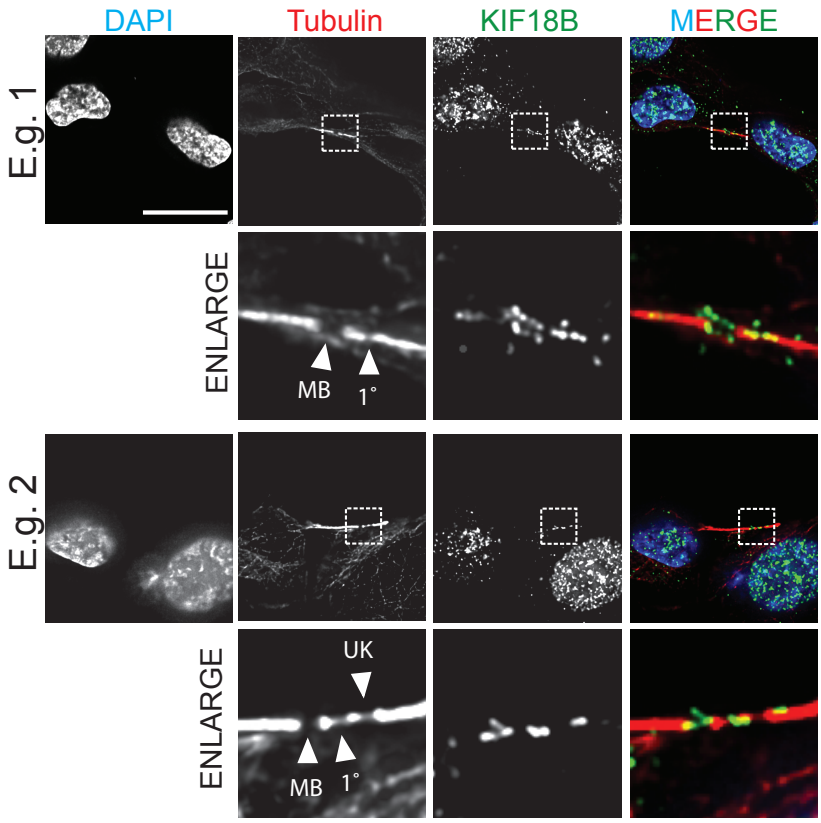

Figure 2.12. KIF18B localisation to abscission cut site during cytokinesis

Immunofluorescence of KIF18B and Tubulin in hTERT-RPE1 cells. DAPI staining is presented in blue (1st column), Tubulin is in red (2nd column), and KIF18B in green (3rd column). The three images are merged in the last column. The second and fourth rows are showing the enlarged image which is indicated as a white square in images. Images of the final stage of cytokinesis, abscission are shown as two examples. “MB”: midbody, “1°”: primary cut site, “UK”: unknown. The scale bar represents 25μm.

2.4.5. Preliminary investigation on the regulation of KIF18B localisation to the midbody

We have shown KIF18B localises to the midbody as well as EB1, from early to late cytokinesis, and compared the localisation pattern of KIF18B and Aurora B at the midbody (Figure 2.10., 2.11.). Since Aurora B is involved in all pathways related to cell division and abscission and in another word, it is known as the chief regulator of abscission (Barr and Gruneberg, 2007; van der Waal et al., 2012), we investigated whether KIF18B localisation to the midbody is regulated by Aurora B (Figure 2.13.).

In addition, the checkpoint effector Checkpoint Kinase 1 (CHK1) has also been reported to regulate cytokinesis and in coordination with Aurora B, ensures appropriate chromosome segregation (Peddibhotla et al., 2009). Therefore, we also tested if the KIF18B localisation at the midbody is regulated by CHK1 protein (Figure 2.13.).

Moreover, Both DNA-PK and ATM have been located in the midbody (Lee et al., 2011; Yang et al., 2011). Therefore, we assessed the potential regulation of KIF18B by the three DDR PIKKs including ATM, ATR (ATM- and Rad3-related), and DNA-PK (Figure 2.13.).

We stained RPE1 cells for KIF18B and tubulin after inhibition of CHK1 and Aurora B as well as ATM, ATR, and DNA-PK kinase activity via the treatment of the cells with chemical inhibitors. The average KIF18B signal intensity at the midbody was reduced upon Aurora B inhibition to one-tenth but, not significantly changed upon CHK1 inhibition. The DNA-PK and ATM inhibition caused more than one-third reduction in the KIF18B signal intensity at the midbody, while ATR inhibition had no effect (Figure 2.13.).

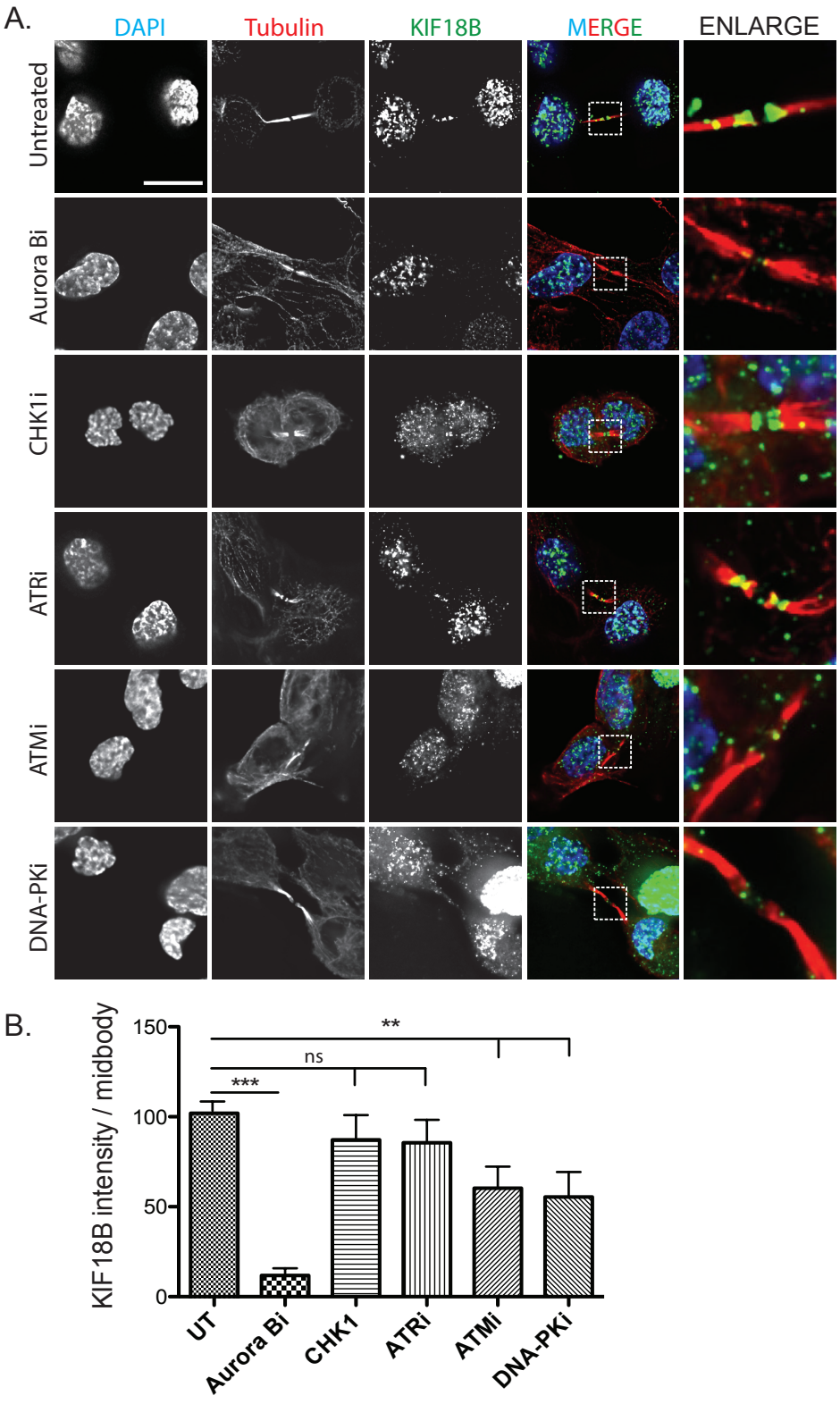
A.
DAPI
Tubulin
KIF18B
MERGE
ENLARGE
Untreated
Aurora Bi
CHK1i
ATRi
ATMi
DNA-PKi
B.
KIF18B intensity / midbody
150
100
50
0
**
ns
***
UT
Aurora Bi
CHK1
ATRi
ATMi
DNA-PKi

Figure 2.13.

Figure 2.13. KIF18B localisation is depending on the Aurora B, ATM, and DNA-PK kinase activity

(A) Representative images of immunofluorescence of Tubulin and KIf18B in cytokinetic RPE1 cells in different conditions including untreated and treated with Aurora B, CHK1, ATR, ATM, and DNA-PK inhibitors, before fixation as indicated on the left. DAPI staining presented as blue, Tubulin as red and KIF18B as green (1st, 2nd and 3rd column, respectively). The three channels are merged in the fourth column. The fifth column is the enlargement of the selection in the fourth column. The scale bar represents 25μm. (B) The quantification of KIF18B intensity at the midbody including midzone and arms in all different conditions. The quantification was performed by Fiji ImageJ version 1.52n software through defining a region of interest at the midbody and measurement of the KIF18B signal intensity within the region of interest (ROI). 10 cytokinetic cells were tested in each condition and each bar in the graph shows the mean of KIF18B signal intensity in each condition. The error bars represent the SEM of 3 independent repeats. Student's t-test analyses revealed the results were significant ***P<0.001, **P<0.01, and not significant (ns).

2.4.6. Loss of KIF18B results in fewer cytokinetic cells

To further investigate the role of KIF18B in cytokinesis, we carried out cytokinetic profiling upon KIF18B depletion. In this assessment, we also depleted ATR and NUP153 as controls for conditions with decreased and increased number of cytokinetic cells, respectively (Mackay et al., 2010; Okowa, 2018).

ATR, as one of the apical kinases, regulating DDR, is also a central player in several checkpoint pathways aiming to preserve the genome integrity during the cell cycle (Friedel et al., 2009). Loss of ATR also results in failed abscission and the formation of binucleated cells (Eykelenboom et al., 2013). Our laboratory has recently identified a non-canonical role for ATR in the regulation of abscission timing (Okowa, 2018). ATR was demonstrated to localise to the midbody at cytokinesis to delay abscission while interacting with the ESCRT III subunit CHMP4B. Chemical inhibition or genetic depletion of ATR reduced the number of cells in cytokinesis as cells progressing more quickly through abscission upon loss of ATR function (Okowa, 2018).

Nucleopore Complex (NPC) proteins are the components of nucleopore baskets essential for trafficking mRNA and proteins between the nucleus and cytoplasm (Mackay et al., 2010). It has been shown that the disruption of NPC by depletion of NUP153, one of the main components of NPC, results in Aurora B mediated abscission

delay. This acts as a checkpoint mechanism for cytokinetic progression and the increase in cytokinetic cells (Mackay and Ullman, 2011).

Performing cytokinetic profiling, HeLa cells were fixed and stained for tubulin and ANCHR, a marker of midbodies, 48 h after depletion of ATR, NUP153, and KIF18B (Figure 2.14.). Cells in cytokinesis were identified by the intense tubulin signal at the midbody canal. Moreover, the localisation of ANCHR to the midbody served as an indicator for cytokinesis (Figure 2.14.). Depletion of ATR reduced the number of cells in cytokinesis by half, compared to the control. The number of cytokinetic cells doubled upon NUP154 depletion compared to control.

KIF18B depletion resulted in reduction in the number of cytokinetic cells similar to that of ATR depletion. This preliminary data is consistent with a possible role for KIF18B in cytokinesis.

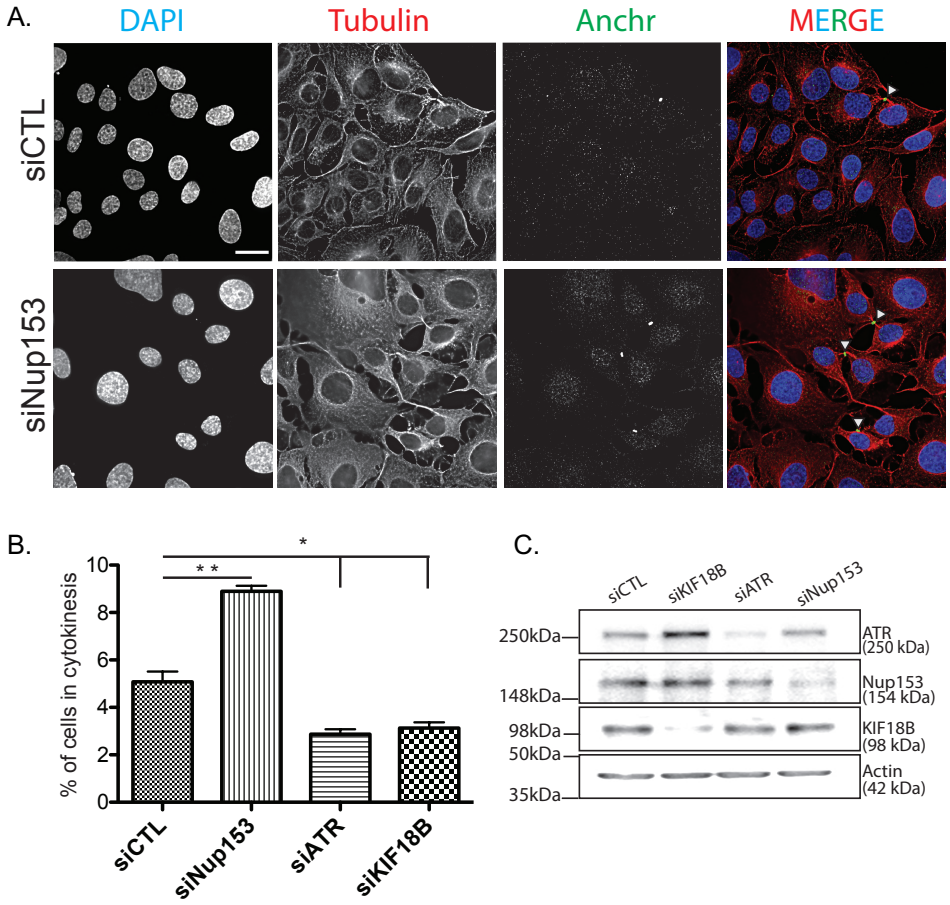

Figure 2.14. Loss of KIF18B reduces the number of cells in cytokinesis

(A) Representative images of immunofluorescence of Tubulin and ANCHR, in control (transfected with siCTL) and NUP153 depleted (transfected with siNUP153) HeLa cells. ANCHR is a marker of the midbody and indicative of cytokinesis. The images of ATR and KIF18B depleted cells are not shown as cytokinetic cells were barely detectable. The scale bar represents 25μm. (B) Quantification of the number of cells in cytokinesis in control and upon KIF18B, ATR, and Nup153 depletion. Cells in cytokinesis were scored manually. The bars in the graph show the average number of cytokinetic cells from three independent experiments. The number of cells per experiment was ≥400. Student t-test used for comparison of the results of treated cells with control which showed the significance with *P <0.1 and **P <0.01. (C) The western blot for confirmation of the efficient knockdown of proteins is presented, which is performed according to the methods described in the Materials and Methods section using the indicated primary antibodies. Actin was used as a loading control.

2.5. Discussion

In this chapter, we studied the subcellular localisation of KIF18B, in normal cells and the regulation of its expression throughout the cell cycle.

The staining of three different cell lines for KIF18B showed different intensities. Therefore, we checked if KIF18B is cell cycle-regulated. The cell cycle regulation of KIf18B proved through three different examination methods. This was not the first time showing KIF18B cell cycle regulation. It has been examined by Lee et al. as a cell-cycle regulated kinesin when they published the first paper exclusively about KIF18B (Lee et al., 2010). However, their report was not quite convincing as the WB quality was unfavourable and their intervals of cell harvesting after double thymidine block look insufficient. Moreover, they have used their own developed antibody for KIF18B which was never tested before, so this result required to be confirmed with a different antibody. We also found KIF18B to be cell-cycle regulated but in a slightly different way from that described by Lee et al., They argued KIF18B is undetectable in G1 and at G1/S transition and started to appear at G2/M in a similar pattern with Cyclin B while we found KIF18B quite detectable in G1 and at G1/S transition with a steady increase as it progresses toward G2 and M to reach the peak of expression. However, Cyclin B shows an increase in late G2 and M but actually, it peaks in mitosis while KIF18B has an ascending slope toward mitosis.

Moreover, we found KIF18B and Cyclin B maximum expression around 10 to 12 hours post thymidine release while Lee et al. showed the peak at 9 hours which can be attributed to differences between cell line batches, the probable difference in methodology, and the level of cell synchronization.

The KIF18B localisation within the cell throughout the cell cycle is highly variable and complex. In interphase, unlike most kinesins, KIF18B showed to be predominantly nuclear which is consistent with

previous studies (Lee et al., 2010; Tanenbaum et al., 2011) however, we observed a higher KIF18B signal intensity around the dark areas of the nucleus, reflective of nucleoli (Pontvianne et al., 2016) and dense DAPI stained areas, reflecting the possibility of correlation with heterochromatic DNA and suggestive to have a role in the nucleus.

In mitosis, however, it is only described to localise at the astral microtubule plus ends (Lee et al., 2010; Tanenbaum et al., 2011), we observed KIF18B on the microtubules everywhere in the cell with slightly more concentration on astral microtubule plus ends. This observation is in accordance with the previously reported movement of KIF18B on microtubules with a relatively high speed (635 ± 163 nm/s; mean ± s.d.) without depolymerizing them (Tanenbaum et al., 2014) and also consistent with a recent study reporting KIF18B as a highly processive protein, able to walk along the microtubules and once reached the microtubule plus ends, lands there for a considerable time (McHugh et al., 2018).

Interestingly, we observed KIF18B localisation to midbody in cytokinesis, which to the best of our knowledge, is not reported in any of the literature so far. KIF18B showed a dynamic localisation to the midbody from early to late cytokinesis by moving from the midzone in early cytokinesis to the midbody arms at the later time points. We also showed KIF18B localisation at the primary cut site, forming prior to final abscission.

EB1 and MCAK are reported as KIF18B interacting partners, coordinating with KIF18B in astral microtubule length regulation (McHugh et al., 2018; Stout et al., 2011; Tanenbaum et al., 2011). EB1 is required for KIF18B localisation on the plus end of microtubules. In this regard, spindle dislocation is shown as the consequence of KIF18B mis-localisation due to EB1 depletion (McHugh et al., 2018). We have also shown that EB1 localises to the midbody. This preliminary data proposes a probable role for KIF18B coordinated with EB1 in abscission progress. The hypothesis is that KIF18B localises to the midzone and then midbody arms, accompanied by EB1 to

depolymerise the microtubule filaments and facilitate the final cleavage between the two daughter cells. Investigating the cytokinetic cells stained for MCAK and KIF18B would be able to better describe the mechanism of KIF18B's action at the midbody.

The ability of microtubule-binding of the KIF18B's C-terminus depends on phosphorylation by Aurora kinases. Inhibition of the kinase activity of Aurora kinases will lead to longer astral microtubules in mitotic cells, regarding the known conventional role of KIF18B (McHugh et al., 2018). Similarly, we showed KIF18B to have a 10-fold decrease in localisation at the midbody upon Aurora B kinase activity inhibition.

Aurora kinases including Aurora B shown to interact with CHK1, policing the abscission timing (Mackay and Ullman, 2015; Zhang and Hunter, 2014). On the other hand, CHK1 is required for launching the DNA damage checkpoints (Patil et al., 2013; Zhang and Hunter, 2014). As we tested, the KIF18B signal intensity at the midbody of cytokinetic cells did not change significantly upon CHK1 inhibition. This result suggests, the Aurora B dependent regulation of KIF18B at the midbody is not regulated by CHK1 dependent Aurora B phosphorylation. This refers to uncharacterized signalling pathways upstream of Aurora B which is not fully understood yet (Mackay and Ullman, 2015)

ATR is also implicated to contribute to abscission timing in the interest of genome integrity preserving while localising at the midbody (Eykelenboom et al., 2013; Mackay and Ullman, 2015; Okowa, 2018). Moreover, ATR has an important role in CHK1 activation and the progress of the final steps of cytokinesis. As we tested, KIF18B localisation at the midbody was not ATR dependent.

An Aurora B dependent phosphorylated form of ATM at Serin 1403 is reported to localise to the midbody. This ATM phosphorylation is required for ATM mitotic activity in undamaged normal cells (Yang et al., 2011). The mitotic spindle structure is shown to be affected by either chemical ATM kinase activity inhibition or genetically ATM

depletion (Palazzo et al., 2014). The loss of ATM will result in mitotic abnormalities such as chromosome misalignment, multipolar spindles, scrambled astral microtubules, and spindle dislocation (Palazzo et al., 2014; Shen et al., 2005). These features as the consequence of loss of ATM activities resemble the role of KIF18B mitosis, maintaining the length of astral microtubule and spindle orientation (McHugh et al., 2018; Tanenbaum et al., 2011), proposing a possible relationship between KIF18B and ATM activities during mitosis confirmed by the reduction in KIF18B signal intensity at the midbody by ATM inhibition.

The phosphorylated form of DNA-PK at T2609 is reported to localise at the centrosomes, kinetochores, and midbody during mitosis (Lee et al., 2011) Kyung-Jong Lee for the first time reported that the DNA-PK has a critical regulatory role in mitosis in normal cells, in addition to its established role in DNA damage response. Mitotic-induced phosphorylation of DNA-PK is closely related to spindle conformation at centrosomes and kinetochores. Depletion or inhibition of DNA-PK will result in chromosome misalignment and aneuploidy due to mitotic catastrophe as the mitotic progression will be perturbed (Lee et al., 2011). The significant reduction in KIF18B signal intensity upon DNA-PK inhibition could be indicative of the role of DNA-PK in mitosis regulation that affects the KIF18B localisation at the midbody as it modulates microtubule dynamic and chromosome segregation.

DNA-PK is recently identified as a negative regulator of ATM in DNA damaged cells (Liu et al., 2019). In addition, another study showed downregulation of ATM is a common feature of DNA-PK$^{-/-}$ cells (Neal and Meek, 2019). Accordingly, the effect of DNA-PK and ATM inhibition on KIF18B midbody localisation could be related to DNA-PK and ATM interactions as they can phosphorylate each other, or a caveat would be that they conduct their effect separately according to their DDR-independent roles in mitosis. Nevertheless, all inhibitory functions of the chemical inhibitors used requires to be approved by genetically depletion of the proteins as well.

Regarding the localisation of KIF18B at the midbody, we have done a cytokinetic profile upon KIF18B depletion in RPE1 cells. Our result revealed the reduction in the number of cytokinetic cells upon KIF18B depletion, possibly attributed to the incapability of the cells in entering cytokinesis reflecting the role of KIF18B in earlier time points in mitosis; maintaining the astral microtubule length and spindle orientation. Although, it is shown that KIF18B and MCAK cooperating to regulate the astral microtubules dynamic and co-depletion of both does not have additional effects on the microtubule length, indicating their epistatic interaction (McHugh et al., 2018). Another explanation would be the reduction in the number of cytokinetic cells is due to the role of KIF18B in abscission timing, proposing KIF18B to act as a checkpoint for abscission. An auxin-inducible degron (AID) system which is ideal as a tool to achieve rapid and inducible protein degradation (Sathyan et al., 2019), can be used to target KIF18B in synchronised cells, to better define the role of KIF18B in cytokinesis and particularly in abscission.

Chapter 3: KIF18B interacts with 53BP1 to promote an efficient double-strand break repair

3.1. Summary

53BP1 is a DNA damage response mediator, which plays an important role in repair pathway choice and inhibiting HR. Inhibition of resection is one of the 53BP1 functions in preserving genome integrity (Bunting et al., 2010). As it determines the efficiency of PARPi treatments of BRCA1 deficient cancers (Bouwman et al., 2010), it is privileged in DNA damage response proteins to be investigated.

Investigating the mechanism of 53BP1 involvement in DNA damage, a quantitative proteomic screen (SILAC) was carried out previously in our lab to study the 53BP1 interactome and discover potential functions of 53BP1 (see Appendix IV.). Interestingly, a kinesin-8 family member, KIF18B, highly scored as a 53BP1 interacting partner. We have shown that KIF18B colocalises with 53BP1 at IRIF in gamma-irradiated cells and nuclear bodies in undamaged cells. Furthermore, impairment of 53BP1 focal recruitment to IRIFs and TIFs is shown to be dependent on KIF18B. H4K20me2 is considered as one of the influential chromatin modifications required for 53BP1 focal recruitment at DSBs. We ruled out if the dependence of efficient 53BP1 recruitment on KIF18B is through affecting H4K20 dimethylation. 53BP1 interacting domain (TIM) as well as the motor domain of KIF18B shown to be involved in de-protected telomere fusion as well as 53BP1 recruitment to Telomere Dysfunction-Induced Foci, TIFs. Additionally, we showed microtubules disruption and KIF18B depletion are having an epistatic effect on 53BP1 efficient focal recruitment at IRIF.

Based on the involvement of the KIF18B motor domain in DDR besides its localisation at DNA damaged sites, we propose probable microtubule mediated KIF18B motor activity in 53BP1 dependent damage response process.

3.2. Introduction

Double-Strand Breaks (DSBs) are the most destructive damage to DNA. Depending on the extent of the damage and the cell's ability to repair it, the outcome ranges from a fully functional genome to cell death or cancer (Harper and Elledge, 2007).

Following the DSBs formation, a subset of proteins will be recruited to the damage sites to sense, mediate and conduct the repair via two main pathways, H and NHEJ (Schooley et al., 2012b).

The tumour suppressor 53BP1 is a key mediator protein in DNA damage response (DDR) playing an important role in repair pathway choice and promoting NHEJ by repressing the resection required for HR (Bekker-Jensen and Mailand, 2010).

The precise mechanism of 53BP1 recruitment to and retention at DSB has been the subject of much investigation but is still not clearly understood.

Histones PTMs involved in 53BP1 recruitment to the DSB are reported to be mainly H4k20me2 and H2A(X)K15ub, interacting with the Tudor domain of 53BP1. The histone H4 mono-, di- and tri- methylation is mediated by KMT5A, KMT5B, and KMT5C methyl transferases respectively (Girish et al., 2016; Nishioka et al., 2002).

In addition to promoting the NHEJ pathway, 53BP1 has reported roles in telomere maintenance and immunoglobulin V(D)J recombination and class switch recombination (Dimitrova et al., 2008; Ward et al., 2004). Moreover, it has been recently shown that 53PB1 promotes microtubule-dependent DSBs mobility through interaction with the LINC complex, mediating the fusion of de-protected telomeres (Lottersberger et al., 2015).

In mammalian cells, the shelterin complex protects telomeres from being considered as DNA broken ends and consequently, activation of the damage response cascade (Palm and de Lange, 2008). Upon removing the shelterin complex by TRF2 depletion, Telomere -Induced

Foci (TIFs) will form at the site of de-protected telomeres (Takai et al., 2003). Since these de-protected telomeres are considered as DSBs, they will ultimately be fused through the NHEJ pathway mediated by 53BP1 in an ATM-dependent manner (Dimitrova et al., 2008).

To elucidate 53BP1 biology, a quantitative proteomic screen was performed in our lab on affinity-purified 53BP1 extracted from unirradiated and irradiated exponentially growing chicken DT40 cells. In addition to previously identified 53BP1 interacting partners, KIF18B, a kinesin 8 family member, was identified as a novel interactor (Frizzell, 2015) (See Appendix IV.). More recent work in our laboratory has established a direct interaction of KIF18B via a short motif near its C-terminus with the Tudor domain of 53BP1(Frizzell, 2015). Hence, the 53BP1 Tudor domain interacting motif has been dubbed, the Tudor Interacting Motif or TIM.

Kinesins are members of a molecular motor superfamily and have an essential role in cell survival and a multitude of processes involved in the active movement (Vale, 2003). Involvement of a kinesin in the DNA damage response has been suggested before, as KIF4A was reported to be involved in BRCA2/RAD51 mediated H(Wu et al., 2008). KIF4A also retaining genome stability through maintenance of heterochromatin by regulation of ADP-ribosylation of core and linker histones. Moreover, KIF4A is required for chromatin assembly proteins recruitment (Mazumdar et al., 2004).

We found KIF18B, which is mainly nuclear in interphase, colocalises with 53BP1 at IRIF as well as nuclear bodies in G1 cells. Moreover, we have shown KIF18B is required for efficient 53BP1 focal recruitment to IRIFs and TIFs through direct interaction of KIF18B ‘s TIM domain at the C-terminal with 53BP1 Tudor domain. We uncovered the involvement of KIF18B ‘s motor domain as well as the TIM domain in the DSB repair process.

3.3. Materials and methods

3.3.1. Cell Culture

Cells were cultured at 37°C in a humidified atmosphere of 5% CO^2. U2OS, HeLa and HEK293T cells were cultured using DMEM supplemented with 10% FBS (Sigma Aldrich) and 1% penicillin-streptomycin (Sigma Aldrich). hTERT immortalized RPE-1 cells were cultured in DMEM-F12 media supplemented with 10% FBS and 1% penicillin-streptomycin (Sigma Aldrich). HeLa (Tet inducible) cells were cultured in DMEM supplemented with 10% Tet free FBS (approved to be tetraCycline free) and 1% penicillin-streptomycin (Sigma Aldrich).

3.3.2. Drug treatments

U2OS cells at 70-80% confluency were treated with a concentration of 100ng/ml Nocodazole and 200 ng/ml Taxol, 30 minutes before 3Gy irradiation. Cells were harvested for western blotting and immunofluorescent staining 1h post-irradiation.

3.3.3. Protein Extraction

Protein extracts were prepared by lysing cells in lysis buffer (50mM Tris-HCl, 0.5% Triton X-100, 150mM NaCl, 10% glycerol, 1mM MgCl2, protease and phosphatase inhibitors cocktail, Abcam (ab201119)) and a 1:1000 dilution of Benzonase nuclease (Sigma Aldrich) for 45 min at 4°C. Samples were then centrifuged for 20 min at 14,000 rpm at 4°C, the supernatant was then used for downstream applications. The protein concentrations were measured using Bradford reagent.

3.3.4. Western Blotting

The concentration of proteins was adjusted to be the same and diluted with 4X sample buffer (2.0 ml 1M Tris-HCl pH 6.8, 0.8 g SDS, 4.0 ml 100% glycerol, 0.4 ml 14.7 M β-mercaptoethanol, 1.0 ml 0.5 M EDTA, 8 mg Bromophenol Blue). The separation of proteins performed using sodium dodecyl sulphate polyacrylamide gel electrophoresis (SDS-PAGE). Proteins were transferred to a nitrocellulose membrane using 0.35 mAmps for 1h on a BioRad power supply at 4°C. Membranes were blocked in 5% milk-TBS with 0.1% Tween20 for 20 min at RT. The conditions for probing with the primary antibody are mentioned in Table 3.1. Following overnight probing for the primary Ab, membranes were washed three times in TBST buffer and subsequently incubated with the relevant secondary antibody at 1:5000 dilution in 5% milk-TBS with 0.1% Tween20 for 60 min at RT.

Specifically, to probe the membrane with H4K20me2 antibody, following the protein transfer, the membrane was blocked in 10% milk-TBST for 1h then incubated with the H4K20me2 diluted 1/1000 in 5% milk-TBST for 1h. One wash with H_2O will be followed by three washes in TBST and incubation with secondary antibody for 1h. Three washes with TBST and 5 min incubation with ECL and finally 3 washes with H2O would be the last step.

The membrane imaged with Fusion FX Vilber imager and H4K20me2 bands intensity were quantified by Fusion software v18.05. The Band Analysis tools of software were used to select and determine the background-subtracted density of the bands in all the gels and blots.

Table 3.1. List of antibodies and conditions used for western blotting

Antibody	Dilution	Blocking	Species	Manufacturer	Catalogue Number
53BP1	1:10000	5% milk	Rabbit	Bethyl	A300-272A
53BP1	1:10000	5% milk	Rabbit	Novus	NB100-304
KIF18B	1:1000	5% milk	Rabbit	Sigma Aldrich	HPA024205
Actin	1:5000	5% milk	Rabbit	Sigma Aldrich	A2066
AcTubulin	1:2000	5% milk	Mouse	Millipore	MABT868
TRF2	1:1000	5% milk	Rabbit	Novus	NB110-57130
H4k20me2	1:10000	10%milk	Rabbit	Millipore	07-367
Goat Anti-Rabbit IgG	1:5000	5%milk	Goat	Thermoscientific	31460
Anti-mouse IgG	1:5000	5%milk	Rabbit	Thermoscientific	31450

3.3.5. Immunofluorescence staining

The coverslips were sterilized under UV for 20 min before seeding cells. Counted $1.5x10^5$ to $2.5x10^5$ (depending on the purpose of experiment) U2OS, HeLa, or hTERT RPE-1 cells were grown on a sterile coverslip in DMEM with 10% FBS and 1% penicillin-streptomycin. 24 to 48 h following the seeding, coverslips which cells were grown on them, rinsed twice with PBS. Cells were fixed in 4% PFA for 10 min at RT, or in ice-cold methanol for 20 min at -20°C depending on the antibody staining required. Coverslips were then washed three times in PBS and permeabilised with 0.25% Triton X-100 for 5-10 min at room temperature. The cells were again washed in PBS three times before blocking in 5 % BSA for 1h at RT or overnight in 4°C and followed by 1h at RT. The primary and secondary antibody staining conditions are mentioned in Table 3.2. The coverslips were generally incubated with primary and secondary antibodies for 1h at 37°C in dark. There would be three washes with

PBS between primary and secondary antibody incubations. Following the final three PBS washing, slides were mounted using vectashield media with DAPI. Images were captured on a Deltavision using Softworx software (Applied Precision, Issaquah). 0.2-0.5µm Z-stacks were collected, deconvolved using Huygens software, projected, merged, and analysed using FIJI ImageJ version 1.52n software.

Table 3.2. List of antibodies and conditions used for immunofluorescence staining

Primary Antibodies					
Antibody	**Dilution**	**Blocking**	**Species**	**Manufacturer**	**Catalogue Number**
53BP1	1:500	5% BSA	Mouse	Thanos	None-commercial
53BP1	1:500	5% BSA	Rabbit	Novus	NB100-304
KIF18B	1:200	5% BSA	Rabbit	Sigma Aldrich	HPA024205
αTubulin-B512	1:200	5% BSA	Mouse	Sigma Aldrich	T5168
γH2AX	1:1000	5% BSA	Mouse	Millipore	05-636
Secondary Antibodies					
FITC anti-mouse IgG	1:200	5% BSA	Goat	Jackson Immunoresearch	115-096-062
FITC anti-rabbit IgG	1:200	5% BSA	Goat	Jackson Immunoresearch	111-096-045
TRITC anti-mouse IgG	1:200	5% BSA	Donkey	Jackson Immunoresearch	711-025-152
TRITC anti-rabbit IgG	1:200	5% BSA	Donkey	Jackson Immunoresearch	711-025-151

3.3.6. siRNA Transfection

Counted $1.5x10^5$ RPE1 or U2OS cells were seeded in 35 mm dishes and transfected with 40pmol of siRNA targeting Luciferase (Eurofins) as control, and independent KIF18B targeting siRNAs (Eurofins) with 6 µl of Oligofectamine (Invitrogen) in 0.8 ml of Optimem (Invitrogen)

per 35 mm dish. 3 h post-transfection, 0.5 ml of DMEM (without penicillin and streptomycin) supplemented with 20% FBS and 4 mM L-glutamine was added to the media. After 24 hours, 1 ml of DMEM with 10% FBS and 1% penicillin/streptomycin was added. Cells were harvested 48 h following the siRNA transfection. Biological triplicates were used for each siRNA treatment. siRNA sequences are listed in Table 2.3.

3.3.7. cDNA transfection

HeLa cells were grown to 80-90% confluency and transfected with 1µg of DNA and 2µl of Lipofectamine2000 (Life Technologies) diluted in 500 µl Opti-MEM (Gibco) added into 2ml DMEM with 10% FBS per 35 mm dish. Cells were grown for 48 h prior to analysis by immunofluorescence and western blot.

3.3.8. Metaphase Spreads

Before trypsinising the cells, they were treated with 0.5 µg/ml Colcemid for 2 h. Cells were then trypsinised and the pellet was resuspended in 5 ml of pre-warmed (37°C) hypotonic solution (75 mM KCl) and incubated for 25 min at 37°C. Five millilitres ice-cold fixative (methanol/acetic acid, 3:1) was added to the swelled cells to stop the hypotonic progress. Cells were then centrifuged for 5 min at 1200rpm. The pellet resuspended dropwise in 5ml cold fixative. This fixation step was repeated, and cells were finally resuspended in approximately 200µl of fixative solution. Cells can be stored at -20 °C.

For spreading, 12µl of fixed cells were dropped onto superfrost or polylysine coated slides from the distance of 1cm and air-dried overnight at RT to age the chromosomes.

3.3.9. Telomere FISH

Slides were immersed in PBS for 15 min before fixation in 4% paraformaldehyde in PBS for 4 min at 37°C. Slides were washed twice in PBS at 37°C for 5 min and incubated with 500ul of RNAse A (100ug/ml in 2X saline-sodium citrate buffer, SSC) for 1h at 37°C. Slides were washed three times in 2x SSC and once in ddH2O for 30 sec prior to treatment with pepsin (0.005% solution pH 2.0) for 4 min at 37°C. After a brief rinse in PBS, the paraformaldehyde fixation and PBS washes were repeated, and the slides were dehydrated in a cold ethanol series (1 min in 70%, 85%, and 100% ice-cold ethanol) and air-dried.

Hybridization buffer containing 60% formamide, 20 mM Na_2HPO_4 pH 7.4, 20 mM Tris pH 7.4, 0.1ug/ml salmon sperm DNA, 2X SSC buffer, and 200nM telomere PNA (TelC-FAM, Eurogentec, Seraing, Belgium) probe was denatured at 90°C for 5 min while slides were incubated at 85°C for 5 min. 50µl of denatured hybridisation probe was added to the slide and a coverslip was placed on top to prevent evaporation. Slides were incubated with the probe for 10 min at 85°C in hybridisation chamber and then incubated for 1-2 h at RT in the dark. Slides were rinsed in wash solution (2XSSC containing 0.1% Tween 20) at RT and then washed twice in pre-warmed (60°C) wash solution for 10 min at 60°C, and then once more washed at room temperature for 1 min. Slides were then washed for 2 min in 2XSSC, 1XSSC, and deionised water prior to air-drying and mounting with Vectashield and DAPI (Vector Laboratories). Slides were sealed with a coverslip and images were captured using 100x magnification and 0.2µm Z stacks on a Deltavision using softworx software (Applied Precision, Issaquah) and deconvolved using Huygens software and analysed.

3.3.10. Telomere fusion assay and cDNA rescue

$1.5x10^5$ HeLa Tet-inducible cells were seeded 24h prior to the first day of the experiment. DoxyCycline was retained at the concentration of

1µg/ml from day 1 to 7 in culturing media to induce efficient TRF2 depletion.

siRNA transfection targeting KIF18B has done using Oligofectamin on days 1 and 3. Expression of KIF18B full length and mutated versions to check the phenotype rescue, carried out on day 5. Using Lipofectamin, the cells co-transfected with siKIF18B and RNAi-insensitive full length KIF18B-GFP, KIF18B-GFP$^{\Delta TIM}$, and KIF18B-GFP^{MD}. Finally, on day 7 cells were harvested for WB, IF and metaphase spread.

3.3.11. Statistical methods

For quantified microscopy experiments three biological replicates were completed with a constant number of cells per condition per biological replicate which is indicated in each figure legend. Sample sizes were selected to be as large as biologically and technically feasible within our experimental conditions. The mean difference of each condition was individually compared to control via Student t-test. The variance was similar between the groups that are being compared. GraphPad Prism 8.2.1 software was used for all standard statistical analyses.

3.4. Results

3.4.1. KIF18B co-localises with 53BP1 at IRIF

In the SILAC proteomic screening carried out in our laboratory to investigate the 53BP1 interactome, KIF18B had a relatively high score, placing amongst known interacting partners of 53BP1, such as p53, Usp28, and Plk1. The interaction score describes the relative enrichment of the peptide detected compared to negative control cell extracts with untagged 53BP1. *In vivo,* co-immunoprecipitation of KIF18B with 53BP1 has been shown previously in our lab (See appendix IV) and the interacting motif of KIF18B with 53BP1 has mapped (Frizzell, 2015).

Followed by showing the *in vivo* interaction of KIF18B and 53BP1, we sought to investigate if KIF18B and 53BP1 Co-localise in damaged cells concerning 53BP1 IRIF (Figure 3.1.). 53BP1 is known to have a critical role in repair pathway choice and as one of the vanguard proteins recruited to the DSB contributing to foci formation (Chapman et al., 2012a). We gamma irradiated HeLa cells with 3 Gy and subsequently stained them for KIF18B and 53BP1 after 45 min. As shown in Figure 3.1. A, 53BP1 formed, IRIF in irradiated cells and nuclear bodies, also known as G1 bodies, in unirradiated cells. Interestingly, KIF18B co-localised with 53BP1 at both IRIF and nuclear bodies (Figure 3.1. A). The same result was reproduced in U2OS cells (Figure 3.1 B). To confirm that the co-localisation is not due to bleed-through from one channel into the other, we stained cells for 53BP1 only, using Tetramethylrhodamine (TRITC) and imaged in both red and green channels (Figure 3.1.C). Reciprocally, stained cells for KIF18B only using Fluorescein isothiocyanate (FITC) and imaged them in green and red channels (Figure 3.1.D). Analysis of the images showed no bleed-through between these channels.

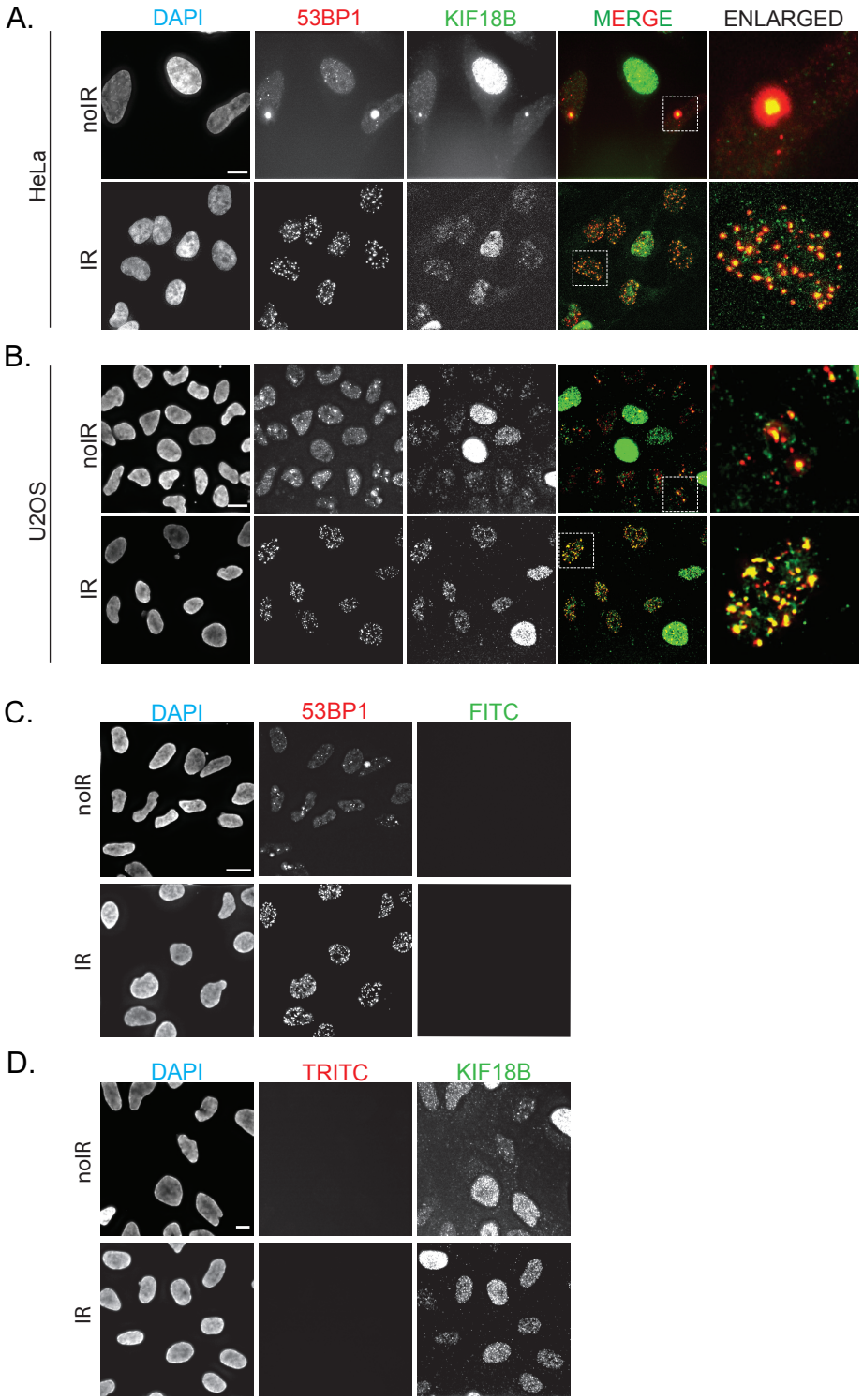
A.
DAPI
53BP1
KIF18B
MERGE
ENLARGED
HeLa
noIR
IR
B.
U2OS
noIR
IR
C.
DAPI
53BP1
FITC
noIR
IR
D.
DAPI
TRITC
KIF18B
noIR
IR

Figure 3.1.

Figure 3.1. KIF18B and 53BP1 co-localisation in human cells

Immunofluorescence of KIF18B and 53BP1 in HeLa (A) and U2OS (B) cells in both conditions of unirradiated (control, noIR) and 45 min post 3Gy irradiated (IR) as indicated on the left. DNA staining by DAPI is presented in blue, 53BP1 staining is shown as red and KIF18B as green (Columns 1, 2, and 3, respectively). The fourth column presents the merged fluorescence of green and red channels. The fifth column in panel A and B shows an enlargement of the area highlight by a white box in the fourth column. (C) U2OS cells were stained for 53PB1 only to confirm no bleed through in FITC channel. (D) U2OS cells were stained for KIF18B only to confirm no bleed through in TRITC channel. The scale bars represent 25μm.

To authenticate the co-localisation of 53BP1 and KIF18B, and to rule out any unspecific binding of the antibodies, we used another technique called the Supernova tagging system. In this system, the cells are co-transfected with two plasmids. One of them encodes the protein of interest, which is tagged with up to 24 copies of an epitope from the budding yeast transcription regulator, GCN4, with intervening linker sequences (Sun-tagged protein). The other plasmid encodes the single-chain variable antibody fragment (scFv) specific to the epitope from GCN4 (scFv-GCN4) fused to GFP for visualisation (scFv-GCN4-GFP). As a result of the binding of GFP-scFv to the tandem repeats, the tagged protein would glow up with 24 GFP molecules, resulting in a bright signal (Tanenbaum et al., 2014) (Figure 3.2.A). Another version of GFP-scFv containing NLS sequence can be used in this system to sequester the unbound GFP-scFv proteins to the nucleus when visualisation of cytoplasmic proteins is desired. First, to control the proper expression of the proteins in this system, we expressed only the GFP-scFv in HeLa cells, which resulted in a diffuse GFP signal all over the cell including cytoplasm and nucleus (Figure 3.2. B). We also expressed the GFP-scFv-NLS to check if we can use it to better visualise nuclear KIF18B, but due to the high amount of GFP signal in the nucleus, it was impossible to distinguish between $KIF18B^{SN}$ and unbound GFP-scFv-NLS (Figure 3.2. B). We have used a SUN-tagged truncated version of kinesin-1 (K560) to control the expression of another tagged protein other than KIF18B. The expression of $K560^{SN}$-GFP-scFv in HeLa cells resulted in a cytoplasmic GFP signal representing K560 as expected (Figure 3.2. B). To investigate the co-localisation of KIF18B and 53BP1, we co-

expressed SUN-tagged KIF18B and GFP-SCFV in HeLa cells (Figure 3.2. C). The cells were irradiated (45min post 3Gy) and treated with cytoskeletal extraction buffer (CSK) prior to fixation to extract proteins that are not stably anchored to cell structures. Cells were stained for 53BP1 and KIF18B was detectable with GFP signal. Similar to our prior IF experiments, this approach also showed co-localisation of KIF18B and 53BP1 at IRIFs.

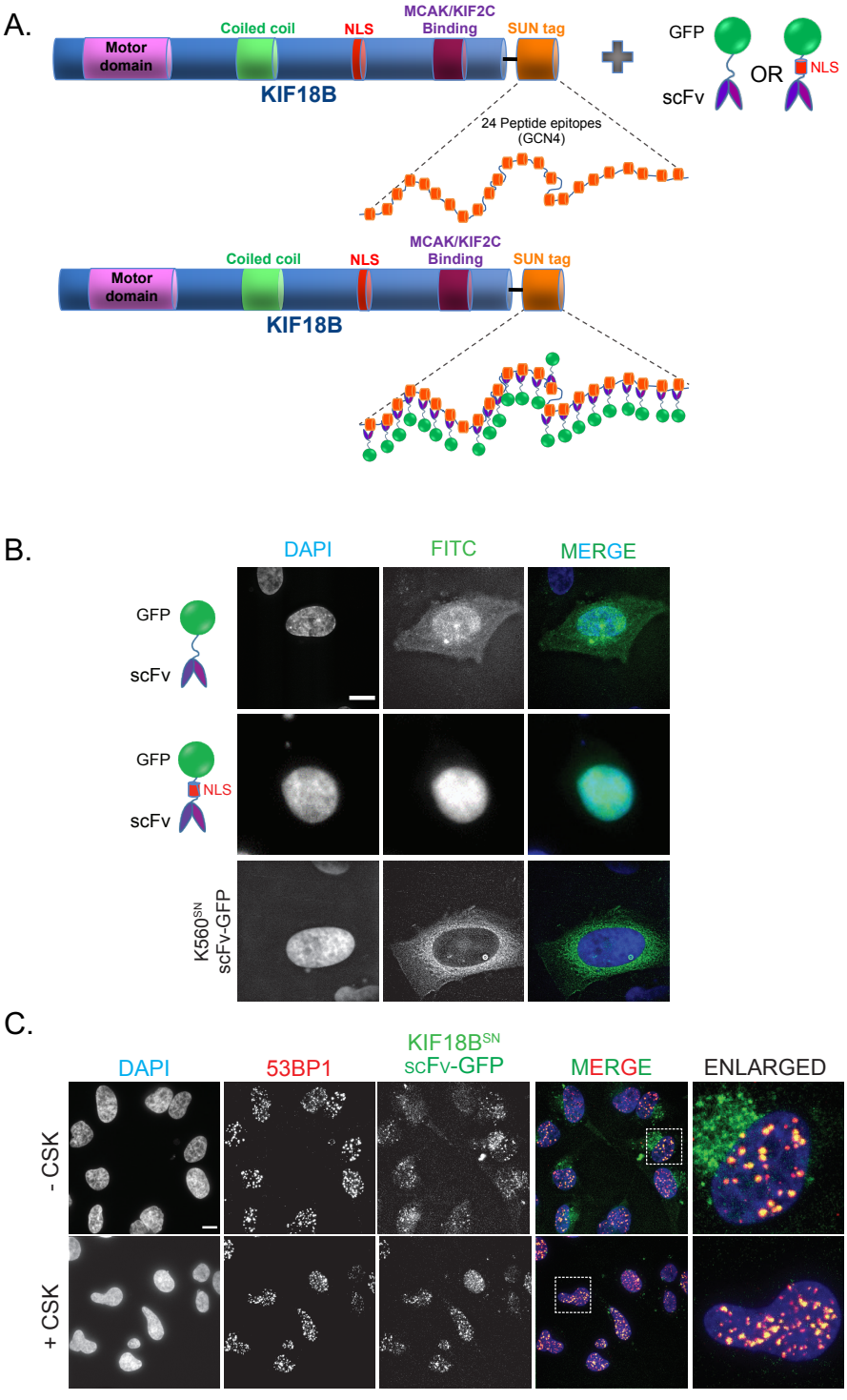
A.
Motor domain
Coiled coil
NLS
MCAK/KIF2C Binding
SUN tag
KIF18B
GFP
scFv
OR
NLS
24 Peptide epitopes (GCN4)
B.
DAPI
FITC
MERGE
GFP
scFv
NLS
K560SN scFv-GFP
C.
DAPI
53BP1
KIF18BSN scFv-GFP
MERGE
ENLARGED
- CSK
+ CSK

Figure 3.2.

Figure 3.2. Detection of KIF18B by using the Supernova tagging system

(A) Schematic of the supernova tagging system; showing the protein of interest, KIF18B, tagged to a polypeptide composed of 24 tandem GCN4 repeats recognised by GFP tagged scFv having an NLS or not. (B) The first row shows a representative HeLa cell transfected only with the cDNA encoding scFV-GFP, fixed after 48 h of transfection. The second row shows a representative HeLa cell transfected with the cDNA encoding scFV-NLS-GFP, sequestering the expressed GFP fusion proteins to the nucleus, fixed after 48 h of transfection. The third row shows a representative HeLa cell which was co-transfected with K560-24GCN4 construction and scFV-GFP, fixed after 48 h of transfection. The first column represents DAPI staining. The second column represents GFP in FITC channel and the third column is the merge of DAPI and FITC. (C) Immunofluorescence staining of 53BP1 in HeLa cells, co-transfected with KIF18B-24GCN4 and GFP-scFv, with and without CSK treatment as indicated on the left. Forty-eight hours after transfection, cells were irradiated (45 min post 3Gy) and stained with 53BP1. DAPI-stained DNA is shown in blue, 53BP1 in red, and $KIF18B^{SN}$ in green (columns 1^{st} to 3^{rd}). In the fourth column, all three channels are merged. The fifth column represents the enlargement of the selection in the merged image. The scale bar represents 25 μm.

3.4.2. Recruitment of 53BP1 is dependent on KIF18B

We have observed co-localisation of KIF18B with 53BP1 at DSBs (Figure 3.1. & 3.2.). To determine if KIF18B is required for the localisation of 53BP1 to the vicinity of DSBs, we examined 53BP1 focal recruitment to IRIF in the presence or absence of KIF18B by using siRNA-mediated depletion (Figure 3.3 A). We quantified the absolute number of 53BP1 foci per cell before and after 15, 30- and 60-minutes post 3Gy irradiation in U2OS cells (Figure 3.3. B). In un-irradiated cells, very few foci were detected, typically five, which includes the large bright foci seen in G1 cells that have been characterised as 53BP1 Nuclear Bodies (Lukas et al., 2011), as well as smaller and less intense foci that presumably correspond to sites of endogenous DNA damage (Figure 3.3.A). At 15 minutes post IR; control cells averaged 37 of 53BP1 IRIFs, which increased to 44 at 30 minutes followed by decreasing back to 37 at 60 minutes (Figure 3.3.B). KIF18B depleted cells displayed significantly fewer 53BP1 IRIF at all time-points, corresponding to 23, 29, and 29 at 15-, 30- and 60-minutes post IR while KIF18B depletion was efficient at all time-points (Figure 3.3.C). The difference in 53BP1 IRIF in control and KIF18B depleted cells suggests a role for KIF18B in 53BP1 recruitment to IR-induced foci at DSBs.

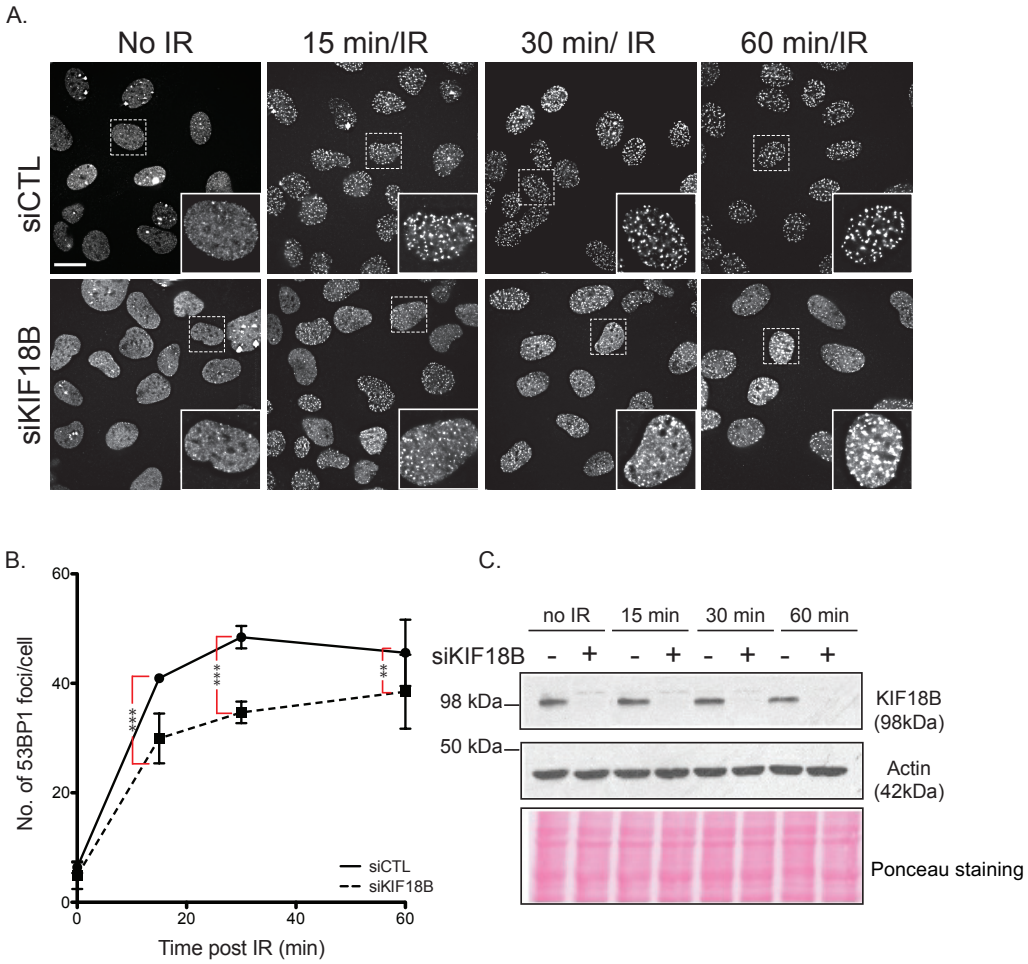

Figure 3.3. 53BP1 recruitment to the IR-induced foci depends on KIF18B

(A) Representative images of 53BP1 immunofluorescence in U2OS cells, transfected with control and KIF18B targeting siRNAs as indicated on the left. It is showing un-irradiated cells (No IR, as control cells) versus 3Gy irradiated U2OS cells at three time points (15, 30, and 60 minutes after irradiation). The inlet in each panel shows an enlarged example of a selected cell in the panel. The scale bar is equal to 25μm. (B) Quantification of 53BP1 IR-induced foci (IRIF) using Fiji ImageJ version 1.52n software. 200 cells were counted per condition in each experiment. Three replicates were carried out and Student t-test was used to statistically analyse the significance of the difference between 53BP1 IRIF average numbers in control and KIF18B depleted cells. Statistical analysis performed using GraphPad Prism 8.2.1. The error bars represent the SEM across 3 independent repeats. The significance of the difference is presented as ***P<0.0001 and **P<0.001 (C) Western blot indicating the efficient knockdown of KIF18B in unirradiated cells and three time points post 3Gy irradiation. The detection of actin in the extracts and the Ponceau S staining of the blotting membrane served as loading controls.

3.4.3. KIF18B depletion decrease the rate of DSBs repair

Phosphorylation of the histone variant H2AX at serine 139 in its C-terminal tail (ASQEY motif) in megabase domains of chromatin flanking DSBs, is an early event in the response to DSBs that correlates with their repair (Rogakou et al., 1998). The peak for γH2AX foci formation following low to moderate doses of IR has shown to be from 15 to 30 minutes immediately after damage and then will decrease gradually within few hours. However, 10% of γH2AX is detectable up to 48 hours after IR and corresponds to a slow component of DSB to repair corresponding to heterochromatin (Goodarzi et al., 2008; Nakamura et al., 2010).

As KIF18B depletion resulted in the abrogation of 53BP1 focal recruitment to IRIF (Figure 3.3.), we hypothesised, this defect might result in inefficient DSB repair. To assess the rate of DSB repair, we monitored the number of γH2AX foci per cell in control and KIF18B depleted cells at 15, 30- and 60-minutes post 3Gy irradiation (Figure 3.4.). Consistent with the amount of 53BP1 foci, detected in un-irradiated U2OS cells (Figure 3.3.), we similarly observed around 5 γH2AX foci counted in un-irradiated cells. This amount increased to 60 at 15 minutes post IR before falling to averages of 57 and 45 γH2AX IRIF/cell at 30- and 60-minutes post IR indicative of ongoing repair (Figure 3.4. B). In KIF18B-depleted cells γH2AX IRIF persisted for longer throughout the time course, corresponding to an average of 64, 69, and 62 γH2AX IRIF per cell at 15, 30- and 60-minutes post irradiation. Based on the observed persistence of γH2AX IRIFs as a proxy for defective DSB repair, this data suggests that KIF18B plays a role in facilitating the efficient repair of DSB.

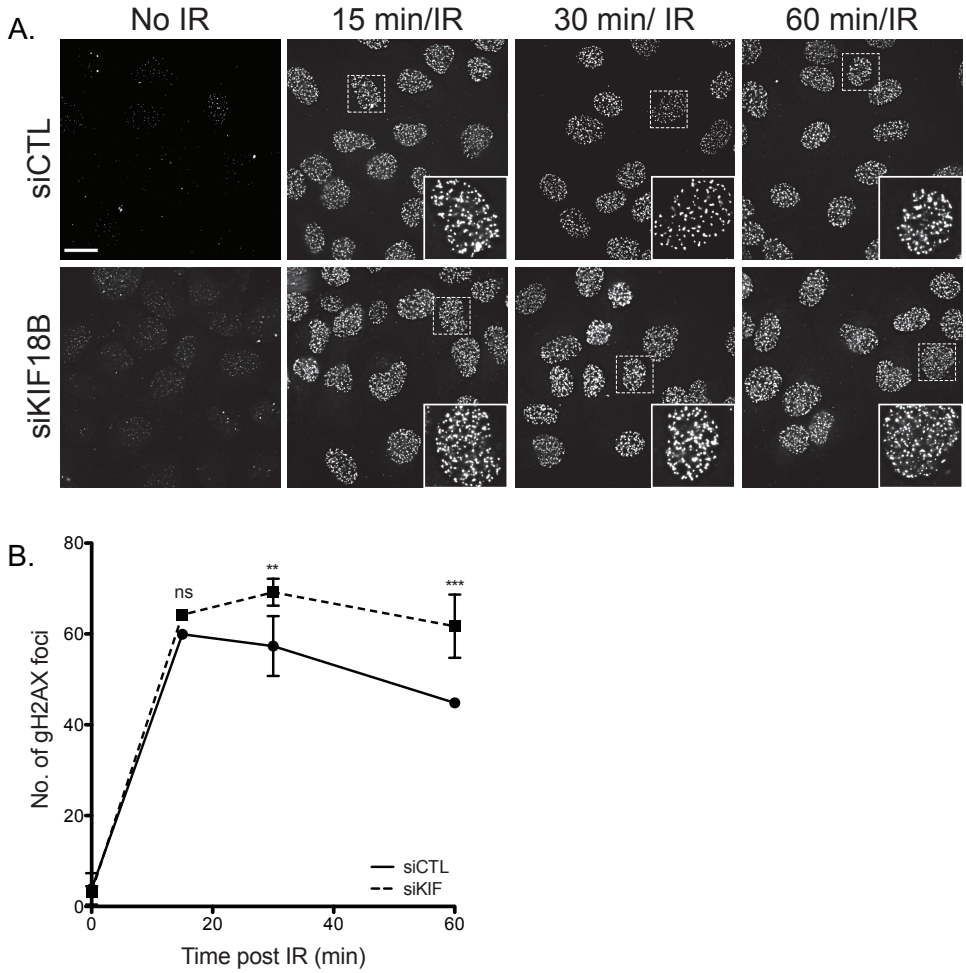

Figure 3.4. KIF18B is required for efficient double-strand break repair

(A) Representative immunofluorescence images of γH2AX in U2OS cells, transfected with control and KIF18B targeting siRNAs as indicated on the left. The panels show un-irradiated cells (NoIR) versus 3Gy irradiated cells at three time points (15, 30, and 60 minutes) as indicated on the top. The scale bar is equal to 25µm. (B) Quantification of γH2AX foci was performed using Fiji ImageJ version 1.52n software. 200 cells were counted per condition in each experiment. Three replicates were carried out and Student t-test was used to statistically analyse the difference between γH2AX foci average number in control and KIF18B depleted cells. Statistical analysis performed using GraphPad Prism 8.2.1. The error bars represent the SEM of 3 independent repeats. The significance of the difference is presented as ***P<0.0001, **P<0.001, and ns: not significant.

3.4.4. KIF18B depletion has no impact upon H4K20 di-methylation

We have shown that KIF18B is required for efficient 53BP1 recruitment to IRIF (Figure 3.3.); Furthermore, previous results from our laboratory have shown that KIF18B also interacts with H4K20me2 but distinctively to that of binding to 53BP1 (Frizzell, 2015). In fact, the KIF18B'S TIM domain, an H4K20me2 peptide, and Tudor domain of 53BP1 form a trimetric complex while the presence of TIM domain enhances the binding of the Tudor domain to H4K20me2 (Naoyuki Sarai, et al., Unpublished) (Figure 3.5. A). To determine if KIF18B has any effect on the H4K20 di-methylation level, which could impact the formation of 53BP1 IRIFs, we examined the level of H4K20me2 in HeLa, hTERT-RPE1, and U2OS cells upon KIF18B depletion (Figure 3.5. B)

Based on the quantification of H4K20me2 in western blots of the HeLa, hTERT-RPE1, and U2OS cells extracts, KIF18B depletion did not have any effect on global H4K20 di-methylation in these cells (Figure 3.5. B). Thus, the dependence of 53BP1 recruitment to the DSBs on KIF18B could be explained by the direct interaction of the KIF18B TIM domain with the Tudor domain of 53BP1.

A.

Residues required for TIM - Tudor Interaction:	Residues required for H4K20me2 -Tudor interaction:
W1495A S1495A – reduced interaction S1497A – reduced interaction S1495A/S1497 C1525A	W1495A Y1502A D1521A

B.

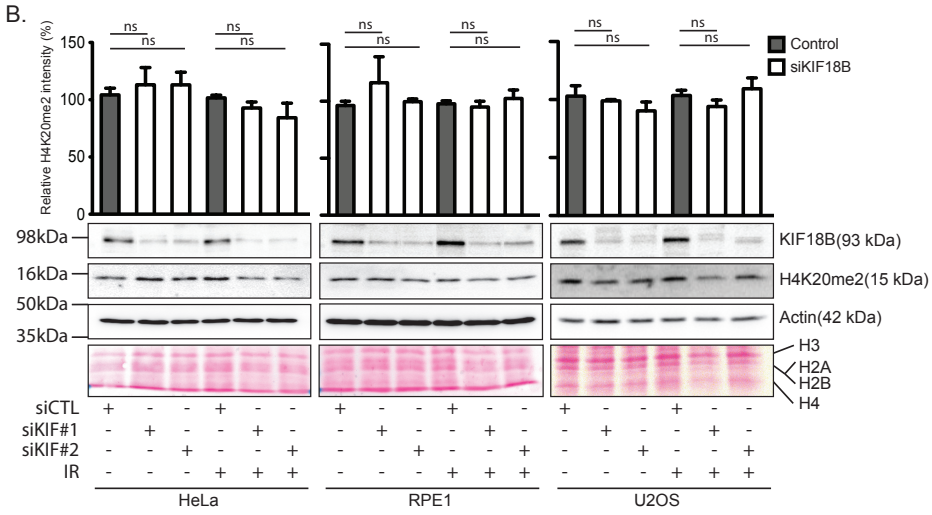

Figure 3.5. H4K20 di-methylation is not affected by KIF18B depletion

(A)The table shows the essential residues of 53BP1 Tudor domain for its interaction with KIF18B's TIM domain and H4K20me2 (Naoyuki Sarai, et al., unpublished). (B) Western blot analysis of H4K20me2 in HeLa, U2OS, and RPE1 cells after KIF18B depletion in un-irradiated (Control) and 3Gy irradiated cells. Two independent siRNAs were used to knockdown KIF18B. The quantification of the western blot bands density probed for H4K20me2 was carried out using Fusion software v18.05. The error bars represent the SEM across 3 independent repeats. Student t-test was used to compare the difference between control and KIF18B depleted cells in both non-irradiated and 3Gy irradiated conditions. ns: not significant. Statistical analysis performed using GraphPad Prism 8.2.1. Actin detection and Ponceau S staining served as loading controls of the extracts. Representative western blots are shown.

3.4.5. KIF18B is required for fusion of de-protected telomeres

Our work has characterised a previously unreported interaction between human 53BP1 and KIF18B (Figure III.1) (Frizzell, 2015), as well as their co-localisation at DSBs (Figure 3.1.). Given that the efficient recruitment of 53BP1 to IRIF is dependent upon KIF18B (Figure 3.3.), we sought to test if the role of 53BP1 in the fusion of de-protected telomeres is also dependent upon KIF18B (Figure 3.6.).

We used a previously developed human HeLa cell line, stably expressing a Tet-inducible shRNA targeting *TRF2* upon the addition of DoxyCycline. (Grolimund et al., 2013). We examined the role of KIF18B along with 53BP1 in the fusion of de-protected telomeres, occurring by NHEJ of the DSBs resulted from telomere de-protection. Efficient depletion of the TRF2 protein to de-protect telomeres was achieved by incubating the cells with DoxyCycline (1ug/ml) for 7 days. To maintain siRNA-mediated depletion of KIF18B and 53BP1 during the 7-day induction of telomere de-protection, siRNAs were transfected three times on days 1, 3, and 5 of the experimental protocol (Figure 3.6. A). This protocol resulted in the efficient depletion of TRF2.

Un-transfected cells without depletion of TRF2 (UT, no Dox) showed no evidence for chromosome fusion (Figure 3.6. C & D). Addition of Dox (UT, +Dox) to induce depletion of TRF2 resulted in an average of 5.0 fusions per spread. Similarly, in control siRNA transfected cells (siCTL/+Dox) an average of 5.1 chromosome fusion events were observed. However, in cells depleted of both 53BP1 and TRF2 (si53BP1/+Dox) the average number of chromosome fusions was reduced from approximately 5 to just 0.7, confirming that 53BP1 is required for fusion of de-protected telomeres.

Two independent siRNAs targeting KIF18B (siRNA#1 and #2) were used to assess the role of KIF18B in the fusion of de-protected telomeres. The first (siRNA#1) resulted in an average of 1.3 and the second (siRNA#2), 0.4 fusions of de-protected telomeres per

metaphase spread, suggesting a role for KIF18B in this process similar to that of 53BP1. To assess the relationship between KIF18B and 53BP1 in de-protected telomere fusion, we assessed the effect of both proteins' depletion. The double knockdown (siKIF18B #1 and si53BP1) resulted in an average of 1.0 fusions per spread, similar to either of the single depletions (Figure 3.6. B & C).

Altogether, this data confirmed the previous studies indicating a role for 53BP1 in the fusion of de-protected telomeres (Dimitrova et al., 2008), and extends this observation to suggest that KIF18B is also required for efficient telomeric fusion. Furthermore, as double depletion of both 53BP1 and KIF18B did not result in an additive defect in telomeric fusion, it suggests an epistatic relationship between 53BP1 and KIF18B. Thus, 53BP1 and KIF18B may function in the same pathway with respect to the fusion of de-protected telomeres.

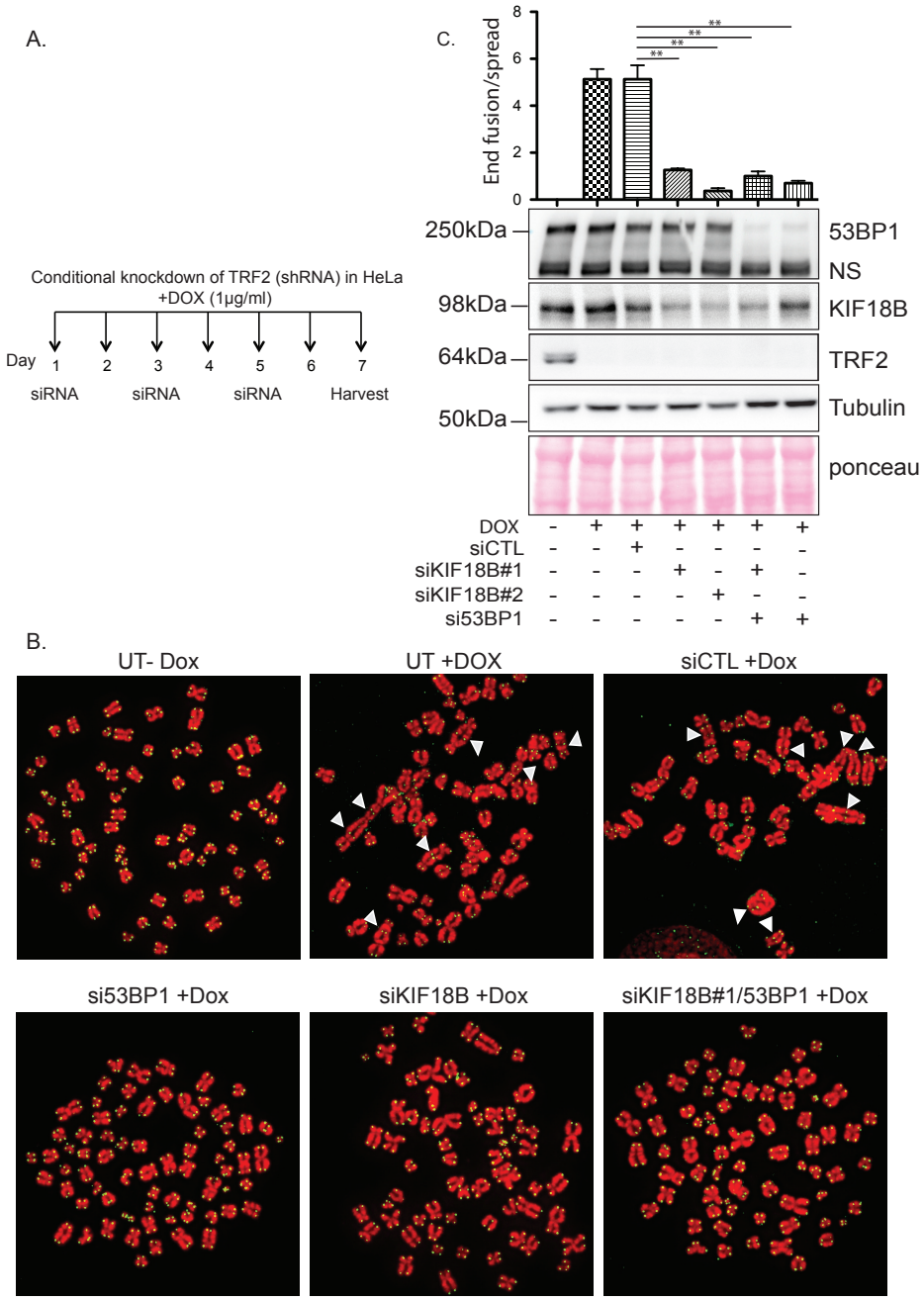

Figure 3.6. KIF18B is required for fusion of de-protected telomeres along with 53BP1

(A) Schematic of the experiment plan indicating culturing HeLa cells with media containing 1 µg/ml Dox for 7 days and also the cells were transfected with siRNA on days 1, 3, and 5. (B) Representative images of telomere FISH (Fluorescent In Situ Hybridisation) of HeLa cells upon de-protection of telomeres in controls (UT: Untransfected and siCTL: control siRNA), KIF18B depleted cells (siKIF18B), 53BP1 depleted cells (si53BP1) and Kif18B-53BP1 co-depleted cells (siKIF18B#1/53BP1). (C) The western blot indicating efficient knockdown of KIF18B, 53BP1, and TRF2. The Tubulin and Ponceau S staining used as loading and protein transfer control. Quantification of fusions at both ends of chromosomes was carried out manually in 30 spreads per condition in three repeats. Error bars represent the SEM of the three repeats. Student t-test was used to compare the difference between control and KIF18B, 53BP1 and KIF18B/53BP1 depleted cells. **P<0.005.

3.4.6. Both motor domain and TIM domain of KIF18B are required for fusion of unprotected telomeres

We have shown the requirement of KIF18B along with 53BP1 for fusion of de-protected telomeres (Figure 3.6.). Depletion of KIF18B with two independent siRNAs, resulted in the loss of telomere fusion similarly to 53BP1 depletion. However, to provide further confirmation, we asked whether the re-expression of KIF18B in cells, in which expressed KIF18B from the endogenous *KIF18B* gene has been depleted, could rescue the defect in chromosome fusions. To perform this rescue experiment, we needed to express the KIF18B cDNA from an expression construct at endogenous levels, which proved challenging.

We used a KIF18B-GFP cDNA construct (Tanenbaum et al., 2011), which hugely overexpressed KIF18B-GFP with respect to the endogenous KIF18B gene (Figure 3.7. A). To reduce KIF18B-GFP expression to close to endogenous KIF18B levels we tried several approaches. Firstly, we diluted the cDNA construct expressing KIF18B-GFP with its empty vector at different dilutions, which did not make a considerable difference in expression level (*data not shown*). Secondly, we used site-directed mutagenesis to abrogate the CMV promoter driving KIF18B-GFP expression. We made three different mutations within the TATA box of the CMV promoter, as well as a version in which the TATA box was totally removed. However, as Figure 3.7. B & C show, although KIF18B-GFP expression, reduced but was still significantly overexpressed in comparison with the endogenous level. Thirdly, we replaced the CMV promoter with HSV-TK promoter with different truncations which were previously introduced as a suitable promoter to overcome the overexpression of the exogenous proteins (Figure 3.7. D) (Ali et al., 2018). Using HSV-TK promoters TSC and 2ST also did not reduce KIF18B-GFP levels to close to the levels from the endogenous KIF18B (WB not shown). Fourthly, we decided to screen the stable cell lines expressing the KIF18B-GFP cDNA and search for a clone expressing it at close to

endogenous level. However, for reasons we could not decipher, while the KIF18B-GFP cDNA was expressed at early passages (Figure 3.7.E), at later passages it was not detectable (Figure 3.7.F).

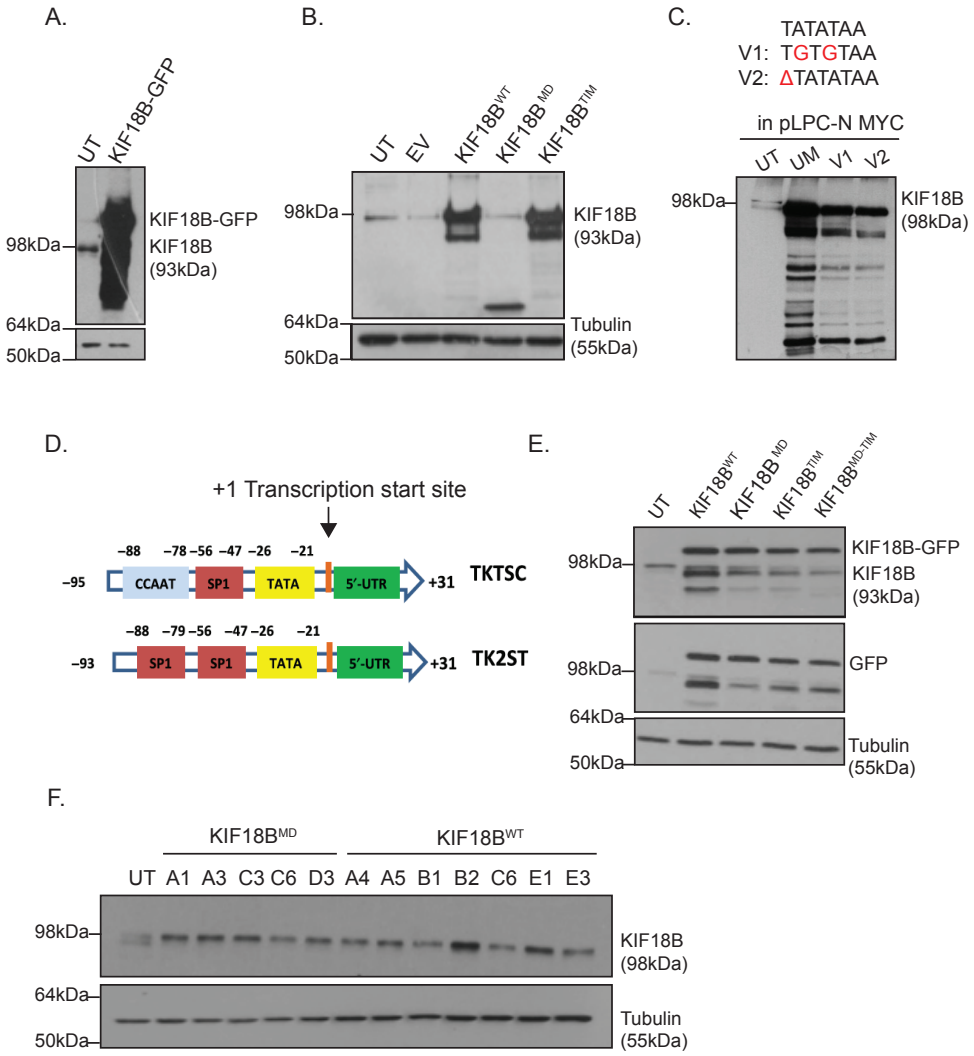

Figure 3.7. Troubleshooting of the exogenous KIF18B expression prior to the rescue experiment for de-protected telomere fusion

(A) Western blot indicating the exogenous KIF18B-GFP overexpression in comparison to the endogenous KIF18B. (B) Expressing KIF18B-GFP (WT, MD, and ΔTIM) with TATA box mutations within the CMV promoter, indicating WT and ΔTIM overexpression and MD degradation. The detection of Tubulin served as a loading control (C) Changing vector to pLPC-N MYC and TATA box mutation which did not reduce the KIF18B-GFP overexpression. (D) Schematic demonstration of truncated versions of the HSV-TK promoter (schematic adapted from Ali et al., 2018) (E) Transient successful expression of KIF18B-GFP (WT, MD, and ΔTIM) to raise the optimum expressing clones and making stables. The detection of Tubulin served as a loading control. (F) KIF18B-GFP degradation in selected clones as indicated on the top.

Finally, we devised a protocol involving transient expression of the RNAi-insensitive-KIF18B-GFP cDNA, coupled with two independent siRNAs transfections to express the cDNA at close to endogenous levels. This protocol uses one siRNA specific to the endogenous *KIF18B* gene, which the KIF18B-GFP construct is resistant to it, and another independent siRNA that targets both the endogenous and the exogenously expressed KIF18B-GFP cDNA (see Table 2.3. for siRNA sequences). As shown in Figure 3.8. A and B, in this protocol transfection of siRNAs carried out on days 1, 3 and 5 to keep the KIF18B depleted, while Dox inducible TRF2 shRNA expression is ongoing. On day 5, the siRNA transfection is coupled with transfection of KIF18B-GFP (WT as well as mutant versions) cDNA constructs, which is, 48 h prior to harvesting the cells. This protocol allowed KIF18B-GFP and mutant versions to be expressed at levels close to endogenous KIF18B while the endogenously expressed KIF18B is depleted.

As shown in Figure 3.8. B & C, KIF18^{WT}-GFP rescued the average number of chromosome fusions to levels very similar to that observed in control cells (UT/+Dox and siCTL/+Dox), supporting a role for KIF18B in this process.

To further investigate the mechanism of KIF18B involvement in de-protected telomere fusion, we used two mutated versions of KIF18B-GFP in our cDNA rescue assay of the de-protected telomere fusion defect upon KIF18B depletion. One of the mutated versions lacks the Tudor Interaction Motif (KIF18B$^{\Delta TIM}$-GFP) to determine whether the direct interaction of KIF18B with 53BP1 is required for fusion of de-protected telomeres. The other mutated version corresponds to a motor defective version of KIF18B (KIF18^{MD}-GFP) (Tanenbaum et al., 2011), harbouring the H300A, R304A, and K307A mutations (kind gift from René H Medema, University Medical Centre Utrecht).

Un-transfected cells lacking TRF2 (UT/+Dox), as well as those transfected with control siRNA (siCTL/+Dox) both displayed an

average of approximately 5 fusions per metaphase spread which reduced to less than one (0.8) upon KIF18B depletion, as expected based on our previous result (Figure 3.6. B & C, Figure 3.8. B & C). While KIF18B^{WT}-GFP was able to rescue the telomere fusion to an average of approximately 5 fusion per spread, chromosome fusion events remained at 1.4 and 1.2 fusion per spread upon expression of KIF18B$^{\Delta TIM}$-GFP and KIF18^{MD}-GFP (Figure 3.8. B & C). This result suggests that KIF18B requires both, the interaction with 53BP1 as well as its motor function, for the fusion of de-protected telomeres.

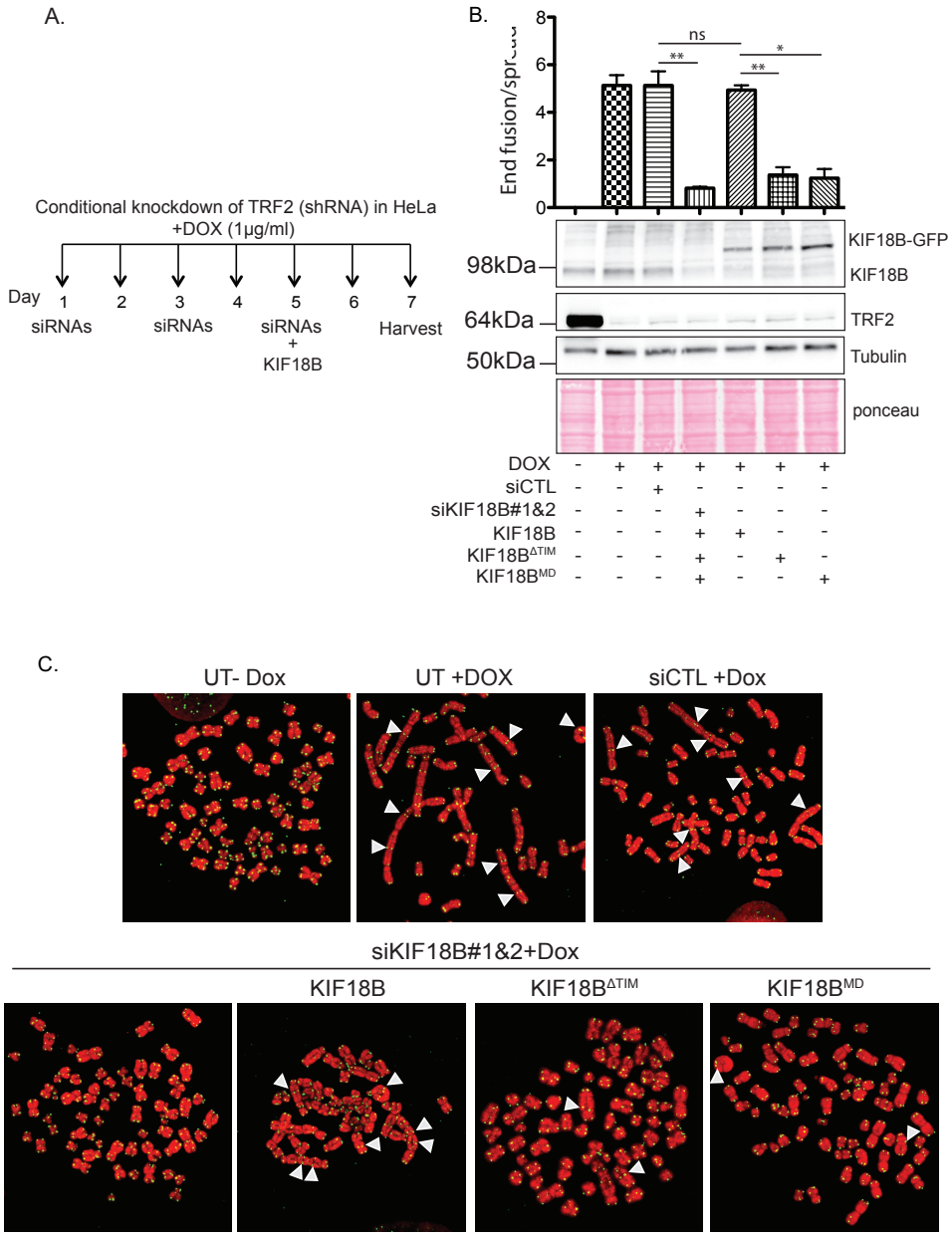

Figure 3.8. TIM domain and motor domain of KIF18B are required for fusion of de-protected telomeres

(A) Schematic showing the experimental design in which, HeLa Tet-inducible cells were treated with 1 µg/ml DoxyCycline (Dox) for 7 days prior to harvest. Cells were transfected with KIF18B targeting siRNA on days 1, 3, and 5. On day 5, cells simultaneously transfected with siRNA and KIF18B^{WT}-GFP, KIF18B$^{\Delta TIM}$-GFP, and KIF18B^{MD}-GFP (B) Graph showing quantification of telomere fusions per metaphase spread. The Fusion of chromosome ends scored manually and 30 spread analysed per condition. The data are indicating the average of three independent experiments and error bars represent the SEM of the three repeats. Statistical analysis was carried out using Student t-test by GraphPad Prism 8.2.1 software. The differences between control and KIF18B depleted cells as well as KIF18B^{WT}-GFP transfected cells and mutated versions shown as *P<0.05, **P<0.005, and ns: not significant. The western blot indicates the efficient knockdown of KIF18B and TRF2 as well as expression of KIF18B-GFP close to the endogenous level. The Tubulin and Ponceau S staining used as loading and protein transfer control. (C) Representative images of telomere FISH (Fluorescent In Situ Hybridisation) of HeLa cells in different conditions as indicated in (B).

3.4.7. KIF18B is required for 53BP1 recruitment to Telomere Dysfunction-Induced Foci

Formation of γH2AX and consequent accumulation of DDR proteins, including 53BP1, RAD17, ATM, and MRE11, upon de-protection of telomeres has been referred to as a Telomere Dysfunction-Induced Focus (TIF), which can be easily detected by immunofluorescence staining with the appropriate antibodies (Takai et al., 2003).

We quantified TIFs as another readout to confirm the involvement of KIF18B in fusion of de-protected telomeres using our cDNA rescue protocol (Figure 3.9. A). As before, DoxyCycline was used to induce expression of TRF2 shRNA expression, resulting in depletion of TRF2 which leads to uncapping or de-protection of telomeres. TIFs were detected by using an antibody specific to 53BP1. We considered cells with more than 4 TIFs as being TIF positive cells. Note that many exponentially growing cells display large bright 53BP1 foci corresponding to 53BP1 nuclear bodies that form in G1 cells (Lukas et al., 2011). We quantified 16% of cells as TIF positive in untreated condition, which increased to 63% and 58% upon addition of Dox to both un-transfected (UT/+Dox) and control siRNA transfected (siCTL/ +Dox) cells (Figure 3.9. B). Upon depletion of KIF18B, the TIF positive cells reduced to 38%, which increased to 55% by re-expression of KIF18B^{WT}-GFP. Upon expression of KIF18B-GFP lacking Tudor Interacting Motif (KIF18B$^{\Delta TIM}$-GFP), the motor defective (KIF18B^{MD}-GFP) and the double mutated (KIF18B$^{\Delta TIM+MD}$-GFP), the percentage of TIF positive cells drops to 34%, 42%, and 41% respectively (Figure 3.9. B). Quantification of the average number of 53BP1 TIFs per cell also showed an increase from 0.2 in untreated cells to 5.5 and 4.4 in Dox treated, un-transfected, and siCTL transfected cells respectively. KIF18B depletion reduced the TIF numbers to 2.7, which was rescued by KIF18B^{WT}-GFP expression to 4.5 and remained at 2.1, 2.6 and 2.7 by expressing KIF18B^{MD}-GFP, KIF18B$^{\Delta TIM}$-GFP and the double mutant KIF18B$^{MD+\Delta TIM}$-GFP in endogenous KIF18B depleted cells, respectively. This result supports the KIF18B requirement for 53BP1

recruitment to the TIFs in order to mediate deprotected telomere fusion through NHEJ. Furthermore, we have shown mechanistically both TIM and motor domains of KIF18B are necessary for fulfilment of its role in 53BP1 recruitment to TIFs and fusion of de-protected telomeres.

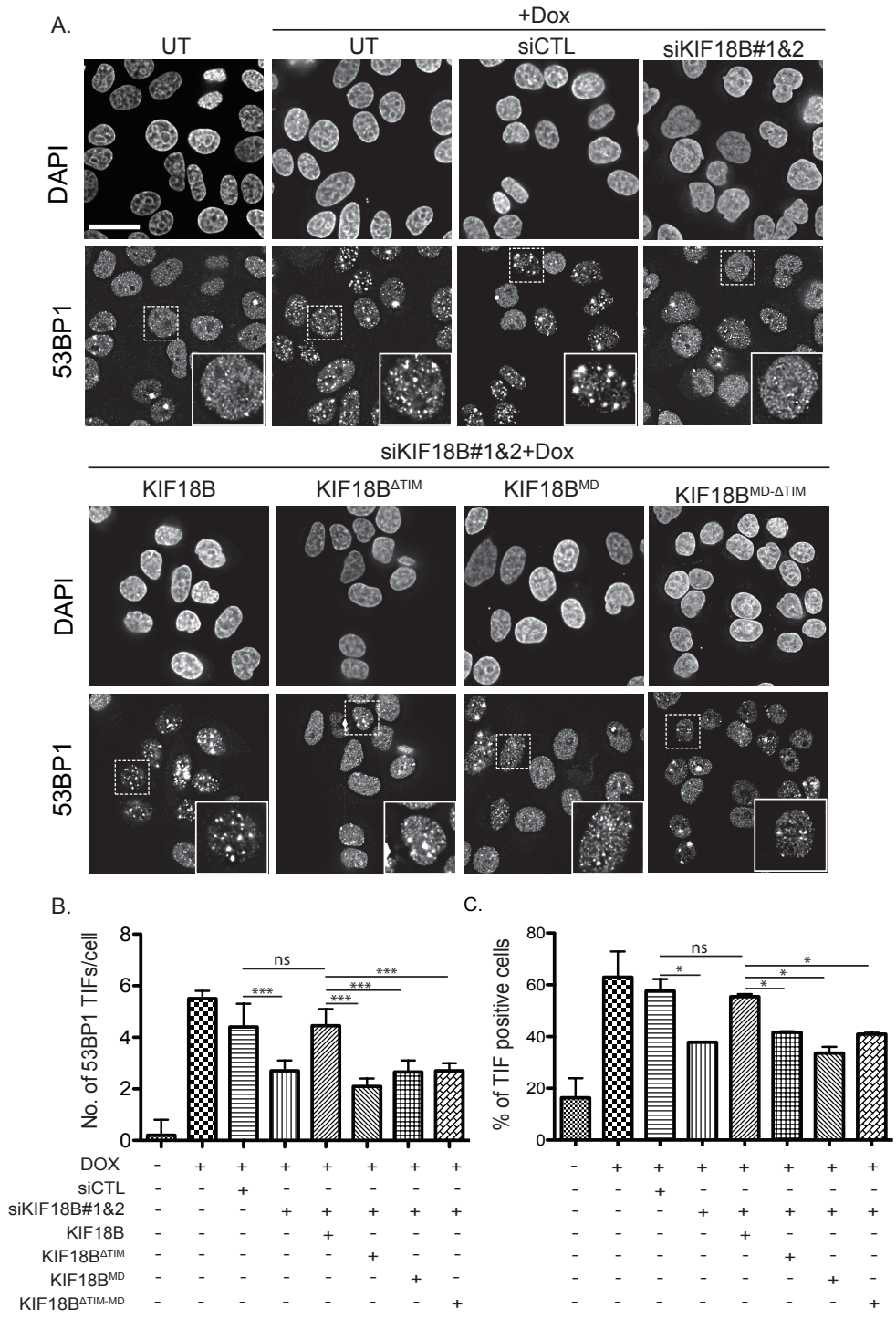
A.
+Dox
UT
UT
siCTL
siKIF18B#1&2
DAPI
53BP1
siKIF18B#1&2+Dox
KIF18B
KIF18B^ΔTIM
KIF18B^MD
KIF18B^MD-ΔTIM
DAPI
53BP1
B.
No. of 53BP1 TIFs/cell
ns
***
***
***
***
C.
% of TIF positive cells
ns
*
*
*
*
DOX
siCTL
siKIF18B#1&2
KIF18B
KIF18B^ΔTIM
KIF18B^MD
KIF18B^ΔTIM-MD

Figure 3.9.

Figure 3.9. The Telomere Dysfunction-Induced Foci formation upon telomeres de-protection requires both KIF18B's TIM and motor domains.

(A) Representative images of immunofluorescence of 53BP1 in HeLa Tet-inducible cells upon telomere de-protection in control and KIF18B depleted cells as well as conditions in which KIF18B wild type, ΔTIM, and MD were ectopically expressed while endogenous KIF18B was depleted. The first row of each block indicates DAPI staining and the second row shows 53BP1 staining. The scale bar is equal to 25μm. (B) Quantification of the number of Telomere Dysfunction-Induced Foci (TIFs) per cell in indicated conditions in (A). (C) Quantification of the percentage of TIF positive cells in indicated conditions in (A). Quantification of TIFs is performed using FIJI ImageJ version 1.52n. Three independent experiments carried out and error bars represent the SEM of the three repeats. >300 cells were analysed per condition in each experiment and Student t-test was used to compare the difference between Control and KIF18B depleted cells as well as KIF18BWT-GFP transfected cells and mutated versions. ***P<0.0001, *P<0.05 and ns: not significant.

3.4.8. Microtubule poisons and KIF18B depletion are epistatic in 53BP1 recruitment to IRIF

In agreement with the involvement of the motor domain of KIF18B in focal recruitment of 53BP1 at the DBSs, we hypothesised that there might be a dependency of the 53BP1 IRIF on microtubule filaments, as the KIF18B trajectory. To address this question, we used microtubule poisons to investigate if they have any effect on 53BP1 IRIF. We used Nocodazole as a microtubule depolymerising agent (Hoebeke et al., 1976a) and Taxol as a microtubule stabiliser (Hoebeke et al., 1976b). We quantified the number of 53BP1 IRIFs in U2OS cells, treated with Nocodazole and Taxol post 3Gy irradiation and compared it with KIF18B depleted and irradiated cells (Figure 3.10.).

In un-irradiated control cells, 9 53BP1 foci were counted as the basal level of DNA damage (Figure 3.10. B). We counted an average of 51 foci/cell in untreated cells post irradiation which decreased to 40 and 35 foci/cell upon Nocodazole and Taxol treatment respectively, compared to 37 foci/cell after KIF18B depletion. We also treated the KIF18B depleted cells with Nocodazole and Taxol and an average of 36 foci/cell were quantified in both cases.

Altogether, our data is showing the disruption of the microtubule network reduced 53BP1 focal recruitment to the DSBs, in accordance with a previous study reporting the role of microtubules in the

trafficking of the proteins involved in DDR including 53BP1 (Poruchynsky et al., 2015). In this work trafficking of the DNA damage response proteins into the nucleus was shown to be dependent upon microtubules as treatment of cells with microtubule poisons resulted in DDR proteins being sequestered into the cytoplasm. Besides, we showed the efficient focal recruitment of 53BP1 does not only depends on the microtubules but also requires a functional KIF18B. Finally, the KIF18B depleted cells treatment with microtubule poisoning agent does not show any additive effect on 53BP1 IRIF abrogation, which can suggest that KIF18B and microtubules are working in the same pathway for 53BP1 focal recruitment to the DSBs.

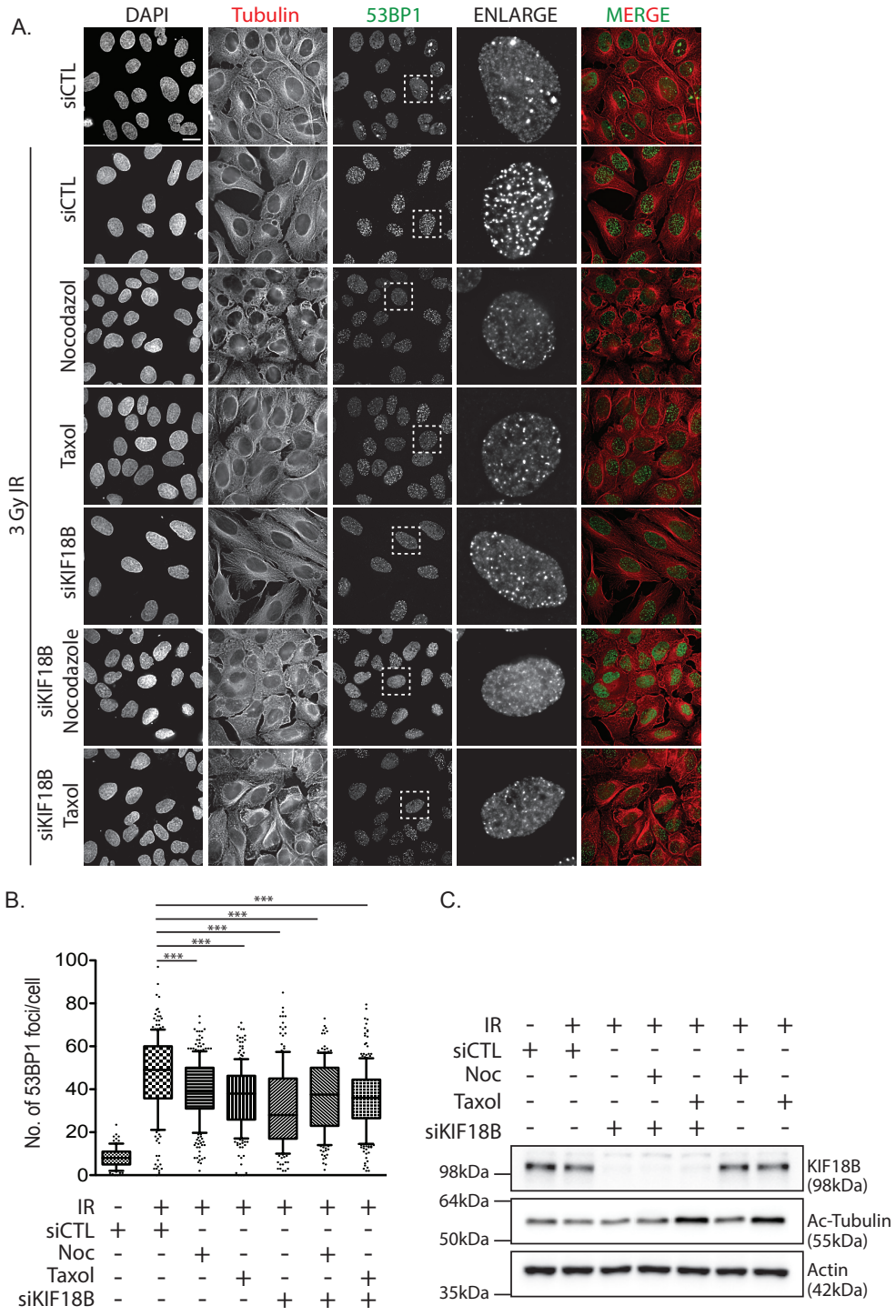
A.
DAPI
Tubulin
53BP1
ENLARGE
MERGE
siCTL
siCTL
Nocodazol
Taxol
siKIF18B
siKIF18B Nocodazole
siKIF18B Taxol
3 Gy IR
B.
No. of 53BP1 foci/cell
100
80
60
40
20
0
***
IR - + + + + + +
siCTL + + - - - - -
Noc - - + - - + -
Taxol - - - + - - +
siKIF18B - - - - + + +
C.
IR - + + + + + +
siCTL + + - - - - -
Noc - - - + - + -
Taxol - - - - + - +
siKIF18B - - + + + - -
98kDa
64kDa
50kDa
35kDa
KIF18B (98kDa)
Ac-Tubulin (55kDa)
Actin (42kDa)

Figure3.10.

Figure 3.10. Microtubule poisoning and KIF18B depletion resulted in 53BP1 abrogation at IRIF.

(A) Representative images of 53BP1 immunofluorescence in HeLa cells showing control unirradiated cells versus those treated with Taxol, Nocodazole, and KIF18B siRNA post 3Gy irradiation as indicated on left. The first column presents DAPI. Tubulin and 53BP1 are shown in the second and third columns. The fourth column is the enlargement of the selection in thde third column. The fifth column is the merge of Tubulin in red and 53BP1 in green. The scale bar represents 25 μm. (B) Graph showing quantification of the number of 53BP1 foci per cell in different conditions using FIJI ImageJ version 1.52n. >250 cells were analysed per condition. The mean of three independent experiments is shown and error bars represent SEM of these repeats. Student t-tests were used to compare the difference between siControl transfected cells and the cells upon different treatments after irradiation. ***P<0.0001 (C) Western blots confirm the efficient KIF18B depletion as well as tubulin hyperacetylation upon Taxol treatment. Actin detection served as a loading control.

3.5. Discussion

The proteomic screening carried out in our lab to investigate the 53BP1 interactome revealed a relatively uncharacterised kinesin 8 family member, KIF18B, as a highly scored interacting partner. Mapping the region of KIF18B that interacts with 53BP1 resulted in recognition of a Tudor Interaction Motif (TIM) near the C-terminal of KIF18B that interacts with the 53BP1 Tudor domain.

We have shown KIF18B is a 53BP1 interacting partner that co-localises with 53BP1 at DSBs. Immunofluorescent staining of endogenous KIF18B and 53BP1 showed their co-localisation at IRIF in gamma irradiated cells. This co-localisation was also confirmed by observation of overexpressed Sun-tagged KIF18B co-localising with 53BP1 at IRIF. Together, KIF18B recognition as a 53BP1-interacting partner and co-localisation with 53BP1 at DSBs suggested that KIF18B is involved in the DDR.

In addition, KIF18B co-localised with 53BP1 at the nuclear bodies in G1 cells. Nuclear bodies are proposed to be comprised of un-replicated DNA remnants from the S phase. Recruitment of 53BP1 to these nuclear bodies indicates recognition of them as DNA damage sites by cell repair machinery and KIF18B co-localisation with 53BP1 at these spots suggested that KIF18B is involved in the DDR.

The nuclear localisation of KIF18B during interphase, its biochemical interaction with 53BP1 in cellular extracts, and co-localisation with 53BP1 at IRIF suggested that KIF18B may be involved in 53BP1 recruitment to IRIF. In support of this. we found that 53BP1 focal recruitment to IRIF was abrogated in KIF18B depleted cells. However, it is possible that the role of KIF18B in 53BP1 recruitment was either through direct interaction of its C-terminal with 53BP1 Tudor domain or indirectly via affecting other essential factors for 53BP1 recruitment. We ruled out the loss of H4K20 di-methylation upon KIF18B depletion by showing that H4K20me2 level in HeLa, U2OS, and hTERT-RPE1 cells were unaffected by KIF18B depletion. In addition, it has been shown recently in our laboratory that KIF18B also interacts with H4K20me2 (Naoyuki Sarai, unpublished data). In fact, the 53BP1 Tudor domain interacts with both KIF18B and H4K20me2 using neighbouring but different amino acids residues. *In vitro* assessment of this trimeric complex showed that the addition of KIF18B peptide corresponding to its TIM domain resulted in a more stable binding of the 53BP1 Tudor domain to H4K20me2. Thus, the KIF18B protein may be required to enhance the interaction between 53BP1 and H4K20me2 modified nucleosomes *in vivo*.

H2AX phosphorylation at DSBs is one of the earliest detectable events which can be used as an indicator of DSB; the gradual decrease in γH2AX foci number is a sign of repair (Löbrich et al., 2010). In normal cells, γH2AX foci detection starts from 3 minutes post IR and the decrease is identifiable from approximately 30 minutes post IR after reaching the peak, depending on the DNA content and severity of damage (Löbrich et al., 2010). When we depleted KIF18B, we observed a significant delay in γH2AX foci resolution, further implicating KIF18B in DNA damage repair.

The fusion of de-protected telomeres is a 53BP1 and NHEJ mediated process (Dimitrova et al., 2008). We have shown that KIF18B is also required for these fusion events and probably does so in a pathway

shared with 53BP1, as both genes appear to function epistatically in the fusion of de-protected telomeres.

Importantly, re-expression of exogenous KIF18B was able to rescue the loss of telomere fusion in KIF18B depleted cells, allowing us to rule out the off-target effect of the siRNA used. Further investigation of the role of KIF18B in dysfunctional telomere fusions revealed that both the motor function of KIF18B as well as its TIM domain are required for the fusion.

In addition to regulating fusion of de-protected telomeres, KIF18B depletion reduced 53BP1 focal recruitment to TIFs as well as to 53BP1 IRIFs. Furthermore, we showed that efficient focal recruitment of 53BP1 to Telomere Dysfunction-Induced Foci (TIFs) depends on both KIF18B motor function as well as the TIM domain, while the double mutant (defective motor domain and deleted TIM) does not cause an additive reduction in 53BP1 TIF formation, indicating that both the motor domain and TIM work in the same way to promote efficient 53BP1 recruitment to TIF.

DDR proteins are trafficked to the nucleus via the microtubule network (Poruchynsky et al., 2015). Abrogation of 53BP1 IRIF formation upon treatment of cells with microtubule poisoning agents is in agreement with the requirement of a microtubule routed kinesin, KIF18B, for 53BP1 focal recruitment to DSBs. Based on the similar effect of KIF18B depletion and microtubule poisoning on 53BP1 IRIF formation, we postulated that KIF18B motor function is required for 53BP1 recruitment to IRIF. As simultaneous microtubule poisoning and KIF18B depletion did not cause any additive reduction in 53BP1 recruitment, KIF18B may require microtubules for displacing 53BP1 to DSBs. Nevertheless, investigation of 53BP1 IRIF formation in cells expressing either KIF18B$^{\Delta TIM}$ or KIF18B^{MD}, with both endogenous KIF18B depletion and microtubule poisoning, has been suggested to support our hypothesis.

Chapter 4: Investigating the existence of microtubules in the nucleus

4.1. Summary

53BP1 is implicated in DSBs mobility including The movement of de-protected telomeres and IR induced DSBs (Mirman and de Lange, 2020). Provided by our results, we have shown 53BP1 interaction with a kinesin, KIF18B, and involvement of KIF18B in DDR. On the other hand, we have shown motor domain of KIF18B is s required for 53BP1 recruitment to IRIFs and TIFs. Kinesins are motor proteins and require microtubules to move along them through ATP hydrolysing.

Followed by published evidence of actin polymerisation in the nucleus upon DNA damage in mammalian cells (Belin et al., 2015), as well as formation of DNA damage-inducible intranuclear microtubule filaments (DIMs) inside the nucleus of budding yeast (Oshidari et al., 2018), we sought to investigate the existence of microtubules in the nucleus.

We constructed a cDNA to express a GFP labelled microtubule-binding protein inside the nucleus as a biomarker to track any possible microtubule inside the nucleus. The preliminary results are promising and require more optimisation to find a definite answer to this controversial question.

4.2. Introduction

53BP1 is reported to promote microtubule-dependent DSBs mobility and maintain the fusion of de-protected telomeres (Lottersberger et al., 2015). Moreover, 53BP1 along with other damage response proteins including ATM, DNA-PK, and Ku80 is involved in pairing of DSB induced foci indicating the direct movement of neighbouring foci which reduced by 53BP1 depletion (Yamauchi et al., 2017)

Our data indicates the requirement of the KIF18B motor domain as well as the TIM domain for fusion of the de-protected telomeres and 53BP1 stained TIF formation. Moreover, we have shown the dependence of 53BP1 efficient IRIF formation upon damage on KIF18B. Since KIF18B is a kinesin, and the motor function is an inevitable feature of it, it is not very unlikely to find the involvement of 53BP1 IRIF on the motor domain of KIF18B in accordance with the fact that disruption of microtubule filaments abrogates 53BP1 focal recruitment to IRIF.

We know the microtubules are the path for kinesins to move along them upon ATP hydrolysing to transport the cargos across the cell. Microtubules are abundant cytoplasmic fibres that have not been reported in the nuclei of eukaryotes that undergo open mitoses. Although in eukaryotes such as yeasts, which have closed mitoses, they are present, by definition, within the nucleus (Laporte et al., 2013). DNA damage-inducible intranuclear microtubule filaments (DIMs) also specifically showed to be involved in repair in budding yeast, through promoting the damaged DNA mobility and cooperating with Kar3 as a kinesin-14 family member (Oshidari et al., 2018).

To address the mechanism of KIF18B motor domain involvement in DDR through interaction with 53BP1, a provocative hypothesis is that the motor function of KIF18B is microtubule-dependent within the nucleus transporting 53BP1 and facilitating DSBs movement. Proving this possibility would require nuclear microtubules to exist in the nucleus under rare circumstances. For example, such fibres might

only be present at very low concentration, be very short-lived and be relatively short in length.

To investigate the probability of microtubule existence in the nucleus, we constructed a cDNA, encoding the GFP tagged, microtubule-binding domain of the Tau protein sequestered to the nucleus via three NLSs in its sequence.

By expression of the construct in U2OS cells confirmed the binding of the construct to the microtubule from observing the mitotic cells. The expression level of the cDNA should be optimized to avoid overexpression resulting in odd structures in the cells.

4.3. Materials and Methods

4.3.1. Cell culture

Cells were cultured at 37°C in a humidified atmosphere of 5% CO_2. U2OS, HeLa, and HEK293T were cultured using DMEM supplemented with 10% FBS (Biosciences). hTERT immortalized RPE-1 cells were cultured in DMEM-F12 media supplemented with 10% FBS. All cell lines were cultured in 1% penicillin-streptomycin (Biosciences).

4.3.2. Protein extraction

Protein extracts were prepared by lysing cells in lysis buffer (50mM Tris-HCl, 0.5% NP40, 150mM NaCl, 10% glycerol, 1mM $MgCl_2$, protease and phosphatase inhibitors) and a 1:1000 dilution of Benzonase nuclease (Sigma Aldrich) for 45 min at 4°C. Samples were centrifuged for 20 min at 14,000 rpm at 4°C, the supernatant was used for downstream applications. The protein concentrations were measured using Bradford reagent.

4.3.3. Western blotting

The concentration of proteins was adjusted to be the same and diluted with 4X sample buffer (2.0 ml 1M Tris-HCl pH 6.8, 0.8 g SDS, 4.0 ml 100% glycerol, 0.4 ml 14.7 M β-mercaptoethanol, 1.0 ml 0.5 M EDTA, 8 mg Bromophenol Blue). The separation of proteins carried out on sodium dodecyl sulphate polyacrylamide gel electrophoresis (SDS-PAGE). Proteins were transferred to a nitrocellulose membrane using 0.35 mA for 1h at 4°C. Membranes were blocked in 5% milk-TBST for 20 min at RT. The conditions for probing with the primary and secondary antibody are mentioned in Table 4.1. Following overnight probing for the primary Ab, membranes were washed 3 times with TBST and incubated with the relevant secondary antibody for 60 min at RT.

Table 4.1. List of antibodies and conditions used for western blotting

Antibody	Dilution	Blocking	Species	Manufacturer	Catalogue Number
KIF18B	1:1000	5% milk	Rabbit	Sigma Aldrich	HPA024205
Actin	1:5000	5% milk	Rabbit	Sigma Aldrich	A2066
Goat Anti-Rabbit IgG	1:5000	5%milk	Goat	Thermoscientific	31460

4.3.4. Immunofluorescence staining

Coverslips sterilized under UV for 20 min before seeding cells. $2.5x10^5$ to $1.5x10^5$ (depending on the purpose of thd experiment) cells were grown on a sterile coverslip. 24 to 48 h following the seeding, coverslips were briefly washed twice with PBS. Cells were fixed in 4% PFA for 10 min at RT, or in ice-cold methanol for 20 min at -20°C Coverslips were washed three times in PBS. Slides were mounted using vectashield media with DAPI. Images were captured on a Deltavision integrated microscope system mounted on an IX71 Olympus microscope and using Softworx software. 0.2-0.5 µm Z-stacks were collected, deconvolved, projected, and merged. Microscopy analysis performed using ImageJ 1.52n software.

4.3.5. Generation of microtubule-binding plasmid

Microtubule binding domain (MBD) of the Tau protein amplified from PRk5-EGFP-Tau using MBD-Nhe1-Fw and MBD-Age1-Rv primers (Table 4.2). The UTR230 (Actin binding domain) cut out from the UTR230-EGFP-3xNLS using Cla1 and Sal1. The MBD was cloned into the EGFPC1-3xNLS to generate MDB-Tau-GFP-3xNLS.

4.3.6. Site-directed mutagenesis

A pair of forward and reverse primer were designed to contain the targeted mutation (Table 4.2). After running PCR, 1 µl Dpn1 added to the tubes and incubated for 2-3 h at 37˚C. The PCR product purified and eluted in 30 µl elution buffer (Macherey-Nagel Ref: 740609.50). 3µl of the purified DNA transformed into Competent cells (Top10). The extracted Plasmid (using Macherey-Nagel Ref: 740588.50) was screened by restriction digest and sequencing.

Table 4.2. List of primers

Name	Sequence (5'-3')
MBD-Nhe1-Fw	ATACTGTCTAGAATGAAGAGCCGCCTGCAGACAGC
MBD-Age1-Rv	ttttttACCGGTaaTGGCGACTTGTACACGATCTCCG
Mutagen v1-Fw	TGTACGGTGGGAGGTCTgTATAAGCAGAGCTGGTTTAGT
Mutagen v1-Rv	ACTAAACCAGCTCTGCTTATAcAGACCTCCCACCGTACA
Mutagen v2-Fw	TGTACGGTGGGAGGTCTgTgTAAGCAGAGCTGGTTTAGT
Mutagen v2-Rv	ACTAAACCAGCTCTGCTTAcAcAGACCTCCCACCGTACA
Mutagen v3-Fw	TGTACGGTGGGAGGTCTAGCAGAGCTGGTTTAGT
Mutagen v3-Rv	ACTAAACCAGCTCTGCTAGACCTCCCACCGTACA

4.3.7. cDNA transfection

Cells were grown to 80-90% confluency and transfected with 1µg of DNA and 2µl of Lipofectamine2000 (Life Technologies) diluted in 500 µl Opti-MEM (Gibco) added into 2ml DMEM with 10% FBS per 35 mm dish. Cells were grown for 48 h prior to analysis by immunofluorescence and western blot.

4.4. Results

4.4.1. Microtubule targeting cDNA construction

To explore the possible existence of microtubules in the nucleus, first, we needed to construct a cDNA expressing a traceable microtubule-binding protein as a biomarker.

Microtubules are formed from $\alpha\beta$-tubulin heterodimers which are stabilized through binding to microtubule-associated proteins (MAPs). MAPs bind directly to the polymerised or depolymerised tubulin. Tau protein is categorized as a type2 MAP that binds to the inner microtubule surface via a conserved repeated PGGG sequence at the C-terminal (Kar, 2003). The Tau microtubule-binding repeats with 60-70% similarity to the other MAPs, conserved from Drosophila to human (Heidary and Fortini, 2001).

Inspired by the recent paper that showed the actin filaments polymerization in the nucleus after DNA damage through expressing the actin-binding domain sequestered to the nucleus via 3XNLS (Belin et al., 2015), We cloned the microtubule-binding domain (MBD) of the Tau protein including four tandem repeats and the linker sequence to pEGFP-C1-3XNLS. The MBD-Tau-pEGFP-3XNLS construct would be able to express the GFP tagged-Tau microtubule-binding domain sequestered to the nucleus (Figure 4.1.).

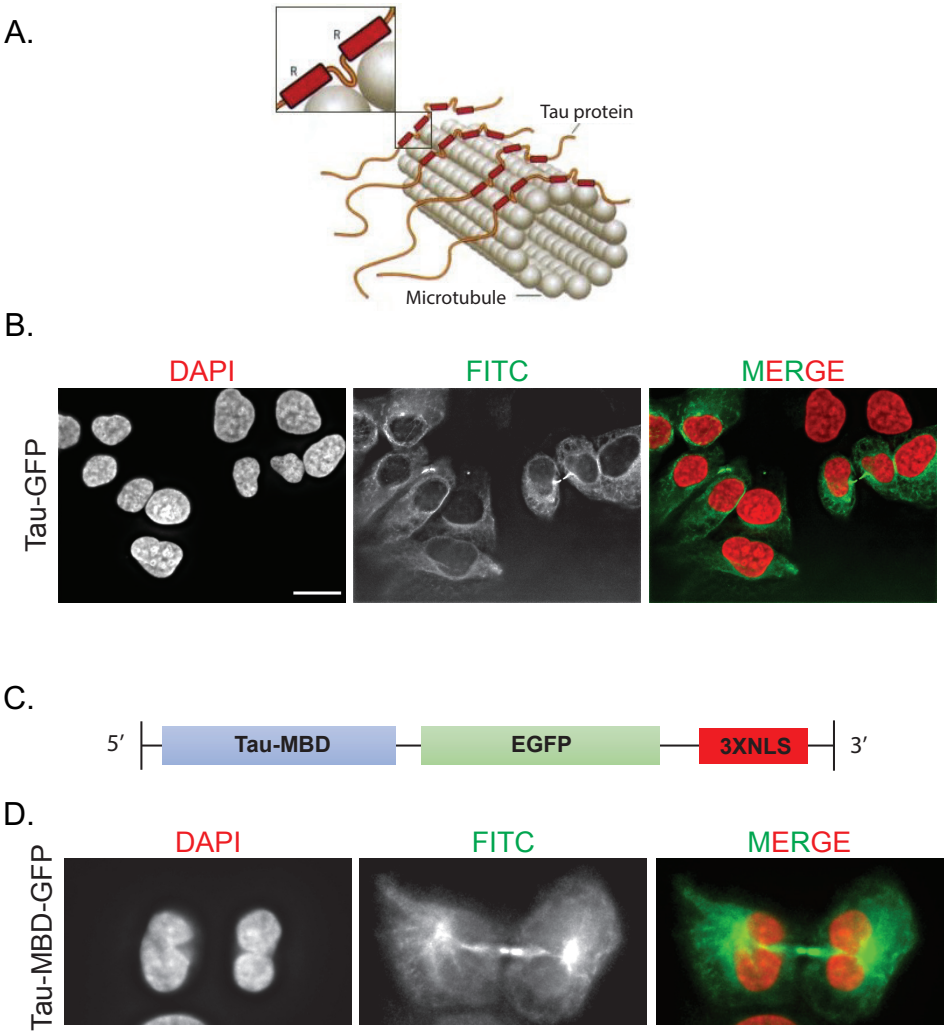

Figure 4.1. Construction and expression of MBD-Tau-pEGFP-3XNLS cDNA

(A) Schematic of Tau tetrameric protein binding to microtubule filaments. [Adapted from (Goode and Feinstein, 1994)] (B) Tau-GFP expression in U2OS cells. DAPI stained DNA is shown in the1st panel, Tau-GFP is shown in the 2nd panel representing the microtubules. In the 3rd panel the two channels are merged and DAPI shown in red whereas Tau-GFP presented in green, the scale bar represents 25µm. (C) Schematic structure of the constructed plasmid to express Tau-MBD-GFP to be sequestered into the nucleus via the 3xNLs and target microtubules. (D) Representative image of a mitotic cell, expressing MBD-Tau-pEGFP-3XNLS. DAPI stain is shown in the1st panel, MBD-Tau-pEGFP expression shown in the 2nd panel confirming the Tau-MBD binding to microtubules. In the 3rd panel, the two channels are merged and DAPI is shown in red and MBD-Tau-pEGFP is presented in green.

4.4.2. MBD-Tau-pEGFP-3XNLS expression

We expressed the MBD-Tau-pEGFP-3XNLS in U2OS cells to detect any GFP signal in the nucleus indicating the probability of microtubule existence in the nucleus. First, we checked the construct's capability to bind microtubules. As it has shown in figure 4.1., the Tau-MBD binds to the spindle microtubules in a mitotic cell. However, by looking at the GFP illuminated mitotic spindle, it is apparent that Tau-MBD is greatly overexpressed.

In order to lower the expression of MBD-Tau-pEGFP-3XNLS and optimize it to rule out any artefactual green signal observed in the nucleus out of overexpression, we have mutated the TATA box within the CMV promoter of the constructed plasmid. Using site-directed mutagenesis, we incorporated two types of A/G substitution point mutation, and one deletion mutation which completely removed the TATA box from the promoter (Figure 4.2.).

Comparing the expression level of the version 2 and 3 harbouring A/G mutation and TATA box deletion respectively, the level of expression is reduced by more than one-tenth in version 2 and approximately one-twentieth in version 3. The microscopic images also showing more structural patterns in mutated versions comparing to the unmutated which mostly showed artefactual overexpression.

The expression level of the MBD-Tau-pEGFP-3XNLS needs to be more evaluated to make sure it is expressing at the right expression level with more proper controls.

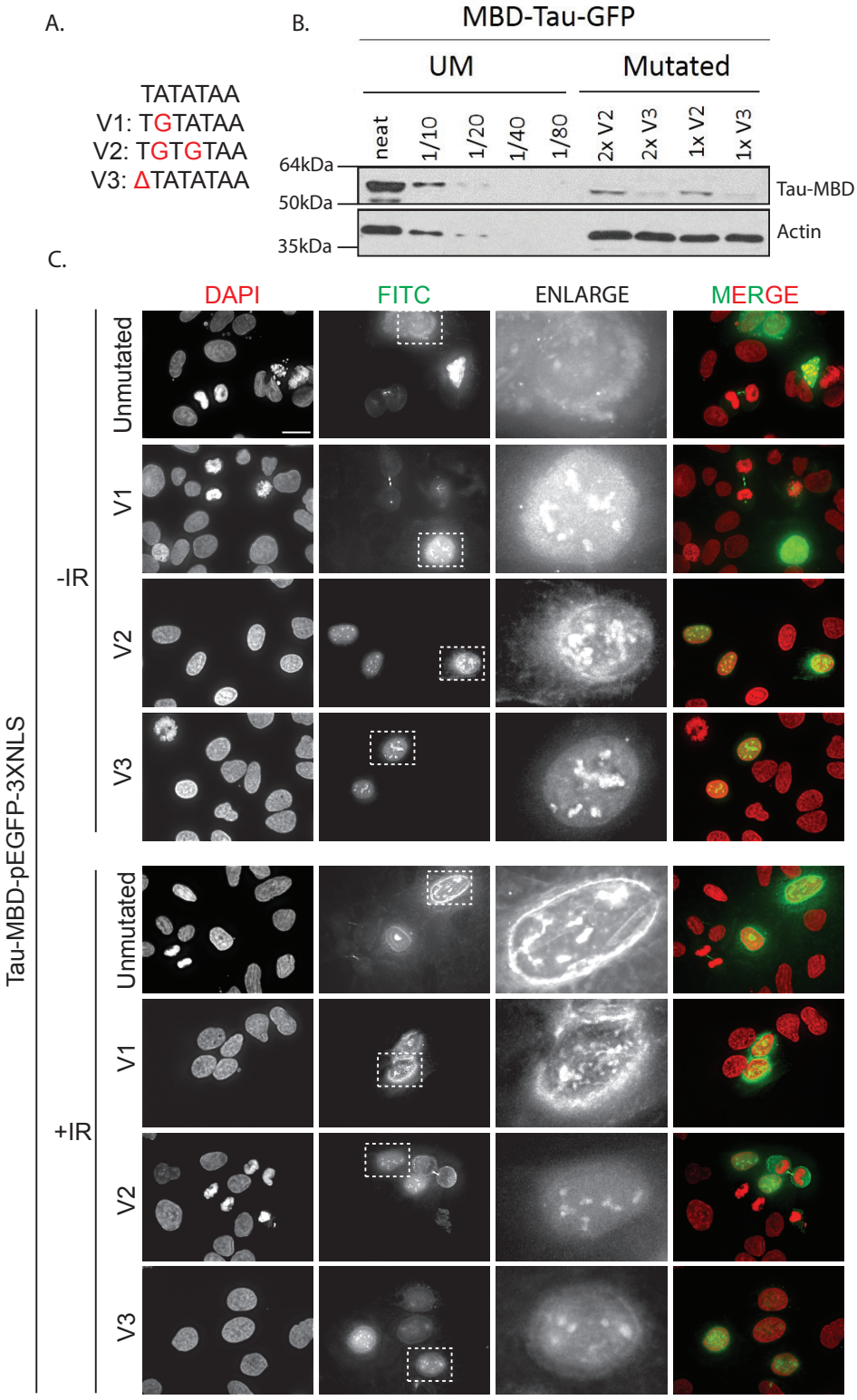
A.
TATATAA
V1: TGTATAA
V2: TGTGTAA
V3: ΔTATATAA
B.
MBD-Tau-GFP
UM
Mutated
neat
1/10
1/20
1/40
1/80
2x V2
2x V3
1x V2
1x V3
64kDa
50kDa
35kDa
Tau-MBD
Actin
C.
DAPI
FITC
ENLARGE
MERGE
Tau-MBD-pEGFP-3XNLS
-IR
+IR
Unmutated
V1
V2
V3

Figure 4.2.

Figure 4.2. MBD-Tau-pEGFP-3XNLS expression optimisation

(A) Three different versions of mutation in TATA box, including one and two A/G point mutations plus its complete deletion. (B) Western blot of mutated versions 2 and 3 (cell extracts are loaded neat (1X) and in double (2X)) along with the diluted extracts (Neat, 1/10. 1/20, 1/40, and 1/80) of unmutated cells to compare the reduction of overexpression of ectopically expressed MBD-Tau-GFP. Actin is used as the loading control. (C) Unmutated and three types of CMV promoter MBD-Tau-pEGFP-3XNLS mutated versions expression in U2OS cells before and after 3Gy irradiation as indicated on the left. DAPI staining, FITC channel indicating expression of Tau-MBD-GFP-3XNLS are shown in the first and second columns respectively. The third column is the enlargement of the selection in the second column. The fourth column is the merge of DAPI in red and Tau-MBD-3xNLS in green.

4.5. Discussion

Microtubules are highly dynamic polymers composed of α and β tubulin dimers. There are range of critical functions for microtubules such as cytoskeletal foundation, vesicle and organelle transportation, cilia and flagella formation, and cell division. Microtubules have a close collaboration with kinesin and dynein in terms of transportation of cargos in the cytoskeleton.

We have shown the interaction of KIF18B as a member of the kinesin 8 superfamily with 53BP1 to promote efficient DSBs repair. KIF18B requirement for efficient 53BP1 IRIF and TIF formation and fusion of de-protected telomeres are pieces of evidence of KIF18B involvement in DDR while interacting with 53BP1. Moreover, microtubule poisoning agent treatment of cells abrogates the 53BP1 IRIF formation as KIF18B depletion does. It is reported that microtubules are regulating the damage response proteins traffic within the nucleus (Poruchynsky et al., 2015). As 53BP1 was implicated in the repair of distal DSB via NHEJ (Dimitrova et al., 2008), one hypothesis could be that the motor domain of KIF18B might be required to facilitate the movement of distally located breaks. Whether or not this might also involve microtubules in the nucleus remains a controversial question given that orthodoxy indicates that microtubules do not exist in the nucleus.

So far, the lack of evidence indicating the existence of microtubules in the nucleus of eukaryotic cells which undergo open mitosis might be

due to a lack of molecular tools for detecting microtubules in the nucleus without affecting cytoplasmic microtubules.

There are some possible reasons to explain our inability to show the possible existence of microtubule in the nucleus with the currently available technologies. Probably they are too short, or their dynamic is different from the cytoskeleton and too fast to capture. Another reason might be the strong signal from the cytoplasmic microtubules masking the weak signal of the nuclear microtubules providing their existence. Constructing a signalling biosensor to detect and bind the presumptive microtubules is the plan of our laboratory to reveal microtubules in the nucleus and clear the mechanism of the KIF18B motor domain in DNA repair.

As recently reviewed, there are supporting shreds of evidence for the involvement of another filamentous polymer, nuclear actin in DSB repair via H(Hurst et al., 2019). Actin-binding protein 2/3, APR 2/3 are reported to be involved in this process through binding to the break sites, mediating clustering, and homology-directed repair (Schrank et al., 2018). Interestingly, F-actin polymerisation is also reported and implicated in the DDR (Belin et al., 2015). To elucidate actin polymers in the nucleus upon DNA damage, Belin BJ et al. used UTR230, a short variant of the most stable sub-populations of actin filaments, GFP, and 3XNLS on the pEGFP-C1 backbone (Belin et al., 2015). Similarly, we selected the Tau as one of the well-known microtubule-associated proteins that interact with microtubules through conserved domains.

Expressing the MBD-Tau-pEGFP-3XNLS in U2OS cells resulted in GFP signal in the nucleus while the binding of the GFP tagged expressed protein was confirmed in mitotic cells. But the construction was overexpressed and probably causing artefactual signals in the cells. Although reduced expression of the MBD-Tau was observed upon TATA box mutation within the CMV promoter but yet the microscopic images of transfected U2OS cells showing GFP illuminated structures in the nucleus are inconclusive as they are the

same in both irradiated and unirradiated cells. On the other hand, the microtubules maybe having a constant structure as part of nucleoskeleton beside numerus identified filaments in the nucleus (Simon and Wilson, 2011), irrespective to healthy or damaged condition, and at the event of damage serve as kinesin trajectories for DSBs movement and 53BP1 mediated repair.

To further investigate the microtubule existence in the nucleus we can use another MAP such as XMAP215 which is also highly conserved and interact with the plus end of microtubules. Exploring the other members of the tubulin superfamily such as γ, δ, ε and ζ would be other attempts to elucidate the existence of microtubules in the nucleus.

Chapter 5: Conclusion and future perspectives

5.1. Conclusion and future perspectives

The two major DSB repair pathways, NHEJ and HR, safeguard the genome's integrity against the endogenous and exogenous DNA damaging agents. 53BP1, one of the key mediators of the DDR, has a critical role in repair pathway choice by inhibiting the BRCA1-dependent resection required for HR and thereby promoting NHEJ (Guo et al., 2018). An additional function attributed to 53BP1 that ensures DSB repair fidelity is DSB mobilization (Lottersberger et al., 2015; Mirman and de Lange, 2020). Therefore, finding a kinesin, which has motor activity, as an interacting partner of 53BP1 in the proteomic screening performed in our laboratory (Maretto et al., unpublished) was intriguing to investigate.

The localisation of KIF18B was investigated by immunofluorescence. KIF18B showed primarily nuclear localisation, co-localising preferentially with the dense DAPI stained regions in the nucleus, suggestive of interaction with heterochromatin. The range of KIF18B signal intensity among exponentially growing cells was attributed to its cell cycle regulated expression. Our results showed that KIF18B has low expression level at G1, particularly early G1, and steadily increases with cell cycle progression with peak expression being reached in late G2/M. While being predominantly nuclear during interphase, in mitosis it is localised to microtubules with high levels of localisation to the plus ends of astral microtubules. This would be consistent with KIF18B's ability to 'walk' along the microtubules without destabilizing them (Tanenbaum et al., 2014) until it reaches a plus end where, in concert with MCAK, its microtubule depolymerising function is activated to ensure the correct microtubule dynamics required for the successful completion of mitosis.

Interestingly, and for the first time, we showed KIF18B localisation to the midbody during cytokinesis suggesting a role in cytokinesis that remains to be characterised. Since this KIF18B localisation to midbody is Aurora B dependent, this could suggest that either KIF18B is

involved in the regulation of the abscission checkpoint, or that it functions in microtubule dynamics as a microtubule depolymeriser facilitates abscission.

EB1 and MCAK are known KIF18B interacting partners in depolymerising astral microtubules at the plus end (Stout et al., 2011; Tanenbaum et al., 2011). We have shown that EB1 also localises to midbody in cytokinesis. Therefore, by imaging the cytokinetic cells stained for MCAK, and by monitoring cytokinesis events by live cell imaging in the presence and absence of KIF18B and its interacting partners—such as EB1, MCAK, and other DDR proteins—we can gain a foundational view about KIF18B's role in cytokinesis. Expression of KIF18B mutants either lacking the TIM domain or the motor defective version in KIF18B depleted cells would further elucidate the mechanism of KIF18B involvement in cytokinesis.

KIF18B co-localises with 53BP1 at IRIF and nuclear bodies; this is detectable in cells with low to medium levels of KIF18B. This observation indicates that either these two proteins have a cell cycle regulated interaction and co-localisation, or that this co-localisation is constant during interphase but the certain amount of KIF18B co-localised with 53BP1 is overwhelmed by the high level of KIF18B signal intensity in the nucleus when highly expressed.

We have implicated KIF18B in DNA damage repair by showing 53BP1 dependency on KIF18B for recruitment to IRIF for timely efficient DSB repair, detectable by γH2AX resolution at time points after damage. However, H4K20me2, which serves as a critical marker for 53BP1 recruitment to IRIF, was ruled out to be affected by KIF18B. Therefore, the dependence of 53BP1 on KIF18B for recruitment to DSBs is likely to be through the direct interaction of the KIF18B TIM domain and the Tudor domain of 53BP1. However, investigating the number and intensity of FK2 foci—a ubiquitination marker—in irradiated cells upon KIF18B depletion would be a good way to verify the effect of KIF18B on H2AK15 ubiquitination, another important factor for 53BP1 recruitment to IRIF.

Furthermore, 53BP1 is reported to promote NHEJ-mediated fusion of de-protected telomeres by increasing chromatin mobility (Dimitrova et al., 2008). The required force for this chromatin mobility is proposed to be transmitted from dynamic microtubules outside the nucleus to the 53BP1 proteins that bind chromatin, through the linker proteins between the cytoskeleton and the nucleoskeleton known as the LINC complex (Lottersberger et al., 2015).

In this work, we have shown that both the KIF18B motor domain and TIM domain are required for de-protected telomere fusion and 53BP1 recruitment to TIFs. A caveat based on existing models is: the possible involvement of KIF18B in producing the sufficient force, transmitted through the LINC complex from outside of the nucleus, to facilitate the repair of damaged DNA inside the nucleus via mobilization. Alternative speculation would be the existence of microtubules in the nucleus in a limited amount and certain circumstances, mediating the 53BP1-dependent directional movement of damaged DNA. Hypothetically, the latter model proposes that KIF18B interacts with 53BP1 as cargo via the TIM domain, and transports it within the nucleus via an active movement on the proposed microtubules, which will be discussed below.

As it is understood based on our results, abrogated 53BP1 focal recruitment to IRIFs upon disruption of microtubules is similar to the effect of KIF18B depletion. Besides, KIF18B's motor domain is involved in de-protected telomere fusion and 53BP1 recruitment to TIFs. While KIF18B co-localises with 53BP1 at IRIFs inside the nucleus, it would be hard to explain a paradoxical model for damaged DNA transportation through the movement of KIF18B on the microtubules outside of the nucleus.

A recent study characterised DNA damage-inducible intranuclear microtubule filaments (DIMs) inside the nucleus of budding yeast (Oshidari et al., 2018). In addition, Lamins, γTubulin, actin, myosin, and some kinesins (KIF4A, KIF17B, KIF18A, KIF18B, MCAK) are

shown as dynamical components in the nucleoskeleton (Simon and Wilson, 2011). Furthermore, actin polymerization in the nucleus upon DNA damage induction is reported in human cells (Belin et al., 2015).

Hence, after years of controversy, it is time to find the best technology to explore the possibility of the existence of microtubules in mammalian cells nucleus and to challenge the current orthodox belief.

There are some possible reasons to explain our inability to show the existence of microtubule in the nucleus with the currently available technologies. For one, nuclear microtubules would likely be very short and have different dynamics from cytoplasmic microtubules that are too fast to capture. Another reason might be the strong signal from the cytoplasmic microtubules masks the weak signal of the nuclear microtubules. Constructing a signalling biosensor to detect and bind the presumptive microtubules was our start point to reveal microtubules in the nucleus and provide a clear reason for the mechanism of the KIF18B motor domain involvement in DNA repair.

KIF18B is implicated as a carcinogenic driver gene; a bioinformatic study revealed more than 100 times *KIF18B* overexpression in breast, ovarian, kidney, liver, and lung cancers (Itzel et al., 2015). Moreover, in a very recent study, *KIF18B* proved to be up-regulated in hepatocellular carcinoma and linked with poor prognosis via lymph invasion and metastasis (Yang et al., 2020). Mutations in KIF18B are also shown in familial glioma as a type of fatal brain tumour (Jalali et al., 2015). Logically, as a protein with mitotic function, it is not surprising to find upregulation of KIF18B in malignancies but, based on our evidence on the involvement of KIF18B in DNA damage repair, KIF18B overexpression could also be the cells' defensive response to DNA damage. Therefore, further investigation on the mechanism of involvement of KIF18B in the DDR and its interaction with 53BP1 will help effective cancer therapy

References

Abe, S., Nagasaka, K., Hirayama, Y., Kozuka-Hata, H., Oyama, M., Aoyagi, Y., Obuse, C., and Hirota, T. (2011). The initial phase of chromosome condensation requires Cdk1-mediated phosphorylation of the CAP-D3 subunit of condensin II. Genes Dev. *25*, 863–874.

Abraham, R.T. (2004). PI 3-kinase related kinases: 'big' players in stress-induced signaling pathways. DNA Repair (Amst). *3*, 883–887.

Adhikari, D., Liu, K., and Shen, Y. (2012). Cdk1 drives meiosis and mitosis through two different mechanisms. Cell Cycle *11*, 2763–2764.

Ahel, I., Rass, U., El-Khamisy, S.F., Katyal, S., Clements, P.M., McKinnon, P.J., Caldecott, K.W., and West, S.C. (2006). The neurodegenerative disease protein aprataxin resolves abortive DNA ligation intermediates. Nature *443*, 713–716.

Ali, R., Ramadurai, S., Barry, F., and Nasheuer, H.P. (2018). Optimizing fluorescent protein expression for quantitative fluorescence microscopy and spectroscopy using herpes simplex thymidine kinase promoter sequences. FEBS Open Bio *8*, 1043–1060.

Allers, T., and Lichten, M. (2001). Differential Timing and Control of Noncrossover and Crossover Recombination during Meiosis. Cell *106*, 47–57.

Amiard, S., Doudeau, M., Pinte, S., Poulet, A., Lenain, C., Faivre-Moskalenko, C., Angelov, D., Hug, N., Vindigni, A., Bouvet, P., et al. (2007). A topological mechanism for TRF2-enhanced strand invasion. Nat. Struct. Mol. Biol. *14*, 147–154.

Andres, S.N., Vergnes, A., Ristic, D., Wyman, C., Modesti, M., and Junop, M. (2012). A human XRCC4–XLF complex bridges DNA. Nucleic Acids Res. *40*, 1868–1878.

Aymard, F., and Legube, G. (2016). A TAD closer to ATM. Mol. Cell. Oncol. *3*, e1134411.

Bakkenist, C.J., and Kastan, M.B. (2003). DNA damage activates ATM through intermolecular autophosphorylation and dimer dissociation. Nature *421*, 499–506.

Bakkenist, C.J., and Kastan, M.B. (2004). Initiating Cellular Stress Responses. Cell *118*, 9–17.

Barazas, M., Annunziato, S., Pettitt, S.J., de Krijger, I., Ghezraoui, H., Roobol, S.J., Lutz, C., Frankum, J., Song, F.F., Brough, R., et al. (2018). The CST Complex Mediates End Protection at Double-Strand Breaks and Promotes PARP Inhibitor Sensitivity in BRCA1-Deficient Cells. Cell Rep. *23*, 2107–2118.

Barnum, K.J., and O'Connell, M.J. (2014). Cell cycle regulation by checkpoints. Methods Mol. Biol.

Barr, F.A., and Gruneberg, U. (2007). Cytokinesis: Placing and Making the Final Cut. Cell *131*, 847–860.

Bartek, J., and Lukas, J. (2001). Mammalian G1- and S-phase checkpoints in response to DNA damage. Curr. Opin. Cell Biol. *13*, 738–747.

Becker, J.R., Cuella-Martin, R., Barazas, M., Liu, R., Oliveira, C., Oliver, A.W., Bilham, K., Holt, A.B., Blackford, A.N., Heierhorst, J., et al. (2018). The ASCIZ-DYNLL1 axis promotes 53BP1-dependent non-homologous end joining and PARP inhibitor sensitivity. Nat. Commun. *9*, 5406.

Bekker-Jensen, S., and Mailand, N. (2010). Assembly and function of DNA double-strand break repair foci in mammalian cells. DNA Repair (Amst). *9*, 1219–1228.

Belin, B.J., Lee, T., and Mullins, R.D. (2015). DNA damage induces nuclear actin filament assembly by Formin-2 and Spire-1/2 that promotes efficient DNA repair. Elife *4*.

Benjamin, R.C., and Gill, D.M. (1980). ADP-ribosylation in mammalian cell ghosts. Dependence of poly(ADP-ribose) synthesis on strand breakage in DNA. J. Biol. Chem. *255*, 10493–10501.

Bennardo, N., Cheng, A., Huang, N., and Stark, J.M. (2008). Alternative-NHEJ Is a Mechanistically Distinct Pathway of Mammalian Chromosome Break Repair. PLoS Genet. *4*, e1000110.

Bernstein, N.K., Williams, R.S., Rakovszky, M.L., Cui, D., Green, R., Karimi-Busheri, F., Mani, R.S., Galicia, S., Koch, C.A., Cass, C.E., et al. (2005). The Molecular Architecture of the Mammalian DNA Repair Enzyme, Polynucleotide Kinase. Mol. Cell *17*, 657–670.

Bertoli, C., Skotheim, J.M., and de Bruin, R.A.M. (2013). Control of cell cycle transcription during G1 and S phases. Nat. Rev. Mol. Cell Biol. *14*, 518–528.

References

Bétermier, M., Bertrand, P., and Lopez, B.S. (2014). Is Non-Homologous End-Joining Really an Inherently Error-Prone Process? PLoS Genet. *10*, e1004086.

Bilaud, T., Brun, C., Ancelin, K., Koering, C.E., Laroche, T., and Gilson, E. (1997). Telomeric localization of TRF2, a novel human telobox protein. Nat. Genet. *17*, 236–239.

Bjursell, G., and Reichard, P. (1973). Effects of thymidine on deoxyribonucleoside triphosphate pools and deoxyribonucleic acid synthesis in Chinese hamster ovary cells. J. Biol. Chem. *248*, 3904–3909.

Boboila, C., Oksenych, V., Gostissa, M., Wang, J.H., Zha, S., Zhang, Y., Chai, H., Lee, C.-S., Jankovic, M., Saez, L.-M.A., et al. (2012). Robust chromosomal DNA repair via alternative end-joining in the absence of X-ray repair cross-complementing protein 1 (XRCC1). Proc. Natl. Acad. Sci. *109*, 2473–2478.

Booher, R.N., Holman, P.S., and Fattaey, A. (1997). Human Myt1 Is a Cell Cycle-regulated Kinase That Inhibits Cdc2 but Not Cdk2 Activity. J. Biol. Chem. *272*, 22300–22306.

BOSTOCK, C. (1971). An evaluation of the double thymidine block for synchronizing mammalian cells at the G1-S border*1. Exp. Cell Res. *68*, 163–168.

Botuyan, M.V., Lee, J., Ward, I.M., Kim, J.-E., Thompson, J.R., Chen, J., and Mer, G. (2006). Structural Basis for the Methylation State-Specific Recognition of Histone H4-K20 by 53BP1 and Crb2 in DNA Repair. Cell *127*, 1361–1373.

Bouwman, P., Aly, A., Escandell, J.M., Pieterse, M., Bartkova, J., van der Gulden, H., Hiddingh, S., Thanasoula, M., Kulkarni, A., Yang, Q., et al. (2010). 53BP1 loss rescues BRCA1 deficiency and is associated with triple-negative and BRCA-mutated breast cancers. Nat. Struct. Mol. Biol. *17*, 688–695.

Brady, S., Lasek, R., and Allen, R. (1982). Fast axonal transport in extruded axoplasm from squid giant axon. Science (80-.). *218*, 1129–1131.

Brouwer, I., Zhang, H., Candelli, A., Normanno, D., Peterman, E.J.G., Wuite, G.J.L., and Modesti, M. (2017). Human RAD52 Captures and Holds DNA Strands, Increases DNA Flexibility, and Prevents Melting of Duplex DNA: Implications for DNA Recombination. Cell Rep. *18*, 2845–2853.

Bruce, A. (2008). Molecular Biology of The Cell. 1601.

Bryan, T.M., Englezou, A., Dalla-Pozza, L., Dunham, M.A., and Reddel, R.R. (1997). Evidence for an alternative mechanism for maintaining telomere length in human tumors and tumor-derived cell lines. Nat. Med. *3*, 1271–1274.

Bunting, S.F., Callén, E., Wong, N., Chen, H.-T., Polato, F., Gunn, A., Bothmer, A., Feldhahn, N., Fernandez-Capetillo, O., Cao, L., et al. (2010). 53BP1 Inhibits Homologous Recombination in Brca1-Deficient Cells by Blocking Resection of DNA Breaks. Cell *141*, 243–254.

Burke, B. (2001). The nuclear envelope: filling in gaps. Nat. Cell Biol. *3*, E273–E274.

Burma, S., Chen, B.P., Murphy, M., Kurimasa, A., and Chen, D.J. (2001). ATM Phosphorylates Histone H2AX in Response to DNA Double-strand Breaks. J. Biol. Chem. *276*, 42462–42467.

Busino, L., Donzelli, M., Chiesa, M., Guardavaccaro, D., Ganoth, D., Valerio Dorrello, N., Hershko, A., Pagano, M., and Draetta, G.F. (2003). Degradation of Cdc25A by β-TrCP during S phase and in response to DNA damage. Nature *426*, 87–91.

Bzymek, M., Thayer, N.H., Oh, S.D., Kleckner, N., and Hunter, N. (2010). Double Holliday junctions are intermediates of DNA break repair. Nature *464*, 937–941.

Cadet, J., and Wagner, J.R. (2013). DNA Base Damage by Reactive Oxygen Species, Oxidizing Agents, and UV Radiation. Cold Spring Harb. Perspect. Biol. *5*, a012559–a012559.

Callen, E., Di Virgilio, M., Kruhlak, M.J., Nieto-Soler, M., Wong, N., Chen, H.-T., Faryabi, R.B., Polato, F., Santos, M., Starnes, L.M., et al. (2013). 53BP1 Mediates Productive and Mutagenic DNA Repair through Distinct Phosphoprotein Interactions. Cell *153*, 1266–1280.

Canman, C.E. (1998). Activation of the ATM Kinase by Ionizing Radiation and Phosphorylation of p53. Science (80-.). *281*, 1677–1679.

Capalbo, L., Mela, I., Abad, M.A., Jeyaprakash, A.A., Edwardson, J.M., and D'Avino, P.P. (2016). Coordinated regulation of the ESCRT-III component CHMP4C by the chromosomal passenger complex and centralspindlin during cytokinesis. Open Biol. *6*, 160248.

Carlton, J.G., Caballe, A., Agromayor, M., Kloc, M., and Martin-Serrano, J. (2012). ESCRT-III Governs the Aurora B-Mediated Abscission Checkpoint Through CHMP4C. Science (80-.). *336*, 220–225.

Carmena, M., Wheelock, M., Funabiki, H., and Earnshaw, W.C. (2012). The chromosomal passenger complex (CPC): from easy rider to the godfather of mitosis. Nat. Rev. Mol. Cell Biol. *13*, 789–803.

Caron, P., Choudjaye, J., Clouaire, T., Bugler, B., Daburon, V., Aguirrebengoa, M., Mangeat, T., Iacovoni, J.S., Álvarez-Quilón, A., Cortés-Ledesma, F., et al. (2015). Non-redundant Functions of ATM and DNA-PKcs in Response to DNA Double-Strand Breaks. Cell Rep. *13*, 1598–1609.

Ceballos, S.J., and Heyer, W.-D. (2011). Functions of the Snf2/Swi2 family Rad54 motor protein in homologous recombination. Biochim. Biophys. Acta - Gene Regul. Mech. *1809*, 509–523.

Ceccaldi, R., Rondinelli, B., and D'Andrea, A.D. (2016). Repair Pathway Choices and Consequences at the Double-Strand Break. Trends Cell Biol. *26*, 52–64.

Celli, G.B., and de Lange, T. (2005). DNA processing is not required for ATM-mediated telomere damage response after TRF2 deletion. Nat. Cell Biol. *7*, 712–718.

Celli, G.B., Denchi, E.L., and de Lange, T. (2006). Ku70 stimulates fusion of dysfunctional telomeres yet protects chromosome ends from homologous recombination. Nat. Cell Biol. *8*, 885–890.

Chapman, J.R., Taylor, M.R.G., and Boulton, S.J. (2012a). Playing the End Game: DNA Double-Strand Break Repair Pathway Choice. Mol. Cell *47*, 497–510.

Chapman, J.R., Sossick, A.J., Boulton, S.J., and Jackson, S.P. (2012b). BRCA1-associated exclusion of 53BP1 from DNA damage sites underlies temporal control of DNA repair. J. Cell Sci. *125*, 3529–3534.

Chapman, J.R., Barral, P., Vannier, J.-B., Borel, V., Steger, M., Tomas-Loba, A., Sartori, A.A., Adams, I.R., Batista, F.D., and Boulton, S.J. (2013). RIF1 Is Essential for 53BP1-Dependent Nonhomologous End Joining and Suppression of DNA Double-Strand Break Resection. Mol. Cell *49*, 858–871.

Chen, H.T. (2000). Response to RAG-Mediated V(D)J Cleavage by

NBS1 and gamma-H2AX. Science (80-.). *290*, 1962–1964.

Chen, J., Li, P., Song, L., Bai, L., Huen, M.S.Y., Liu, Y., and Lu, L.-Y. (2020). 53BP1 loss rescues embryonic lethality but not genomic instability of BRCA1 total knockout mice. Cell Death Differ. *27*, 2552–2567.

Chen, M.-S., Ryan, C.E., and Piwnica-Worms, H. (2003). Chk1 Kinase Negatively Regulates Mitotic Function of Cdc25A Phosphatase through 14-3-3 Binding. Mol. Cell. Biol. *23*, 7488–7497.

Cheung-Ong, K., Giaever, G., and Nislow, C. (2013). DNA-Damaging Agents in Cancer Chemotherapy: Serendipity and Chemical Biology. Chem. Biol. *20*, 648–659.

Chiolo, I., Minoda, A., Colmenares, S.U., Polyzos, A., Costes, S. V., and Karpen, G.H. (2011). Double-Strand Breaks in Heterochromatin Move Outside of a Dynamic HP1a Domain to Complete Recombinational Repair. Cell *144*, 732–744.

Cho, N.W., Dilley, R.L., Lampson, M.A., and Greenberg, R.A. (2014). Interchromosomal Homology Searches Drive Directional ALT Telomere Movement and Synapsis. Cell *159*, 108–121.

Christ, L., Raiborg, C., Wenzel, E.M., Campsteijn, C., and Stenmark, H. (2017). Cellular Functions and Molecular Mechanisms of the ESCRT Membrane-Scission Machinery. Trends Biochem. Sci. *42*, 42–56.

Chu, T.W., and Autexier, C. (2016). Telomeres and Chromosome Stability. In The Functional Nucleus, (Cham: Springer International Publishing), pp. 127–154.

Chung, D.K.C., Chan, J.N.Y., Strecker, J., Zhang, W., Ebrahimi-Ardebili, S., Lu, T., Abraham, K.J., Durocher, D., and Mekhail, K. (2015). Perinuclear tethers license telomeric DSBs for a broad kinesin- and NPC-dependent DNA repair process. Nat. Commun. *6*, 7742.

Ciccia, A., and Elledge, S.J. (2010). The DNA Damage Response: Making It Safe to Play with Knives. Mol. Cell *40*, 179–204.

Cimprich, K.A., and Cortez, D. (2008). ATR: an essential regulator of genome integrity. Nat. Rev. Mol. Cell Biol. *9*, 616–627.

Clouaire, T., and Legube, G. (2019). A Snapshot on the Cis Chromatin Response to DNA Double-Strand Breaks. Trends Genet.

35, 330–345.

Cobb, J.A. (2005). Replisome instability, fork collapse, and gross chromosomal rearrangements arise synergistically from Mec1 kinase and RecQ helicase mutations. Genes Dev. *19*, 3055–3069.

Cortez, D. (2015). Preventing replication fork collapse to maintain genome integrity. DNA Repair (Amst). *32*, 149–157.

Costantini, S., Woodbine, L., Andreoli, L., Jeggo, P.A., and Vindigni, A. (2007). Interaction of the Ku heterodimer with the DNA ligase IV/Xrcc4 complex and its regulation by DNA-PK. DNA Repair (Amst). *6*, 712–722.

Cottingham, F.R., and Hoyt, M.A. (1997). Mitotic Spindle Positioning in Saccharomyces cerevisiae Is Accomplished by Antagonistically Acting Microtubule Motor Proteins. J. Cell Biol. *138*, 1041–1053.

Coverley, D., Laman, H., and Laskey, R.A. (2002). Distinct roles for cyclins E and A during DNA replication complex assembly and activation. Nat. Cell Biol. *4*, 523–528.

Crisp, M., Liu, Q., Roux, K., Rattner, J.B., Shanahan, C., Burke, B., Stahl, P.D., and Hodzic, D. (2006). Coupling of the nucleus and cytoplasm: Role of the LINC complex. J. Cell Biol. *172*, 41–53.

D'Avino, P.P., Giansanti, M.G., and Petronczki, M. (2015). Cytokinesis in Animal Cells. Cold Spring Harb. Perspect. Biol. *7*, a015834.

Dantzer, F., de la Rubia, G., Ménissier-de Murcia, J., Hostomsky, Z., de Murcia, G., and Schreiber, V. (2000). Base Excision Repair Is Impaired in Mammalian Cells Lacking Poly(ADP-ribose) Polymerase-1 †. Biochemistry *39*, 7559–7569.

deCastro, M.J., Fondecave, R.M., Clarke, L.A., Schmidt, C.F., and Stewart, R.J. (2000). Working strokes by single molecules of the kinesin-related microtubule motor ncd. Nat. Cell Biol. *2*, 724–729.

Dekker, J., and Mirny, L. (2016). The 3D Genome as Moderator of Chromosomal Communication. Cell *164*, 1110–1121.

Della-Maria, J., Zhou, Y., Tsai, M.-S., Kuhnlein, J., Carney, J.P., Paull, T.T., and Tomkinson, A.E. (2011). Human Mre11/Human Rad50/Nbs1 and DNA Ligase IIIα/XRCC1 Protein Complexes Act Together in an Alternative Nonhomologous End Joining Pathway*. J.

Biol. Chem. *286*, 33845–33853.

Denchi, E.L., and de Lange, T. (2007). Protection of telomeres through independent control of ATM and ATR by TRF2 and POT1. Nature *448*, 1068–1071.

Deng, Y., Guo, X., Ferguson, D.O., and Chang, S. (2009). Multiple roles for MRE11 at uncapped telomeres. Nature *460*, 914–918.

Derbyshire, D.J. (2002). Crystal structure of human 53BP1 BRCT domains bound to p53 tumour suppressor. EMBO J. *21*, 3863–3872.

Dev, H., Chiang, T.-W.W., Lescale, C., de Krijger, I., Martin, A.G., Pilger, D., Coates, J., Sczaniecka-Clift, M., Wei, W., Ostermaier, M., et al. (2018). Shieldin complex promotes DNA end-joining and counters homologous recombination in BRCA1-null cells. Nat. Cell Biol. *20*, 954–965.

Dianov, G., and Lindahl, T. (1994). Reconstitution of the DNA base excision—repair pathway. Curr. Biol. *4*, 1069–1076.

Difilippantonio, S., Gapud, E., Wong, N., Huang, C.-Y., Mahowald, G., Chen, H.T., Kruhlak, M.J., Callen, E., Livak, F., Nussenzweig, M.C., et al. (2008). 53BP1 facilitates long-range DNA end-joining during V(D)J recombination. Nature *456*, 529–533.

Dimitrova, N., and de Lange, T. (2009). Cell Cycle-Dependent Role of MRN at Dysfunctional Telomeres: ATM Signaling-Dependent Induction of Nonhomologous End Joining (NHEJ) in G1 and Resection-Mediated Inhibition of NHEJ in G2. Mol. Cell. Biol. *29*, 5552–5563.

Dimitrova, N., Chen, Y.-C.M., Spector, D.L., and de Lange, T. (2008). 53BP1 promotes non-homologous end joining of telomeres by increasing chromatin mobility. Nature *456*, 524–528.

Dion, V., Kalck, V., Horigome, C., Towbin, B.D., and Gasser, S.M. (2012). Increased mobility of double-strand breaks requires Mec1, Rad9 and the homologous recombination machinery. Nat. Cell Biol. *14*, 502–509.

DiTullio, R.A., Mochan, T.A., Venere, M., Bartkova, J., Sehested, M., Bartek, J., and Halazonetis, T.D. (2002). 53BP1 functions in an ATM-dependent checkpoint pathway that is constitutively activated in human cancer. Nat. Cell Biol. *4*, 998–1002.

Doksani, Y., Wu, J.Y., de Lange, T., and Zhuang, X. (2013). Super-

Resolution Fluorescence Imaging of Telomeres Reveals TRF2-Dependent T-loop Formation. Cell *155*, 345–356.

DOUGLAS, P., SAPKOTA, G.P., MORRICE, N., YU, Y., GOODARZI, A.A., MERKLE, D., MEEK, K., ALESSI, D.R., and LEES-MILLER, S.P. (2002). Identification of in vitro and in vivo phosphorylation sites in the catalytic subunit of the DNA-dependent protein kinase. Biochem. J. *368*, 243–251.

Downs, J.A., and Jackson, S.P. (2004). A means to a DNA end: the many roles of Ku. Nat. Rev. Mol. Cell Biol. *5*, 367–378.

Downs, J.A., Lowndes, N.F., and Jackson, S.P. (2000). A role for Saccharomyces cerevisiae histone H2A in DNA repair. Nature *408*, 1001–1004.

Dueva, R., and Iliakis, G. (2013). Alternative pathways of non-homologous end joining (NHEJ) in genomic instability and cancer. Transl. Cancer Res.

Early, A., Drury, L.S., and Diffley, J.F.X. (2004). Mechanisms involved in regulating DNA replication origins during the cell cycle and in response to DNA damage. Philos. Trans. R. Soc. London. Ser. B Biol. Sci. *359*, 31–38.

Endow, S.A., and Higuchi, H. (2000). A mutant of the motor protein kinesin that moves in both directions on microtubules. Nature *406*, 913–916.

Endow, S.A., Kull, F.J., and Liu, H. (2010). Kinesins at a glance. J. Cell Sci. *123*, 3420–3424.

Escribano-Díaz, C., Orthwein, A., Fradet-Turcotte, A., Xing, M., Young, J.T.F., Tkáč, J., Cook, M.A., Rosebrock, A.P., Munro, M., Canny, M.D., et al. (2013). A Cell Cycle-Dependent Regulatory Circuit Composed of 53BP1-RIF1 and BRCA1-CtIP Controls DNA Repair Pathway Choice. Mol. Cell *49*, 872–883.

Evans, T., Rosenthal, E.T., Youngblom, J., Distel, D., and Hunt, T. (1983). Cyclin: A protein specified by maternal mRNA in sea urchin eggs that is destroyed at each cleavage division. Cell *33*, 389–396.

Eykelenboom, J.K., Harte, E.C., Canavan, L., Pastor-Peidro, A., Calvo-Asensio, I., Llorens-Agost, M., and Lowndes, N.F. (2013). ATR Activates the S-M Checkpoint during Unperturbed Growth to Ensure Sufficient Replication Prior to Mitotic Onset. Cell Rep. *5*, 1095–1107.

Falck, J., Mailand, N., Syljuåsen, R.G., Bartek, J., and Lukas, J. (2001). The ATM–Chk2–Cdc25A checkpoint pathway guards against radioresistant DNA synthesis. Nature *410*, 842–847.

Fededa, J.P., and Gerlich, D.W. (2012). Molecular control of animal cell cytokinesis. Nat. Cell Biol. *14*, 440–447.

Feng, L., Huang, J., and Chen, J. (2009). MERIT40 facilitates BRCA1 localization and DNA damage repair. Genes Dev. *23*, 719–728.

Findlay, S., Heath, J., Luo, V.M., Malina, A., Morin, T., Coulombe, Y., Djerir, B., Li, Z., Samiei, A., Simo-Cheyou, E., et al. (2018). SHLD2/FAM35A co-operates with REV7 to coordinate DNA double-strand break repair pathway choice. EMBO J. *37*.

Flynn, R.L., and Zou, L. (2011). ATR: a master conductor of cellular responses to DNA replication stress. Trends Biochem. Sci. *36*, 133–140.

Fortini, P. (2003). The base excision repair: mechanisms and its relevance for cancer susceptibility. Biochimie *85*, 1053–1071.

Fradet-Turcotte, A., Canny, M.D., Escribano-Díaz, C., Orthwein, A., Leung, C.C.Y., Huang, H., Landry, M.-C., Kitevski-LeBlanc, J., Noordermeer, S.M., Sicheri, F., et al. (2013). 53BP1 is a reader of the DNA-damage-induced H2A Lys 15 ubiquitin mark. Nature *499*, 50–54.

Fraschini, R. (2020). Cytokinesis in Eukaryotic Cells: The Furrow Complexity at a Glance. Cells *9*, 271.

Friedel, A.M., Pike, B.L., and Gasser, S.M. (2009). ATR/Mec1: coordinating fork stability and repair. Curr. Opin. Cell Biol. *21*, 237–244.

Frizzell, L. (2015). The kinesin KIF18B interacts with 53BP1 and is required for efficient double strand break repair. 233.

FUNG, T., and POON, R. (2005). A roller coaster ride with the mitotic cyclins. Semin. Cell Dev. Biol. *16*, 335–342.

Furuno, N., den Elzen, N., and Pines, J. (1999). Human Cyclin a Is Required for Mitosis until Mid Prophase. J. Cell Biol. *147*, 295–306.

Gandhi, M., Evdokimova, V.N., T.Cuenco, K., Nikiforova, M.N., Kelly,

L.M., Stringer, J.R., Bakkenist, C.J., and Nikiforov, Y.E. (2012). Homologous chromosomes make contact at the sites of double-strand breaks in genes in somatic G0/G1-phase human cells. Proc. Natl. Acad. Sci. *109*, 9454–9459.

Gao, S., Feng, S., Ning, S., Liu, J., Zhao, H., Xu, Y., Shang, J., Li, K., Li, Q., Guo, R., et al. (2018). An OB-fold complex controls the repair pathways for DNA double-strand breaks. Nat. Commun. *9*, 3925.

Gavet, O., and Pines, J. (2010). Progressive Activation of CyclinB1-Cdk1 Coordinates Entry to Mitosis. Dev. Cell *18*, 533–543.

Gheghiani, L., Loew, D., Lombard, B., Mansfeld, J., and Gavet, O. (2017). PLK1 Activation in Late G2 Sets Up Commitment to Mitosis. Cell Rep. *19*, 2060–2073.

Giglia-Mari, G., Zotter, A., and Vermeulen, W. (2011). DNA Damage Response. Cold Spring Harb. Perspect. Biol. *3*, a000745–a000745.

Girish, T.S., McGinty, R.K., and Tan, S. (2016). Multivalent Interactions by the Set8 Histone Methyltransferase With Its Nucleosome Substrate. J. Mol. Biol. *428*, 1531–1543.

Goldberg, M., Stucki, M., Falck, J., D'Amours, D., Rahman, D., Pappin, D., Bartek, J., and Jackson, S.P. (2003). MDC1 is required for the intra-S-phase DNA damage checkpoint. Nature *421*, 952–956.

Goodarzi, A.A., Noon, A.T., Deckbar, D., Ziv, Y., Shiloh, Y., Löbrich, M., and Jeggo, P.A. (2008). ATM Signaling Facilitates Repair of DNA Double-Strand Breaks Associated with Heterochromatin. Mol. Cell *31*, 167–177.

Goode, B., and Feinstein, S. (1994). Identification of a novel microtubule binding and assembly domain in the developmentally regulated inter-repeat region of tau. J. Cell Biol. *124*, 769–782.

Goshima, G., Wollman, R., Stuurman, N., Scholey, J.M., and Vale, R.D. (2005). Length Control of the Metaphase Spindle. Curr. Biol. *15*, 1979–1988.

Grant, G.D., Brooks, L., Zhang, X., Mahoney, J.M., Martyanov, V., Wood, T.A., Sherlock, G., Cheng, C., and Whitfield, M.L. (2013). Identification of cell cycle–regulated genes periodically expressed in U2OS cells and their regulation by FOXM1 and E2F transcription factors. Mol. Biol. Cell *24*, 3634–3650.

Greenberg, R.A., Chin, L., Femino, A., Lee, K.-H., Gottlieb, G.J., Singer, R.H., Greider, C.W., and DePinho, R.A. (1999). Short Dysfunctional Telomeres Impair Tumorigenesis in the INK4aΔ2/3 Cancer-Prone Mouse. Cell *97*, 515–525.

Griffith, J.D., Comeau, L., Rosenfield, S., Stansel, R.M., Bianchi, A., Moss, H., and de Lange, T. (1999). Mammalian Telomeres End in a Large Duplex Loop. Cell *97*, 503–514.

Grolimund, L., Aeby, E., Hamelin, R., Armand, F., Chiappe, D., Moniatte, M., and Lingner, J. (2013). A quantitative telomeric chromatin isolation protocol identifies different telomeric states. Nat. Commun. *4*, 2848.

Grundy, G.J., Rulten, S.L., Zeng, Z., Arribas-Bosacoma, R., Iles, N., Manley, K., Oliver, A., and Caldecott, K.W. (2012). APLF promotes the assembly and activity of non-homologous end joining protein complexes. EMBO J. *32*, 112–125.

Guan, K.L., Jenkins, C.W., Li, Y., Nichols, M.A., Wu, X., O'Keefe, C.L., Matera, A.G., and Xiong, Y. (1994). Growth suppression by p18, a p16INK4/MTS1- and p14INK4B/MTS2-related CDK6 inhibitor, correlates with wild-type pRb function. Genes Dev.

Gudjonsson, T., Altmeyer, M., Savic, V., Toledo, L., Dinant, C., Grøfte, M., Bartkova, J., Poulsen, M., Oka, Y., Bekker-Jensen, S., et al. (2012). TRIP12 and UBR5 Suppress Spreading of Chromatin Ubiquitylation at Damaged Chromosomes. Cell *150*, 697–709.

Guo, X., Bai, Y., Zhao, M., Zhou, M., Shen, Q., Yun, C.-H., Zhang, H., Zhu, W.-G., and Wang, J. (2018). Acetylation of 53BP1 dictates the DNA double strand break repair pathway. Nucleic Acids Res. *46*, 689–703.

Gupta, M.L., Carvalho, P., Roof, D.M., and Pellman, D. (2006). Plus end-specific depolymerase activity of Kip3, a kinesin-8 protein, explains its role in positioning the yeast mitotic spindle. Nat. Cell Biol. *8*, 913–923.

Gupta, R., Somyajit, K., Narita, T., Maskey, E., Stanlie, A., Kremer, M., Typas, D., Lammers, M., Mailand, N., Nussenzweig, A., et al. (2018). DNA Repair Network Analysis Reveals Shieldin as a Key Regulator of NHEJ and PARP Inhibitor Sensitivity. Cell *173*, 972-988.e23.

Hagting, A., Karlsson, C., Clute, P., Jackman, M., and Pines, J. (1998). MPF localization is controlled by nuclear export. EMBO J. *17*,

4127–4138.

Hanahan, D., and Weinberg, R.A. (2011). Hallmarks of Cancer: The Next Generation. Cell *144*, 646–674.

Harper, J.W., and Elledge, S.J. (2007). The DNA Damage Response: Ten Years After. Mol. Cell *28*, 739–745.

Hartmann, N., and Scherthan, H. (2005). Characterization of the telomere complex, TERF1 and TERF2 genes in muntjac species with fusion karyotypes. Exp. Cell Res. *306*, 64–74.

Heidary, G., and Fortini, M.E. (2001). Identification and characterization of the Drosophila tau homolog. Mech. Dev. *108*, 171–178.

Henson, J.H., Ditzler, C.E., Germain, A., Irwin, P.M., Vogt, E.T., Yang, S., Wu, X., and Shuster, C.B. (2017). The ultrastructural organization of actin and myosin II filaments in the contractile ring: new support for an old model of cytokinesis. Mol. Biol. Cell *28*, 613–623.

Hilario, J., Amitani, I., Baskin, R.J., and Kowalczykowski, S.C. (2009). Direct imaging of human Rad51 nucleoprotein dynamics on individual DNA molecules. Proc. Natl. Acad. Sci. *106*, 361–368.

Hirokawa, N. (1998). Kinesin and Dynein Superfamily Proteins and the Mechanism of Organelle Transport. Science (80-.). *279*, 519–526.

Hoebeke, J., Van Nijen, G., and De Brabander, M. (1976a). Interaction of oncodazole (R 17934), a new anti-tumoral drug, with rat brain tubulin. Biochem. Biophys. Res. Commun. *69*, 319–324.

Hoebeke, J., Van Nijen, G., and De Brabander, M. (1976b). Interaction of oncodazole (R 17934), a new anti-tumoral drug, with rat brain tubulin. Biochem. Biophys. Res. Commun. *69*, 319–324.

Hoffelder, D., Luo, L., Burke, N., Watkins, S., Gollin, S., and Saunders, W. (2004). Resolution of anaphase bridges in cancer cells. Chromosoma *112*.

Honda, R., Lowe, E.D., Dubinina, E., Skamnaki, V., Cook, A., Brown, N.R., and Johnson, L.N. (2005). The structure of cyclin E1/CDK2: implications for CDK2 activation and CDK2-independent roles. EMBO J. *24*, 452–463.

Howard, J., Hudspeth, A.J., and Vale, R.D. (1989). Movement of microtubules by single kinesin molecules. Nature *342*, 154–158.

Huertas, P. (2010). DNA resection in eukaryotes: deciding how to fix the break. Nat. Struct. Mol. Biol. *17*, 11–16.

Hunter, A.W., Caplow, M., Coy, D.L., Hancock, W.O., Diez, S., Wordeman, L., and Howard, J. (2003). The Kinesin-Related Protein MCAK Is a Microtubule Depolymerase that Forms an ATP-Hydrolyzing Complex at Microtubule Ends. Mol. Cell *11*, 445–457.

Hurd, D.D., and Saxton, W.M. (1996). Kinesin mutations cause motor neuron disease phenotypes by disrupting fast axonal transport in Drosophila. Genetics *144*, 1075–1085.

Hurst, V., Shimada, K., and Gasser, S.M. (2019). Nuclear Actin and Actin-Binding Proteins in DNA Repair. Trends Cell Biol. *29*, 462–476.

Iacovoni, J.S., Caron, P., Lassadi, I., Nicolas, E., Massip, L., Trouche, D., and Legube, G. (2010). High-resolution profiling of γH2AX around DNA double strand breaks in the mammalian genome. EMBO J. *29*, 1446–1457.

Itzel, T., Scholz, P., Maass, T., Krupp, M., Marquardt, J.U., Strand, S., Becker, D., Staib, F., Binder, H., Roessler, S., et al. (2015). Translating bioinformatics in oncology: guilt-by-profiling analysis and identification of KIF18B and CDCA3 as novel driver genes in carcinogenesis. Bioinformatics *31*, 216–224.

Iwabuchi, K., Bartel, P.L., Li, B., Marraccino, R., and Fields, S. (1994). Two cellular proteins that bind to wild-type but not mutant p53. Proc. Natl. Acad. Sci. *91*, 6098–6102.

Iyer, D., and Rhind, N. (2017). The Intra-S Checkpoint Responses to DNA Damage. Genes (Basel). *8*, 74.

Izumi, T., and Maller, J.L. (1993). Elimination of cdc2 phosphorylation sites in the cdc25 phosphatase blocks initiation of M-phase. Mol. Biol. Cell *4*, 1337–1350.

Jackman, J., and O'Connor, P.M. (1998). Methods for Synchronizing Cells at Specific Stages of the Cell Cycle. Curr. Protoc. Cell Biol. *00*.

Jacobs, A.L., and Schär, P. (2012). DNA glycosylases: in DNA repair and beyond. Chromosoma *121*, 1–20.

Jalali, A., Amirian, E.S., Bainbridge, M.N., Armstrong, G.N., Liu, Y., Tsavachidis, S., Jhangiani, S.N., Plon, S.E., Lau, C.C., Claus, E.B., et al. (2015). Targeted Sequencing in Chromosome 17q Linkage Region Identifies Familial Glioma Candidates in the Gliogene Consortium. Sci. Rep. *5*, 8278.

Jiang, W. (1999). Mammalian Cdc7-Dbf4 protein kinase complex is essential for initiation of DNA replication. EMBO J. *18*, 5703–5713.

Johnson, E.S., and Kornbluth, S. (2012). Phosphatases Driving Mitosis. In Progress in Molecular Biology and Translational Science, pp. 327–341.

Jones, J.M., and Gellert, M. (2004). The taming of a transposon: V(D)J recombination and the immune system. Immunol. Rev. *200*, 233–248.

Jossen, R., and Bermejo, R. (2013). The DNA damage checkpoint response to replication stress: A Game of Forks. Front. Genet. *4*.

Kakarougkas, A., and Jeggo, P.A. (2014). DNA DSB repair pathway choice: an orchestrated handover mechanism. Br. J. Radiol. *87*, 20130685.

Kamileri, I., Karakasilioti, I., Sideri, A., Kosteas, T., Tatarakis, A., Talianidis, I., and Garinis, G.A. (2012). Defective transcription initiation causes postnatal growth failure in a mouse model of nucleotide excision repair (NER) progeria. Proc. Natl. Acad. Sci. *109*, 2995–3000.

Kanu, N., and Behrens, A. (2007). ATMIN defines an NBS1-independent pathway of ATM signalling. EMBO J. *26*, 2933–2941.

Kapitein, L.C., Peterman, E.J.G., Kwok, B.H., Kim, J.H., Kapoor, T.M., and Schmidt, C.F. (2005). The bipolar mitotic kinesin Eg5 moves on both microtubules that it crosslinks. Nature *435*, 114–118.

Kar, S. (2003). Repeat motifs of tau bind to the insides of microtubules in the absence of taxol. EMBO J. *22*, 70–77.

Karlseder, J., Hoke, K., Mirzoeva, O.K., Bakkenist, C., Kastan, M.B., Petrini, J.H.J., and Lange, T. de (2004). The Telomeric Protein TRF2 Binds the ATM Kinase and Can Inhibit the ATM-Dependent DNA Damage Response. PLoS Biol. *2*, e240.

Kim, A.J., and Endow, S.A. (2000). A kinesin family tree. J. Cell Sci.

113 Pt 21, 3681–3682.

Kim, Y.-J., and M. Wilson III, D. (2012). Overview of Base Excision Repair Biochemistry. Curr. Mol. Pharmacol. *5*, 3–13.

Kim, S.-T., Lim, D.-S., Canman, C.E., and Kastan, M.B. (1999). Substrate Specificities and Identification of Putative Substrates of ATM Kinase Family Members. J. Biol. Chem. *274*, 37538–37543.

Kimura, K. (1998). Phosphorylation and Activation of 13S Condensin by Cdc2 in Vitro. Science (80-.). *282*, 487–490.

King, M.-C. (2003). Breast and Ovarian Cancer Risks Due to Inherited Mutations in BRCA1 and BRCA2. Science (80-.). *302*, 643–646.

Kleiner, R.E., Verma, P., Molloy, K.R., Chait, B.T., and Kapoor, T.M. (2015). Chemical proteomics reveals a γH2AX-53BP1 interaction in the DNA damage response. Nat. Chem. Biol. *11*, 807–814.

Kolas, N.K., Chapman, J.R., Nakada, S., Ylanko, J., Chahwan, R., Sweeney, F.D., Panier, S., Mendez, M., Wildenhain, J., Thomson, T.M., et al. (2007). Orchestration of the DNA-Damage Response by the RNF8 Ubiquitin Ligase. Science (80-.). *318*, 1637–1640.

Krawczyk, P.M., Borovski, T., Stap, J., Cijsouw, T., Cate, R. t., Medema, J.P., Kanaar, R., Franken, N.A.P., and Aten, J.A. (2012). Chromatin mobility is increased at sites of DNA double-strand breaks. J. Cell Sci. *125*, 2127–2133.

Kumagai, A., Lee, J., Yoo, H.Y., and Dunphy, W.G. (2006). TopBP1 Activates the ATR-ATRIP Complex. Cell *124*, 943–955.

de Lange, T. (2018). Shelterin-Mediated Telomere Protection. Annu. Rev. Genet. *52*, 223–247.

Laporte, D., Courtout, F., Salin, B., Ceschin, J., and Sagot, I. (2013). An array of nuclear microtubules reorganizes the budding yeast nucleus during quiescence. J. Cell Biol. *203*, 585–594.

Lawrence, C.J., Dawe, R.K., Christie, K.R., Cleveland, D.W., Dawson, S.C., Endow, S.A., Goldstein, L.S.B., Goodson, H. V., Hirokawa, N., Howard, J., et al. (2004). A standardized kinesin nomenclature. J. Cell Biol. *167*, 19–22.

Lazzerini-Denchi, E., and Sfeir, A. (2016). Stop pulling my strings —

what telomeres taught us about the DNA damage response. Nat. Rev. Mol. Cell Biol. *17*, 364–378.

Lee, A.J., Endo, M., Hobbs, J.K., and Wälti, C. (2018). Direct Single-Molecule Observation of Mode and Geometry of RecA-Mediated Homology Search. ACS Nano *12*, 272–278.

Lee, C.-S., Lee, K., Legube, G., and Haber, J.E. (2014). Dynamics of yeast histone H2A and H2B phosphorylation in response to a double-strand break. Nat. Struct. Mol. Biol. *21*, 103–109.

Lee, K.-J., Lin, Y.-F., Chou, H.-Y., Yajima, H., Fattah, K.R., Lee, S.-C., and Chen, B.P.C. (2011). Involvement of DNA-dependent Protein Kinase in Normal Cell Cycle Progression through Mitosis. J. Biol. Chem. *286*, 12796–12802.

Lee, Y.M., Kim, E., Park, M., Moon, E., Ahn, S.M., Kim, W., Hwang, K.B., Kim, Y.K., Choi, W., and Kim, W. (2010). Cell cycle-regulated expression and subcellular localization of a kinesin-8 member human KIF18B. Gene *466*, 16–25.

Lees, E. (1995). Cyclin dependent kinase regulation. Curr. Opin. Cell Biol. *7*, 773–780.

Li, G.-M. (2008). Mechanisms and functions of DNA mismatch repair. Cell Res. *18*, 85–98.

Li, L., and Zou, L. (2005). Sensing, signaling, and responding to DNA damage: Organization of the checkpoint pathways in mammalian cells. J. Cell. Biochem. *94*, 298–306.

Li, M., and Wilson, D.M. (2014). Human Apurinic/Apyrimidinic endonuclease 1. Antioxid. Redox Signal. *20*, 678–707.

Li, F., Dong, J., Eichmiller, R., Holland, C., Minca, E., Prakash, R., Sung, P., Yong Shim, E., Surtees, J.A., and Eun Lee, S. (2013). Role of Saw1 in Rad1/Rad10 complex assembly at recombination intermediates in budding yeast. EMBO J. *32*, 461–472.

Li, X., Zhang, X.-P., Solinger, J.A., Kiianitsa, K., Yu, X., Egelman, E.H., and Heyer, W.-D. (2007). Rad51 and Rad54 ATPase activities are both required to modulate Rad51-dsDNA filament dynamics. Nucleic Acids Res. *35*, 4124–4140.

Lindahl, T. (1974). An N-Glycosidase from Escherichia coli That Releases Free Uracil from DNA Containing Deaminated Cytosine

Residues. Proc. Natl. Acad. Sci. *71*, 3649–3653.

Lindqvist, A., van Zon, W., Karlsson Rosenthal, C., and Wolthuis, R.M.F. (2007). Cyclin B1–Cdk1 Activation Continues after Centrosome Separation to Control Mitotic Progression. PLoS Biol. *5*, e123.

Lindqvist, A., Rodríguez-Bravo, V., and Medema, R.H. (2009). The decision to enter mitosis: feedback and redundancy in the mitotic entry network. J. Cell Biol. *185*, 193–202.

Lisby, M., Mortensen, U.H., and Rothstein, R. (2003). Colocalization of multiple DNA double-strand breaks at a single Rad52 repair centre. Nat. Cell Biol. *5*, 572–577.

Liu, S., Bekker-Jensen, S., Mailand, N., Lukas, C., Bartek, J., and Lukas, J. (2006). Claspin Operates Downstream of TopBP1 To Direct ATR Signaling towards Chk1 Activation. Mol. Cell. Biol. *26*, 6056–6064.

Liu, S., Shiotani, B., Lahiri, M., Maréchal, A., Tse, A., Leung, C.C.Y., Glover, J.N.M., Yang, X.H., and Zou, L. (2011). ATR Autophosphorylation as a Molecular Switch for Checkpoint Activation. Mol. Cell *43*, 192–202.

Liu, Y., Chen, S., Wang, S., Soares, F., Fischer, M., Meng, F., Du, Z., Lin, C., Meyer, C., DeCaprio, J.A., et al. (2017). Transcriptional landscape of the human cell cycle. Proc. Natl. Acad. Sci. *114*, 3473–3478.

Liu, Y., Efimova, E. V., Ramamurthy, A., and Kron, S.J. (2019). Repair-independent functions of DNA-PKcs protect irradiated cells from mitotic slippage and accelerated senescence. J. Cell Sci. *132*, jcs229385.

Löbrich, M., Shibata, A., Beucher, A., Fisher, A., Ensminger, M., Goodarzi, A.A., Barton, O., and Jeggo, P.A. (2010). γH2AX foci analysis for monitoring DNA double-strand break repair: Strengths, limitations and optimization. Cell Cycle *9*, 662–669.

Locke, J., Joseph, A.P., Peña, A., Möckel, M.M., Mayer, T.U., Topf, M., and Moores, C.A. (2017). Structural basis of human kinesin-8 function and inhibition. Proc. Natl. Acad. Sci. *114*, E9539–E9548.

Lohka, M.J., Hayes, M.K., and Maller, J.L. (1988). Purification of maturation-promoting factor, an intracellular regulator of early mitotic events. Proc. Natl. Acad. Sci. *85*, 3009–3013.

Lottersberger, F., Bothmer, A., Robbiani, D.F., Nussenzweig, M.C., and de Lange, T. (2013). Role of 53BP1 oligomerization in regulating double-strand break repair. Proc. Natl. Acad. Sci. *110*, 2146–2151.

Lottersberger, F., Karssemeijer, R.A., Dimitrova, N., and de Lange, T. (2015). 53BP1 and the LINC Complex Promote Microtubule-Dependent DSB Mobility and DNA Repair. Cell *163*, 880–893.

Lou, Z., Minter-Dykhouse, K., Franco, S., Gostissa, M., Rivera, M.A., Celeste, A., Manis, J.P., van Deursen, J., Nussenzweig, A., Paull, T.T., et al. (2006). MDC1 Maintains Genomic Stability by Participating in the Amplification of ATM-Dependent DNA Damage Signals. Mol. Cell *21*, 187–200.

Lovejoy, C.A., and Cortez, D. (2009). Common mechanisms of PIKK regulation. DNA Repair (Amst). *8*, 1004–1008.

Lowndes, N.F. (2010). The interplay between BRCA1 and 53BP1 influences death, aging, senescence and cancer. DNA Repair (Amst). *9*, 1112–1116.

Lowndes, N.F., and Murguia, J.R. (2000). Sensing and responding to DNA damage. Curr. Opin. Genet. Dev. *10*, 17–25.

Lu, L., Ladinsky, M.S., and Kirchhausen, T. (2011). Formation of the postmitotic nuclear envelope from extended ER cisternae precedes nuclear pore assembly. J. Cell Biol. *194*, 425–440.

Lu, X., Tang, M., Zhu, Q., Yang, Q., Li, Z., Bao, Y., Liu, G., Hou, T., Lv, Y., Zhao, Y., et al. (2019). GLP-catalyzed H4K16me1 promotes 53BP1 recruitment to permit DNA damage repair and cell survival. Nucleic Acids Res. *47*, 10977–10993.

Lucca, C., Vanoli, F., Cotta-Ramusino, C., Pellicioli, A., Liberi, G., Haber, J., and Foiani, M. (2004). Checkpoint-mediated control of replisome–fork association and signalling in response to replication pausing. Oncogene *23*, 1206–1213.

Lukas, C., Savic, V., Bekker-Jensen, S., Doil, C., Neumann, B., Sølvhøj Pedersen, R., Grøfte, M., Chan, K.L., Hickson, I.D., Bartek, J., et al. (2011). 53BP1 nuclear bodies form around DNA lesions generated by mitotic transmission of chromosomes under replication stress. Nat. Cell Biol. *13*, 243–253.

Lukas, J., Herzinger, T., Hansen, K., Moroni, M.C., Resnitzky, D., Helin, K., Reed, S.I., and Bartek, J. (1997). Cyclin E-induced S phase without activation of the pRb/E2F pathway. Genes Dev. *11*, 1479–

1492.

Lupardus, P.J. (2002). A requirement for replication in activation of the ATR-dependent DNA damage checkpoint. Genes Dev. *16*, 2327–2332.

Ma, T. (2000). Cell cycle-regulated phosphorylation of p220NPAT by cyclin E/Cdk2 in Cajal bodies promotes histone gene transcription. Genes Dev. *14*, 2298–2313.

Ma, Y., Pannicke, U., Schwarz, K., and Lieber, M.R. (2002). Hairpin Opening and Overhang Processing by an Artemis/DNA-Dependent Protein Kinase Complex in Nonhomologous End Joining and V(D)J Recombination. Cell *108*, 781–794.

Maciejowski, J., Li, Y., Bosco, N., Campbell, P.J., and de Lange, T. (2015). Chromothripsis and Kataegis Induced by Telomere Crisis. Cell *163*, 1641–1654.

Mackay, D.R., and Ullman, K.S. (2011). Coordinating postmitotic nuclear pore complex assembly with abscission timing. Nucleus *2*, 283–288.

Mackay, D.R., and Ullman, K.S. (2015). ATR and a Chk1-Aurora B pathway coordinate postmitotic genome surveillance with cytokinetic abscission. Mol. Biol. Cell *26*, 2217–2226.

Mackay, D.R., Makise, M., and Ullman, K.S. (2010). Defects in nuclear pore assembly lead to activation of an Aurora B–mediated abscission checkpoint. J. Cell Biol. *191*, 923–931.

Mahajan, K.N., Nick McElhinny, S.A., Mitchell, B.S., and Ramsden, D.A. (2002). Association of DNA Polymerase μ (pol μ) with Ku and Ligase IV: Role for pol μ in End-Joining Double-Strand Break Repair. Mol. Cell. Biol. *22*, 5194–5202.

Malivert, L., Ropars, V., Nunez, M., Drevet, P., Miron, S., Faure, G., Guerois, R., Mornon, J.-P., Revy, P., Charbonnier, J.-B., et al. (2010). Delineation of the Xrcc4-interacting Region in the Globular Head Domain of Cernunnos/XLF*. J. Biol. Chem. *285*, 26475–26483.

Manis, J.P., Morales, J.C., Xia, Z., Kutok, J.L., Alt, F.W., and Carpenter, P.B. (2004). 53BP1 links DNA damage-response pathways to immunoglobulin heavy chain class-switch recombination. Nat. Immunol. *5*, 481–487.

Manning, A.L., Ganem, N.J., Bakhoum, S.F., Wagenbach, M.,

Wordeman, L., and Compton, D.A. (2007). The Kinesin-13 Proteins Kif2a, Kif2b, and Kif2c/MCAK Have Distinct Roles during Mitosis in Human Cells. Mol. Biol. Cell *18*, 2970–2979.

Mansour, W.Y., Rhein, T., and Dahm-Daphi, J. (2010). The alternative end-joining pathway for repair of DNA double-strand breaks requires PARP1 but is not dependent upon microhomologies. Nucleic Acids Res. *38*, 6065–6077.

Mao, Z., Bozzella, M., Seluanov, A., and Gorbunova, V. (2008). DNA repair by nonhomologous end joining and homologous recombination during cell cycle in human cells. Cell Cycle *7*, 2902–2906.

Mari, P.-O., Florea, B.I., Persengiev, S.P., Verkaik, N.S., Bruggenwirth, H.T., Modesti, M., Giglia-Mari, G., Bezstarosti, K., Demmers, J.A.A., Luider, T.M., et al. (2006). Dynamic assembly of end-joining complexes requires interaction between Ku70/80 and XRCC4. Proc. Natl. Acad. Sci. *103*, 18597–18602.

Marnef, A., and Legube, G. (2017). Organizing DNA repair in the nucleus: DSBs hit the road. Curr. Opin. Cell Biol. *46*, 1–8.

Martin, R.G., and Stein, S. (1976). Resting state in normal and simian virus 40 transformed Chinese hamster lung cells. Proc. Natl. Acad. Sci. *73*, 1655–1659.

Masson, M., Niedergang, C., Schreiber, V., Muller, S., Menissier-de Murcia, J., and de Murcia, G. (1998). XRCC1 Is Specifically Associated with Poly(ADP-Ribose) Polymerase and Negatively Regulates Its Activity following DNA Damage. Mol. Cell. Biol. *18*, 3563–3571.

Matos, J., Blanco, M.G., Maslen, S., Skehel, J.M., and West, S.C. (2011). Regulatory Control of the Resolution of DNA Recombination Intermediates during Meiosis and Mitosis. Cell *147*, 158–172.

Matsumoto, Y., and Kim, K. (1995). Excision of deoxyribose phosphate residues by DNA polymerase beta during DNA repair. Science (80-.). *269*, 699–702.

Mattiroli, F., Vissers, J.H.A., van Dijk, W.J., Ikpa, P., Citterio, E., Vermeulen, W., Marteijn, J.A., and Sixma, T.K. (2012). RNF168 Ubiquitinates K13-15 on H2A/H2AX to Drive DNA Damage Signaling. Cell *150*, 1182–1195.

Mayr, M.I., Hümmer, S., Bormann, J., Grüner, T., Adio, S., Woehlke, G., and Mayer, T.U. (2007). The Human Kinesin Kif18A Is a Motile

Microtubule Depolymerase Essential for Chromosome Congression. Curr. Biol. *17*, 488–498.

Mazumdar, M., Sundareshan, S., and Misteli, T. (2004). Human chromokinesin KIF4A functions in chromosome condensation and segregation. J. Cell Biol. *166*, 613–620.

McClintock, B. (1941). The Stability of Broken Ends of Chromosomes in Zea Mays. Genetics *26*, 234–282.

McDonald, H.B., Stewart, R.J., and Goldstein, L.S.B. (1990). The kinesin-like ncd protein of Drosophila is a minus end-directed microtubule motor. Cell *63*, 1159–1165.

McHugh, T., Gluszek, A.A., and Welburn, J.P.I. (2018). Microtubule end tethering of a processive kinesin-8 motor Kif18b is required for spindle positioning. J. Cell Biol. *217*, 2403–2416.

Mehta, A., and Haber, J.E. (2014). Sources of DNA Double-Strand Breaks and Models of Recombinational DNA Repair. Cold Spring Harb. Perspect. Biol. *6*, a016428–a016428.

Mendoza, M., Norden, C., Durrer, K., Rauter, H., Uhlmann, F., and Barral, Y. (2009). A mechanism for chromosome segregation sensing by the NoCut checkpoint. Nat. Cell Biol. *11*, 477–483.

Methot, S.P., and Di Noia, J.M. (2017). Molecular Mechanisms of Somatic Hypermutation and Class Switch Recombination. In Advances in Immunology, pp. 37–87.

Mierzwa, B., and Gerlich, D.W. (2014). Cytokinetic Abscission: Molecular Mechanisms and Temporal Control. Dev. Cell *31*, 525–538.

Miki, H., Okada, Y., and Hirokawa, N. (2005). Analysis of the kinesin superfamily: insights into structure and function. Trends Cell Biol. *15*, 467–476.

Mimitou, E.P., and Symington, L.S. (2009). Nucleases and helicases take center stage in homologous recombination. Trends Biochem. Sci. *34*, 264–272.

Mirman, Z., and de Lange, T. (2020). 53BP1: a DSB escort. Genes Dev. *34*, 7–23.

Mirman, Z., Lottersberger, F., Takai, H., Kibe, T., Gong, Y., Takai, K.,

References

Bianchi, A., Zimmermann, M., Durocher, D., and de Lange, T. (2018). 53BP1–RIF1–shieldin counteracts DSB resection through CST- and Polα-dependent fill-in. Nature *560*, 112–116.

Mladenov, E., and Iliakis, G. (2011). Induction and repair of DNA double strand breaks: The increasing spectrum of non-homologous end joining pathways. Mutat. Res. Mol. Mech. Mutagen. *711*, 61–72.

Moore, J.D. (2003). Unmasking the S-Phase-Promoting Potential of Cyclin B1. Science (80-.). *300*, 987–990.

Morgan, D.O. (1997). CYCLIN-DEPENDENT KINASES: Engines, Clocks, and Microprocessors. Annu. Rev. Cell Dev. Biol. *13*, 261–291.

Morrical, S.W. (2015). DNA-pairing and annealing processes in homologous recombination and homology-directed repair. Cold Spring Harb. Perspect. Biol. *7*, a016444.

Muller, J.H. (1938). The remaking of chromosomes. Collect. Net.

Murray, A.W. (2004). Recycling the Cell Cycle. Cell *116*, 221–234.

Nakamura, A.J., Rao, V.A., Pommier, Y., and Bonner, W.M. (2010). The complexity of phosphorylated H2AX foci formation and DNA repair assembly at DNA double-strand breaks. Cell Cycle *9*, 389–397.

Neal, J.A., and Meek, K. (2019). Deciphering phenotypic variance in different models of DNA-PKcs deficiency. DNA Repair (Amst). *73*, 7–16.

Nick McElhinny, S.A., Snowden, C.M., McCarville, J., and Ramsden, D.A. (2000). Ku Recruits the XRCC4-Ligase IV Complex to DNA Ends. Mol. Cell. Biol. *20*, 2996–3003.

Nicolette, M.L., Lee, K., Guo, Z., Rani, M., Chow, J.M., Lee, S.E., and Paull, T.T. (2010). Mre11–Rad50–Xrs2 and Sae2 promote 5′ strand resection of DNA double-strand breaks. Nat. Struct. Mol. Biol. *17*, 1478–1485.

Nimonkar, A. V., Genschel, J., Kinoshita, E., Polaczek, P., Campbell, J.L., Wyman, C., Modrich, P., and Kowalczykowski, S.C. (2011). BLM-DNA2-RPA-MRN and EXO1-BLM-RPA-MRN constitute two DNA end resection machineries for human DNA break repair. Genes Dev. *25*, 350–362.

Nishioka, K., Rice, J.C., Sarma, K., Erdjument-Bromage, H., Werner, J., Wang, Y., Chuikov, S., Valenzuela, P., Tempst, P., Steward, R., et al. (2002). PR-Set7 Is a Nucleosome-Specific Methyltransferase that Modifies Lysine 20 of Histone H4 and Is Associated with Silent Chromatin. Mol. Cell *9*, 1201–1213.

Noordermeer, S.M., Adam, S., Setiaputra, D., Barazas, M., Pettitt, S.J., Ling, A.K., Olivieri, M., Álvarez-Quilón, A., Moatti, N., Zimmermann, M., et al. (2018). The shieldin complex mediates 53BP1-dependent DNA repair. Nature *560*, 117–121.

Norbury, C.J., and Zhivotovsky, B. (2004). DNA damage-induced apoptosis. Oncogene *23*, 2797–2808.

Norden, C., Mendoza, M., Dobbelaere, J., Kotwaliwale, C. V., Biggins, S., and Barral, Y. (2006). The NoCut Pathway Links Completion of Cytokinesis to Spindle Midzone Function to Prevent Chromosome Breakage. Cell *125*, 85–98.

Nurse, P. (1990). Universal control mechanism regulating onset of M-phase. Nature *344*, 503–508.

O'Farrell, P.H. (2001). Triggering the all-or-nothing switch into mitosis. Trends Cell Biol. *11*, 512–519.

Ochs, F., Karemore, G., Miron, E., Brown, J., Sedlackova, H., Rask, M.-B., Lampe, M., Buckle, V., Schermelleh, L., Lukas, J., et al. (2019). Stabilization of chromatin topology safeguards genome integrity. Nature *574*, 571–574.

Okamoto, K., Bartocci, C., Ouzounov, I., Diedrich, J.K., Yates III, J.R., and Denchi, E.L. (2013). A two-step mechanism for TRF2-mediated chromosome-end protection. Nature *494*, 502–505.

Okowa, C. (2018). ATR mediated regulation of the abscission checkpoint.

Onaka, A.T., Toyofuku, N., Inoue, T., Okita, A.K., Sagawa, M., Su, J., Shitanda, T., Matsuyama, R., Zafar, F., Takahashi, T.S., et al. (2016). Rad51 and Rad54 promote noncrossover recombination between centromere repeats on the same chromatid to prevent isochromosome formation. Nucleic Acids Res. *44*, 10744–10757.

Oshidari, R., Strecker, J., Chung, D.K.C., Abraham, K.J., Chan, J.N.Y., Damaren, C.J., and Mekhail, K. (2018). Nuclear microtubule filaments mediate non-linear directional motion of chromatin and promote DNA repair. Nat. Commun. *9*, 2567.

Oshima, J., Huang, S., Pae, C., Campisi, J., and Schiestl, R.H. (2002). Lack of WRN results in extensive deletion at nonhomologous joining ends. Cancer Res. *62*, 547–551.

Palazzo, L., Della Monica, R., Visconti, R., Costanzo, V., and Grieco, D. (2014). ATM controls proper mitotic spindle structure. Cell Cycle *13*, 1091–1100.

Palm, W., and de Lange, T. (2008). How Shelterin Protects Mammalian Telomeres. Annu. Rev. Genet. *42*, 301–334.

Panier, S., and Boulton, S.J. (2014). Double-strand break repair: 53BP1 comes into focus. Nat. Rev. Mol. Cell Biol. *15*, 7–18.

Patil, M., Pabla, N., and Dong, Z. (2013). Checkpoint kinase 1 in DNA damage response and cell cycle regulation. Cell. Mol. Life Sci. *70*, 4009–4021.

Paull, T.T., and Deshpande, R.A. (2014). The Mre11/Rad50/Nbs1 complex: Recent insights into catalytic activities and ATP-driven conformational changes. Exp. Cell Res. *329*, 139–147.

Paull, T.T., and Gellert, M. (1999). Nbs1 potentiates ATP-driven DNA unwinding and endonuclease cleavage by the Mre11/Rad50 complex. Genes Dev. *13*, 1276–1288.

Paull, T.T., Rogakou, E.P., Yamazaki, V., Kirchgessner, C.U., Gellert, M., and Bonner, W.M. (2000). A critical role for histone H2AX in recruitment of repair factors to nuclear foci after DNA damage. Curr. Biol. *10*, 886–895.

Peddibhotla, S., Lam, M.H., Gonzalez-Rimbau, M., and Rosen, J.M. (2009). The DNA-damage effector checkpoint kinase 1 is essential for chromosome segregation and cytokinesis. Proc. Natl. Acad. Sci. *106*, 5159–5164.

Pelham, R.J., and Chang, F. (2002). Actin dynamics in the contractile ring during cytokinesis in fission yeast. Nature *419*, 82–86.

Perera, S.A., Maser, R.S., Xia, H., McNamara, K., Protopopov, A., Chen, L., F.Hezel, A., Kim, C.F., Bronson, R.T., Castrillon, D.H., et al. (2008). Telomere dysfunction promotes genome instability and metastatic potential in a K-ras p53 mouse model of lung cancer. Carcinogenesis *29*, 747–753.

Perrault, R., Wang, H., Wang, M., Rosidi, B., and Iliakis, G. (2004).

Backup pathways of NHEJ are suppressed by DNA-PK. J. Cell. Biochem. *92*, 781–794.

Peter, M., Heitlinger, E., Häner, M., Aebi, U., and Nigg, E.A. (1991). Disassembly of in vitro formed lamin head-to-tail polymers by CDC2 kinase. EMBO J. *10*, 1535–1544.

Petermann, E., Woodcock, M., and Helleday, T. (2010). Chk1 promotes replication fork progression by controlling replication initiation. Proc. Natl. Acad. Sci. *107*, 16090–16095.

Petersen, B.O. (1999). Phosphorylation of mammalian CDC6 by Cyclin A/CDK2 regulates its subcellular localization. EMBO J. *18*, 396–410.

Petersen, S., Casellas, R., Reina-San-Martin, B., Chen, H.T., Difilippantonio, M.J., Wilson, P.C., Hanitsch, L., Celeste, A., Muramatsu, M., Pilch, D.R., et al. (2001). AID is required to initiate Nbs1/γ-H2AX focus formation and mutations at sites of class switching. Nature *414*, 660–665.

Petrini, J. (2003). The cellular response to DNA double-strand breaks: defining the sensors and mediators. Trends Cell Biol. *13*, 458–462.

Pierce, A.J. (2001). Ku DNA end-binding protein modulates homologous repair of double-strand breaks in mammalian cells. Genes Dev. *15*, 3237–3242.

Pontvianne, F., Carpentier, M.C., Durut, N., Pavlištová, V., Jaške, K., Schořová, Š., Parrinello, H., Rohmer, M., Pikaard, C.S., Fojtová, M., et al. (2016). Identification of Nucleolus-Associated Chromatin Domains Reveals a Role for the Nucleolus in 3D Organization of the A. thaliana Genome. Cell Rep.

Poruchynsky, M.S., Komlodi-Pasztor, E., Trostel, S., Wilkerson, J., Regairaz, M., Pommier, Y., Zhang, X., Kumar Maity, T., Robey, R., Burotto, M., et al. (2015). Microtubule-targeting agents augment the toxicity of DNA-damaging agents by disrupting intracellular trafficking of DNA repair proteins. Proc. Natl. Acad. Sci. *112*, 1571–1576.

Primo, L.M.F., and Teixeira, L.K. (2020). DNA replication stress: oncogenes in the spotlight. Genet. Mol. Biol. *43*.

Prunuske, A.J., and Ullman, K.S. (2006). The nuclear envelope: Form and reformation. Curr. Opin. Cell Biol.

Pytel, D., Rusin, P., Sliwinska, A., Morawiec-Bajda, A., Drzewoski, J., and Majsterek, I. (2007). Role of homologous recombination repair and non-homologous end joining in therapeutic resistance of BCR/ABL-expressing leukemia cells. Gene Ther. Mol. Biol.

Qing, Y., Yamazoe, M., Hirota, K., Dejsuphong, D., Sakai, W., Yamamoto, K.N., Bishop, D.K., Wu, X.H., and Takeda, S. (2011). The epistatic relationship between BRCA2 and the other RAD51 mediators in homologous recombination. PLoS Genet.

Queralt, E., and Uhlmann, F. (2008). Cdk-counteracting phosphatases unlock mitotic exit. Curr. Opin. Cell Biol. *20*, 661–668.

Ramadan, K., Bruderer, R., Spiga, F.M., Popp, O., Baur, T., Gotta, M., and Meyer, H.H. (2007). Cdc48/p97 promotes reformation of the nucleus by extracting the kinase Aurora B from chromatin. Nature *450*, 1258–1262.

Rodgers, K., and McVey, M. (2016). Error-Prone Repair of DNA Double-Strand Breaks. J. Cell. Physiol. *231*, 15–24.

Rogakou, E.P., Pilch, D.R., Orr, A.H., Ivanova, V.S., and Bonner, W.M. (1998). DNA Double-stranded Breaks Induce Histone H2AX Phosphorylation on Serine 139. J. Biol. Chem. *273*, 5858–5868.

Rooney, S., Sekiguchi, J., Zhu, C., Cheng, H.-L., Manis, J., Whitlow, S., DeVido, J., Foy, D., Chaudhuri, J., Lombard, D., et al. (2002). Leaky Scid Phenotype Associated with Defective V(D)J Coding End Processing in Artemis-Deficient Mice. Mol. Cell *10*, 1379–1390.

Rosenbaum, J.L., and Witman, G.B. (2002). Intraflagellar transport. Nat. Rev. Mol. Cell Biol. *3*, 813–825.

Rother, M.B., Pellegrino, S., Smith, R., Gatti, M., Meisenberg, C., Wiegant, W.W., Luijsterburg, M.S., Imhof, R., Downs, J.A., Vertegaal, A.C.O., et al. (2020). CHD7 and 53BP1 regulate distinct pathways for the re-ligation of DNA double-strand breaks. Nat. Commun.

Roukos, V., Voss, T.C., Schmidt, C.K., Lee, S., Wangsa, D., and Misteli, T. (2013). Spatial Dynamics of Chromosome Translocations in Living Cells. Science (80-.). *341*, 660–664.

Russell, P., and Nurse, P. (1987). Negative regulation of mitosis by wee1+, a gene encoding a protein kinase homolog. Cell *49*, 559–567.

Sakaue-Sawano, A., Kurokawa, H., Morimura, T., Hanyu, A., Hama, H., Osawa, H., Kashiwagi, S., Fukami, K., Miyata, T., Miyoshi, H., et al. (2008). Visualizing Spatiotemporal Dynamics of Multicellular Cell-Cycle Progression. Cell *132*, 487–498.

San Filippo, J., Sung, P., and Klein, H. (2008). Mechanism of Eukaryotic Homologous Recombination. Annu. Rev. Biochem. *77*, 229–257.

Santocanale, C., and Diffley, J.F.X. (1998). A Mec1- and Rad53-dependent checkpoint controls late-firing origins of DNA replication. Nature *395*, 615–618.

Sarbajna, S., and West, S.C. (2014). Holliday junction processing enzymes as guardians of genome stability. Trends Biochem. Sci. *39*, 409–419.

Sathyan, K.M., McKenna, B.D., Anderson, W.D., Duarte, F.M., Core, L., and Guertin, M.J. (2019). An improved auxin-inducible degron system preserves native protein levels and enables rapid and specific protein depletion. Genes Dev. *33*, 1441–1455.

Satyanarayana, A., and Kaldis, P. (2009). Mammalian cell-cycle regulation: several Cdks, numerous cyclins and diverse compensatory mechanisms. Oncogene *28*, 2925–2939.

Savic, V., Yin, B., Maas, N.L., Bredemeyer, A.L., Carpenter, A.C., Helmink, B.A., Yang-Iott, K.S., Sleckman, B.P., and Bassing, C.H. (2009). Formation of Dynamic γ-H2AX Domains along Broken DNA Strands Is Distinctly Regulated by ATM and MDC1 and Dependent upon H2AX Densities in Chromatin. Mol. Cell *34*, 298–310.

Saxton, W.M., Hicks, J., Goldstein, L.S.B., and Raff, E.C. (1991). Kinesin heavy chain is essential for viability and neuromuscular functions in Drosophila, but mutants show no defects in mitosis. Cell *64*, 1093–1102.

Schmidt, M., Rohe, A., Platzer, C., Najjar, A., Erdmann, F., and Sippl, W. (2017). Regulation of G2/M Transition by Inhibition of WEE1 and PKMYT1 Kinases. Molecules *22*, 2045.

Schooley, A., Vollmer, B., and Antonin, W. (2012a). Building a nuclear envelope at the end of mitosis: coordinating membrane reorganization, nuclear pore complex assembly, and chromatin de-condensation. Chromosoma *121*, 539–554.

Schooley, A., Vollmer, B., and Antonin, W. (2012b). Building a

nuclear envelope at the end of mitosis: coordinating membrane reorganization, nuclear pore complex assembly, and chromatin de-condensation. Chromosoma *121*, 539–554.

Schrank, B.R., Aparicio, T., Li, Y., Chang, W., Chait, B.T., Gundersen, G.G., Gottesman, M.E., and Gautier, J. (2018). Nuclear ARP2/3 drives DNA break clustering for homology-directed repair. Nature *559*, 61–66.

Schroeder, T.E. (1972). THE CONTRACTILE RING. J. Cell Biol. *53*, 419–434.

Shao, G., Patterson-Fortin, J., Messick, T.E., Feng, D., Shanbhag, N., Wang, Y., and Greenberg, R.A. (2009). MERIT40 controls BRCA1-Rap80 complex integrity and recruitment to DNA double-strand breaks. Genes Dev. *23*, 740–754.

She, Z.-Y., Yu, K.-W., Zhong, N., Xiao, Y., Wei, Y.-L., Lin, Y., Li, Y.-L., and Lu, M.-H. (2020). Kinesin-7 CENP-E regulates chromosome alignment and genome stability of spermatogenic cells. Cell Death Discov. *6*, 25.

Sheaff, R.J., Groudine, M., Gordon, M., Roberts, J.M., and Clurman, B.E. (1997). Cyclin E-CDK2 is a regulator of p27Kip1. Genes Dev. *11*, 1464–1478.

Shechter, D., Costanzo, V., and Gautier, J. (2004). ATR and ATM regulate the timing of DNA replication origin firing. Nat. Cell Biol. *6*, 648–655.

Shelby, R.D., Vafa, O., and Sullivan, K.F. (1997). Assembly of CENP-A into Centromeric Chromatin Requires a Cooperative Array of Nucleosomal DNA Contact Sites. J. Cell Biol. *136*, 501–513.

Shen, K.C., Heng, H., Wang, Y., Lu, S., Liu, G., Deng, C.-X., Brooks, S.C., and Wang, Y.A. (2005). ATM and p21 Cooperate to Suppress Aneuploidy and Subsequent Tumor Development. Cancer Res. *65*, 8747–8753.

Shibata, A. (2017). Regulation of repair pathway choice at two-ended DNA double-strand breaks. Mutat. Res. Mol. Mech. Mutagen. *803–805*, 51–55.

Shiloh, Y. (2003). ATM and related protein kinases: safeguarding genome integrity. Nat. Rev. Cancer *3*, 155–168.

Shimamoto, Y., Forth, S., and Kapoor, T.M. (2015). Measuring Pushing and Braking Forces Generated by Ensembles of Kinesin-5 Crosslinking Two Microtubules. Dev. Cell *34*, 669–681.

Shin, Y., Du, Y., Collier, S.E., Ohi, M.D., Lang, M.J., and Ohi, R. (2015). Biased Brownian motion as a mechanism to facilitate nanometer-scale exploration of the microtubule plus end by a kinesin-8. Proc. Natl. Acad. Sci. *112*, E3826–E3835.

Sibanda, B.L., Critchlow, S.E., Begun, J., Pei, X.Y., Jackson, S.P., Blundell, T.L., and Pellegrini, L. (2001). Crystal structure of an Xrcc4-DNA ligase IV complex. Nat. Struct. Biol.

Silverman, J. (2004). Human Rif1, ortholog of a yeast telomeric protein, is regulated by ATM and 53BP1 and functions in the S-phase checkpoint. Genes Dev. *18*, 2108–2119.

Simon, D.N., and Wilson, K.L. (2011). The nucleoskeleton as a genome-associated dynamic “network of networks.” Nat. Rev. Mol. Cell Biol. *12*, 695–708.

Simsek, D., and Jasin, M. (2010). Alternative end-joining is suppressed by the canonical NHEJ component Xrcc4–ligase IV during chromosomal translocation formation. Nat. Struct. Mol. Biol. *17*, 410–416.

van Sluis, M., and McStay, B. (2015). A localized nucleolar DNA damage response facilitates recruitment of the homology-directed repair machinery independent of cell cycle stage. Genes Dev. *29*, 1151–1163.

Smogorzewska, A., Karlseder, J., Holtgreve-Grez, H., Jauch, A., and de Lange, T. (2002). DNA Ligase IV-Dependent NHEJ of Deprotected Mammalian Telomeres in G1 and G2. Curr. Biol. *12*, 1635–1644.

Soniat, M.M., Myler, L.R., Kuo, H.-C., Paull, T.T., and Finkelstein, I.J. (2019). RPA Phosphorylation Inhibits DNA Resection. Mol. Cell *75*, 145-153.e5.

Soutoglou, E., and Misteli, T. (2007). Mobility and immobility of chromatin in transcription and genome stability. Curr. Opin. Genet. Dev. *17*, 435–442.

Spagnolo, L., Rivera-Calzada, A., Pearl, L.H., and Llorca, O. (2006). Three-Dimensional Structure of the Human DNA-PKcs/Ku70/Ku80 Complex Assembled on DNA and Its Implications for DNA DSB

Repair. Mol. Cell *22*, 511–519.

Starr, D.A., and Fridolfsson, H.N. (2010). Interactions Between Nuclei and the Cytoskeleton Are Mediated by SUN-KASH Nuclear-Envelope Bridges. Annu. Rev. Cell Dev. Biol. *26*, 421–444.

Steigemann, P., and Gerlich, D.W. (2009). Cytokinetic abscission: cellular dynamics at the midbody. Trends Cell Biol. *19*, 606–616.

Steigemann, P., Wurzenberger, C., Schmitz, M.H.A., Held, M., Guizetti, J., Maar, S., and Gerlich, D.W. (2009). Aurora B-Mediated Abscission Checkpoint Protects against Tetraploidization. Cell *136*, 473–484.

Stewart, G.S., Wang, B., Bignell, C.R., Taylor, A.M.R., and Elledge, S.J. (2003). MDC1 is a mediator of the mammalian DNA damage checkpoint. Nature *421*, 961–966.

Stout, J.R., Yount, A.L., Powers, J.A., LeBlanc, C., Ems-McClung, S.C., and Walczak, C.E. (2011). Kif18B interacts with EB1 and controls astral microtubule length during mitosis. Mol. Biol. Cell *22*, 3070–3080.

Strecker, J., Gupta, G.D., Zhang, W., Bashkurov, M., Landry, M.-C., Pelletier, L., and Durocher, D. (2016). DNA damage signalling targets the kinetochore to promote chromatin mobility. Nat. Cell Biol. *18*, 281–290.

Strickfaden, H., McDonald, D., Kruhlak, M.J., Haince, J.-F., Th'ng, J.P.H., Rouleau, M., Ishibashi, T., Corry, G.N., Ausio, J., Underhill, D.A., et al. (2016). Poly(ADP-ribosyl)ation-dependent Transient Chromatin Decondensation and Histone Displacement following Laser Microirradiation. J. Biol. Chem. *291*, 1789–1802.

Sturzenegger, A., Burdova, K., Kanagaraj, R., Levikova, M., Pinto, C., Cejka, P., and Janscak, P. (2014). DNA2 Cooperates with the WRN and BLM RecQ Helicases to Mediate Long-range DNA End Resection in Human Cells. J. Biol. Chem. *289*, 27314–27326.

Sugawara, N., Paques, F., Colaiacovo, M., and Haber, J.E. (1997). Role of Saccharomyces cerevisiae Msh2 and Msh3 repair proteins in double-strand break-induced recombination. Proc. Natl. Acad. Sci. *94*, 9214–9219.

Sun, Y., Jiang, X., Chen, S., Fernandes, N., and Price, B.D. (2005). A role for the Tip60 histone acetyltransferase in the acetylation and activation of ATM. Proc. Natl. Acad. Sci. *102*, 13182–13187.

Sung, P., and Klein, H. (2006). Mechanism of homologous recombination: mediators and helicases take on regulatory functions. Nat. Rev. Mol. Cell Biol. *7*, 739–750.

Svoboda, K., and Block, S.M. (1994). Force and velocity measured for single kinesin molecules. Cell *77*, 773–784.

Symington, L.S. (2014). End Resection at Double-Strand Breaks: Mechanism and Regulation. Cold Spring Harb. Perspect. Biol. *6*, a016436–a016436.

Symington, L.S., and Gautier, J. (2011). Double-Strand Break End Resection and Repair Pathway Choice. Annu. Rev. Genet. *45*, 247–271.

Takai, H., Smogorzewska, A., and de Lange, T. (2003). DNA Damage Foci at Dysfunctional Telomeres. Curr. Biol. *13*, 1549–1556.

Takisawa, H., Mimura, S., and Kubota, Y. (2000). Eukaryotic DNA replication: from pre-replication complex to initiation complex. Curr. Opin. Cell Biol. *12*, 690–696.

Takizawa, C.G., and Morgan, D.O. (2000). Control of mitosis by changes in the subcellular location of cyclin-B1–Cdk1 and Cdc25C. Curr. Opin. Cell Biol. *12*, 658–665.

Tanenbaum, M.E., Macurek, L., van der Vaart, B., Galli, M., Akhmanova, A., and Medema, R.H. (2011). A Complex of Kif18b and MCAK Promotes Microtubule Depolymerization and Is Negatively Regulated by Aurora Kinases. Curr. Biol. *21*, 1356–1365.

Tanenbaum, M.E., Gilbert, L.A., Qi, L.S., Weissman, J.S., and Vale, R.D. (2014). A Protein-Tagging System for Signal Amplification in Gene Expression and Fluorescence Imaging. Cell *159*, 635–646.

Taylor, W.R., and Stark, G.R. (2001). Regulation of the G2/M transition by p53. Oncogene *20*, 1803–1815.

Tercero, J.A., and Diffley, J.F.X. (2001). Regulation of DNA replication fork progression through damaged DNA by the Mec1/Rad53 checkpoint. Nature *412*, 553–557.

Tercero, J.A., Longhese, M.P., and Diffley, J.F.X. (2003). A Central Role for DNA Replication Forks in Checkpoint Activation and Response. Mol. Cell *11*, 1323–1336.

Thoresen, S.B., Campsteijn, C., Vietri, M., Schink, K.O., Liestøl, K., Andersen, J.S., Raiborg, C., and Stenmark, H. (2014). ANCHR mediates Aurora-B-dependent abscission checkpoint control through retention of VPS4. Nat. Cell Biol. *16*, 547–557.

Thorslund, T., Ripplinger, A., Hoffmann, S., Wild, T., Uckelmann, M., Villumsen, B., Narita, T., Sixma, T.K., Choudhary, C., Bekker-Jensen, S., et al. (2015). Histone H1 couples initiation and amplification of ubiquitin signalling after DNA damage. Nature *527*, 389–393.

Tirnauer, J.S., and Bierer, B.E. (2000). Eb1 Proteins Regulate Microtubule Dynamics, Cell Polarity, and Chromosome Stability. J. Cell Biol. *149*, 761–766.

Trenz, K., Smith, E., Smith, S., and Costanzo, V. (2006). ATM and ATR promote Mre11 dependent restart of collapsed replication forks and prevent accumulation of DNA breaks. EMBO J. *25*, 1764–1774.

Tsouroula, K., Furst, A., Rogier, M., Heyer, V., Maglott-Roth, A., Ferrand, A., Reina-San-Martin, B., and Soutoglou, E. (2016). Temporal and Spatial Uncoupling of DNA Double Strand Break Repair Pathways within Mammalian Heterochromatin. Mol. Cell *63*, 293–305.

Uematsu, N., Weterings, E., Yano, K., Morotomi-Yano, K., Jakob, B., Taucher-Scholz, G., Mari, P.-O., van Gent, D.C., Chen, B.P.C., and Chen, D.J. (2007). Autophosphorylation of DNA-PKCS regulates its dynamics at DNA double-strand breaks. J. Cell Biol. *177*, 219–229.

Uziel, T. (2003). Requirement of the MRN complex for ATM activation by DNA damage. EMBO J. *22*, 5612–5621.

Vale, R.D. (2003). The Molecular Motor Toolbox for Intracellular Transport. Cell *112*, 467–480.

VALE, R., REESE, T., and SHEETZ, M. (1985). Identification of a novel force-generating protein, kinesin, involved in microtubule-based motility. Cell *42*, 39–50.

Varga, V., Leduc, C., Bormuth, V., Diez, S., and Howard, J. (2009). Kinesin-8 Motors Act Cooperatively to Mediate Length-Dependent Microtubule Depolymerization. Cell *138*, 1174–1183.

Vitre, B., Coquelle, F.M., Heichette, C., Garnier, C., Chrétien, D., and Arnal, I. (2008). EB1 regulates microtubule dynamics and tubulin sheet closure in vitro. Nat. Cell Biol. *10*, 415–421.

W.-L. Toh, G., Sugawara, N., Dong, J., Toth, R., Lee, S.E., Haber, J.E., and Rouse, J. (2010). Mec1/Tel1-dependent phosphorylation of Slx4 stimulates Rad1–Rad10-dependent cleavage of non-homologous DNA tails. DNA Repair (Amst). *9*, 718–726.

van der Waal, M.S., Hengeveld, R.C.C., van der Horst, A., and Lens, S.M.A. (2012). Cell division control by the Chromosomal Passenger Complex. Exp. Cell Res. *318*, 1407–1420.

Walczak, C.E., Zong, H., Jain, S., and Stout, J.R. (2016). Spatial regulation of astral microtubule dynamics by Kif18B in PtK cells. Mol. Biol. Cell *27*, 3021–3030.

Walker, R.A., Salmon, E.D., and Endow, S.A. (1990). The Drosophila claret segregation protein is a minus-end directed motor molecule. Nature *347*, 780–782.

Wang, H., and Xu, X. (2017). Microhomology-mediated end joining: new players join the team. Cell Biosci. *7*, 6.

Wang, A., Kolhe, J.A., Gioacchini, N., Baade, I., Brieher, W.M., Peterson, C.L., and Freeman, B.C. (2020). Mechanism of Long-Range Chromosome Motion Triggered by Gene Activation. Dev. Cell *52*, 309-320.e5.

Wang, B., Hurov, K., Hofmann, K., and Elledge, S.J. (2009). NBA1, a new player in the Brca1 A complex, is required for DNA damage resistance and checkpoint control. Genes Dev. *23*, 729–739.

Wang, R.C., Smogorzewska, A., and de Lange, T. (2004). Homologous Recombination Generates T-Loop-Sized Deletions at Human Telomeres. Cell *119*, 355–368.

Ward, I.M., Reina-San-Martin, B., Olaru, A., Minn, K., Tamada, K., Lau, J.S., Cascalho, M., Chen, L., Nussenzweig, A., Livak, F., et al. (2004). 53BP1 is required for class switch recombination. J. Cell Biol. *165*, 459–464.

Watanabe, N., Arai, H., Nishihara, Y., Taniguchi, M., Watanabe, N., Hunter, T., and Osada, H. (2004). M-phase kinases induce phospho-dependent ubiquitination of somatic Wee1 by SCF -TrCP. Proc. Natl. Acad. Sci. *101*, 4419–4424.

West, S.C., Blanco, M.G., Chan, Y.W., Matos, J., Sarbajna, S., and Wyatt, H.D.M. (2015). Resolution of Recombination Intermediates: Mechanisms and Regulation. Cold Spring Harb. Symp. Quant. Biol. *80*, 103–109.

Williams, R.S., Bernstein, N., Lee, M.S., Rakovszky, M.L., Cui, D., Green, R., Weinfeld, M., and Glover, J.N.M. (2005). Structural basis for phosphorylation-dependent signaling in the DNA-damage response. Biochem. Cell Biol. *83*, 721–727.

Williams, R.S., Williams, J.S., and Tainer, J.A. (2007). Mre11–Rad50–Nbs1 is a keystone complex connecting DNA repair machinery, double-strand break signaling, and the chromatin templateThis paper is one of a selection of papers published in this Special Issue, entitled 28th International West Coast Chromatin a. Biochem. Cell Biol. *85*, 509–520.

Wold, M.S. (1997). Replication protein A: a heterotrimeric, single-stranded DNA-binding protein required for eukaryotic DNA metabolism. Annu. Rev. Biochem. *66*, 61–92.

Wordeman, L. (2010). How kinesin motor proteins drive mitotic spindle function: Lessons from molecular assays. Semin. Cell Dev. Biol. *21*, 260–268.

Wright, W.D., Shah, S.S., and Heyer, W.-D. (2018). Homologous recombination and the repair of DNA double-strand breaks. J. Biol. Chem. *293*, 10524–10535.

Wu, G., Zhou, L., Khidr, L., Guo, X.E., Kim, W., Lee, Y.M., Krasieva, T., and Chen, P.-L. (2008). A novel role of the chromokinesin Kif4A in DNA damage response. Cell Cycle *7*, 2013–2020.

Wu, J., Huen, M.S.Y., Lu, L.-Y., Ye, L., Dou, Y., Ljungman, M., Chen, J., and Yu, X. (2009). Histone Ubiquitination Associates with BRCA1-Dependent DNA Damage Response. Mol. Cell. Biol. *29*, 849–860.

Yamauchi, M., Shibata, A., Suzuki, K., Suzuki, M., Niimi, A., Kondo, H., Miura, M., Hirakawa, M., Tsujita, K., Yamashita, S., et al. (2017). Regulation of pairing between broken DNA-containing chromatin regions by Ku80, DNA-PKcs, ATM, and 53BP1. Sci. Rep. *7*, 41812.

Yan, J., and Jetten, A.M. (2008). RAP80 and RNF8, key players in the recruitment of repair proteins to DNA damage sites. Cancer Lett. *271*, 179–190.

Yang, B., Wang, S., Xie, H., Wang, C., Gao, X., Rong, Y., Liu, Z., and Lu, Y. (2020). KIF18B promotes hepatocellular carcinoma progression through activating Wnt/β-catenin-signaling pathway. J. Cell. Physiol. *235*, 6507–6514.

Yang, C., Tang, X., Guo, X., Niikura, Y., Kitagawa, K., Cui, K., Wong,

S.T.C., Fu, L., and Xu, B. (2011). Aurora-B Mediated ATM Serine 1403 Phosphorylation Is Required for Mitotic ATM Activation and the Spindle Checkpoint. Mol. Cell *44*, 597–608.

Yang, S.-H., Zhou, R., Campbell, J., Chen, J., Ha, T., and Paull, T.T. (2012). The SOSS1 single-stranded DNA binding complex promotes DNA end resection in concert with Exo1. EMBO J. *32*, 126–139.

Yano, K., Morotomi-Yano, K., Wang, S., Uematsu, N., Lee, K., Asaithamby, A., Weterings, E., and Chen, D.J. (2008). Ku recruits XLF to DNA double-strand breaks. EMBO Rep. *9*, 91–96.

Zgheib, O., Pataky, K., Brugger, J., and Halazonetis, T.D. (2009). An Oligomerized 53BP1 Tudor Domain Suffices for Recognition of DNA Double-Strand Breaks. Mol. Cell. Biol. *29*, 1050–1058.

Zhang, Y., and Heermann, D.W. (2014). DNA double-strand breaks: linking gene expression to chromosome morphology and mobility. Chromosoma *123*, 103–115.

Zhang, Y., and Hunter, T. (2014). Roles of Chk1 in cell biology and cancer therapy. Int. J. Cancer *134*, 1013–1023.

Zhao, H., Watkins, J.L., and Piwnica-Worms, H. (2002). Disruption of the checkpoint kinase 1/cell division cycle 25A pathway abrogates ionizing radiation-induced S and G2 checkpoints. Proc. Natl. Acad. Sci. *99*, 14795–14800.

Zhu, C., Bossy-Wetzel, E., and Jiang, W. (2005). Recruitment of MKLP1 to the spindle midzone/midbody by INCENP is essential for midbody formation and completion of cytokinesis in human cells. Biochem. J. *389*, 373–381.

Zhu, J., Petersen, S., Tessarollo, L., and Nussenzweig, A. (2001). Targeted disruption of the Nijmegen breakage syndrome gene NBS1 leads to early embryonic lethality in mice. Curr. Biol. *11*, 105–109.

Zimmermann, M., Lottersberger, F., Buonomo, S.B., Sfeir, A., and de Lange, T. (2013). 53BP1 Regulates DSB Repair Using Rif1 to Control 5' End Resection. Science (80-.). *339*, 700–704.

Appendix I: Funding and poster presentations

I.1. Scholarship funding

- Hardiman scholarship by National University of Ireland awarded for completion of this PhD in four years.
- Awarded a Beckman Fund Scholarship in 2018
- Awarded Thomas Crawford Hayes Scholarship in 2019

I.2. Poster presentations

1. **Scientific Advisory Board, Centre for Chromosome Biology, Galway, November 2015**
   Title: The role of KIF18B, a novel 53BP1 interactor, in DNA damage repair
2. **SFI midterm review, December 2016, Galway.**
   Title: KIF18B a newly identified 53BP1 partner is required for DSB repair.

The role of KIF18B, a novel 53BP1 interactor, in DNA damage repair

Louise Frizzell, Silvia Maretto, Shideh Sakhteh, Muriel Voisin, Noel F Lowndes.

Genome Stability Laboratory - Centre for Chromosome Biology,
School of Natural Sciences, National University of Ireland, Galway

1. Introduction

53BP1, a DNA damage response (DDR) mediator was first identified as a p53 binding partner. It is involved early in the DDR and also has a role in cell cycle checkpoint control. Upon treatment with ionizing radiation, 53BP1 is rapidly recruited to double strand breaks (DSBs) forming ionizing radiation-induced foci (IRIF) [1]. While 53BP1 is not required for repair by homologous recombination (HR), nor for 'classical' non-homologous end joining (NHEJ), it is required for long-distance NHEJ. In addition, both class switch recombination and telomeric fusion is dependent upon 53BP1 [2, 3]. In the latter case 53BP1 regulates the increased mobility of deprotected telomeres, thereby facilitating their NHEJ-dependent fusion [2].

Preliminary data: The kinesin KIF18B was identified as a novel 53BP1 interactor in a quantitative proteomic screen.
Hypothesis: The motor activity of KIF18B is required for the repair of distal DSBs.

2. KIF18B depleted cells are sensitive to IR and have a defect in DNA damage repair

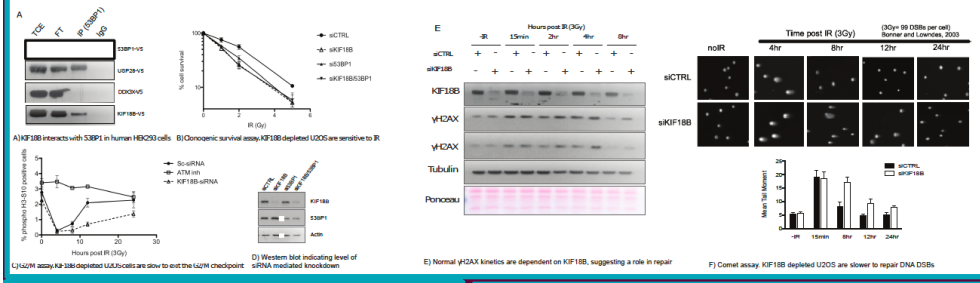

3. Abrogated 53BP1 focal recruitment in KIF18B depleted cells

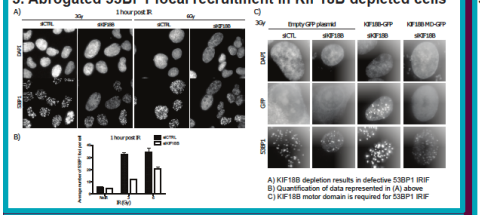

4. Cellular localisation of KIF18B

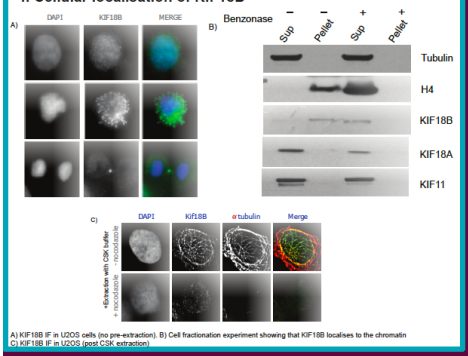

5. KIF18B is required for long range NHEJ

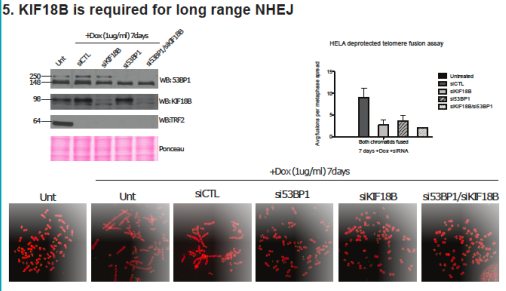

6. Evidence for nuclear microtubule filaments?

To adress this question we are constructing a plasmid containing tubulin binding domain to bind microtubules, GFP to visulise, 3X Nuclear localisation sequence to centralize in nucleus.

7. Model

A role for nuclear microtubules in DSB repair??

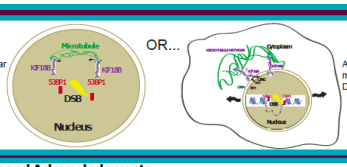

OR...

A role for cytoplasmic microtubules in DSB repair??

8. Conclusions and Future work

Our data (IR sensitivity, defective checkpoint exit, persistent γH2AX, persistent DSBs, KIF18B motor domain-dependent 53BP1 IRIFs, defective deprotected telomere fusion) is consistent with a role for KIF18B in long range DSB repair. To further investigate our hypothesis:

- Confirm evidence for nuclear microtubule network (required for distal NHEJ??)
- Is it DNA damage dependent?
- Is long range NHEJ dependent on molecular motors and microtubule filaments?

References and Acknowledgments

1. Schultz, L., Chehab N H., Malikzay, A., Halazonetis T D. p53 Binding Protein 1 (53BP1) Is an Early Participant in the Cellular Response to DNA Double-Strand Breaks. J. Cell. Biol. 151, 1381-1390 (2000).
2. Dimitrova, N., Chen, Y-C M., Spector, D L., de Lange, T. 53BP1 promotes non-homologous end joining of telomeres by increasing chromatin mobility. Nature Letters. 456, 524-528 (2008).
3. Ward, I M., Reina-San-Martin, B., Olaru, A., Minn, K., Tamada, K., Lau, J S., Cascalho, M., Chen, L., Nussenzweig, A., Livak, F., Nussenzweig, M C., Chen, J. 53BP1 is required for class switch recombination. J. Cell. Biol. 165, 459-464 (2004).

We would like to thank Rene Medema, Wankee Kim, Lunardi Frederic, Titia deLange, Hideaki Ogiwara and Brian McStay for valuable reagents.

This work was supported by a Science Foundation Ireland principal investigator award to N. Lowndes, a NUI Galway College of Science Scholarship and the Beckman Fund Scholarship.

KIF18B, a newly identified 53BP1 partner, is required for DSB repair

Louise Frizell, Nikolay Tsanov, Maryam Sakteh, Silvia Maretto, Muriel Voisin, and Noel Lowndes

Genome Stability Laboratory - Centre for Chromosome Biology, School of Natural Sciences, National University of Ireland, Galway

1. Introduction

- We identified the microtubule motor KIF18B in a SILAC proteomic screen for unknown 53BP1-interacting partners
- KIF18B is chromatin-bound and interacts with both 53BP1 and histones
- We mapped the interaction regions and showed that KIF18B binds the TUDOR domain of 53BP1 via a short peptide motif
- The knockdown of KIF18B results in DSB repair defects and IR sensitivity, and phenocopies 53BP1 knockdown
- KIF18B colocalises with 53BP1 at DSBs and deprotected telomeres

- Our results suggest that KIF18B plays a role with 53BP1 in DSB repair
- We are currently investigating an interaction model whereby KIF18B may provide an additional interaction surface for 53BP1 and histones at DSBs
- To study the role of the motor domain of KIF18B, we are setting up technology to visualise the movement of single molecules of KIF18B in the nucleus, and to address the existence of nuclear microtubules

2. KIF18B binds the TUDOR domain of 53BP1

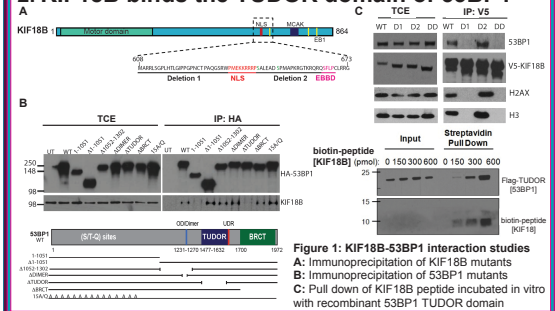

Figure 1: KIF18B-53BP1 interaction studies
A: Immunoprecipitation of KIF18B mutants
B: Immunoprecipitation of 53BP1 mutants
C: Pull down of KIF18B peptide incubated in vitro with recombinant 53BP1 TUDOR domain

3. KIF18B functions with 53BP1 in DSB repair

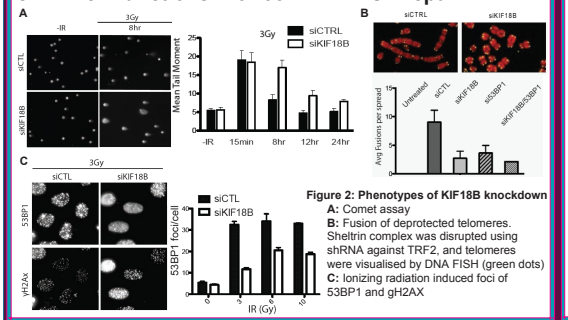

Figure 2: Phenotypes of KIF18B knockdown
A: Comet assay
B: Fusion of deprotected telomeres. Sheltrin complex was disrupted using shRNA against TRF2, and telomeres were visualised by DNA FISH (green dots)
C: Ionizing radiation induced foci of 53BP1 and gH2AX

4. KIF18B colocalises with 53BP1 at DSBs

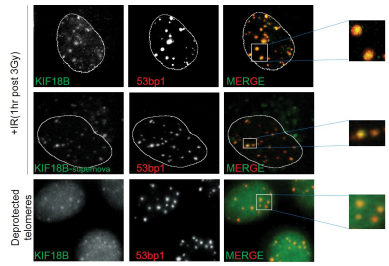

Figure 3: Subcellular localisation of KIF18B
Up: KIF18B and 53BP1 IRIFs visualised by immunofluorescence
Middle: Supernova tagged-KIF18B colocalosation with 53BP1 at IRIFs
Low: Localisation of KIF18B and 53BP1 at deprotected telomeres. Sheltrin complex was disrupted using shRNA against TRF2

5. Interaction model

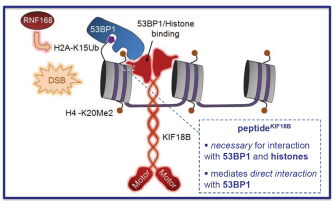

Figure 4: Model for recruitment of 53BP1 to DSBs via KIF18B
KIF18B could provide an additional interaction surface for both 53BP1 and histones

6. Investigating the role of KIF18B motor domain

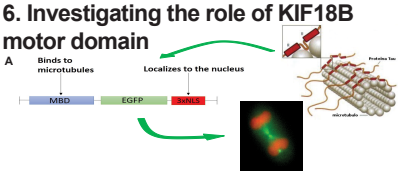

Figure 5: Optimisation of technology for visualisation of microtubules and KIF18B microtubule motor
A: Expressing MBD-Tau-EGFP-NLS to explore the probability of microtubules existence in the nucleus
B: Take advantage of Supernova tagging system to visualise KIF18B single molecules

7. Future directions

- Set up the chromosome movement assay and study the effect of KIF18B knockdown on DSB movement
- Live cell imaging of KIF18B single molecules using Supernova-tagging system
- Optimization of Tau-MBD expression levels in the nucleus to address the existence of nuclear microtubules
- Screening KIF18B motor domain inhibitors designed in silico by Leif Eriksson (Gothenburg University, Sweden)
- Test the interaction model using biochemistry
- TUDOR mutagenesis to indentify the residues interacting with KIF18B peptide
- Solve the NMR structure of the TUDOR - peptideKIF18B complex with Peter Crowley (Chemistry department, NUI Galway)

References and Acknowledgments

1. Botuyan MV. et al. Cell. 2006 Dec 29;127(7):1361-73.
2. Fradet-Turcotte A. et al. Nature. 2013 Jul 4;499(7456):50-4.
3. Roukos V. et al. Science. 2013 Aug 9;341(6146):660-4.
4. Tanenbaum ME. et al. Cell. 2014 Oct 23;159(3):635-46.

This work was supported by a Science Fundation Ireland principal investigator award to N. Lowndes and a Hardiman Scholarship was awarded to MS.

Appendix II: protocols

II.1. siRNA transfection

Adjust the final concentration of the siRNA to 0.1nmol by dilution with RNase free water.

Plate 1-1.5x10^5 cells/well in a 6-well or 35mm plate (for adherent cells) using media W/O PEN/STREP.

Transfect siRNA after 24 hours using Oligofectamine

6μl of Oligofectamine + 14μl Optimem per sample accumulatively in one tube.

Example: for 10 samples, mix 60 μl Oligofectamine and 140 μl optimum in one tube.

For the first time, the amount of siRNA and the ratio to Optimem requires to be optimized. Thus, it is better to start with following concentrations.

0 nM siRNA: 0μl siRNA + 180μl Optimem

10 nM siRNA: 0,5μl siRNA + 179,5μl Optimem

50 nM siRNA: 2,5μl siRNA + 177,5μl Optimem

100 nM siRNA: 5μl siRNA + 175μl Optimem

Add 20μl Oligofectamine to each siRNA sample, label and vortex them well.

Incubate 20min at RT

Prior to addition of the siRMA mixture, wash cells with PBS

Add 800μl of Optimem to each well and then 200μl of incubated siRNA

Incubate for 3h at 37C

Add 500μl of 3xDMEM (DMEM with 3x FBS and 3x glutamine)

Next day add 1ml of media with P/S

The cells can be harvested 24 to 48 h after transfection regarding to the cell type and the siRNA.

II.2. Immunofluorescent staining

Grow the adherent cells on 20 minutes UV sterilized coverslips. Depending on the cell type you will need 70-80% confluency.

At the time of harvesting, gently wash the cells with PBS for 3 times and try not to wash out the cells which are not fixed.

The fixation method depends on what you are staining the cells for. Mainly the cells are going to be fixed with either methanol (best fixation for microtubules) or PFA.

- Methanol fixation –following the 3X PBS washes, add ice-cold methanol to the coverslip, put in freezer for 20 min. you can keep the cells on methanol in freezer for few days given that they do not get dry.
- PFA fixation – add 4% PFA to the cells after 3X PBS washes for 10minutes at room temperature (dilute 16% stock under the fume hood 1 in 4 using PBS and has to be freshly made)
- Wash 3 times in PBS

  Following PFA fixation;

- Permeabilise the cells using 0.250% TritonX (diluted in PBS). Incubate for 5min at room temperature
- Wash 3 times in PBS.

  If fixing the cells with methanol, there is no need for permeabilization.

- Block in 5% BSA diluted in PBS (BSA should be filtered after dilution and before use) for 1 hin 37˚C incubator. This can be overnight (or a day or two) in the fridge followed by 1hat room temperature.

Primary Antibody Staining

- Dilute antibody in 1% BSA (often 1 in 200 is a good place to start optimisation)
- Place 50µl of the diluted Ab on to parafilm attached inside an IF box
- Invers the coverslip and place in the Ab droplet in a way that cells face down and contact with Ab.
- Humidify the box with a wet tissue in one corner to prevent drying of the cells.
- Incubate with a lid on at 37˚C for 1 h
- Put coverslips back into dish to wash 3 times

Secondary Antibody staining

- Repeat as primary antibody staining for 45 min to 1hr.
- Put coverslips back into the dish and wash 3X with PBS.
- Put a small drop Vectashield plus DAPI onto a slide and place coverslip cell side down onto it.

Take the execs mounting fluid by placing the slide and coverslip together face down on a piece of Whatman paper and very gently pressing to the paper.

- Seal the edges of the coverslip with nail varnish.

Cytoskeletal (CSK) pre-extraction buffer

CSK should be freshly made and pre-warmed to 37°C before use.

Incubate coverslip with CSK buffer for10 minutes at room temp prior to fixation

CSK buffer

	STOCK	Dil. Factor	10ml
100mM NaCl	5M	50x	200ul
300mM Sucrose	2M	6.6x	1.5ml
10mM PIPES pH7	200mM	20x	500ul
3mM $MgCl_2$	1M	333x	30ul
0.2% Triton X-100	10%		200ul

Notes: You can vary Triton X-100 concentration or try NP40 depending on the protein you want to visualise. Also, you can add RNase/DNase.

II.3. Protein extraction and western blotting

Protein extraction and measurement:

- Followed by trypsinising cells, wash them tree times with PBS and then the pellet can be stored in -20˚C for few weeks.
- Once defrosted, wash the pellet with PBS and lyse the cells with lysis buffer. Usually, 30-50 µl of lysis buffer is adequate for 35 mm dishes. For bigger pellet more lysis buffer is required which needs to be optimised.
- Lyse the cells on ice for 45-60 minutes. During this time vortex the samples occasionally.
- Spin down the lysed cells 15-20 minutes at maximum speed in 4˚C.
- Transfer the supernatant into a new tube.
- Measure the protein concentration using Bradford reagent. (Dilute the lysis 1/1000 with deionised water then add 500µl of Bradford reagent. Prepare one tube as blank containing just water and Bradford reagent. Read the absorbance of the

samples using spectrophotometer against the blank at 595 nm) for the concentration calculation you will need to make a standard curve made by serial dilution of known concentrations of BSA. I divide the Abs by 0.0305 based on the standard to have the concentration in mg/ml.

- The lysate can be stored for unlimited time at -80˚C
- Based on the required amount of the protein to be loaded on gel dilute it with Laemmli buffer with freshly added 10% 2 β-mercaptoethanol. (Usually I load 20 µg)
- Samples also can be stored at -80˚ C in Laemmli buffer.
- Boil the samples before loading on gel for 5 minutes at 95˚C.

Polyacrylamide gel preparation:

- Wash and dry glass plates and then clean with a tissue and 70% ethanol.
- Assemble the glasses with spacer and fix them. Make sure there won't be any leaking with small amount of water and pour out the water. Then take the exes water with a tissue or Whatman paper.
- Pour acrylamide mix (5ml for small and 20ml for large gels).
- Add 1ml 100% isopropanol on top of the running gel to prevent it from drying out.
- Leave the gel to set for 15-20min.
- Remove Isopropanol and rinse out the top of the gel with milliQ H2O.
- Add stacking gel and insert comb.
- Leave to set for 15-20min.
- Assemble the gel in the running apparatus and fill with Running buffer.
- Remove the comb and flush out the wells with running buffer.
- Note: APS needs to be fresh for the gel. It can be stored at 4°C for 1 week or you can make aliquots and store in -20˚C.

Dilute 100 mg of ammonium persulfate in 1ml of water to make 1ml of 10% APS.

- APS and TEMED should be the last components added to the gel as they will cause polymerisation of the gel once added.

The polymerised gel can be stored in fridge for 1-2 days while wrapped in a wet tissue and placed in a plastic bag to prevent from drying.

Running:

- Load 4 µl of ladder or marker which can be any brand and the size is depend on the protein of interest size. (I usually use Seeblue 1kb)
- Load the samples beside the ladder on polyacrylamide gel and Run them on 80 V up until they reach to the end of staking gel. Then increase the voltage to 120V.
  (The electrophoresis tank should be filled with running buffer)
- Once the proteins run as desired (normally once the blue line exit the gel), stop running and set up the transfer tank and place a Nitrocellulose membrane while sandwiched between Whatman papers and sponges.

Transferring:

Setting the transfer cassette:

- Submerge the nitrocellulose membrane as well as the Whatman papers and sponges in transfer buffer.
- Sandwich the gel and membrane in following order into the cassette;
  1. Black side of the cassette
  2. Sponge
  3. 3x Whatman papers
  4. Gel
  5. Membrane
  6. 3x Whatman papers

7. Sponge
8. White side of the cassette

- Role with a roller or tube over the packed membrane to remove any bobbles.
- Load the cassette into the transfer tank and fill it with transfer buffer.

- Transfer on ice for 1hat 100V.
- Finishing the transfer, open the packed membrane and put it in a proper container and wash with water.
- Through the membrane in ponceau-s (5% Acetic acid and 0.5% Ponceau), to check the successful transfer of proteins. After short exposure to ponceau, wash the execs and place it in a poly pocket to scan it.
- Wash the membrane with TBST to clean up the ponceau while rocking for a while

Probing:

- Role the membrane and put it in a falcon tube and block using 5% milk in PBS for 45 minutes. (*NB. If using a phospho-antibody, use TBS-tween for blocking, washing etc.)
- Pour the diluted primary antibody in 5%milk and incubate it overnight at 4˚C (cold-room) on rotator. It should be avoided to overlap the membrane as it won't expose properly to the Ab.
- Wash the membrane 3 x10 min with TBST (Empty the primary Ab to another tube which can be stored in freezer for using more couple of times).
- Pour the secondary antibody diluted in 5% milk.
- Incubate the tube on roller at room temperature for 1hr.
- Wash the membrane 3X with TBST
- Incubate the membrane with the mix of equal amount of ECL reagents 1 and 2 for 2 minutes.
- Place the membrane in a poly pocket and fix it in a radiology cassette to develop it either manually or using the developer

Machine or alternatively image it by the Vilber imager.

Lysis Buffer (10ml)

	Final	**Stock**	**Volume (for 10ml)**
H_2O			6.6ml
Glycerol	20%	100%	2ml
NP40	0.5%	10%	500µl
NaCl	150mM	5M	300µl
Tris-HCl pH7.5	50mM	1M	500µl
Protease Inhibitor Cocktails		100x	100µl
Phosphatase Inhibitor Cocktails		50x	200µl
$MgCl_2$	1 mM	1M	10µl
Benzonase (if required)		1000x	Use 1ul in 1ml

Laemmli Buffer (4x)

	Final	**Stock**
Tris-HCl pH6.8	250mM	1M
SDS	8%	20%
Glycerol	30%	100%
Bromophenol Blue	0.02%	Powder

Polyacrylamide gel (SDS-PAG) recipe:

Gel concentrations	6%	8%	10%	12%	STACKING
H2O	2.7 ml	2.3 ml	2.0 ml	1.7 ml	1.4 ml
ACRYLAMIDE/BIS ACR 30%	1 ml	1.3 ml	1.7 ml	2 ml	0.380 ml
1.5 M Tris Ph:8.8	1.3 ml	1.3 ml	1.3 ml	1.3 ml	0.250 ml (1M, PH: 6.8)
20% SDS	25 µl	25 µl	25 µl	25 µl	10 µl
10% APS	50 µl	50 µl	50 µl	50 µl	30 µl
TEMED	4 µl	3 µl	2 µl	2 µl	2 µl

Running Buffer (1L)

100ml of 10x TG (Tris-Glycine) buffer

5ml of 20% SDS (1% final Conc)

Water up to 1L

Transfer Buffer (1L)

100ml of 10x TG (Tris-Glycine) buffer

0.5ml of 20% SDS (0.1% final Conc)

200ml Methanol (20% final Conc)

Water up to 1L

10x TBS (1L)

121.14g Trizma Base

90g NaCl

pH7.5 (with HCl)

ddH2O up to 1L

TBST (1L)

100 ml of 10X TBS

100 µl of tween

ddH2O up to 1L

II.4. Membrane staining for H4K20me2

- Perform SDS-polyacrylamide gel electrophoresis (SDS-PAGE) on an acid-extracted protein sample and transfer the proteins to nitrocellulose. Wash the blotted nitrocellulose twice with water.
- Block the blotted nitrocellulose in freshly prepared TBS containing 10% non-fat dry milk and with 0.05% Tween 20 for 1 hour at room temperature with constant agitation.
- Incubate the nitrocellulose with a 1:1,000 to 1:10,000 dilution of anti- dimethyl-Histone H4 (Lys 20), diluted in freshly prepared TBST-MLK for 2 hours with agitation at room temperature.
- Wash the nitrocellulose twice with water.
- Incubate the nitrocellulose in the secondary reagent of choice (a goat anti-rabbit HRP conjugated IgG, 1:5000 dilution was used) in TBST-MLK for 1 hour with agitation at room temperature.
- Wash the nitrocellulose twice with water.
- Wash the nitrocellulose in TBS-0.05% Tween-20 for 3-5 minutes.
- Rinse the nitrocellulose in 4-5 changes of water.
- Use detection method of choice (enhanced chemiluminescence was used

II.5. Double thymidine block

- Make sure your cells are happy
- Cells should be around 75-85% confluency at the time of release.
- Everything has to be kept in 37˚C including media, washing media and PBS and avoid keeping cells out of incubator for long time.
- Use as less as possible media as making conditioned media would be easier for cells. 5 ml media would be enough for 10cm dish for short time release and use 6-7 ml for longer time release.
- Always give the plate enough swirl to make sure the cells are not clamping and well spread.
- Seed HeLa cells on 50-60% density in number of 10 cm dishes according to the number of time points you are planning to harvest the cells. Consider one dish for asynchronized cells.
- Add 100 µl of 100 mM thymidine (1 mM final concentration). Thymidine is not very soluble in water so use PBS to make the 100 mM stock
- Incubate for 16 h.
- Aspirate the medium and wash the cells 3x with pre-warm PBS or medium.
- Add 10 ml growth medium supplemented with 25 µM deoxycytidine and 25 µM thymidine.
- Incubate for 9 h.
- Add 250 µl of 100 mM thymidine.
- Incubate for 16 h.
- Aspirate the medium and wash the cells 3x with 10 ml pre-warm PBS or medium.
- Add 10 ml growth medium supplemented with 25 µM deoxycytidine and return the cells to the incubator.
- Harvest the cells at different time points for analysis.

- Typically, cells are harvested every 2 or 3 h for up to 24 h to cover at least one cell cycle.

II.6. cell surface staining for FACs analysis

- Resuspend the trypsinised and PBS washed cells in 1ml cold PBS.
- Transfer the cell suspension into a 15ml Falcon containing 3ml ice-cold 100% ethanol while vertexing to have final concentration of 75% ethanol. (Falcon tubes with ethanol should be kept in -20ºC at least 20min prior to fixation. The vertexing is required to prevent the cells from clumping and blocking the FACS machine)
- The fixed cells can be stored in -20˚C, up to two months.

Antibody staining:

- Add 3ml PBS to the samples and pellet the cells at 1200rpm x 5min.
- Remove supernatant and transfer cells in 1ml PBS into a new 1.5ml microtube (low adherent tubes are not suitable as the cell will stick to the side of the tube.) Alternatively, if you have several samples, resuspend the cells in 200µl PBS and transfer to a round-bottom 96-well plate, and then use 200µl volume for all washes and an extra wash step each time and pellet cells at 1200rpm.
- Pellet the cells at 2000rpm x 2min at 4ºC (It is best to use a swing-out rotor to prevent losing the cells which stick to the microtube wall in each centrifuge.
- Remove the PBS.
- Resuspend the cells in 50ul PBS containing 1%BSA, 0.5% Triton X-100 and 1µl H3pS10 antibody (millipore).
- Incubate with the 1º antibody for 2h at RT.
- Wash the cells three times in 1ml PBS containing 1%BSA.
- Resuspend the cells in 50µl PBS containing 1%BSA, 0.5% Triton X-100 and 1ul anti-rabbit FITC 2º antibody.

- Incubate in the dark at RT for 1hr.
- Wash cells three times in PBS containing 1% BSA.
- Resuspend the cells in 300 µl PBS containing 40µg/ml Propiodium Iodide and 250 µg/ml RNase A. Then filter them through a 0.2-micron filter into FACS tube to prevent FACS machine blockage.
- Incubate the cells for 30-60 min in the dark on ice.

FACS analysis:

The required controls are including

- no stain control (just fixed cells), a
- no PI control (just fixed cells stained with H3pS10 antibody and the FITC 2ºantibody)
- no FITC control (just fixed cells with PI). This is required for compensate for overlapping of the PI with FITC and vice versa.

Draw the following plots on the BD-FACS Diva Software:

- Scatter plot FSC vs. SSC (to see all events)
- Scatter plot FSC-A vs. FSC-H (to exclude doublets)
- Scatter plot PE-Cy7 (x-axis) vs. FITC (y-axis) (to see mitotic staining)
- Histogram of PE-Cy7 (to see cell cycle distribution)
- Also create a statistic view to read of the percentage of mitotic cells.

Note: FSC, SSC and PE-Cy7 channel should all be on a normal scale, while FITC should be on a log scale.

- Run no stain control first, gate for single cell population (P1) on the FSC vs. SSC scatter plot (Note, voltage for both FSC and SSC will need to be adjusted depending on the cell type used).
- Then gate out the doublets (FSC-A vs. FSC-H).
- Next run the PI only control. Adjust the voltage for PE-Cy7, so that the G1 peak (1st peak) is at 100 and the G2 peak (2nd peak) is at 200. This ensures that your cells are single cells with a normal DNA content.

- Then adjust the FITC channel, so that all FITC negative cells fall just below 10^3.
- The FITC only control should give a distinct population above $10^{3.}$
- Use a quadrant gate with the horizontal axis just above 10^3 and the vertical axis at 150. The top right quadrant is the number of mitotic cells for each sample.
- Run all sample through the FACS on low throughput (this should be around 200-400 events per second) and collect a minimum of 20,000 to 30,000 cells per sample. Use SIT flush after each sample.
- Plot the percentage of mitotic cells v. time.

II.7. Metaphase spread

- Grow cells to around 60-70% confluency
- Arrest cells in metaphase with 0.05 ug/ml Colcemid for 2 h (stock is 1mg/ml in PBS dilute 1 in 20,000)
- Harvest cells using trypsin (keep media as it may contain dislodged mitotic cells, the media, the PBS used for wash and the trypsinised cells should spin down together)
- Spin down cells (1200 rpm x 5min)
- Discard supernatant (okay to leave a drop)
- Resuspend pellet slowly in 1ml pre-warmed (37˚C) hypotonic solution (75 mM KCl), then add 4 ml hypotonic solution dropwise. (Volume of hypotonic solution can be optimised; you need a slightly cloudy solution)
- Incubate adherent cell types for 25-30 min at 37˚C (Suspension cells – around 10min)
- Using a 1ml pipette, add one ml of fresh ice-cold fixative (methanol/acetic acid - 3:1 ratio) per ml of hypotonic solution used. Add dropwise to the tube and invert to mix. This stops the hypotonic process and pre-fixes the cells
- Spin the cell suspension (1200 rpm x 5min), remove the supernatant carefully, leaving a drop
- Add 5ml fresh ice-cold fixative dropwise down the side of the tube, very slowly, gently flicking the pellet all the time
- Pellet cells, repeat fixation step and pellet again
- Add between 200 ul-1 ml of ice-cold fixative to the pellet dropwise, flick to mix. The final volume of fixative is determined by the desired concentration of cells on your slide. It should be slightly cloudy, yet translucent when hold up in light.
- This can now be stored at -20 C up to one year or dropped onto slides
- Drop cell suspension (~12 µl) onto preferably polylysine slide from a height of about 1 cm.

- Immediately put them on metal plate and place them on the surface of water in 56˚ C prewarmed water bath.
- Air dry slides and check them with an invert microscope (in TC) to ensure the good quality of the spreads.
- Leave them over night in dark and dry place to be aged.
- stain as desired (GIEMSA/DAPI/FISH)

II.8. FISH

Solutions

Hybridization buffer	40 ml
20 mM Na2HPO4, pH 7.4	1.6 ml of 0.5 M
20 mM Tris, pH 7.4	800 ul of 1 M
60% formamide	24 ml
2 X SSC	4 ml of 20 X SSC
1 ug/ml salmon sperm DNA	20 µl of 2 mg/ml stock
DD H2O up to volume	9.6 ml

It is advised to make 500 µl aliquots of Hybridisation buffer and keep them at -20˚C as it contains formamide which is not stable.

RNAse A	1 ml
100ug/ml RNAse A in 2xSSC	20 ul RNAse from 5 mg/ml stock 100 ul 20 X SSC 899 ul Water

Pepsin 0.005% solution

2.5mg pepsin in 50ml 0.01M HCl (water and 42ul of 37%HCl) (make fresh and **warm** to 45 degrees)

Wash solution 1

70% formamide

10 mM Tris, pH 7.2

Wash solution 2

0.05 M Tris, 0.15 M NaCl pH 7.5

0.05% Tween

Probe preparation

I am using a Telomere PNA probe from Eurogentec (TelC-FAM) – green

- Resuspend 5nmol lyophilized PNA probe in 100ul milliQ water to make 50uM stock.
- Use at 40x (i.e. final concentration 100nM)
- Denature 20ul of probe in hybridization per slide at 90 degrees for 5min
- (100ul hybridization buffer and 2.5ul probe)

Pre-treat slides (metaphase spreads)

- Immerse in PBS for 5min
- Fix in 4% formaldehyde in PBS for 2min at 37˚C
- Three 5 min washes in PBS at 37 ˚C
- Put 500 µl of RNAaseA solution onto parafilm and place slides face down onto it for 1 hat 37˚C (in humidified box)
- Three washes in 2X SSC and one in DW (deionized water)
- Immerse in Pepsin 0.005% for 10min at 37˚C
- Brief rinse with PBS
- Fix in 4% formaldehyde in PBS for 2min at 37˚C
- Three 5min washes in PBS at 37˚C
- Dehydrate slides in cold ethanol series (1min in 70%, 85%, 100%)
- Air dry slide

Hybridization

- Incubate slides at 80 degrees for 5min (in hybridisation chamber)
- Add 50ul of probe in hybridization buffer to marked area (heat at 90 degrees for 5min first)
- Cover with long coverslip and stick parafilm on top to prevent drying
- Incubate for 5 min at 85˚C (80 – 90˚C)
- Incubate in the dark at room temp for 2 hour or overnight (in humidified box. I usually seal them in a polypocket with a damp tissue inside to ensure that they won't dry)

Wash

- Wash twice with wash solution 1 at room temperature for 15 min
- Three 5 min washes with wash solution 2
- Dehydrate slides in cold ethanol series (1 min in 70%, 85%, 100%)
- Air dry

Visualising

- Add DAPI with vectashield and a coverslip, then seal with nail varnish
- Use 100x magnification to visualise telomere

Appendix III: Top 53BP1 interactors In SILAC Screen

A.

Protein Description	53BP1/W
53Bp1	20.675
53Bp1 (216kDa isoform)	12.702
p53	9.6166
USP28	6.1894
Kinesin-like protein KIF18B	4.4999
serine/threonine-protein kinase Nek4	4.2237
similar to olfactory receptor MOR41-1	1.6558
signal recognition particle 14kDa protein	1.649
PLK1	1.5361
Vimentin	1.5116
Ubiquitin carboxyl -terminal hydrolase 7	1.4189
Polyadenylate-binding protein -interacting protein 2	1.2021
DEAD box polypeptide 17	1.174
Tripartite motif-containing protein 71	1.1328
eukaryotic translation initiation factor 3 subunit H	1.0806
similar to gag protein	1.0224
clathrin light chain B	1.0205
Isoform 2 of alpha-actinin-2	1.0205
lamin-B2	1.0176
Thioredoxin domain containing 4	0.98635

B.

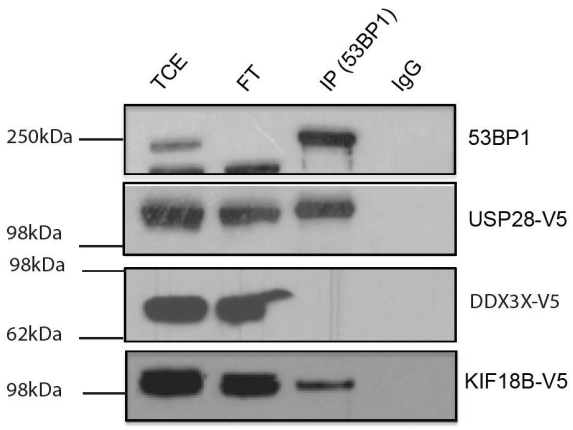

Figure III.1. 53BP1 interacting proteins.

(A) Top 53BP1 interacting proteins in the proteomic screening (SILAC) including KIF18B among the published 53BP1 interacting partners which highlighted in green. (B) Immunoprecipitation of 53BP1 and KIF18B. the USP28 used as a positive control and DDX3X used as a negative control to show interaction with 53BP1.(The immunoprecipitation is performed by Dr. Silvia Maretto)